

Some illustrations have been removed for copyright restrictions.

Pages 137, 138, 257, 258, 259 and 260 have been removed for copyright restrictions.

# **MYOPIA: STRUCTURAL AND FUNCTIONAL CORRELATES**

Manbir Kaur Nagra

Doctor of Philosophy

Aston University

August 2010

This copy of the thesis has been supplied on condition that anyone who consults it is understood to recognise that its copyright rests with its author and that no quotation from the thesis and no information derived from it may be published without proper acknowledgement.

Aston University

## **MYOPIA: STRUCTURAL AND FUNCTIONAL CORRELATES**

Manbir Kaur Nagra

Doctor of Philosophy

August 2010

### **SUMMARY**

Ocular dimensions are widely recognised as key variants of refractive error. Previously, accurate depiction of eye shape *in vivo* was largely restricted by limitations in the imaging techniques available. This thesis describes unique applications of the recently introduced 3-dimensional magnetic resonance imaging (MRI) approach to evaluate human eye shape in a group of young adult subjects ( $n=76$ ) with a range of ametropia (MSE= -19.76 to +4.38D). Specific MRI derived parameters of ocular shape are then correlated with measures of visual function.

Key findings include the significant homogeneity of ocular volume in the anterior eye for a range of refractive errors, whilst significant volume changes occur in the posterior eye as a function of ametropia. Anterior *vs.* posterior eye differences have also been shown through evaluations of equivalent spherical radius; the posterior 25% cap of the eye was shown to be relatively steeper in myopes compared to emmetropes. Further analyses showed differences in retinal quadrant profiles; assessments of the maximum distance from the retinal surface to the presumed visual axes showed exaggerated growth of the temporal quadrant in myopic eyes. Comparisons of retinal contour values derived from transformation of peripheral refraction data were made with MRI; flatter retinal curvature values were noted when using the MRI technique.

A distinctive feature of this work is the evaluation of the relationship between ocular structure and visual function. Multiple aspects of visual function were evaluated through several vehicles: multifocal electroretinogram testing, visual field sensitivity testing, and the use of psychophysical methods to determine ganglion cell density.

The results show that many quadrantic structural and functional variations exist. In general, the data could not demonstrate a significant correlation between visual function and associated measures of ocular conformation either within or between myopic and emmetropic groups.

**Key words: Ocular shape, Peripheral refraction, Visual fields, Multifocal Electroretinography, Ganglion cell density**

## ACKNOWLEDGEMENTS

I would like to begin by thanking my principal supervisor, Professor Bernard Gilmartin, for providing endless guidance, enthusiasm, and for sharing his academic wisdom.

I would also like to thank my associate supervisors: Dr Nicola Logan, Professor Krish Singh, and Professor Paul Furlong for helping set up the MRI aspect of the project. I am indebted to Dr Mark Dunne for his assistance with the *RetFit* program. I am especially grateful to Professor Stephen Anderson for his advice on the ganglion cell density experiment.

Furthermore, I would like to thank both Andrea Scott and Dr Ian Fawcett for their assistance with the mfERG data collection. I am also appreciative of the time and effort Elizabeth Wilkinson, Dr Jade Thai, and Jon Wood spent acquiring the MRI data presented in this thesis. Thank you to Dr Bill Cox, Dr Robert Cubbidge, and Hetal Patel for their relative contributions to the data analysis. I am appreciative of the time given by all participants who volunteered for the studies which comprise this thesis.

The College of Optometrists (UK) is gratefully acknowledged for the award of a three year PhD Research Scholarship and travel bursary. Advantage West Midlands (UK) and the Lord Dowding Fund for Humane Research (UK) are also acknowledged for their funding contributions to this project.

A special thank you to Jagdeep Sangha for the many hours spent helping me with my computer related problems over the past few years.

And finally, I would like to thank my family: my parents, Manjit and Balbir, for all their support throughout this process, and my sister Harbir for the tremendous hours of help and feedback she gave. Thank you.

## CONTENTS

<b>SUMMARY</b>	2
<b>ACKNOWLEDGEMENTS</b>	3
<b>CONTENTS</b>	4
<b>LIST OF TABLES</b>	10
<b>LIST OF APPENDICES</b>	20
1 INTRODUCTION .....	21
2 OCULAR SHAPE IN MYOPIA .....	23
2.1 Factors influencing eye growth.....	23
2.2 Ocular biometric studies .....	24
2.3 Axial length in myopia.....	24
2.3.1 Axial length variables .....	25
2.4 Cornea and myopia .....	27
2.5 Anterior chamber depth and myopia.....	29
2.6 Eye shape and retinal contour in myopia.....	30
2.7 MRI use in ocular imaging .....	31
2.8 Summary .....	33
3 PERIPHERAL REFRACTIVE ERROR AND OCULAR SHAPE .....	35
3.1 Introduction.....	35
3.2 Peripheral refraction techniques .....	35
3.3 Peripheral astigmatism.....	36
3.3.1 Peripheral astigmatism and refractive error .....	37
3.4 Computational approach to deriving retinal contour .....	39
3.5 Retinal profile and peripheral refraction.....	40
3.5.1 Vertical peripheral refraction .....	42
3.6 Summary .....	43
4 VISUAL FIELDS AND AMETROPIA .....	44
4.1 Definition .....	44

4.2	Perimetry.....	45
4.2.1	Reliability indices in automated perimetry .....	45
4.2.2	Refractive correction.....	46
4.3	Visual pathway.....	47
4.3.1	Distribution of retinal photoreceptors .....	48
4.3.2	Photoreceptor function in ametropia.....	49
4.4	Visual fields and ametropia .....	49
4.5	Summary .....	50
5	ELECTROPHYSIOLOGY AND MYOPIA.....	51
5.1	Introduction.....	51
5.2	The electroretinogram .....	51
5.3	The multifocal electroretinogram (mfERG) .....	52
5.3.1	First and second order kernels .....	54
5.3.2	Tools for mfERG analysis .....	54
5.4	Cellular origins of response .....	55
5.5	Myopia and electrophysiology findings.....	57
5.5.1	Myopia and ERG .....	57
5.5.2	MfERG and myopia.....	58
5.5.3	Reasons for reduced electrical response in myopia .....	61
5.6	Summary .....	62
6	GANGLION CELL DENSITY AND OCULAR SHAPE.....	63
6.1	Introduction.....	63
6.2	Distribution of ganglion cells.....	63
6.3	Receptive fields.....	64
6.3.1	Magnocellular and Parvocellular cells.....	65
6.4	Sampling theorem, aliasing and the Nyquist limit.....	66
6.5	Peripheral visual function .....	66
6.6	Myopia, eye size and peripheral ganglion cell function .....	67

6.7	Summary .....	69
7	INSTRUMENTATION .....	70
7.1	Introduction.....	70
7.2	Shin Nippon Autorefractor .....	70
7.3	Zeiss <i>IOL Master</i> .....	71
7.4	Zeiss Humphrey Visual Fields Analyser .....	73
7.5	Oculus Pentacam.....	74
7.6	Magnetic Resonance Imaging (MRI).....	75
7.7	Summary .....	77
8	SUMMARY OF AIMS AND OBJECTIVES .....	78
9	DEPICTION OF OCULAR SHAPE AS DERIVED FROM 3-DIMENSIONAL MAGNETIC RESONANCE IMAGING (MRI) .....	79
9.1	Introduction.....	79
9.2	3 Dimensional MRI.....	79
9.2.1	Ocular Volume.....	81
9.2.2	Generation of quadrant and radius band values .....	82
9.2.3	Angle $\alpha$ .....	85
9.2.4	Previous reports using the Aston University MR scanning protocol.....	86
9.3	Purpose.....	88
9.4	Hypothesis.....	88
9.5	Methods.....	88
9.5.1	Radius bands .....	89
9.5.2	Ocular volumes .....	90
9.5.3	Quadrant data .....	90
9.5.4	Stretch index .....	91
9.5.5	Interval Variation (IV) .....	91
9.5.6	Surface areas .....	92
9.5.7	Inter eye differences.....	92

9.6	Results.....	92
9.6.1	Radius bands .....	92
9.6.2	Ocular volumes .....	96
9.6.3	Quadrant data .....	100
9.6.4	Inter eye differences.....	125
9.7	Discussion and conclusions .....	133
9.8	Summary .....	135
10	SUPPORTING PUBLICATIONS .....	137
11	PERIPHERAL REFRACTION AND OCULAR SHAPE .....	139
11.1	Introduction.....	139
11.2	Peripheral astigmatism.....	140
11.3	Purpose.....	142
11.4	Hypothesis.....	142
11.5	Instrumentation .....	142
11.6	Methods.....	142
11.7	Results.....	143
11.8	Discussion and conclusions .....	160
11.9	Summary .....	162
12	VISUAL FIELD SENSITIVITY AND OCULAR SHAPE .....	163
12.1	Introduction.....	163
12.2	Purpose.....	164
12.3	Hypothesis.....	164
12.4	Instrumentation .....	164
12.5	Methods.....	164
12.6	Results.....	168
12.6.1	Discussion and conclusions .....	175
12.7	Summary .....	176
13	MULTIFOCAL ELECTRORETINOGRAM AND OCULAR SHAPE .....	177

13.1	Introduction.....	177
13.2	Purpose.....	179
13.3	Methods and instrumentation.....	179
13.4	Results.....	182
13.5	Discussion and conclusions .....	190
13.6	Summary .....	192
14	INVESTIGATION OF GANGLION CELL DENSITY WITH REFERENCE TO OCULAR SHAPE .....	193
14.1	Introduction.....	193
14.2	Purpose.....	194
14.3	Hypothesis.....	194
14.4	Methods.....	194
14.5	Instrumentation .....	196
14.5.1	Stimulus detection.....	196
14.5.2	Stimulus direction discrimination .....	197
14.5.3	Validity .....	197
14.6	Results.....	197
14.6.1	Detection and direction discrimination experiments .....	197
14.6.2	The effect of eye conformation on ganglion cell receptors .....	203
14.7	Case study .....	210
14.7.1	Discussion and conclusions .....	214
14.7.2	Possible causes for the absence of a relationship between ganglion cell density and ocular shape .....	215
14.8	Summary .....	217
15	GENERAL DISCUSSION .....	218
15.1	Introduction.....	218
15.2	Eye shape and its role in myopia .....	218
15.3	Visual Function and ocular shape .....	220

15.4	Further work.....	222
15.4.1	Orbital size versus ocular size.....	222
15.4.2	Advanced data analysis and development of myopia treatments .....	222
15.4.3	Extending peripheral refraction work .....	222
15.4.4	Identifying high risk cases of myopia .....	223
15.4.5	Anterior eye biometric and functional investigations.....	223
15.4.6	Histological studies .....	224
15.5	Summary .....	224
	<b>REFERENCES</b>	226
	<b>APPENDICES</b>	238

## LIST OF TABLES

Table 1 The site of retinal damage and its consequence for the mfERG response waveform (after Hood, 2002).....	57
Table 2 Magno- and Parvocellular differences .....	65
Table 3 The distribution of refractive error within the cohort .....	89
Table 4 The mean percentage along the axis at which the maximal point was noted .....	110
Table 5 Mean maximum distance for each quadrant by refractive group. SD indicates the standard deviation of the maximum distance values for each refractive group.....	113
Table 6 Lists the distance in mean percentage along the axis at which the maximal point was noted.....	114
Table 7 Showing the maximum distance for each quadrant by refractive group. SD indicates the standard deviation .....	117
Table 8 The refractive errors of the 18 subjects for whom right and left eyes were compared. Axial length are taken from MR data .....	125
Table 9 The approximate distance from the fovea towards the anterior eye in millimetres which would correspond to each field angle using a schematic eye (after Dunne, 1995)....	145
Table 10 The average MSE in dioptres (D) and standard deviations for each refractive category, right and left eyes .....	146
Table 11 Mean MSE at each eccentricity for right eyes, for each refractive group $\pm$ standard deviations ( $n$ = nasal retina, $t$ = temporal retina). Results for eccentricity 15 degrees temporal were omitted due to effect of the optic nerve head. ....	147
Table 12 Mean difference in MSE between central and peripheral locations, right eyes ....	149
Table 13 Mean $J_{180}$ values right eye listed by angle of eccentricity and refractive group....	151
Table 14 $J_{45}$ right eye, listed by angle of eccentricity and refractive group .....	153
Table 15 Cylindrical component as calculated from vector components $J_{180}$ and $J_{45}$ , right eyes .....	155
Table 16 The relative differences between the two techniques at different field angles.....	158
Table 17 Mean differences in $y$ values between the MR data and RetinaFit program values (in mm).....	159
Table 18 Mean MS response for each quadrant.....	170
Table 19 Mean TD of responses for each XQ quadrant .....	171
Table 20 Mean TD of responses for each +Q quadrant .....	171
Table 21 Surface area values and standard deviations for each quadrant.....	173

Table 22 Mean IV values for each quadrant, based on MRI data for the posterior 25% of the eye .....	175
Table 23 Central and peripheral refractions (at ~40° temporal to fovea) of subjects corrected with full trial aperture lenses (right eyes) .....	195
Table 24 Biometric data of subjects.....	195
Table 25 Detection task results (mean values with standard deviations where repeat runs were carried out). Blank cells indicate that either the subject was unable to complete the test at a particular spatial frequency or correct responses had fallen to below 50% and thus there was no need for further measurements. ....	198
Table 26 Direction discrimination task results (mean values with standard deviations where repeat runs were carried out).....	203
Table 27 Calculated index of ocular stretch and Nyquist limit (NL) estimates calculated for each subject (in %). NB a higher % for index of stretch indicates a smaller eye .....	205
Table 28 Refractive and ocular biometric data for subject R.C.....	210
Table 29 Estimates of threshold values and indices of ocular stretch .....	212
Table 30 Mean MSE at each eccentricity for left eyes .....	295
Table 31 Mean difference in MSE values between central and peripheral locations, data is shown for left eyes .....	296
Table 32 Mean $J_{180}$ values left eye based on eccentricity .....	297
Table 33 $J_{45}$ left eye, based on eccentricity.....	298
Table 34 Cylindrical component calculated from vector components $J_{180}$ and $J_{45}$ . Left eye data is shown.....	299
Table 35 Graphical representation of the cylindrical component, left eyes only .....	299
Table 36 Biometry data for subject RC measured using the Zeiss IOL Master (in mm) ....	315
Table 37 Ocular biometry data for subject JP (in mm).....	316

## LIST OF FIGURES

Figure 1 Demonstrates the strong correlation between a longer axial length and myopia (axial length measured using the Zeiss IOL Master and Mean Spherical Error (MSE) with the Shin Nippon SRW 5000 autorefractor, $n=71$ , $p < 0.01$ , $r = -0.891$ ). Data from subject dataset .....	25
Figure 2 Graphical representation of the AL:CR ratio as calculated from readings taken with the Zeiss IOL Master ( $n=66$ ). Data presented from subject dataset .....	28
Figure 3 Graphical representation of the average keratometry reading as measured with the Zeiss IOL Master against MSE ( $n=66$ ). Data presented from subject dataset.....	29
Figure 4 Graphical representation of anterior chamber depth (as measured with the Zeiss IOL Master) with MSE $n=69$ ( $p < 0.01$ , $r = 0.427$ ). Data presented from subject dataset....	30
Figure 5 (a) The height and (b) the width measurements taken from MR images (from Atchison et al. 2004).....	32
Figure 6 The effect of a steeper retina (R) on the tangential (T) and sagittal (S) image shells (Dunne, 1995) .....	36
Figure 7 The effect of a flatter retina on the tangential and sagittal image shells (Dunne, 1995) .....	37
Figure 8 Plot showing the average astigmatic axis direction and magnitude in the central $44^\circ$ for each of the three main refractive groups (from Seidemann et al. 2002) .....	39
Figure 9 (a) The uniform expansion of a myopic eye shown in Taiwanese - Chinese eyes (b) the asymmetrical expansion of the nasal aspect shown in Caucasian subjects (from Logan et al. 2004). .....	41
Figure 10 Diagram representing Traquair's depiction of the island of vision (right eye).....	44
Figure 11 Diagram showing the human visual pathway (LGN denotes the position of the lateral geniculate nucleus). The diagram shows the crossover of the nasal fibres (temporal field) to the contralateral side. The messages are relayed through the LGN and onto the primary visual cortex located in the occipital lobe of the brain.....	48
Figure 12 Typical ERG waveform.....	52
Figure 13 Hexagon stimulus used in mfERG testing (from Marmor et al. ISCEV guidelines 2003) .....	53
Figure 14 Typical waveform response from the mfERG (from Marmor et al. ISCEV guidelines, 2003).....	54
Figure 15 3-dimensional topography plot of mfERG response (figure taken from subject data set, left eye).....	55

Figure 16 Cellular responses in mfERG (after Hood et al. 2002) .....	56
Figure 17 Diagrammatical representation of the concentric ring averages analysed, note ring 1 denotes the presumed foveal response. ....	58
Figure 18 Diagrammatical representation of the quadrant average analysis undertaken by Kawabata and chi-Usami 1997. N.B the horizontal and vertical meridians have been omitted, presumably to ensure equal hexagonal responses from each quadrant and also to exclude the optic nerve head .....	59
Figure 19 On-centre ganglion cells and sinusoidal grating .....	64
Figure 20 Visual resolution limit in cycles per degree at an eccentricity of 25°, at radial locations around the retina (Anderson et al. 1992) .....	67
Figure 21 (a) Equatorial stretching (b) Global expansion (c) Posterior Pole (after Strang et al. 1998) .....	68
Figure 22 Graph showing the predicted decline in resolution with increasing myopia for each of the three myopic models, (optical cut-off is marked at 45 cpd, represents the optical limit of the eye) (after Strang et al. 1998) .....	69
Figure 23 An example of a Pentacam output. The output shows the corneal thickness for an emmetropic subject (MSE: +0.50D). Further outputs are given for parameters such as corneal curvature and aberrations. ....	75
Figure 24 The MR scanner and head coil (c/o Aston University Day Hospital).....	80
Figure 25 The three different views presented in mri3dX. Each view shows one slice .....	81
Figure 26 The division of anterior and posterior volume measurements is shown by the dashed line (after Gilmartin et al. 2008) .....	82
Figure 27 Graphic depicting the 3-dimensional MRI process. The first image shows the raw T2 weighted MR image. The second image shows the same scan once shaded using the mri 3dX program. The third image is a representation of the eye once the polygonal envelope has collapsed around the shaded voxels producing a rough corrugated model of the eye (Singh, Logan, & Gilmartin 2006). The final two pictures illustrate 3 dimensional models post smoothing; radius bands (as described in Methods) are visible in the final picture. ....	83
Figure 28 The direction in which data points are collapsed to generate data for the XQ. The same methodology was applied to the +Q .....	84
Figure 29 The diagram shows the conversion of 3D data to 2D. Figure provided c/o Professor Bernard Gilmartin .....	85
Figure 30 Diagrammatical representation of the various parameters of ocular shape measured as part of this study. ....	89

Figure 31 Data plotted for the region 15-100% along the axis. 2 <sup>nd</sup> order polynomial fitted for the region 25-75%.....	91
Figure 32 The equivalent radius of curvature by refractive group. Each data set is fitted with a moving average trendline; averaging every second point.....	93
Figure 33 Shows the standard deviation error bars for the emmetropic refractive group in the region 15-92% along the axis .....	94
Figure 34 Shows the standard deviation error bars for the low myopic refractive group in the region 15-92% along the axis .....	94
Figure 35 Shows the standard deviation error bars for the highly myopic refractive group in the region 15-92% along the axis.....	95
Figure 36 Shows the standard deviation error bars for the hyperopic refractive group in the region 15-92% along the axis .....	95
Figure 37 The equivalent radius data fitted with 6 <sup>th</sup> order polynomials to expose subtle changes in shape .....	96
Figure 38 The anterior volumes (below in grey) and posterior volumes (above in black) plotted as a function of MSE. Data is shown for RE only (n=73).....	97
Figure 39 The volume for the posterior 25% plotted as a function of MSE.....	98
Figure 40 The posterior volume minus the posterior 25% volume .....	99
Figure 41 Corneal volume (via the Oculus Pentacam) vs. MSE (D) (p>0.05, r = -0.173) ...	100
Figure 42 A graphical representation of the retinal contours by quadrant .....	102
Figure 43 Nasal and temporal chord distances. Temporal chord distances were subtracted from nasal and plotted graphically. The same methodology was used for S-I, SN-IT and ST-IN quadrants.....	103
Figure 44 Differences between the nasal and temporal chords in each refractive group ....	104
Figure 45 Differences between the superior and inferior chords in each refractive group...	105
Figure 46 Standard deviations for each refractive group, nasal-temporal quadrants .....	106
Figure 47 Standard deviations for each refractive group, superior-inferior quadrants.....	106
Figure 48 The differences between the SN and IT chords for each refractive group .....	107
Figure 49 The differences between the ST and IN chords for each refractive group. NB scaling differences of y axis compared to SN-IT chord differences graph.....	108
Figure 50 Standard deviations for each of the refractive groups SN-IT quadrants .....	109
Figure 51 Standard deviations for each of the refractive groups ST-IN quadrants .....	109
Figure 52 The maximum distance values at 5% or 2.5% increments along the presumed visual axis.....	110

Figure 53 The maximum distance values at 5% or 2.5% increments along the presumed visual axis.....	111
Figure 54 The maximum distance values at 5% or 2.5% increments along the presumed visual axis.....	111
Figure 55 The maximum distance values at 5% or 2.5% increments along the presumed visual axis.....	112
Figure 56 Maximal distance from the presumed visual axis to the retinal surface for each quadrant.....	112
Figure 57 Maximum distance values at 5% or 2.5% increments along the presumed visual axis .....	115
Figure 58 Maximum distance values at 5% or 2.5% increments along the presumed visual axis .....	115
Figure 59 Maximum distance values at 5% or 2.5% increments along the presumed visual axis .....	116
Figure 60 Maximum distance values at 5% or 2.5% increments along the presumed visual axis .....	116
Figure 61 Maximal distance from the presumed visual axis to the retinal surface for each quadrant.....	117
Figure 62 The mean $x^2$ coefficient values for each quadrant divided further by refractive group .....	119
Figure 63 The mean $x^2$ coefficient values for the polynomial curves fitted to data representing the posterior 25% cap of the eye. Data are separated by refractive group.....	119
Figure 64 The mean $x^2$ coefficient values for each quadrant divided further by refractive group .....	120
Figure 65 The mean $x^2$ coefficient values for the polynomial curves fitted to data representing the posterior 25% cap of the eye. Data are separated by refractive group.....	121
Figure 66 The mean Interval Variance (IV) shown for the XQ.....	122
Figure 67 The mean Interval Variance (IV) for the XQ meridians .....	123
Figure 68 The mean Interval Variance (IV) for the +Q in the 25-75% region.....	124
Figure 69 The mean Interval Variance (IV) for +Q meridians .....	125
Figure 70 The mean differences between the right and left eyes of emmetropic and myopic refractive groups for the nasal and temporal quadrants. ....	126
Figure 71 The mean difference between the right and left eyes of emmetropic and myopic refractive groups for the superior and inferior quadrants .....	127
Figure 72 Standard deviations (SD) for the nasal and temporal inter eye differences .....	127

Figure 73 Standard deviations (SD) for the superior and inferior inter eye differences.....	128
Figure 74 The mean difference between the right and left eyes of emmetropic and myopic refractive groups for the SN and IT quadrants.....	129
Figure 75 The mean difference between the right and left eyes of emmetropic and myopic refractive groups for the ST and IN quadrants.....	129
Figure 76 Standard deviations (SD) for the SN and IT inter eye differences.....	130
Figure 77 Standard deviations (SD) for the ST and IN inter eye differences.....	130
Figure 78 Central corneal thickness versus MSE (in D) as measured by the Oculus Pentacam ( $n=42$ ). All subjects from the MRI subject group were invited for Pentacam readings to be taken, results are shown for subjects who responded ( $p= 0.051$ , $r= -0.262$ ). .....	131
Figure 79 Corneal thickness values (in microns) for the XQ, obtained using the Oculus Pentacam ( $n=40$ ) .....	133
Figure 80 Graph of the mean uncorrected peripheral refractive error for right eyes fitted with 2 <sup>nd</sup> order polynomial curves (references to nasal and temporal refer to retinal not field locations, $n=42$ ) .....	148
Figure 81 Graphical representation of the mean difference in MSE between central and peripheral locations, right eyes (linear fit used for emmetropic group, 2 <sup>nd</sup> order polynomials for myopic groups).....	149
Figure 82 Mean $J_{180}$ values for right eyes, fitted with 2 <sup>nd</sup> order polynomial curves.....	152
Figure 83 Mean $J_{45}$ values for right eyes, fitted with linear trend lines.....	154
Figure 84 Graphical representation of cylindrical component, for right eyes only .....	156
Figure 85 The difference in retinal contour data as derived by MRI and RetinaFit by field angle (combined average of $n=41$ ) .....	157
Figure 86 Mean difference for y values between the MRI and RetinaFit techniques, with reference to refractive error .....	159
Figure 87 The technique used to divide visual fields plots into quadrants. The greyed-out regions show the position of the blind spot and the point directly above the blind spot, these two points were excluded from analysis (as is standard in visual fields research). The circles show the points which lie on the axes and the arrows show the quadrant into which these circled points were included .....	166
Figure 88 The significant relationship between axial length (in mm) and mean spherical error (MSE in D, $n=40$ ) (one tailed Pearson's correlation coefficient $p<0.001$ , $r = -0.854$ ).....	168
Figure 89 Graph showing the mean sensitivity for each of the XQ quadrants, error bars show standard deviations.....	169

Figure 90 Graph showing the mean MS response for each of the +Q quadrants, error bars show standard deviations .....	169
Figure 91 Mean TD per XQ quadrant, error bars show standard deviations .....	170
Figure 92 Mean TD per +Q quadrant, error bars show standard deviations.....	171
Figure 93 Mean surface areas for each XQ quadrant are shown for the posterior 25% cap of the eye. Error bars show standard deviations.....	172
Figure 94 Mean surface areas for each +Q quadrant are shown for the posterior 25% cap of the eye. Error bars show standard deviations.....	173
Figure 95 IV indices per retinal quadrant, error bars show standard deviations .....	174
Figure 96 IV per retinal quadrant, error bars show standard deviations.....	174
Figure 97 The fixation monitor visible to the investigator, the top left shows the signal recorded.....	180
Figure 98 The method by which mfERG rings and quadrants configurations were divided before responses from each region were averaged and analysed .....	181
Figure 99 Schematic representation of the angular subtense by the mfERG stimulus (NB not to scale) .....	182
Figure 100 The PCI axial length against the mean spherical error (MSE) as measured by the Shin Nippon autorefractor ( $n=23$ , left eye data) .....	183
Figure 101 N1 amplitudes shown as a function of retinal eccentricity (R5 indicates the ring furthest from the fovea). Error bars show standard deviation of the dataset .....	183
Figure 102 P1 amplitudes shown as function of retinal eccentricity. Error bars show standard deviation of the dataset.....	184
Figure 103 The N1 response amplitudes for +Q (LE data). Error bars show standard deviation of the dataset .....	185
Figure 104 The P1 response amplitudes for +Q (LE data). Error bars show standard deviation of the dataset .....	185
Figure 105 Surface areas and implicit times for the inferior-nasal retinal quadrant .....	186
Figure 106 Shows the N1 response amplitudes for XQ (LE data) .....	187
Figure 107 The P1 response amplitudes for the XQ (LE data). Error bars indicate the standard deviation .....	188
Figure 108 Shows P1 Implicit times for the XQ (LE data). Error bars indicate the standard deviations .....	188
Figure 109 Surface areas and N1 implicit times for the inferior retinal quadrant .....	189
Figure 110 Diagram showing the experimental setup (not to scale) .....	195

Figure 111 Subject OH, MSE: -8.62D. Vertical lines express 95% confidence limits, solid lines show confidence limits for the detection function and dashed line for the direction discrimination .....	199
Figure 112 Subject MN, MSE: -3.00D .....	200
Figure 113 Subject AS, MSE: +0.50D .....	201
Figure 114 Subject JA, MSE: +0.19D .....	202
Figure 115 Diagrammatical representation of the surface area calculation of the ocular surface. The grey band represents the 60-80% region for which area was calculated (not to scale) .....	205
Figure 116 Graphical representation of the spatial frequencies at which 50% of responses are correct, plotted as a function of stretch index. Circles denote detection and stars indicate direction discrimination. Case study RC is also included (see below). .....	206
Figure 117 Calculated index of stretch for subject OH: 93%. The graph shows the point situated 40° from the presumed foveal location; the horizontal lines denote the distance from the 40° location to the presumed visual axis (RE) Negative values denote the temporal region and positive numbers denote the nasal. ....	207
Figure 118 Calculated index of stretch for subject MN: 91% (RE). Negative values denote the temporal region and positive numbers denote the nasal .....	208
Figure 119 Calculated index of stretch for subject AS: 99% (RE). Negative values denote the temporal region and positive numbers denote the nasal .....	209
Figure 120 Calculated index of stretch for subject JA: 92% (RE). Negative values denote the temporal region and positive numbers denote the nasal .....	210
Figure 121 Case study: RC right eye .....	211
Figure 122 Case study: RC left eye .....	212
Figure 123 Calculated index of stretch, subject RC, left eye: 104%. Negative values denote the temporal region and positive numbers denote the nasal .....	213
Figure 124 Calculated index of stretch, subject RC, right eye: 81%. Negative values denote the temporal region and positive numbers denote the nasal .....	214
Figure 125 Schematic illustration of the retinal layers of the human eye .....	220
Figure 126 Scanned copy of Aston University project consent by the Ethics Committee ...	242
Figure 127 Graph of the mean peripheral refractive error for left eyes fitted with 2 <sup>nd</sup> order polynomial curves .....	295
Figure 128 Graphical representation of the mean difference in MSE between the central and peripheral locations, left eyes .....	296
Figure 129 Mean J <sub>180</sub> values for left eyes, fitted with 2 <sup>nd</sup> order polynomial curves.....	297

Figure 130 Mean $J_{45}$ values for left eyes, fitted with linear trend lines .....	298
Figure 131 Peripheral refraction MSE results for subject RC .....	315
Figure 132 MSE results for subject JP, with and without contact lenses in situ .....	316

## LIST OF APPENDICES

APPENDIX 1: LIST OF ABBREVIATIONS	240
APPENDIX 2: STUDY ETHICAL CONSENT FORMS AND INFORMATION	241
APPENDIX 3: OCULAR HEALTH AND HISTORY QUESTIONNAIRE	274
APPENDIX 4: MRI DERIVED AXIAL LENGTHS AND VOLUMES	277
APPENDIX 5: QUADRANT DATA FOR MRI WORK	282
APPENDIX 6: LEFT PERIPHERAL REFRACTION DATA	295
APPENDIX 7: RIGHT PERIPHERAL REFRACTION AND RETFIT DATA	300
APPENDIX 8: VISUAL FIELDS	317
APPENDIX 9: MFERG RING CONFIGURATION RESPONSES	330
APPENDIX 10: GANGLION CELL DENSITY: DETECTION TASK DATA	340
APPENDIX 11: GANGLION CELL DENSITY: DIRECTION DISCRIMINATION TASK DATA	341

## 1 INTRODUCTION

Myopia is a refractive, and in some cases, pathological condition of the eye. Its prevalence is widespread; in America an estimated 33.1% of the population have myopic refractive errors (Vitale et al. 2008) and in the Far East the figures are much greater with approximately 70% of Chinese adults affected (Edwards & Lam 2004). The worldwide prevalence of myopia, the rapid increase in incidence over the past three decades (Bar et al. 2005; Vitale et al. 2009), and its association with potential ocular morbidity and reduced quality of life, has rightfully justified myopia as a key research topic in vision science, optometry, and ophthalmology. In recent years myopia research has focused on identifying causes of myopic development; subsequently specific types of ocular shape have been recognised as possible precipitants of myopic development.

Higher levels of myopia are closely associated with a larger eye size. The expansion of the eye can lead to adverse effects on the retinal tissue through tissue stretch and thinning. These events may lead to reduced visual function, and less frequently, ocular morbidity.

Previously, imaging the eye has been limited to 2-dimensional approaches. The introduction of 3-dimensional (3D) MR imaging permits a more accurate depiction of eye shape. The 3D MRI provides a unique insight into previously inaccessible ocular areas, analysis of which can be used to construct more comprehensive models of eye shape in myopia. Use of these models can help further explain the processes by which ocular shape may cause or be affected by myopic development.

The generation of myopic models, developed through ocular imaging, can also assist in exploring theories of myopic ocular stretch and reduced visual function (Chen et al. 2006a; Chui et al. 2005). Light sensitivity investigated through visual field testing has shown that myopia as little as 2 dioptres (D) is capable of producing a significant reduction in sensitivity compared with emmetropic (control) subjects (Martin-Boglund, 1991). Furthermore, reduced responses in electrophysiological testing, more specifically mfERG have been noted in myopic subjects (Chen et al. 2006a).

Although a strong association between reduced visual function and the presence of myopia exists, the actual aspect of myopia causing the reduction remains equivocal. One possible cause, and of particular interest to this study, is the theory that myopic ocular expansion causes retinal stretch which leads to either retinal cell damage or reduced cell density and

subsequently a reduction in visual sensitivity. It has been predicted that approximately 15D of refractive error leads to twice the spacing between retinal neurons compared to that found in an emmetrope (Chui et al. 2005).

In this study the functional responses from different retinal layers are evaluated through measurements obtained from various investigative techniques. Findings are then compared with specific indices of ocular shape obtained through 3-dimensional MR imaging. One of the principal aims of the present study is to correlate localised areas of retinal shape with tests of visual functionality in myopic and emmetropic subjects. It is envisaged that this type of investigation will help determine whether retinal shape affects the visual function of the eye.

This thesis is comprised of two main sections; the first part describes investigations of ocular shape through use of 3-dimensional MRI, peripheral refraction, and further biometric measurements taken through use of commercially available instruments such as the Zeiss *IOL Master* and Oculus Pentacam. The second part of the thesis focuses on aspects of visual function determined by visual field tests, multifocal electroretinograms, and ganglion cell density. The tests of visual function are then correlated with specific indices of ocular shape as derived through MR imaging.

The thesis concludes by outlining the principal findings and discusses their relevance to clinical practice. Scope for further research is provided with explanations of how the current data set could be expanded to investigate further parameters of ocular structure and function.

## **2 OCULAR SHAPE IN MYOPIA**

Myopia is well established as a refractive and structural defect of the eye. An excessively long vitreous chamber depth relative to the corneal and lenticular refracting properties renders the eye myopic. Expansion of the eye in myopia is not, however, limited to the axial meridian; both the width and height of the eye have been reported to increase in size (Atchison et al. 2005). Accurate representation of eye shape is the centrepiece to understanding myopia, as shape can provide clues to the course of ocular expansion taken by the myopic eye, the possible effects on visual function, and facilitate the development of therapies against myopia.

### **2.1 Factors influencing eye growth**

The eye is a unique organ; both its physical and sensory development is dependent on visual experience, albeit to differing amounts. In a similar way to many bodily organs, the eye has reportedly shown a subtle form of homeostatic control with regards to ametropic development, (Wallman & Winawer, 2004). The control, however, is defective because in many cases ametropia still develops.

Animal studies in general have shown that in the developing eyes of neonate animals, myopic defocus produced by the introduction of positive power spectacle lenses can inhibit the natural elongation of the eye, or promote excessive elongation with negative lenses (i.e. hyperopic defocus). Positive lenses have been found to elicit a much more powerful response than negative lenses. The choroid is known to thicken transiently with the introduction of positive lenses and choroidal thinning occurs with negative lenses (Wallman & Winawer, 2004; Zhu et al. 2005). The exact mechanisms by which the eye recognises the defocus is unknown, although it appears that a trial and error method is unlikely (Zhu et al. 2005). A parallel can be drawn with form deprivation studies in animals, where depriving the eye of visual experience, fully or partially, can cause the globe to expand. Similar findings have also been reported in human subjects in whom congenital defects such as ptosis or corneal defects have created a barrier to visual input (Twomey et al. 1990; O'Leary & Millodot, 1970). There is no definitive answer to the question of why form deprivation causes such excessive growth. One idea used to explain growth during form deprivation is that the fovea recognises there is no visible image anterior to it and so the only other possible location is posterior; and thus in an attempt to achieve a focused image the eye elongates. In

effect the eye is ‘searching’ for the image’ (Wallman & Winawer, 2004). Alongside the reported increase in ametropia with form deprivation, runs the theory that a peripheral refractive error which is more hyperopic than the central refraction, may precipitate axial growth (see 3.1).

The fact that visual experience could influence development of ametropia is significant to development of therapies in myopia prevention. The refractive status of the peripheral and central visual fields could be manipulated by the use of optical corrections such as custom made contact lenses; minimising the relative peripheral hyperopia. The prospect of pharmacological therapies to prevent myopia has also been studied in depth (Bartlett et al. 2003; Gilmartin, 2004; McBrien et al. 2008; Siatkowski et al. 2004).

## **2.2 Ocular biometric studies**

In addition to the differences in global eye shape and size, characteristics of internal ocular refractive components have been associated with myopia. One of the most influential ocular biometric studies was that of Stenström (1948), he concluded that axial length was the principal cause of all refractive error. Many others went on to reanalyse Stenström’s classic data set and of particular significance is Van Alphen’s analysis (1961). Van Alphen concluded that the myopic eye had a longer axial length and could also be associated with increased corneal curvature and a flatter crystalline lens. Sorsby, (Benjamin et al. 1957; Sorsby & Leary 1969) disputed these reports, arguing that only myopic error greater than 4D could be solely attributable to excessive axial elongation. Sorsby believed that myopia less than 4D could be due to any individual refracting component.

Axial length measurements can be made through numerous methods; currently one of the most popular techniques is the non invasive partial coherence interferometry (PCI) method employed by the Zeiss *IOL Master* (see 7.3).

## **2.3 Axial length in myopia**

There is a plethora of research suggesting increased longitudinal axial length is the main structural correlate of myopia (see Figure 1). The ocular region which contributes most to the increase in axial length is the vitreous chamber (Garner et al. 2006; Goss et al. 1997; McBrien & Millodot 1987). Excessively long axial length appears to be the main structural correlate for both early and late onset myopia (Jiang & Woessner, 1996; McBrien & Adams

1997; McBrien & Millodot 1987). However, it has been shown that lower levels of myopia exist with a range of axial lengths, many of which may fall within ‘normal’ limits for that of an emmetrope. Myopia in these cases may not be purely axial in nature but instead there is a mismatch of principal refracting components: the cornea, crystalline lens, and axial length.

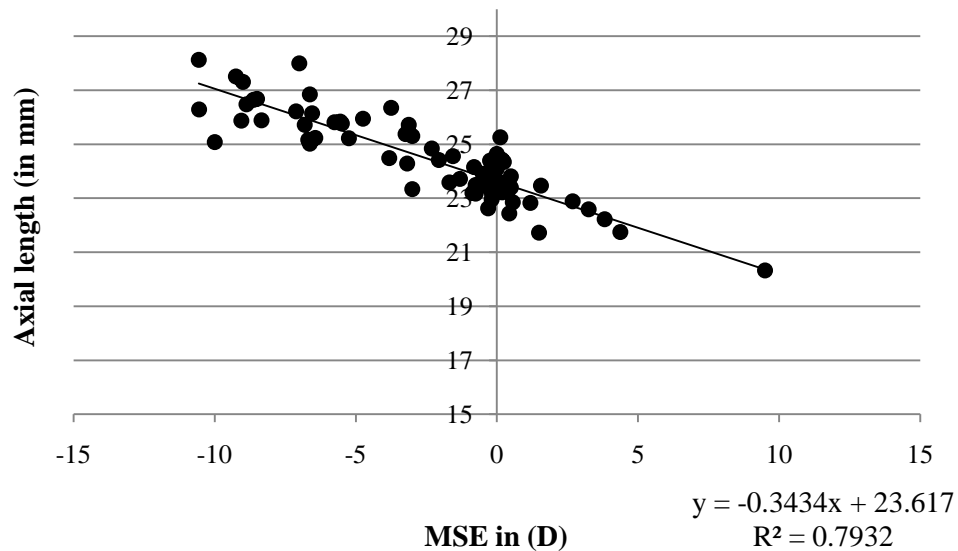


**Figure 1 Demonstrates the strong correlation between a longer axial length and myopia (axial length measured using the Zeiss IOL Master and Mean Spherical Error (MSE) with the Shin Nippon SRW 5000 autorefractor,  $n=71$ ,  $p < 0.01$ ,  $r = -0.891$ ). Data from subject dataset**

### 2.3.1 Axial length variables

#### Genetics

High myopia is generally thought to be hereditary (Farbrother et al. 2004; Wojciechowski et al. 2005). There is evidence for a link between parent and child eye size, more specifically axial length, predisposing the child to myopia (Liang et al. 2004; Zadnik et al. 1994). In children (aged seven years) of a Chinese ethnicity, the prevalence of myopia, is estimated to be three times greater in children who have one myopic parent compared to children who have two non-myopic parents. If both parents are myopic the prevalence is approximately six times greater than children with two non-myopic parents (Yap et al. 1993). Twins have also shown a hereditary link for specific biometric components such as axial length (Dirani et al. 2006).

Pruett (1988) discussed the possibility of an inherited biomechanical weakness of the sclera; specifically, a weakened sclera when exposed to elevated levels of intraocular pressure, which may be associated with accommodation and convergence. A weakened sclera may be

vulnerable to ocular expansion, (Pruett, 1988). With the identification of genes that cause myopia, the mechanisms causing growth may be identified and effective treatment options developed, (Young et al. 2007).

### **Gender**

Gender differences in axial length have been observed in both children and adults. A large scale study on Australian school children found boys to have longer axial length than girls by approximately 2.45% (Ojaimi et al. 2005); similar results have been noted in young adults where average female axial length was approximately 1.97% shorter than males (Logan et al. 2005).

### **Accommodation**

Axial length is thought to increase when accommodation is active, conflicting evidence exists as to whether this increase in axial length is more prominent in myopic or emmetropic subjects (Mallen et al. 2006; O' Donoghue et al. 2005). For near objects convergence is closely associated with accommodation. The isolation of convergence, with little active accommodation, has also shown increases in axial length (Bayramlar et al. 1999).

### **Diurnal variations**

There have been reports of diurnal variations in the axial lengths of both humans and animals (Liu & Farid 1998; Stone & Flitcroft 2004). These fluctuations are thought to be small, between 15-40 $\mu$ m, and present on an irregular basis. In some subjects the diurnal fluctuations may not occur at all. Diurnal variations in axial length may occur due to disruptions in normal light levels or as part of a hormone/neurotransmitter related response.

### **Intraocular pressure (IOP)**

In general it has been agreed that a higher IOP may be associated with longer axial lengths, (Tomlinson & Phillips 1970; Tomlinson & Phillips 1972; Tsutsui et al. 2003). This claim is not supported in children, suggesting the IOP-axial length association may only be present in subjects with fully developed eyes (Lee et al. 1999).

### **Stature**

Saw *et al.* examined the link between height and its relationship with refractive error and ocular biometry in Singaporean Chinese children (aged 7-9 years old), (Saw et al. 2002). They found girls who were taller had longer axial lengths, deeper vitreous chambers, flatter

corneas and their refractions tended to be more myopic. It was also found that boys who were heavier in weight tended to be slightly more hyperopic and have shorter vitreous chambers.

### **Orbit size**

Atchison *et al.* suggested that the growth of the eye was limited by orbit size. They suggested the excessive growth in the axial meridian was a consequence of less restriction by the orbit in the posterior section of the eye, (Atchison *et al.* 2004). The claims are contrary to the findings of a study examining Chinese myopic eyes using MR imaging, where no association was found between ocular and orbit size (Chau *et al.* 2004). Notably ethnic variations in eye shape have previously been reported (Logan *et al.* 2004). Thus far no large scale study has examined the relationship between ocular and orbit size in any other ethnic group.

## **2.4 Cornea and myopia**

The cornea is an avascular and transparent structure covering part of the anterior eye. The typical corneal diameter is approximately  $12.89 \pm 0.60$  mm (Martin & Holden 1982) and typical central thickness readings by ultrasound pachymetry have been reported as  $542 \pm 33$   $\mu\text{m}$  (Marsich & Bullimore 2000). The typical corneal power in an adult eye is 43D, and accounts for approximately two thirds of the eye's total refractive power. Corneal power is related to its curvature. A steeper radius of curvature corresponds to a more myopic corneal power; this is most commonly expressed in millimetres (mm) or dioptres (D). Average corneal curvature is 7.80mm in an adult eye. The cornea is the source of most astigmatic error, although some astigmatism may infrequently originate from the crystalline lens.

### **Corneal curvature**

The cornea in myopia is often studied in reference to the axial length. Grosvenor suggested the presence of a relationship known as the Axial Length: Corneal Radius ratio (AL:CR ratio) (Grosvenor 1988). This method of analysis has subsequently been used in several studies that followed (Goss *et al.* 1997; Grosvenor & Goss 1998). Grosvenor suggested that a high level AL:CR (i.e. greater than 3) was a risk factor for myopic development in emmetropic youths (see Figure 2). In children a higher AL:CR is also believed to be a risk factor for developing myopia, however, for adult onset myopia AL:CR has not proved to be significantly different to emmetropes, (McBrien & Adams 1997).

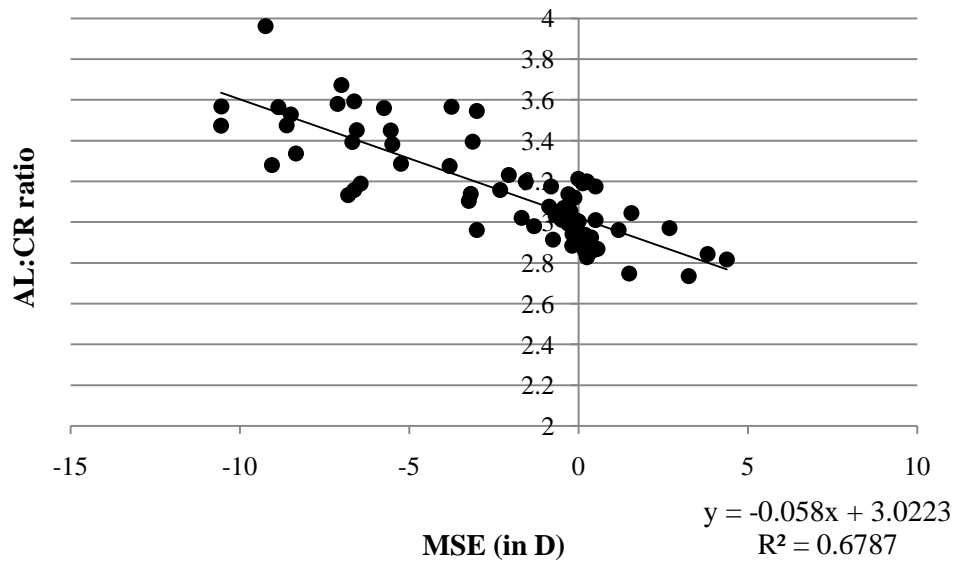


**Figure 2 Graphical representation of the AL:CR ratio as calculated from readings taken with the Zeiss IOL Master ( $n=66$ ). Data presented from subject dataset**

Grosvenor and Goss reported that longer eyes tended to have flatter corneas, this finding has been reconfirmed by more recent work, (Chang et al. 2001). However, myopic eyes have been found to have steeper corneas than those of emmetropes (Garner et al. 2006; Goss et al 1997). In particular it has been reported that in myopes the vertical meridian is steeper than the horizontal, (Goss & Erickson 1990). This finding may help elucidate the direction in which myopic stretch takes place.

Further differences in corneal curvature are noted when examining measurements with reference to ethnicity. Ethnicity differences in corneal curvature have been reported in both adults (Logan et al. 2005) and in children (Twelker et al. 2009). Additionally, gender differences in the corneal curvature of children have also been noted; females have been reported as having significantly steeper corneas compared to males (Gwiazda et al. 2002).

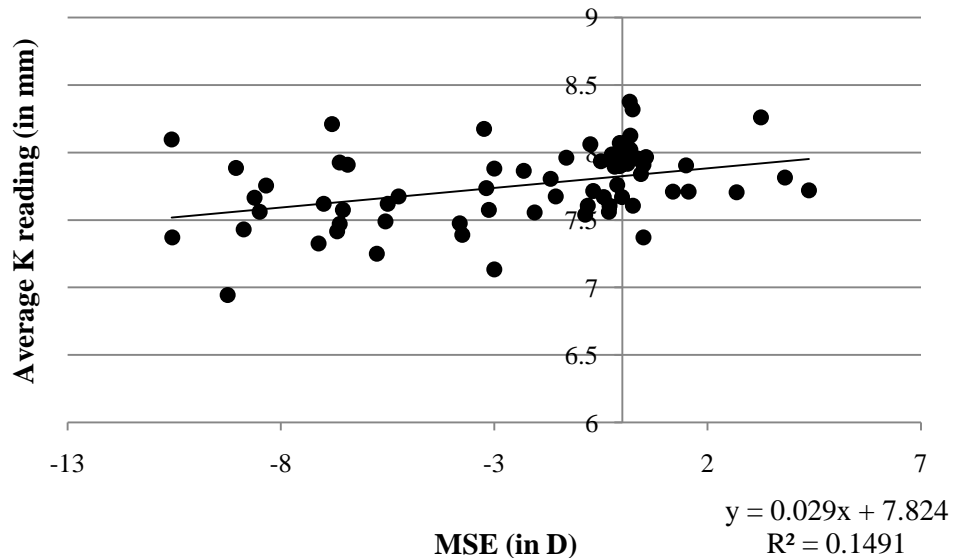


**Figure 3 Graphical representation of the average keratometry reading as measured with the Zeiss IOL Master against MSE ( $n=66$ ). Data presented from subject dataset**

Evaluation of the corneal topography has also produced interesting findings; increasing myopia shows a tendency for the cornea to flatten less rapidly as it approaches the corneal periphery. This is particularly the case for myopic error greater than approximately  $-4.00D$ , (Carney et al. 1997; Zadnik et al. 1999). A reduction in the flattening of the corneal periphery has been noted with increasing vitreous depth (Carney et al. 1997).

### **Corneal thickness**

The average corneal thickness in humans is approximately  $542 \pm 33 \mu m$ . There are many variables for corneal thickness; race, gender, and diurnal variations are all evident (Hamilton et al. 2007). Further physical changes of the cornea, on a cellular level, have shown endothelial cell density to be reduced in myopic subjects. Chang *et al.* indicate that the corneal endothelium is able to operate with very low cell density, therefore a significant effect on visual function is unlikely (Chang et al. 2001).

### **2.5 Anterior chamber depth and myopia**

The average anterior chamber depth is  $3.33 \pm 0.61 mm$  as measured with the *Zeiss IOL Master* (Reddy et al. 2004), this value gradually decreases with age. Both the *Zeiss IOL Master* and the *Oculus Pentacam* allow for rapid non-contact measurements of the anterior chamber (see 7.2 and 7.5).

In general the anterior chamber depth in myopes has been found to be deeper than emmetropes (Bullimore et al. 1992; Garner et al. 2006; Logan et al. 2005). It has been proposed that the thinning of the crystalline lens may contribute to the increased depth of the anterior chamber (Garner et al. 2006), or it may be a consequence of the ocular stretch which is synonymous with increasing myopia. Figure 4 shows the anterior chamber depth measured using the *Zeiss IOL Master* in subjects who formed part of the cohort of the current study.

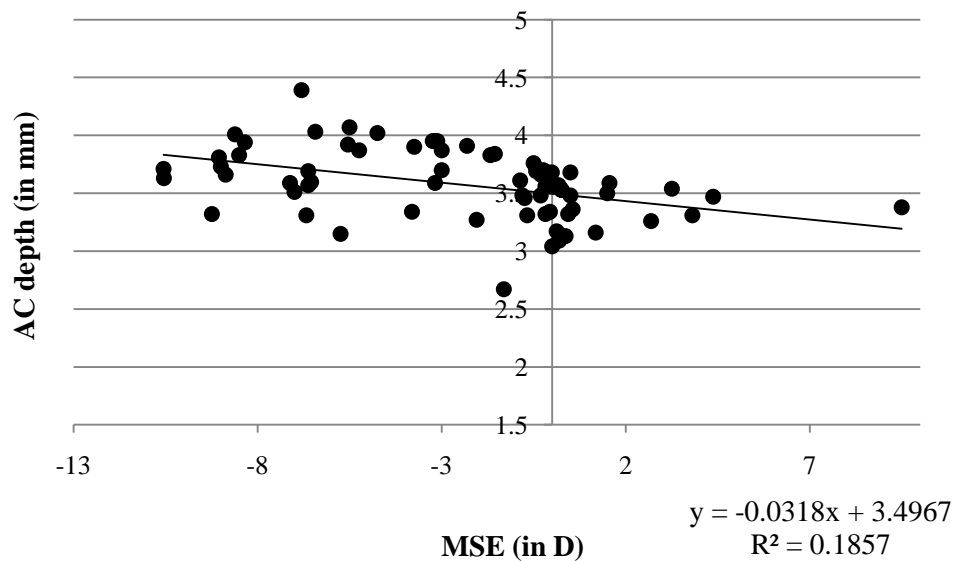


**Figure 4 Graphical representation of anterior chamber depth (as measured with the Zeiss IOL Master) with MSE  $n=69$  ( $p < 0.01$ ,  $r = 0.427$ ). Data presented from subject dataset**

## 2.6 Eye shape and retinal contour in myopia

There is widespread agreement that the average size of the eye in myopia is generally larger than that of an emmetrope or hyperope (Atchison et al. 2004; Atchison et al. 2005; Gilmartin, 2004; Logan et al. 2005; Singh et al. 2006). There is also general agreement that the increase in axial length is the most pronounced of all the changes in the size of the myopic eye. Differences of opinions exist when considering other parameters such as retinal contour, height and width of the eye in myopia. These uncertainties exist largely due to limitations in ocular imaging techniques (Stone & Flitcroft 2004). Many previously employed techniques measured along the axial dimension only, and measures such as retinal contour were inferred rather than directly measured.

Through peripheral refraction studies the myopic eye has typically been found to be prolate or less oblate in shape than emmetropic and hyperopic eyes (Logan et al. 2004). Previous work has also shown that myopes tend to have hyperopic peripheral refractions relative to

the central refraction, (Schmid, 2003; Seidemann et al. 2002), relative hyperopia has also been noted in children (Schmid, 2003). This finding has prompted speculation that the hyperopic periphery stimulates central axial growth (Wallman & Winawer 2004). Other investigators have hypothesised that the expansion of the retina is dictated by the orbit size; as the posterior section of the eye has least restraint from the orbital walls it continues to grow larger than all other parameters (Atchison et al. 2005).

Recent work using 3-dimensional MR imaging has reaffirmed findings of the relatively prolate shape found in myopic eyes (Singh et al. 2006). An attempt was made as part of the current project to quantify the orbit size-eye size relationship using 3-dimensional MRI; however, low resolution has not allowed accurate estimations of orbit size to be made.

In addition to differences found between refractive groups, previous studies have reported ethnicity to be a significant variable in eye shape. In a peripheral refraction study of anisomyopic subjects, nasal-temporal asymmetry in the eyes of white Caucasian subjects has been found, but not in Taiwanese-Chinese subjects, (Logan et al. 2004; Stone & Flitcroft 2004). The CLEERE study also showed ethnic differences; Asian American children were found to have longer axial lengths and based on measurements of peripheral refraction, a relatively more prolate eye shape was noted compared to their African American and Caucasian counterparts (Mutti et al. 2005).

## **2.7 MRI use in ocular imaging**

There have been a handful of studies that have attempted to image the eye through use of MR imaging. The main advantage of MRI is that measurements are independent of the refractive properties of ocular components. A drawback of MR techniques used prior to the introduction of 3-dimensional MR imaging was the thickness of image slices and the 2-dimensional aspect of the data. Nonetheless findings from 2-dimensional MR studies are of direct relevance to the current study and will be discussed further.

One of the earliest investigations using MR imaging to examine ocular shape was by Cheng *et al.* (1992). The cohort's refractive errors ranged from +2.50D to -9.50D (MSE). Subjects were placed into one of the three main refractive groups; hyperopes, emmetropes, or myopes. Apart from a few exceptions the investigators reported similar eye shape for all refractive groups, but eye size was significantly larger in myopes, suggesting a global

expansion model of the myopic eye. The study also measured sclera and choroidal thickness which were uniformly thinner across the globes of the myopic eyes.

Miller *et al.* carried out MRI scans of seventy-eight subjects using a 1.5 tesla MR scanner. A difference in axial length between the hyperopic and myopic eyes was reported. To a lesser extent, equatorial distances of myopic eyes were noted as larger compared to hyperopic eyes (Miller *et al.* 2004). In a similar study Atchison *et al.* (2004) scanned eighty-eight young adult subjects using a 1.5 tesla MR scanner. Specifically differences between emmetropic and myopic eye sizes was investigated; refractive errors ranged from +0.75 to -12D MSE. Notably the number of emmetropes was fewer than myopes; 22 and 66 respectively. The scans were analysed by measuring the width and height in millimetres. Measurements of length were taken from the posterior pole (P) to the anterior cornea (A), measurements of width were taken from the widest regions from nasal (N) to temporal (T) retina, and measurements of height were taken from the superior (S) to inferior (I) retina (see Figure 5).

a

b

**Figure 5 (a) The height and (b) the width measurements taken from MR images (from Atchison *et al.* 2004)**

Myopic eyes were found to be larger in all three meridians. The heights and widths of emmetropic eyes were not significantly different. In myopes the heights were noted to be longer than the widths. Atchison *et al.* went on to mathematically analyse data on retinal shape for the same subject group through fitting of ellipsoids using specialised software; from this work it was reported that the shape of a myopic eye was less oblate than that of an emmetropic eye.

The aforementioned studies have provided valuable data; however, they have all been limited by producing only a 2-dimensional view of the eye (see Figure 5). Furthermore, the

data are limited in the number of MR slices taken. If we assume an axial length of 21mm, a 3mm size slice would equate to seven slices in the axial meridian, thus missing approximately two thirds of the data. Further work by Singh *et al.* (2006) has developed 3-dimensional MR scanning with smaller MR slices and thus a more accurate depiction of ocular shape, (see section 7.6). In brief, the method involves the use of a 3 tesla Siemens whole body MR scanner. Previous MR ocular imaging studies have in general used T1 weighted images; the 3D MR technique uses T2 weighted images. The contrast of the T2 images is optimised to distinguish the fluid filled ocular structures from the bony orbit. The 3-dimensional aspect is achieved through use of a modified version of freeware software MRi3dx. The program allows the eye to be shaded with 1mm<sup>3</sup> voxels, which are assigned x,y coordinates so data can be plotted graphically. Various parameters are generated by the program for example ocular volume (Gilmartin et al. 2008), surface area and radius of curvature (see 9.5).

Since the introduction of 3-dimensional ocular MRI there has been a recent attempt at imaging the eye using a 7 tesla scanner, which enables the production of higher resolution images. The use of higher field strengths does, however, make the image more prone to motion artefacts; in the case of ocular imaging small eye movements may be problematic. Additionally it is more difficult to ascertain specific absorption rate (SAR) safety levels; scanning at higher field strength can create discomfort for subjects. The 3 tesla field strength used for ocular imaging is sufficient for examining ocular volume (Richdale et al. 2009), but for smaller structures such as the ciliary body or crystalline lens a higher field strength would be more appropriate.

## **2.8 Summary**

Imaging the eye *in vivo* has proven problematic; the most widely available technique to derive eye shape appears to be through transformation of peripheral refraction data. Peripheral refraction is often achieved by laboratories customising existing autorefractors. Although peripheral refraction is flexible and relatively inexpensive there is a lack of standardisation and the extent of the field measured is limited by factors such as pupil size. Further evaluations of eye shape have been made through 2-dimensional (2D) MR imaging, however this technique has also demonstrated limitations in accessibility and data analysis. 3-dimensional (3D) MRI, which is used in the current study, overcomes limitations imposed by both 2D MR imaging and peripheral refraction. 3D MRI has shown the ability to

calculate ocular surface curvature and volume, it is envisaged that further biometric parameters will also be analysed using this technique. It is acknowledged that whilst 3D ocular MRI is an invaluable tool for assessing more global parameters such as ocular volume and eye size, higher resolutions are required to detect smaller internal ocular structures. This thesis will attempt to evaluate more global measures of ocular shape in the context of different refractive groups.

### **3 PERIPHERAL REFRACTIVE ERROR AND OCULAR SHAPE**

#### **3.1 Introduction**

Off axis refractive error has been used for several decades to evaluate peripheral aberrations and infer retinal contour. Of particular interest to the field of myopia is the investigation of the theory that relative to the central refractive error a hyperopic peripheral refraction may precipitate axial growth of the eye, which in turn leads to myopic ametropia (Smith et al. 2007; Wallman & Winawer 2004).

#### **3.2 Peripheral refraction techniques**

Peripheral refractive error may be measured through objective or subjective techniques. Earlier studies tended to use a combination of retinoscopy and subjective refraction, similar to standard on-axis refraction. Retinoscopy is an objective, flexible and widely available technique; however, as the angle of eccentricity from the fovea increases there is a concurrent increase in oblique off axis astigmatism making retinoscopy more challenging and prone to errors. Furthermore, retinoscopy is not practical for examining large cohorts due to the time and proficiency required to obtain accurate measurements. Owing to poor peripheral acuity the standard subjective refraction which often follows retinoscopy, in a normal clinical eye test, can be difficult for subjects when attempted away from the visual axis.

Earlier peripheral refraction studies used manual optometers, but their lack of reproducibility and high levels of peripheral aberrations has led to a decline in their usage (Fedtke et al. 2009). More recent peripheral refraction work has made use of commercially available autorefractors which require modifications by investigators in order to present targets off axis. Autorefractors allow an objective measure of refractive error and measurements are free from both practitioner and subject bias. There are, however, a number of limitations: autorefractors are rarely able to measure further than 30-40° eccentricity, additionally they have been shown to overestimate myopia due to the accommodative effort exerted by the subject as he or she becomes aware of the fixation target's proximity to the eye. Use of cycloplegic drugs can temporarily paralyse the accommodative effort and overcome instrument myopia; additionally the mydriatic effect facilitates the measurement of peripheral readings. There are several binocular open view autorefractors available, which can also help reduce levels of instrument myopia.

### 3.3 Peripheral astigmatism

Obliquely incident light rays from objects positioned in the peripheral visual field are limited by the pupil size, consequently they are refracted asymmetrically into two mutually perpendicular planes; tangential and sagittal, giving rise to *oblique* astigmatism. The tangential meridian contains the optic axis and corresponding meridional ray.

The difference between the tangential and sagittal focal lines; the interval of Sturm, represents the magnitude of astigmatic error. Light leaving the eye and into the object plane is also susceptible to oblique astigmatism; this is equal and opposite to the value of oblique astigmatism for light entering the eye. For a given eccentricity the oblique astigmatism value for light *leaving* the eye is equal to the refractive error of the eye. The difference between oblique astigmatism from the object plane and the oblique astigmatism from the image plane can be used to calculate *peripheral* astigmatism. As the angle of eccentricity increases the sagittal image shell falls further away from the retina, becoming increasingly hyperopic. The tangential image shell becomes more myopic with increasing eccentricity (Dunne 1995). The peripheral astigmatism values therefore increase with increasing eccentricity.

**Figure 6 The effect of a steeper retina (R) on the tangential (T) and sagittal (S) image shells (Dunne, 1995)**

**Figure 7 The effect of a flatter retina on the tangential and sagittal image shells (Dunne, 1995)**

### **3.3.1 Peripheral astigmatism and refractive error**

Thomas Young (1801) is often attributed as being the first to note the presence of oblique aberrations in the form of peripheral astigmatism. Young's early attempts at modelling the sagittal and tangential image shell curvatures have been confirmed since by investigations on both human and schematic eyes.

In 1931, Ferree, Rand, and Hardy sought to classify peripheral astigmatism. A Zeiss parallax optometer was used to examine peripheral refraction of 21 eyes at 5° intervals in the horizontal meridian up to a maximum of 60°. 18 of the eyes fell into one of two categories, labelled Type A and Type B. The remaining 3 eyes showed disparity between the nasal and temporal meridians and were classified as a separate entity.

Subjects classed as Type A were shown to be relatively myopic as the angle of eccentricity increased, and the vertical meridian more hyperopic. Type B subjects were shown to be less myopic with increasing eccentricity and more hyperopic in the vertical meridian (Ferree et al. 1931).

Millodot (1981) sought to further examine the inter refractive group variability. Using a cohort of 62 eyes, Millodot measured peripheral refraction with a Topcon refractometer at 10° intervals along the horizontal meridian up to a maximum of 60°. Millodot found the peripheral astigmatic error to increase with increasing eccentricity in 91% of the eyes tested. Three main refractive groups were examined; myopes, hyperopes and near emmetropes. He

noted significant differences in the type of astigmatism between each refractive group, but the magnitude of astigmatism was not significantly different.

Lotmar and Lotmar (1974) analysed results from an earlier study by Rempt *et al.* which had examined 363 subjects using retinoscopy. Through calculation of values for the interval of Sturm, using Gullstrand's schematic model eye, Lotmar and Lotmar sought to classify the eyes into the two sub types (A and B) as proposed by Ferree *et al.* They concluded that a clear distinction into Type A or Type B eyes could not be made.

An insightful method of evaluating peripheral astigmatism by Seidemann *et al.* plotted the average peripheral astigmatic axis in the central 44° for the three main refractive groups (see Figure 8). The two eyes displayed a 'mirror effect' in their axis orientation and degree of astigmatic error (shown in Figure 8). Interestingly, levels of astigmatism were noted to be smaller in the nasal retina compared to the temporal retina and also the fovea. Larger astigmatic error in the temporal retina was also noted by a previous study by Dunne and Barnes (1987). Seidemann *et al.* noted that their results showed unusually high cylindrical errors and thus the mean spherical errors were more myopic in comparison to previous studies.

**Figure 8 Plot showing the average astigmatic axis direction and magnitude in the central 44° for each of the three main refractive groups (from Seidemann et al. 2002)**

### **3.4 Computational approach to deriving retinal contour**

Dunne (1995) utilised the properties of peripheral astigmatism to devise a computer program aimed at profiling retinal contour. The program is based upon the positions of the tangential and sagittal image shells. The fact that a change in retinal contour brings about a change in the two image shells is exploited by the program.

An approximate schematic model is used in which the sagittal image shell travels towards becoming more myopic, and tangential towards a more hyperopic dioptric distance. The two image shells then move towards each other at an equal rate; this process enables the mean spherical error to be calculated, diminishing the effect of peripheral astigmatism.

Corneal asphericity is adjusted so that the peripheral astigmatism matches the measured data. Retinal curvature is then adjusted, and the sagittal and tangential refractive errors calculated. The retinal contour coordinates can be used to estimate values of apical radii and conic constants. These are inputted into further equations to eventually derive values of x and y which can be plotted graphically (see 11.7).

### **3.5 Retinal profile and peripheral refraction**

Ferree, Rand and Hardy's work into peripheral astigmatism served as a basis for the theory that the differences noted on the skiagrams they plotted may originate from changes in the retinal shape (Ferree & Rand, 1933). Certainly for years axial length had been known to be a major structural correlate of central refractive error, however as previously mentioned, peripheral refractive measures may not be directly indicative of axial length. To date, few studies have investigated axial length at peripheral retinal points and correlated it with mean spherical error. Schmid (2003) examined axial length and refractive error in a large cohort of children, at an eccentricity of 30° only. Mallen and Kashyap (2007) investigated the effect in a small group of adults, for the central 80°. A significant correlation between mean spherical error and axial length was noted in both studies. However factors such as lens tilt and curvature may confound off-axis readings and there may be adverse effects from corneal curvature and pupil diameter (Atchison 2004).

In the early 1970s, Rempt, Hoogerheide, and Hoogenboom carried out a series of peripheral refraction studies which triggered tremendous amounts of interest regarding the relationship between progression of myopia and peripheral refraction. A widely cited study (Hoogerheide et al. 1971) investigated the reasons why trainee pilots who were initially emmetropic went on to develop myopia whereas others, who were exposed to the same environmental conditions, did not. Amongst other refractive and functional measures, the investigators used retinoscopy to measure peripheral refractive error. The pilots who went on to develop myopia were generally found to be relatively hyperopic in the periphery. It has since been widely hypothesised that a relatively hyperopic periphery may encourage axial growth and thus myopia (e.g. Chen et al. 2010, Smith et al. 2007; Wallman and Winawer 2004).

The theory that the peripheral retinal shape or refractive error may influence central growth has received further support from studies on infant rhesus monkeys (*Macaca mulatta*). Elimination of central foveal contributions through foveal ablation have shown ocular

growth and emmetropisation processes to be unaffected; leading to the assumption that peripheral vision may independently mediate central growth (Smith et al. 2007).

Studies have examined peripheral refraction with reference to various parameters such as central refraction, ethnicity, age and gender (Logan et al. 2004; Mutti et al. 2000)

Logan *et al.* advanced previous findings by measuring peripheral refraction and using it to determine retinal contour in a group of 56 young adult subjects (Logan et al. 2004). Subjects were sub divided by ethnicity; Caucasian or Taiwanese-Chinese and then by type of myopia; anisometropia or isomyopia (see Figure 9). Cycloplegic peripheral refractions were taken using a Canon R-1 infra red open field autorefractor, in the horizontal meridian at 5° intervals to a maximum eccentricity of 35±5°. Axial length and corneal curvature measures were also taken using commercially available equipment at the time, along with A scan ultrasonography and fundus photography. Logan *et al.*, transformed peripheral refractive data to represent retinal contours by use of a computational approach (Logan et al 1995; Dunne et al. 1995).

**Figure 9 (a) The uniform expansion of a myopic eye shown in Taiwanese - Chinese eyes (b) the asymmetrical expansion of the nasal aspect shown in Caucasian subjects (from Logan et al. 2004).**

Although globe enlargement was noted in both ethnic groups with increasing myopia, asymmetries between the nasal and temporal quadrants were noted in the Caucasian subjects only. Greater expansion was inferred from the nasal retinal periphery. In contrast, Taiwanese-Chinese subjects displayed greater homogeneity between nasal-temporal retinal contours. Nasal-temporal differences have subsequently been noted in many later studies (e.g. Atchison et al. 2006; Mallen and Kashyap, 2007; Pardhan and Rae, 2009). The temporal peripheral refractive errors have been shown to correlate with central refractive error better than nasal ( $r = -0.633$ ,  $p < 0.001$ ) (Pardhan and Rae, 2009).

The general consensus is that myopic eyes tend to be relatively hyperopic in the periphery and hyperopic and emmetropic eyes relatively myopic (Chen et al. 2010). One exception is a study by Seidemann *et al.*, who found all three main refractive groups to be relatively myopic in the periphery. They did, however, acknowledge that their measurements showed unusually large astigmatic errors, which would contribute to a more myopic spherical equivalent. The relative increase in myopia in the periphery of myopes was reported to be less when compared to emmetropic and hyperopic subjects.

The effect of a relatively hyperopic periphery in myopes and the opposite in hyperopes and emmetropes has been reported to be present in younger age groups. Large cohort studies in children ( $n=822$ ) aged 5-14 years, have shown through cycloplegic retinoscopy that myopic children show hyperopic shifts at  $30^\circ$  eccentricity relative to the centre, by an average of  $+0.80 \pm 1.29$  D, (Zadnik et al. 1999).

### **3.5.1 Vertical peripheral refraction**

Very few studies have collected data on vertical peripheral refraction; this is largely due to instrumental limitations in obtaining measurements in this meridian.

Seidemann et al. (2002) used a double pass technique and *Powerrefractor* to measure horizontal peripheral refraction of the three main refractive groups; emmetropic, myopic and hyperopic. The spherical equivalent refraction was found to be more myopic in the superior retina than the inferior by an average of 0.17D for every 10 degrees increase in eccentricity. The results are in line with more recent findings reported by Mallen and Kashyap (2007), who describe a technique to estimate retinal contour using a modified Zeiss *IOL Master*.

The results showed the superior field (inferior retina) in myopic eyes to be relatively hyperopic compared with inferior field.

Atchison *et al.* (2006) compared peripheral refractive error in young adult (18-35 year old) myopic (up to -12D) and emmetropic subjects. Measurements were taken using the Shin Nippon SRW 5000 autorefractor at 5° intervals up to 35° in the horizontal ( $n=116$  eyes) and vertical meridians ( $n=43$  eyes). In the horizontal meridians the temporal spherical equivalent error was significantly affected by central refractive error at eccentricities of 20-25° and beyond, in the nasal aspect these changes occurred much sooner at 5° and beyond. In the vertical meridian all refractive groups were found to have a relatively myopic shift, but not as a function of central myopic error.

### **3.6 Summary**

The retinal area measured by peripheral refractive error is limited by pupil size; few investigators manage to take readings beyond 30-40° eccentricity. Additionally, areas of the retina are missed due to measurements being taken at 5-10° intervals only. Further limitations can arise from refractive component misalignment, and curvature changes with increasing eccentricity from the visual axis.

Despite the limitations, peripheral refractive error is a useful tool in the study of myopia. The technique is non invasive and can be used with other biometric parameters to infer retinal shape. Several attempts have been made to evaluate eye shape through peripheral refractive error, and the results have been reasonably consistent. Myopic eyes tend to be more hyperopic in the periphery than emmetropic and hyperopic eyes. Although data on vertical peripheral refractive error is limited, current work indicates greater myopia in the superior retina.

Further validity of peripheral refraction as an indicator of eye shape can be established through correlation of measurements with the recently introduced 3-dimensional ocular MRI. Experimental data regarding the peripheral refraction vs. 3D MR derived ocular shape are detailed in section 11.7.

## 4 VISUAL FIELDS AND AMETROPIA

### 4.1 Definition

The term monocular visual field, is best described as ‘all the space that one eye can see at any given instant’ (Tate and Lynn, 1977). The human visual field, for each eye, extends approximately 60 degrees superiorly; 75 degrees inferiorly; 100 degrees temporally, and 60 degrees nasally (Choplin and Edwards, 1998).

In humans the two monocular visual fields overlap to produce a binocular stereoscopic zone extending approximately 120 degrees horizontally. Anatomical constraints such as the bridge of the nose, upper lid ptosis, or a prominent brow, may affect the expanse of the visual field.

Visual functionality, quantified though light sensitivity, varies across the visual field. Sensitivity is highest centrally at the point representing the foveal response, and declines towards the periphery. There are notable differences in light sensitivity between the nasal and temporal fields, similarly there are discrepancies between the light sensitivity in the superior and inferior fields. The asymmetry, both spatial and sensory, is perhaps most easily visualised by Traquair’s infamous depiction of the visual field when he described the visual field like an ‘island of vision surrounded by a sea of blindness’, (Traquair, 1924).

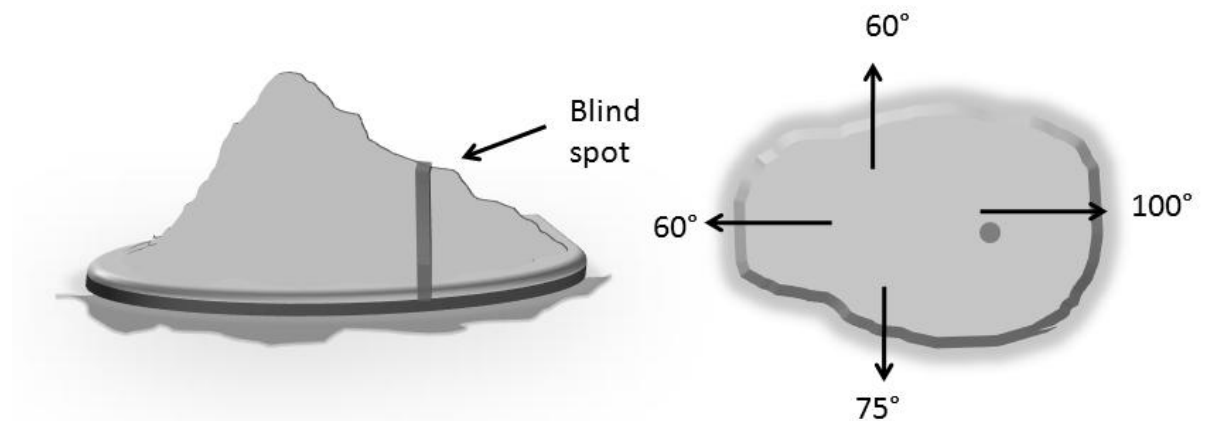


**Figure 10** Diagram representing Traquair's depiction of the island of vision (right eye)

The physiological blind spot is located approximately 15.5 degrees temporal to fixation, and on average extends 5.5° in width and 7.5° in height (Choplin and Edwards, 1998). The blind spot represents the retinal optic nerve head (see Figure 10).

## **4.2 Perimetry**

Perimetry is the assessment of visual field function and may be achieved through both static and kinetic methods.

Kinetic perimetry requires the subject to fixate accurately on a centrally located target while a stimulus of known size and luminance is moved from a non-seeing location (i.e. outside the extent of the visual field) to a location where it is first detected by the subject. Once several directions have been tested with stimuli of equal sensitivity, the points may be joined together to form a map akin to a hill or island of vision. A more comprehensive test may be achieved by using stimuli of different sizes and intensities, allowing the practitioner to retain control over the test by checking areas of decreased sensitivity in more detail.

Although practitioner control and manual manipulation are advantageous, there are several disadvantages of kinetic perimetry: the variations in background conditions, luminance, and stimulus velocity, may all contribute to inaccurate recordings. Furthermore, kinetic perimetry can produce inaccurate recordings as the target is moving and therefore more likely to be detected peripherally rather than centrally due to spatial summation (see 4.3.1).

A more widely used alternative to kinetic perimetry is static perimetry. Automated static perimetry requires the subject to fixate on a centrally located target, while static stimuli are presented in the visual field. The subject confirms the detection of the stimulus through a button buzzer system. The stimulus size remains constant, but the light intensity will vary with each presentation.

A full threshold program will calculate the minimum light intensity detectable at each location in the visual field, normally presented in terms of light sensitivity, which is the reciprocal of light threshold.

### **4.2.1 Reliability indices in automated perimetry**

To ensure accurate recordings it is imperative for the subject to maintain fixation on the central target. The simplest method to monitor fixation is to check repeatedly through use of

a fixation camera and monitor. A more sophisticated technique is the Heijl-Krakau method (Heijl & Krakau, 1975), which entails the automated presentation of a stimulus into the presumed region of the physiological blind spot. If the subject responds to the stimulus, it is believed that the subject is not fixating and a fixation loss is recorded by the perimeter. If fixation losses exceed 20% then accuracy is compromised and the test is deemed unreliable.

In addition to monitoring fixation, reliability can also be checked via assessment of false positive and false negative responses. If a point on the perimeter bowl is retested at a much greater luminance than previously required to elicit a response and the subject fails to respond, a false negative response is recorded. The opposite is true for a false positive response when a subject responds in the absence of stimuli. If the number of false negatives or false positives exceeds 33% then the test results are deemed inaccurate.

Visual field testing has established that there are variations in the sensitivity of different retinal regions. The repeatability of automated perimetry in the superior and nasal quadrants is reported to decrease with increasing eccentricity from the fovea; the temporal quadrant is believed to be the most repeatable (Young et al. 1990).

#### **4.2.2 Refractive correction**

Optimal refractive correction must be worn during perimetry and ideally correct both spherical and cylindrical ametropia. Small amounts of refractive defocus are capable of causing a reduction in retinal sensitivity; particularly in the central 6 degrees around the fovea (Weinreb & Perlman 1986). Contact lenses are preferable particularly in the cases of highly ametropic subjects, particularly myopes (Koller et al. 2001). Contact lenses help counteract the effects of image magnification or minification produced by spectacles. During automated perimetry heat inside the perimeter's bowl may cause soft contact lenses to dehydrate and cause discomfort and defocus which could potentially lead to inaccurate recordings. Subjects wearing coloured aperture contact lenses may find a pinhole effect is created by the lens, preventing the full extent of the visual field to be tested. When clear contact lenses are not used, full aperture trial lenses are required; the larger aperture minimises the risk of artefacts often produced by frame rims of reduced aperture lenses.

### 4.3 Visual pathway

The response to light stimuli originates primarily from the photoreceptor cells in the outer retina. There are two main types of photosensitive cells: rod cells and cone cells. Rod cells are most sensitive in scotopic (low light level) conditions and cone cells in photopic conditions. A third, more recently discovered photosensitive ganglion cell (pRGC) is located in the inner retina (Zaidi et al. 2007). The pRGC is believed to have little involvement with visual field function. Largely, it is the cone pathway that gives rise to the light sensitivity response recorded during a visual fields test.

Cone cells can be broadly classified into three types, short (S), medium (M), and long (L) wavelength cells or red, green and blue cone cells. Each type of cone cell contains photopigments sensitive to particular wavelengths of light. Photons are absorbed by the retinal photoreceptors and light energy converted into electrical signals by 'phototransduction', a process mediated by the opsin protein molecule contained within the cell. Due to the directional sensitivity of the cone cells, light rays entering the pupil at an oblique angle are less effective at stimulating the cones.

The response from the temporal aspect of the visual field originates from the nasal retina of the right eye and temporal retina of the left eye, i.e. the retinal position is contralateral to that of the field (see Figure 11). Therefore, the optic nerve head which is located approximately 15° nasally on the retina produces a blind spot (or scotoma) in the visual field° temporally. Characteristics from visual field defects can often be used to isolate the retinal or neurological location at which pathological change may have occurred.

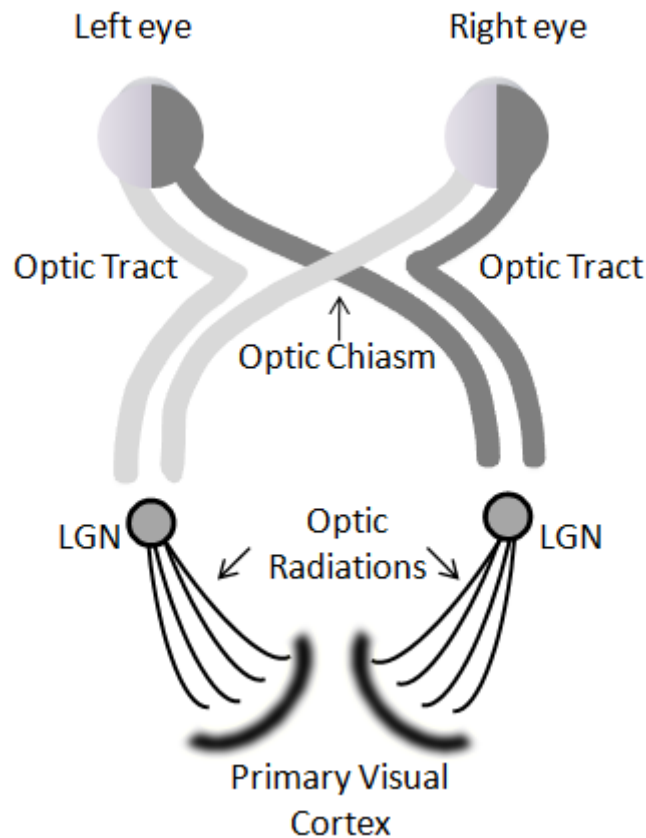


**Figure 11 Diagram showing the human visual pathway (LGN denotes the position of the lateral geniculate nucleus). The diagram shows the crossover of the nasal fibres (temporal field) to the contralateral side. The messages are relayed through the LGN and onto the primary visual cortex located in the occipital lobe of the brain.**

#### **4.3.1 Distribution of retinal photoreceptors**

The outer retinal layer accommodates approximately 4.6 million cones and 92 million rods (Curcio et al. 1990). The distribution of rods and cones across the retina is not uniform. Peak cone density occurs at the fovea (approximately 199,000 cones/mm<sup>2</sup>), and there is a decline in cone density with increasing eccentricity. Conversely, rod density is minimal at the fovea. An area extending 0.350mm<sup>2</sup> around the fovea is completely devoid of rods (Curcio et al. 1990). The peak density of rods occurs in the mid-peripheral retina within an elliptical ring shaped arrangement situated approximately 3-5mm away from the foveola (Curcio et al. 1990; Jonas et al. 1992). The distribution of photoreceptors may help explain the phenomenon of spatial summation

Differences in cone density can be described further by examining each retinal quadrant. The cone density in the nasal meridian is 40-45% higher than the equivalent eccentricity in the temporal meridian (Curcio et al. 1990; Jonas et al. 1990). Cone density in the inferior mid-

peripheral retina has been found to be greater than its superior counterpart (Curcio et al. 1990).

#### **4.3.2 Photoreceptor function in ametropia**

Refractive error may affect visual field recordings in several ways: refractive blur can cause a reduction in light sensitivity, image magnification and minification can lead to inaccurate recordings, axial length may affect luminance levels.

An increase in myopic refractive error and the concurrent enlargement of the eye, principally the vitreous chamber depth, have been well documented. The increase in axial length is believed to cause retinal stretch and subsequently reduced density of retinal cells. Several studies have reported cone receptor density to be significantly lower in myopia than emmetropia (Chui et al. 2008; Kitaguchi et al 2007). Cone density is thought to decrease as a function of increasing axial myopia.

If a mechanical increase in globe size causes reduced density of photoreceptors then it is possible the photoreceptor cells themselves may be damaged or misaligned. Misalignment is particularly important as photoreceptor cells are direction specific, i.e. they respond to light when aligned a specific way only.

#### **4.4 Visual fields and ametropia**

Using both automated static perimetry and manual kinetic perimetry a significant loss in threshold sensitivity for moderate and high levels of axial myopia (-4 to -5D) has been noted (Martin-Boglund, 1991; Aung et al. 2001; Rudnicka & Edgar 1995; Rudnicka & Edgar 1996). One study, using automated static perimetry, noted deterioration in response at much lower levels of myopia  $-2D \pm 1D$  (Czepita & Chmielewska 2004).

Increased axial length is closely associated with a higher level of myopia; axial length greater than 26mm and myopia greater than 5D is reported to be significantly correlated with a decline in visual field sensitivity (Rudnicka & Edgar, 1995). Decline in the superior hemifield (inferior retina), particularly the superior temporal field (inferior nasal retina) is reportedly greater than other quadrants (Rudnicka & Edgar, 1996).

Several explanations have been put forward to explain the visual field sensitivity reduction in myopia: decreased retinal luminance due to a longer axial length, sensory changes in the

photoreceptor cells, decreased photoreceptor density as a consequence of ocular expansion in myopia (see 4.3.2) (Rudnicka & Edgar, 1995), and misdirection or misalignment of photoreceptors caused by an increase in axial length hindering their sensitivity to light. Optic disc tilt is also a commonly reported anomaly noted in myopic individuals; perimetric studies have shown disc tilt to alter visual field sensitivity by lowering of the mean defect (the mean deviation between expected 'normal' values and the measured values), (Tay et al. 2005). Of particular interest to the current study is the notion that ocular expansion may affect visual field sensitivity.

#### **4.5 Summary**

Visual field testing provides a measure of visual function. Ocular expansion which is often a feature of myopia can potentially damage or misdirect retinal cells. Photoreceptor cells are direction specific; if misaligned their functional ability may be hindered. Additionally, myopic eyes may display reduced visual field sensitivity due to the longer distance the light has to travel to reach the retina, increasing the risk of light scatter and absorption by ocular structures. This thesis will aim to address whether ocular shape is correlated with visual field sensitivity using the Humphrey Visual Fields Analyser and specific indices of ocular shape derived from MR imaging.

Further information on the type of perimeter used in this thesis is detailed in section 7.4.

## **5 ELECTROPHYSIOLOGY AND MYOPIA**

### **5.1 Introduction**

Electrophysiological testing allows objective measurement of ocular function through assessment of the retinal electrical responses to a light stimulus. The electrical response from the eye is received by electrodes, which are attached to the subject; the responses are amplified and converted to waveforms.

Electrophysiological testing is widely used as a diagnostic tool in ophthalmology, through several different variants. Two of these variants will be discussed in the context of this thesis; the electroretinogram (ERG) and the multifocal electroretinogram (mfERG).

### **5.2 The electroretinogram**

The electroretinogram (ERG) tests the accumulative electrical retinal cell response to light. The test can be manipulated to examine several different retinal cell types. Electrodes are typically placed on a dormant site such as the forehead, referred to as the reference electrode, and on the cornea to receive the signal; the active electrode. The potential difference between the two electrodes is the response (in nV).

The stimuli are presented using the Ganzfeld method to ensure a uniform luminance across the retina. The patient fixates on a central target, with pupils fully dilated to allow for maximal response from the peripheral retinal areas. The electrical response is amplified and displayed as a waveform, which is interpreted with reference to the characteristics of its amplitude and time course. The response can be contaminated by background electrical interference, subject blinking, and also by facial muscular action such as jaw clenching; therefore each reading should be repeated to allow for an average of two readings to be calculated.

The waveform comprises two components; a negative 'a' wave followed by a positive 'b' wave. The negative 'a' wave response is thought to derive from the hyperpolarisation of the photoreceptors, and the positive 'b' wave is thought to represent the polarisation of the Müller and ON-bipolar cells.

A weak light stimulus is insufficient to stimulate photoreceptors and produce an 'a' wave, in such situations only a 'b' wave will be produced. Conversely if the light stimulus is too bright only an 'a' wave will be produced.

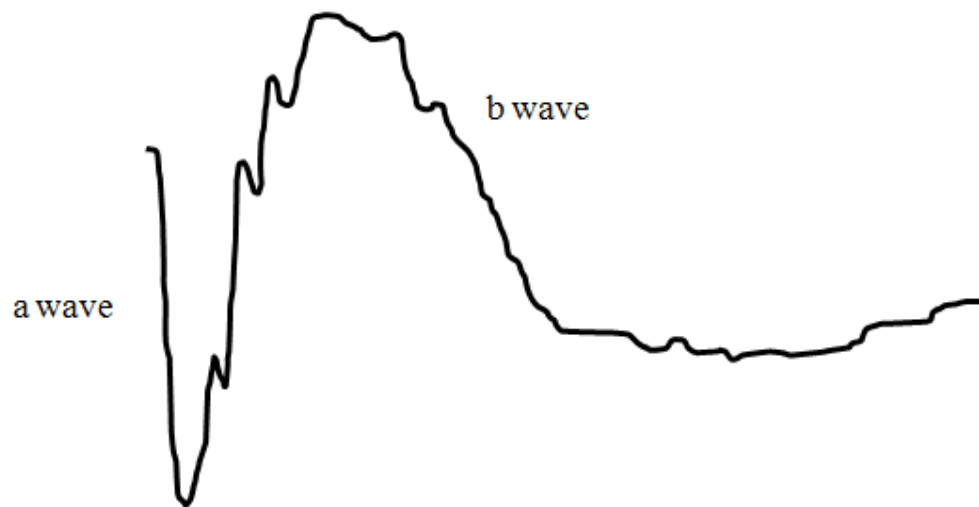


**Figure 12 Typical ERG waveform**

The amplitudes of the a and b waves are recorded. The time from response onset to the trough of the a and peak of the b wave, known as the implicit times are also recorded (see Figure 12).

Although the ERG is still in clinical use today it does have several shortcomings, in particular its lack of sensitivity to localised focal loss of function. Subsequently improvements to the design have been made, namely the multifocal ERG.

### **5.3 The multifocal electroretinogram (mfERG)**

In 1992 the multifocal ERG (mfERG) was introduced by Sutter and Tran (1992). The mfERG allows multiple locations of the retina to be tested simultaneously, providing a topographical representation of electrical activity. Until the introduction of the mfERG, ERGs were often used. The main problem with the ERG was the lack of specificity to a particular area of the retina, and conditions affecting smaller retinal areas could have been left undetected. The mfERG can be described as an ERG of multiple retinal areas (depending on the mfERG paradigm used).

The mfERG stimulates the central 50° of the retina. Stimuli consist of a series of 61, 103 or 241 hexagons; each one may be thought of as independent stimuli stimulating individual retinal areas (Hood et al. 2003). The hexagons are response density scaled to account for the decreasing density of cone cells with increasing eccentricity from the fovea, whereby smaller hexagons are presented in the central regions and larger hexagons are presented in the periphery (see Figure 13). Each hexagon flashes either on (white) or off (black), typically changing every 13.3 milliseconds (Hood 2000). Only half the hexagons are presented at any one time therefore the mean luminance presented is kept constant. The International Society for Clinical Electrophysiology in Vision (ISCEV) guidelines suggest luminance levels of the white hexagons to be between 100-200cd/m<sup>2</sup> (Marmor et al. 2003). The flashing and non flashing of the hexagons may appear to occur randomly, however each hexagon is governed by a pseudo-random binary sequence; an m-sequence. The m sequence assumes two states 0 (no flash), or 1 (flash). At the beginning of a recording each hexagon is in a different phase of the sequence. Each recording takes 4-7 minutes and is often broken down into 15-30 second segments. Longer test durations are associated with decreased subject compliance through blinking and losing fixation of the central target. The response from each presentation is extracted by use of mathematical algorithms to produce an average response for the respective area stimulated. The responses from many hexagons can be grouped together to investigate specific retinal regions.

The interval between flashes can be changed to produce different mfERG recording paradigms. Increasing the interval between flashes produces a waveform response akin to the full field ERG waveform.

**Figure 13 Hexagon stimulus used in mfERG testing (from Marmor et al. ISCEV guidelines 2003)**

### 5.3.1 First and second order kernels

The mfERG waveform bears some similarity to an ERG wave, however instead of an 'a' or 'b' waves as with the ERG, the mfERG wave is comprised of positive and negative components; referred to as P and N respectively.

**Figure 14 Typical waveform response from the mfERG (from Marmor et al. ISCEV guidelines, 2003).**

The most commonly analysed component of the mfERG is the first order kernel; this is obtained by adding all the recordings following a flash (white) stimulus, in a particular hexagon, and subtracting all the recordings following a non flash (black) stimulus, for the same hexagon. It comprises a negative deflection (N1) followed by a positive peak (P1). The second order kernel assesses the effect of the preceding stimulus, which may or may not be a flash stimulus; therefore the second order kernel response is not a true response itself but a calculation based on the first order kernel (see Figure 14). The cellular origins of the second order response have been attributed to the inner retina, but evidence is equivocal.

### 5.3.2 Tools for mfERG analysis

The Visual Evoked Response Imaging System (VERIS) for mfERG recordings has multiple tools which can facilitate analysis. A widely used tool is the averaging of responses. Spatial averaging helps reduce noise from each hexagon, smoothing the waveform (Hood et al. 2008). The averaging tool collates the responses for each of the hexagons and divides by the root mean square. As is the case with all averaging, there is the potential to lose small changes in response. The *Edit groups* function within the VERIS program allows

calculation of the average response from specific areas e.g. concentric rings, quadrants, hemifields. The separation into distinct retinal areas is particularly useful for this thesis; mfERG quadrant responses can be investigated with reference to specific indices of ocular shape for each retinal quadrant as derived by 3D MR imaging.

The VERIS program also allows 3-dimensional topography maps to be generated, by dividing the response amplitude by the area of the hexagon (see Figure 15).

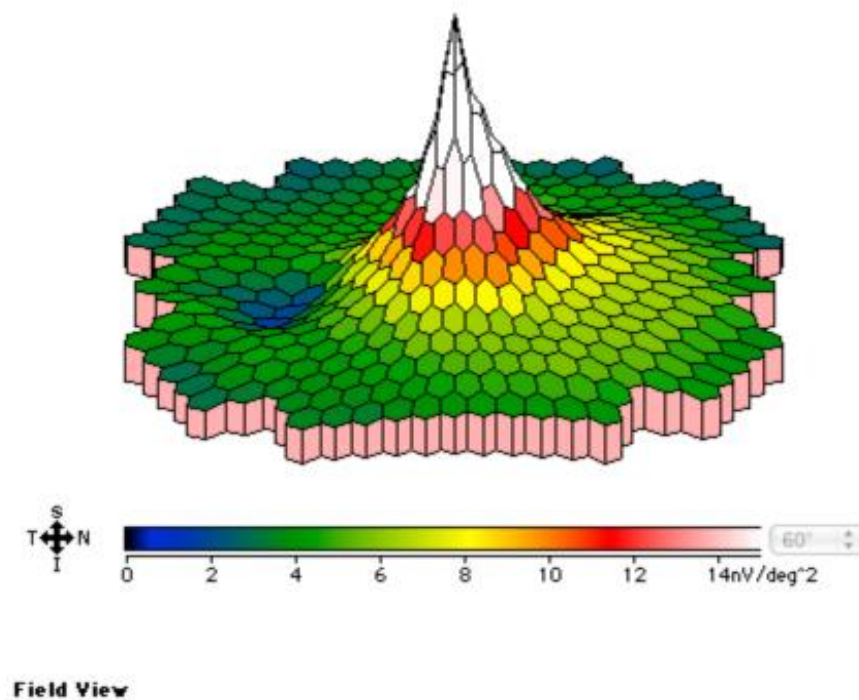


**Figure 15 3-dimensional topography plot of mfERG response (figure taken from subject data set, left eye)**

#### **5.4 Cellular origins of response**

The mfERG response is believed to originate predominately from the bipolar cells with smaller contributions from the photoreceptor (mainly cone) and amacrine cells. The contributions from ganglion cells are thought to be minimal or absent (Hiid et al. 2002).

To evaluate the contributions from various cells, studies on rhesus monkeys have shown that after injection with the chemical tetrodotoxin, TTX, the mfERG response closely resembled that of a human. Using pharmacological agents to further manipulate responses it was concluded that the N1 response was derived from the OFF bipolar cells and in general there

was only a small contribution from the photoreceptors except in the central 6° where the contribution is greater. It was also found that the P1 response originated from the depolarisation of the ON cells and recovery of the OFF cells (Hood et al. 2002). The origin of the N2 response is still uncertain (Hood et al. 2002). There is thought to be little contribution from the ganglion cells to the mfERG response (Hood et al. 2003).

The mfERG has been used successfully to diagnose and investigate a multitude of pathological disorders including retinitis pigmentosa, cone dystrophies, glaucoma and myopia (Chen et al. 2006a;b).

The diagram below (Figure 16) shows the model developed by Hood *et al* (2002) outlining the relative contributions of cells to the mfERG response wave. Damage to, or before, the bipolar cells would cause reduction of the waveform amplitude, (Hood et al. 2003). Damage to the ganglion cells (the inner retina) would not cause a reduction in amplitude (see Table 1).

**Figure 16 Cellular responses in mfERG (after Hood et al. 2002)**

Damage to	Mechanism	P1 ('b wave of') mfERG	
		Amplitude	Implicit time
Cone Receptor	Outer segment damage or cell loss	Smaller	Moderate delay
		Smaller	Normal
Outer plexiform layer	Altered synaptic transmission	Can be normal or larger	Large delay
ON bipolar cells	Cell loss	Smaller	Moderate delay
OFF bipolar cells	Cell loss	Larger	Slightly faster?
Inner plexiform layer	Altered synaptic transmission OR cell loss	Approx. Normal (waveform changes)	Small delay (<3ms)
Ganglion cells	Cell loss	Approx. Normal	Approx. Normal

**Table 1 The site of retinal damage and its consequence for the mfERG response waveform (after Hood, 2002)**

## 5.5 Myopia and electrophysiology findings

A reduction in electrophysiological retinal response with increasing myopia has been reported. The results appear to be inconsistent in the type of response which is reduced i.e. amplitudes, implicit times, or both. Furthermore there is some dispute as to whether it is the level of myopia that causes the reduction or the associated increase in the axial length.

Due to differences in the cellular origins of ERG and mfERG responses the data from each type of test is only related, not the same. Consequently ERG and mfERG responses must be considered separately.

### 5.5.1 Myopia and ERG

A reduction in ERG responses associated with myopia or axial length has been reported (Blach et al. 1966; Perlman et al. 1984; Westall et al. 2001). Blach *et al.* (1966) carried out scotopic ERG recordings (thus eliciting a rod dominated response) on highly myopic subjects with myopia ranging from -9D to -26D. They found both 'a' and 'b' waves to be

affected; a large variation in ERG responses was also noted which they believed to relate to retinal myopic degenerative changes.

Westall *et al.* (2001) carried out standard ERGs on 60 young adult subjects, with refractive errors ranging from +0.75D to -14.50D and axial lengths ranging from 22.2mm to 30.0mm. They found the implicit times were not affected by either myopia or axial length. A significant relationship between reduced amplitude and a longer axial length was noted. Westall *et al.* suggested that should myopia be of lenticular or corneal origin and not associated with increased axial length then theoretically ERG response should not be affected at all.

### 5.5.2 MfERG and myopia

Kawabata and chi-Usami (1997), examined the first order kernel responses on thirty young adult subjects (mean age 26.1 years). The subjects were placed into one of three groups according to refractive error: emmetropia/low myopia ( $MSE \pm sd = -0.78 \pm 0.89D$ ), medium myopia ( $-4.30 \pm 0.81D$ ), and high myopia ( $-10.33 \pm 3.38D$ ). The purpose of the investigation was to evaluate functional changes in myopic eyes. Myopia was believed to be principally of axial origin and not corneal or lenticular. In addition to the more typical mfERG analysis, examining all traces and concentric ring averages, the readings were also divided into quadrants: superior temporal, superior nasal, inferior temporal and inferior nasal (see Figure 18).

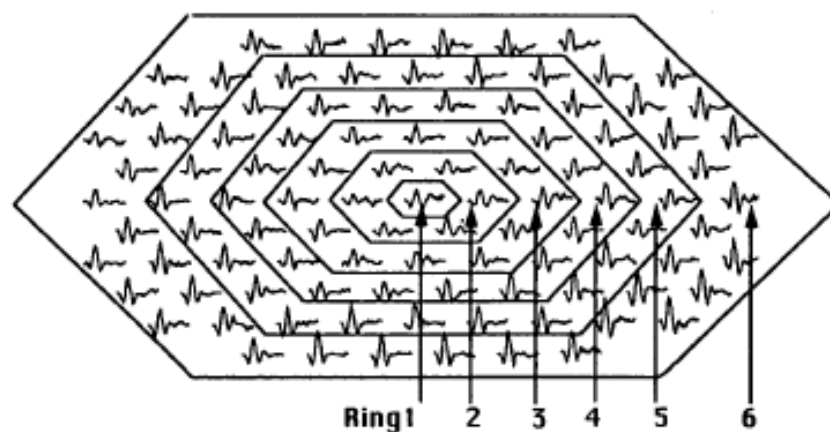


**Figure 17 Diagrammatic representation of the concentric ring averages analysed, note ring 1 denotes the presumed foveal response.**

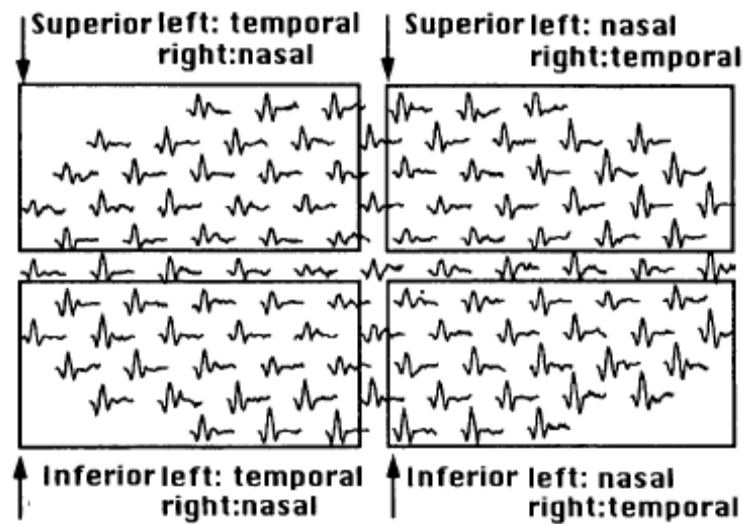


**Figure 18 Diagrammatical representation of the quadrant average analysis undertaken by Kawabata and chi-Usami 1997. N.B the horizontal and vertical meridians have been omitted, presumably to ensure equal hexagonal responses from each quadrant and also to exclude the optic nerve head**

Results showed a decrease in amplitude and an increase in implicit times as myopia increased; N1 amplitudes  $r=0.713$ , and for P1  $r=0.772$ ,  $p<0.0001$  for both cases. Implicit times increased with greater levels of myopia: the first latency  $r=0.603$   $p<0.0004$ , and the second  $r=0.731$   $p<0.0001$ . Amplitudes from the peripheral regions were affected to a greater degree than central regions. Implicit times were delayed more in the inferior regions than superior. Kawabata and chi-Usami (1997) concluded that a reduction in cone cell function in myopia was responsible for the reduced responses noted through mfERG testing.

In a separate study looking at ring responses (Chan and Mohidin, 2003), first order response amplitudes were reportedly affected by increasing axial length, as were paracentral (ring 3) responses. Second order response amplitudes were not affected in the central region, however, the paracentral and peripheral regions showed a reduction in amplitude with increasing axial length (rings 2 to 5). Overall the average of the responses measured showed a decrease in amplitude of 6-10% with every 1mm increase in axial length.

The central response amplitude (P1) originates from the photoreceptors and Chan and Mohidin (2003) suggested the reduced amplitude may relate to central retinal stretch. The first slice of the second order response waveform is believed to originate from the outer plexiform layer (Hood, 2000) and Chan and Mohidin believed that this somehow attributed to the paracentral deterioration in responses.

To elicit whether the main contributory factor to reduced mfERG responses is myopia or axial length Chen *et al.* (2006) carried out a series of mfERG studies using various recording paradigms. In a group of 30 young adult subjects P1 amplitudes and implicit times of standard mfERG recordings were examined with respect to their axial lengths and refractive error. Subjects comprised of 10 emmetropes and 20 myopes, myopic subjects were further classified into stable or progressing myopes. Refractive error ranged from plano to -9.75D. Using ANCOVA statistical analysis the authors accounted for axial length as a covariate of myopia and vice versa. A longer axial length correlated with a longer implicit time and a refractive group effect was also noted. The myopic group was noted to have a longer implicit time of 1.3-3.1ms compared with the emmetropic controls, and as noted by Kawabata and chi-Usami. the delays were greatest in the periphery. Notably, Chen *et al.* (2006) reported statistical differences between the emmetropic and progressing myopia groups only. 15% of the variance in implicit time results was explained through axial length, 27% by refractive error and the remaining believed to be due to inter subject variability. Unlike previous investigations, a detrimental effect of myopia or increased axial length was not noted for the response amplitude.

Further work by the same group using different mfERG recording paradigms has led to the suggestion that the changes are a consequence of myopia and not a precipitating factor of myopia (Chen et al. 2006a;b;c;d). Additionally, the authors found the responses which originated from photoreceptors were not affected by myopia. Most recently, the group has examined oscillatory potentials of mfERG recordings and noted significant differences between stable and progressing myopes (Chen et al. 2006b), which is suggestive of inner retinal contributions to myopic development.

In children mfERG changes (using standard paradigms) have been shown to correlate with greater myopic progression (Luu et al. 2007).

In summary, changes in mfERG readings suggest a greater level of myopia or axial length may produce reduced amplitudes and/or longer implicit times. From previous work examining mfERG responses in adults, it can be hypothesised that the outer retinal layers are affected by myopia, but it is the inner retinal layers which may precipitate myopia.

### **5.5.3 Reasons for reduced electrical response in myopia**

#### **Ocular resistance**

Perlman found an inverse relationship between the b wave response of an ERG and a longer axial length (Perlman et al. 1984). It was believed that increased ocular resistance, that is resistance to the electrical signal by ocular tissues and structures, caused the reduction in ERG response. Perlman believed resistance was more likely to reduce the signal than reduced sampling density or reduced receptor function although a number of studies have disagreed with this proposal (Chen et al. 2006; Kawabata & chi-Usami 1997).

#### **Eye size and shape**

Westall *et al.* 2001 suggest that the increase in axial length and not the level of myopia, acts as a causative factor for reduced ERG responses. The group postulated that myopia of lenticular or corneal origin would not produce differences in ERG responses (Westall et al. 2001). Chan and Mohidin examined the link between axial length and the mfERG and also attributed the reduction in responses to morphological changes associated with increased axial length.

Furthermore, there is a proposal that the retinal cells of highly myopic eyes may be either inherently dissimilar to emmetropic eyes or different as a consequence of myopic damage (Chen et al. 1992). Kawabata and chi-Usami believed the reduction in mfERG responses with myopia was due to cone loss, possibly associated with ocular expansion.

#### **Dopamine**

Dopamine in the human eye is produced in specific amacrine cells within the retina. The role of dopamine is multiplex, it is involved in accommodation, blink rate, iris aperture control and ganglion cell activity (Yeung et al.2001; Spiers, 1969). Recently, it has been suggested that perhaps altered levels of dopamine may influence the human mfERG response (Chen et al. 2006a). Through work conducted largely on animals, depleted levels of the hormone dopamine have been noted in cases of induced myopia (McCarthy et al. 2007). A recent study of myopic development in children noted that sunlight aided the production of dopamine, and reported that although dopamine levels were not measured in the subject group, lower myopic refractive error was noted in children who spent more time outdoors (Rose et al. 2008).

## 5.6 Summary

Electrophysiological testing provides an objective measure of ocular function. The ERG test provides a generalised summed response of ocular function, whilst the mfERG provides a topographical representation of ocular functions. Previous studies have identified reduced responses in both ERG and mfERG with either longer axial length or higher refractive levels of myopia. The effects of higher refractive levels of myopia and axial length are difficult to differentiate as they invariably correlate.

There are many possible explanations for reduced electrical responses in myopic or longer eyes. Often decreased retinal cell density as a result of retinal myopic stretch is attributed with the reduction in response. Many studies have identified loss in paracentral and peripheral regions, whereas others have noted losses to be more central. Thus far most studies have relied upon axial length as a measure of eye size, however this technique is limited. Axial length alone does not indicate eye shape and so is only useful if considering the central hexagon response. The recent development of 3-dimensional ocular MRI enables the comparisons between mfERG responses and individual ocular shape. The findings of this study would help answer the question of whether it is myopia or eye shape that causes the reduction in mfERG response. The thesis addresses correlations of mfERG testing and ocular shape in Chapter 13.

## **6 GANGLION CELL DENSITY AND OCULAR SHAPE**

### **6.1 Introduction**

Ganglion cells reside in the ganglion cell layer in close proximity to the inner retina. The primary function of ganglion cells is the transmission of information as action potentials between the photoreceptors, via horizontal, bipolar and amacrine cells, to the rest of the visual pathway. Ganglion cell axons form the optic nerve, which projects to the occipital cerebral region, specifically the visual cortex.

A single ganglion cell can receive and transmit data from numerous photoreceptors; this process is termed convergence. The ratio of retinal ganglion cells to cone cells in the central foveal region is approximately 2; this ratio declines to approximately 0.5 for retinal regions beyond the central 19° around the fovea, thus there is a greater need for convergence in the peripheral retina (Sjöstrand et al. 1999). The convergence process helps balance the spatial resolution required to detect objects peripherally while still retaining the high level of resolution required to distinguish finer details of objects in the central field. Without convergence a greater number of ganglion cells would be necessary to transmit information to the visual cortex, thus the need for a larger optic nerve head which would in turn produce an intolerably large blind spot in the visual field.

### **6.2 Distribution of ganglion cells**

There are approximately 32000-38000 ganglion cells per mm<sup>2</sup> in the retina; their distribution across the retina is non homogenous (Curcio & Allen 1990; Hebel & Hollander 1983). The cells are arranged in an elliptical ring shape surrounding the fovea, (Curcio et al. 1990). Quadrantic differences in the distribution of ganglion cells have also been noted; a histological study reported nasal density to be 300% greater than that of the temporal retina. The same study noted a greater density of ganglion cells in the superior retina by 60% compared to that of the inferior retina (Curcio et al. 1990). In addition to histological studies, ganglion cell density in humans may also be inferred from psychophysical techniques (Anderson et al. 1992; Anderson et al. 1995; Chui et al. 2008).

### 6.3 Receptive fields

All retinal ganglion cells have a base firing rate which describes the level of spontaneous discharge from the cell in the absence of stimulation. Stimulation in the form of photons (units of light) can increase or decrease the firing rate of the cell.

Studies on mammalian retina, mainly cats, have shown ganglion cells to possess non homogenous circular receptive fields. Two zones arranged in concentric circles have been identified, each with their own stimulation and response characteristics. Stimulation of the central zone has been found to elicit a separate and opposite response to the stimulation of the periphery. A central excitatory region surrounded by a peripheral inhibitory ring is termed an on-centre cell; conversely, a cell with a central inhibitory and peripheral excitatory configuration is termed an off-centre cell (Kuffler, 1953).

The notion of concentric receptive fields in ganglion cells was explored further by use of sinusoidal grating stimuli (Enroth-Cugell & Robson 1966). Two further cell subtypes were identified; X and Y cells. X cell responses were found to increase when an on-centre cell was exposed to light stimuli in the central ring and dark stimuli in the peripheral ring (Figure 19). When the central stimulus was darker than the peripheral, a decline in response was shown. If the sinusoidal grating was positioned to produce a similar stimulus at both the centre and periphery there was no change in the cells response. The X cells were said to show linear spatial summation. Conversely, Y cells responded at the onset of stimulus; the response was unrelated to the stimulus sinusoidal grating phase.

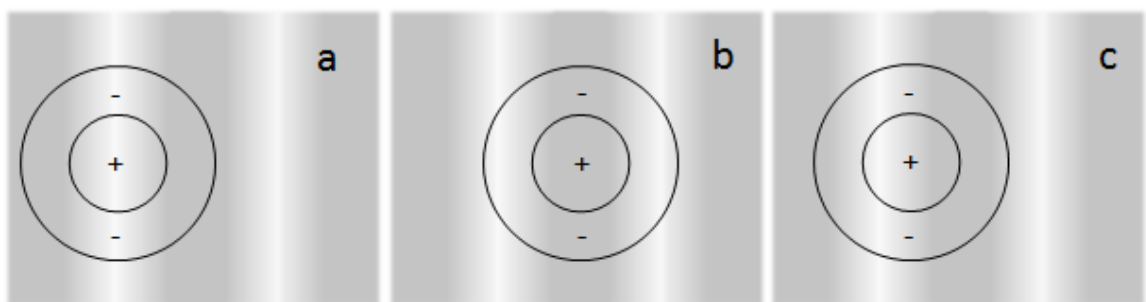


**Figure 19 On-centre ganglion cells and sinusoidal grating**

The X cell response varied with sinusoidal grating phase changes and therefore responded to motion. Y cells, did not respond to movement. It should be noted that the size of ganglion

cell receptive fields is not uniform across the retina; cells located peripherally have larger receptive fields than those located centrally.

### 6.3.1 Magnocellular and Parvocellular cells

Receptive fields in primate retinal ganglion cells follow a similar structure to X and Y cells found in cats. The primate ganglion cells can be broadly divided into two groups; Magnocellular (M) and Parvocellular (P), the names correspond to the cerebral streams followed by each cell type. Although primate ganglion cells resemble cat ganglion cells in many ways, their distribution and properties vary.

Each concentric region of the P cell receptive field possesses an affinity for a particular wavelength of light (De Monasterio & Gouras 1975). This characteristic response to colour is known as colour opponency. Conversely, M cells do not display colour opponency therefore they are often referred to as ‘broadband’ cells,

Earlier studies indicated that M cells showed the ability to respond to motion; however, recent work on humans has demonstrated that P cells can also detect motion at specific retinal eccentricities (Anderson et al. 1995; Galvin et al. 1996).

Further characteristics of M and P cells are listed in Table 2

<b>M cells</b>	<b>P cells</b>
Thicker axons	Thinner axons
Phasic/transient response	Sustained/tonic response
Large cells	Small cells
Broadband	Colour opponency properties
Higher contrast sensitivity	Lower contrast sensitivity
Larger receptive fields with increasing eccentricity from the fovea	

**Table 2 Magno- and Parvocellular differences**

In addition to M and P cells, a third group of ganglion cells, known as K cells (or Koniocellular, originally termed ‘rarely encountered cells’) have been found in primates (Schiller & Malpeli 1977). K cells also display non-linear spatial summation characteristics similar to M cells but at a much slower conduction velocity.

#### **6.4 Sampling theorem, aliasing and the Nyquist limit**

*In vivo* ganglion cell sampling through psychophysical methods exploit the on/off centre arrangement of ganglion cell receptive fields and the sampling theorem. The sampling theorem can be used to describe the limitations placed upon the visual system by the sampling frequency. Assuming ganglion cells are regularly distributed in a given retinal region, the sampling theorem dictates that for a sinusoidal grating to be detected in order to reconstruct the signal accurately, a minimum of two sampling points per cycle are required i.e. one sampling point for the peak of the wave and one for the trough. The limit of the sampling frequency is referred to as the Nyquist limit. If performance falls below the Nyquist limit, (when responses are correct less than 50% of the time); this would produce aliasing or misrepresentation of the signal. In the central foveal region visual optics act as a filter to limit frequencies outside the limits of the bandwidth imposed by the distribution of the foveal cones, to prevent aliasing. High spatial frequency laser interference fringes are independent of the eye’s optics and can be used to induce foveal aliasing.

#### **6.5 Peripheral visual function**

Beyond the foveal region, cone density cannot be relied upon to indicate potential visual acuity due to the decline in cone receptors and the increased amount of signal convergence that takes place. Hence, ganglion cell density is of particular interest in the peripheral retinal regions.

The neural limitations placed upon the visual system in the peripheral retina by ganglion cells are believed to be directly associated with reduced visual resolution (Thibos et al. 1987). However, other factors may also play a role in image degradation: the presence of peripheral aberrations, stimulus contrast and correction of peripheral refractive error.

A study using histological samples found beyond 11-20° eccentricity from the fovea, the relationship between minimum angle of resolution (MAR), receptive fields and retinal ganglion cells to be non linear. The non linearity has been explained by the lack of

differentiation between ganglion cell subtypes in sampling studies (Sjöstrand et al. 1999). Conversely, other studies have noted the relationship of ganglion cell density and visual resolution to be well correlated (Anderson et al. 1992). One study determined ganglion cell density by use of psychophysical techniques in several different retinal locations referencing findings to previously published histological data (Anderson et al. 1992; Curcio & Allen 1990). At an eccentricity of 25°, the greatest resolution acuity was found to be in the nasal quadrant (see Figure 20). This finding correlates well with the increased density of ganglion cells noted in this region (Curcio et al. 1990). Nasal-temporal asymmetries in sensitivity had previously been noted by Anderson *et al.* (1991); at eccentricities of 25-55° the nasal retina was shown to be more sensitive than the temporal. Investigations of the vertical meridian (examining superior-inferior asymmetries) did not find such hemifield differences.

**Figure 20 Visual resolution limit in cycles per degree at an eccentricity of 25°, at radial locations around the retina (Anderson et al. 1992)**

## **6.6 Myopia, eye size and peripheral ganglion cell function**

Of particular interest to the current study is the evidence showing the peripheral retina to be structurally dissimilar between different refractive groups (Atchison et al. 2005). In myopia as the globe expands concurrent retinal expansion and subsequently retinal stretch is believed to take place (Vera-Diaz et al. 2005). As a consequence, retinal receptors may be

misaligned, misdirected, damaged, or decreased in density. Investigation of ganglion cell density in myopic subjects may therefore help clarify the effects of shape and refractive error on peripheral retinal function.

Specifically, ganglion cell density has been found to be reduced in myopes (Chui et al. 2002) and consequently visual resolution believed to be sampling limited (Chui et al. 2005) in direct proportion to the number of ganglion cells (Popovic & Sjöstrand 2005).

One study investigating aliasing at the fovea estimated the Nyquist limit of an emmetropic eye to be 56 cycles per degree (expressed in object space/visual field); the value was calculated by assuming that firstly the maximum foveal proximity of cone receptors is 3 $\mu$ m and secondly that 1° of retina corresponds to 0.29mm. Using this value, a prediction may be made regarding the potential effects of myopia on retinal spacing and thus sampling limits. Strang *et al.* (1998) proposed three models of myopic growth; equatorial stretch, global stretch and posterior pole stretch (see Figure 21).

**Figure 21 (a) Equatorial stretching (b) Global expansion (c) Posterior Pole (after Strang et al. 1998)**

Strang *et al.* made predictions of resolution ability with reference to each myopic model (Strang et al. 1998). The predictions were based upon the parameters set by Williams *et al.* (Williams, 1985). Eyes which followed the equatorial stretch model were expected to have optical rather than neural limitations affecting the resolution. For the posterior pole stretch model, neural resolution was predicted to fall at approximately 5D of myopia, and in the global expansion model resolution was predicted to fall beyond 15D of myopia (see Figure 22). Thirty-four subjects with refractive errors ranging from plano to -14D were examined. The predictions were not confirmed by their findings. This may be due to the models being overly simplistic as it is likely that subjects' eyes were a combination of two or more of the

stretch models. The study failed to explain the reduction in visual resolution through retinal sampling; however, a reduction in visual acuity in some highly myopic subjects was noted.

Thus far it is difficult to ascertain whether eye shape or myopic refractive error has a bearing on ganglion cell density or function.

**Figure 22 Graph showing the predicted decline in resolution with increasing myopia for each of the three myopic models, (optical cut-off is marked at 45 cpd, represents the optical limit of the eye) (after Strang et al. 1998)**

## **6.7 Summary**

Ganglion cell density can be measured *in vivo* through psychophysical techniques by exploiting the sampling theorem. It has been hypothesised that ganglion cell density may be reduced in myopic subjects due to the retinal expansion and stretch which is synonymous with myopia. Only a limited number of investigations have been able to show the decline in density for myopic subjects; optical factors may also play a role in limiting peripheral acuity.

Retinal expansion and stretch, not myopia, are often cited as the causative factors in a hypothetical decline of ganglion cell density, therefore ganglion cell density should be investigated with reference to eye shape; this thesis describes correlations of ganglion cell density with MR derived ocular shape (see 14.4).

## **7 INSTRUMENTATION**

### **7.1 Introduction**

Approximately 17 subjects for the MRI study had been recruited prior to October 2006 (before the PhD studentship began); for the majority of these subjects a range of ocular biometry measurements were obtained by Dr Nicola Logan, Professor Bernard Gilmartin, Professor Krish Singh and Elizabeth Wilkinson.

Subjects were recruited predominantly from the Optometry undergraduate and postgraduate programs at Aston University. A total of 76 subjects were scanned however only 73 are included in the main data set; subjects with refractive error greater than 15D were excluded from general analyses. Ages for the main subject data set ranged from 18 years to 40 years. Subjects were predominantly of White or British Asian ethnicities. Ethical approval was acquired for all experiments and informed consent obtained from subjects.

The range of data collection comprised MR scanning, ocular biometric measures using the Zeiss *IOL Master* and Oculus Pentacam, visual fields testing with the Humphrey Visual Fields Analyser, multifocal ERG VERIS recordings, ganglion cell density, peripheral refraction measurements with the Shin Nippon autorefractor, and the issuing of a questionnaire.

### **7.2 Shin Nippon Autorefractor**

The Shin Nippon SRW 5000 (Japan) is a wide field binocular open view IR autorefractor allowing objective measurement of refractive error. The instrument has been used widely in research (Chat & Edwards, 2001; Logan et al. 2005).

Refractive readings by the S-N SRW 5000 have shown high repeatability and high validity which have been established through correlations with subjective refraction in both adults (Mallen et al. 2001) and children (Chat & Edwards 2001).

The subject is positioned by use of an adjustable chin and fixed head rest. The practitioner is able to view the anterior eye on a small black and white monitor, and through use of a joystick can align and focus the centre of a ring shaped (necklace) mire with the eye. To obtain a reading a minimum pupil size of 2.9mm is recommended by the manufacturer.

Once the subjects' eye is aligned, the practitioner presses the release button in order to take a measurement. Results may be printed and stored; the option to produce electronic copies through connection to a computer also exists, however, this method was not used in the present study.

The instrument is able to measure a wide range of refractive errors;  $\pm 22\text{D}$  spherical component and  $\pm 10\text{D}$  cylindrical component. The values are given to the nearest  $0.125\text{D}$  and the cylindrical axis expressed in  $1^\circ$  increments.

Shin Nippon autorefractors have been used to study accommodation and peripheral refraction. The extensive use of the Shin Nippon range for peripheral refraction has been reviewed (Fedtke et al. 2009) and compared to other techniques and is cited as the principal instrument of choice.

In order to take peripheral refraction measurements with an autorefractor the presentation of the target normally requires a degree of modification. In the current study an attachment was fitted to the Shin Nippon autorefractor casing; the attachment was marked at  $5^\circ$  intervals up to a maximum of  $30^\circ$  right and left from the visual axis ( $0^\circ$ ). The peripheral refraction attachment had been made for previous studies using the Shin Nippon by Dr Leon Davies and Dr Edward Mallen; a fixation target was attached to the autorefractor arm at a viewing distance of 1m.

Prior to obtaining autorefraction readings all subjects were dilated with 1% tropicamide ophthalmic solution (*Minims*<sup>®</sup>, Bausch and Lomb, Surrey, U.K); this ensured maximum pupil size which enabled the acquisition of more peripheral measurements, additionally tropicamide induced a cycloplegic effect which helped to minimise any active accommodation. Prior to the instillation of tropicamide intra-ocular pressure (IOP) readings were obtained using standard commercially available non-contact tonometers, IOP readings were repeated post dilation and advice on possible adverse effects of tropicamide was given.

### **7.3 Zeiss IOL Master**

The *Zeiss IOL Master* is a non-contact device used for measuring ocular biometric parameters. Measurements possible include axial length, corneal radii, anterior chamber depth, and horizontal iris diameter. The *IOL Master* is used extensively in hospitals for calculation of the required intraocular lens power pre cataract surgery.

The operation of the *IOL Master* is much like that of an autorefractor; the subject rests his/her head on the head rest and chin on the adjustable chin rest. The subject fixates upon a target located within the instrument, the practitioner then uses the joystick to adjust the positioning of the unit and focus the mires. Each type of measurement requires the refocusing and realignment of mires, i.e. there are separate sets of mires for keratometry, axial length and anterior chamber depth.

### **Axial length measurements**

The *IOL Master* measures axial length through an adaptation of partial coherence interferometry. A Michelson interferometer splits an infra red light beam ( $\lambda = 780\text{nm}$ ) into a dual beam comprising two partial beams (which reduces any longitudinal eye movements affecting the recording). On entering the eye the dual beam is reflected at two surfaces; the anterior corneal surface and the pigment epithelium. If the path between the partial beams is smaller than the coherence length; an interference signal is detected, (Drexler et al. 1998; Goel et al. 2004). This condition is met through the movement of one of the mirrors within the system. The interference is detected by a photodetector and measured relative to its positioning from the interferometer mirror.

Prior to the introduction of the *IOL Master* axial length measurements were predominantly taken using A-Scan ultrasound. A distinct disadvantage of ultrasound biometry is the higher likelihood of cross infection between subjects owing to the use of a contact probe.

### **Keratometry**

Keratometry is the measurement of the corneal radius of curvature and readings can be used to estimate the degree of corneal cylindrical error. The measurements obtained through the *IOL Master* are comparable to those made by commercially available instruments used in clinical practice, such as the Javal-Schiotz keratometer (Santadomingo et al. 2002; Nemeth et al. 2003).

### **Anterior Chamber Depth (ACD)**

The anterior chamber depth describes the distance along the optic axis from the posterior corneal surface to the anterior crystalline lens surface. The repeatability of ACD measurements with the *IOL Master* have been queried (Lam et al. 2001). Furthermore comparison of ACD measurements from the *IOL Master* with other commercially available instruments have found equivocal results, with some studies reporting comparable results

between instruments (Lackner et al. 2005) and others finding significant differences (Hashemi et al. 2005).

In summary, previous reports suggest that the Zeiss *IOL Master* has good repeatability, for keratometry and axial length measurements, and is a valid instrument of choice for a range of ocular biometric measurement. Results are not, however, interchangeable with those from other ocular biometric instruments.

#### **7.4 Zeiss Humphrey Visual Fields Analyser**

The Zeiss Humphrey Visual Fields Analyser (HVFA) is a well established and widely used automated perimeter in both research and clinical settings; it is generally accepted as the gold standard instrument for automated visual fields testing. In clinical settings the HVFA is often recommended for use in glaucoma patients, i.e. individuals who may have subtle visual field changes.

During the test subject ametropia is fully corrected by use of full aperture trial lenses or by contact lenses. Subjects are positioned by use of adjustable chin and forehead rests, and are required to fixate on a target inside the perimeter bowl.

A push switch is given to a subject, which during the test the subject uses to indicate the presence of a stimulus. The stimulus for most HVFA programs is target size III (4mm<sup>2</sup>); however other sizes may be used to detect more subtle or gross defects. The stimulus will vary in intensity; from 0.8 to 10,000 apostilb (asb), in order to determine the minimum light detected by the subject; known as the differential light threshold. The background luminance within the perimeter will however stay constant at 31.5 asb (Wani et al 2005).

As mentioned previously, the HVFA has extensive software to run various different types of visual field tests. Each test may differ from another by the area of the field covered, number of points tested, or by the way in which the light threshold is determined. The HVFA allows use of the Swedish Interactive Threshold Algorithm (SITA) to determine threshold values. The use of SITA reduces the test time which helps reduce the effect of fatigue associated with longer testing times, thus producing more reliable results.

There are several types of SITA tests; SITA Standard, SITA Fast and FASTPAC. SITA Standard is often used as a replacement for full threshold fields as it is faster and shown to have good repeatability (Chandra et al. 2000). The HVFA provides several reliability

indices as a measure of how valid the test is, these include: fixation losses, false positives and false negatives, (see section 4.2.1).

The Humphrey Visual Field Analyser provides reliable measurements of light sensitivity for the central visual field. In myopic individuals these measurements are a valuable source of information as they can provide information about subtle functional changes. Although studies of automated visual fields in myopia have been previously reported, the approach taken by the current study is unique as it investigates the previously unreported relationship between ocular shape and visual field sensitivity.

### **7.5 Oculus Pentacam**

The Oculus Pentacam (Oculus Optikgeräte GmbH, Wetzlar, Germany) is a relatively new device; it was introduced approximately five years ago. The Pentacam is able to take numerous measurements of the anterior eye, in particular measurements of the cornea (see Figure 23). The Pentacam provides a vast amount of information: corneal pachymetry, corneal volume, higher order aberration maps, and refractive power topographies. The Pentacam is reported to have high repeatability in particular for pachymetry measurements (Khoramnia et al. 2007). The use of the Pentacam has been widely advocated by refractive surgery clinics and hospital services alike.

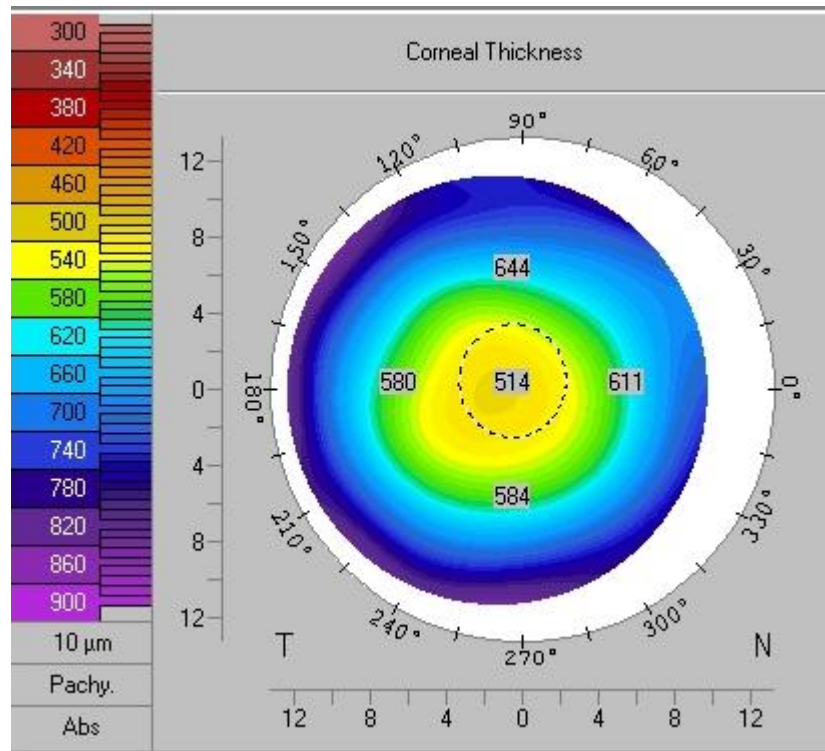


**Figure 23** An example of a Pentacam output. The output shows the corneal thickness for an emmetropic subject (MSE: +0.50D). Further outputs are given for parameters such as corneal curvature and aberrations.

The instrument uses a rotating slit beam camera which is based upon the Scheimpflug principle to take measurements at 25,000 locations within the anterior eye. The Scheimpflug principle describes the relationship between the image plane, object plane and the orientation of the camera lens, required to achieve a focused cross sectional image.

## 7.6 Magnetic Resonance Imaging (MRI)

Magnetic Resonance Imaging, MRI, is a method of imaging used to examine soft internal tissues in humans. MRI is widely used in the field of neurology. The technique works on the basis of an extremely strong magnetic field and exploits the properties on hydrogen atoms which are abundant in the human body. The responses from the magnetic fields are detected by radio waves which are then presented as images.

In the present study a Siemens 3-tesla (Siemens, Erlangen, Germany) whole body scanner was used to scan both eyes. The MRI scanning protocol allowed images to be obtained in five minutes and forty seconds (Singh et al. 2006). To explain how the MRI works it is essential to understand some of the associated background physics.

An atom is a structure constituting a central nucleus which contains both positively charged protons, and neutrons which do not have an electrical charge. The nucleus is surrounded by negatively charged electrons (Westbrook and Kaut, 2003). The atom is electrically stable if the number of protons and electrons is equal. If there is a surplus of either, the atom is electrically unstable and termed an ion.

There are three types of movement within the atom; electrons spinning on their own axis; electrons orbiting the nucleus; and most important for MRI is the spinning of the nucleus on its own axis (Bharatah, 2009). The nucleus of biological tissues contains specific MR sensitive nuclei; these are hydrogen atoms. In general the protons in the hydrogen atom nuclei are randomly aligned. In the presence of a strong magnetic field, such as that introduced by the MR scanner, the orientation of the protons is aligned with the new magnetic field. The protons generally spin around their own axis, however, in the presence of the strong magnetic field they also spin in a rotary pattern about their own axis known as the precessional path. The speed at which this path is followed is known as the precessional frequency, also referred to as the Larmor frequency as it is governed by the Larmor equation (Westbrook and Kaut, 2003). The precessional frequency of hydrogen varies with different magnetic field strengths; a higher field strength of 1.5 tesla would produce a greater frequency than 1.0 tesla.

A pulse of radio frequency waves is applied at the precessional frequency; this causes resonance to occur. The protons gain energy and their orientation is changed, the magnitude of change is termed the flip angle and is usually  $90^\circ$  i.e. the opposite direction to the magnetic field. The radio frequency receiver coil detects the changes in the magnetic field and is able to record from this the MR signal. The receiver coil may be a small localised coil e.g. an ocular coil, or a larger full body coil. A localised coil will provide a higher signal to noise ratio. In this particular study an eight channel phased array head coil was used.

As the radio frequency waves are removed, the energy of the protons is diminished until they realign orientation with the magnetic fields. The loss of radio frequency emitted is termed T1 or T2 decay (Westbrook and Kaut, 2003). T2 weighted images were used in the present study as they optimise organs that are predominantly water based, such as the eye. Each MR slice had a thickness of 1mm and voxel size was 1.0 x 1.0 x 1.0mm. An earlier protocol used 0.5 x 0.5 x 1.0mm voxels (Singh et al. 2006). Further details of how the images were processed and analysed are provided in Chapter 9.

As the MR scanner is the centre of a strong magnetic field it is critical that all metallic objects are removed from the room and from the subjects. In depth screening takes place prior to any scan, and subjects must speak to the radiographer before the procedure.

The scanner comprises a tunnel like chamber and is accessed by the subject through lying on a sliding table. In the current study subjects were asked to fixate on a distant LED target during scans. The images are prone to artefacts therefore movement of the eyes, and other general bodily movement, can cause blurring of the images.

Inside the scanner the environment can be quite noisy owing to changes in the magnetic field strength; referred to as gradients (McRobbie et al. 2003). Ear plugs were provided for all subjects to reduce the loud audio effects of the MR scanner.

## **7.7 Summary**

A number of different techniques are used to assess ocular shape and function as part of the experiments which comprise this thesis. The high validity and repeatability of each instrument or technique has previously been reported, therefore no studies of repeatability or validity have been carried out. Calibration of all lab instruments was maintained throughout the study.

## 8 SUMMARY OF AIMS AND OBJECTIVES

The principal aim of this thesis is to evaluate the relationship between ocular shape and visual function.

Several reports demonstrating reduced visual function in myopia have suggested increased ocular size as a possible causative factor. The increase in ocular size is thought to cause a concurrent decrease in retinal receptor density and subsequently lead to impaired visual function (Chen et al. 2006; Chui et al. 2005). Previously limitations in ocular shape imaging restricted the testing of this hypothesis. Since the introduction of 3-dimensional MR imaging a more comprehensive model of eye shape may be constructed and subsequently correlated with tests of visual function (Singh et al. 2006).

3-dimensional ocular MR imaging allows shape parameters from specific areas of the eye to be evaluated; it is envisaged that evaluations of shape and function will be drawn from specific retinal quartiles. Tests of visual function will include visual field sensitivity testing, multifocal electroretinogram testing, and estimates of ganglion cell density. Previously these tests of have demonstrated reduced responses in myopic eyes.

In order to further evaluate ocular structural aspects, a comparison between peripheral refraction based retinal contours and MRI based retinal contours is envisaged. As peripheral refraction is a more accessible and more widely used technique than 3-dimensional ocular MRI, it is of particular interest to determine whether these two techniques produce comparable and interchangeable results.

Based on previous literature, it is hypothesised that a detrimental effect on visual function will be correlated with the increase in ocular size which is synonymous with myopia.

## **9 DEPICTION OF OCULAR SHAPE AS DERIVED FROM 3-DIMENSIONAL MAGNETIC RESONANCE IMAGING (MRI)**

### **9.1 Introduction**

*In vivo* ocular imaging has proven to be problematic for investigators owing to both optical and anatomical constraints. Two of the most widely used techniques in recent years have been peripheral refraction and 2-dimensional MRI (Atchison et al. 2004; 2005; Logan et al. 2004). Both these methods suffer from relatively large areas of the retina being inaccessible for measurement, and thus assumptions of eye shape in those areas have been made. Peripheral refraction measurements are usually taken over the central 30-40° at 5° intervals; thus not accounting for data from approximately 57% of the area examined. Peripheral refractive studies generally focus on the horizontal meridian; there is limited data for the vertical meridian. Due to difficulties in measurements, information regarding the oblique meridians is rarely acquired. Thus information is missed due to large measurement angles and is also limited to a maximum of two meridians. Furthermore, aberrations created by the eye's optics limit the validity of more peripheral readings. Conversely MRI measurements are independent of the eyes optics; additionally MRI is not limited by pupil size, allowing measurements of the whole eye. Until recently all ocular MRI work was limited to 2-dimensional (2D) methods (Atchison et al. 2005; 2004). Measurements of the height, width and length of the eye were made using MR data (Cheng et al. 1992; Atchison et al. 2004; 2005). Although 2D MR data can provide valuable information on eye size, it has failed accurately to quantify the changes in ocular shape. 2D MR imaging is limited by a number of factors; namely the image slice sizes and methods of data analysis. Despite their relative limitations both techniques, peripheral refraction and MRI, appear to produce similar results; reporting myopic eyes to be relatively prolate or less oblate in the posterior retinal regions compared to emmetropes and hyperopes who tend to be more oblate. 3-dimensional ocular MR imaging bears many advantages over the 2D method. 3D MRI can provide a more comprehensive data set providing information on ocular shape, retinal contour, ocular volume and help to model the shape characteristics of each retinal quadrant.

### **9.2 3 Dimensional MRI**

The acquisition of the MR data is described in more detail in the Instrumentation chapter. In brief, subjects are required meet a strict set of criteria before consideration for MR imaging.

Information regarding the procedure, the prerequisites to scanning, and the possible adverse effects, was supplied through both written and verbal formats prior to scanning. In the current study the information sheets, one of which was an exclusion criteria questionnaire, were read again on the day of the scan. Before committing to the experiment, subjects were briefed again by the registered radiographer present and any positive responses on the questionnaire discussed; positive responses may be regarding issues such as dental work or tattoos. Prior to entering the scanning room all metallic objects were removed from the subjects due to the strong magnetic fields within the room; subjects were asked to either change into hospital gowns or bring a change of clothing which was free of metallic zips and buttons to wear during the procedure. Subjects were then provided with ear plugs to reduce the noise of the scanner before scanning began.

The scan required the subject to assume a supine position on a stretcher bed inside the scanner (see Figure 24). Subjects were asked to fixate on a distant red LED target (located in the MR control room) through use of an inclined mirror system, this target helped to minimise eye movements which could lead to poor MR images.

The scan itself lasts approximately 5 minutes and 40 seconds with an additional 5-10 minutes to set up the subjects and to give the subjects breaks. Throughout the procedure subjects were able to communicate with the radiographer via a two way intercom system.



**Figure 24 The MR scanner and head coil (c/o Aston University Day Hospital)**

Post scanning, a set of Digital Imaging and Communications in Medicine (DICOM) files were generated. DICOM MRI files were converted to image files through use of PC based software MRicro. These image files were then accessed using MAC based freeware software mri3dX.

### **Mri3dX**

The Mri3dX program shows images in three planes; coronal, axial and sagittal. The program allows the user to proceed successively through the image slices, while simultaneously viewing images in the three plane formats (see Figure 25).

The images generated were optimised to show the fluid filled chambers of the eyes at much higher contrast than the surrounding bony orbit (Gilmartin et al. 2008). In the 3D ocular imaging technique images of the two eyes are shaded with  $1\text{mm}^3$  voxels, through use of a flood-filling algorithm. There is a considerable amount of overspill with the automatic shading function therefore manual manipulation is required. Shading manipulation requires careful examination of each MR image slice and it must be ensured that shading is contained within the ocular regions only; any overspill is subsequently corrected. The image slices are 1mm in thickness, therefore there are approximately the same number of slices as millimetres of axial length. Separate shades are used for the right and left eyes to help differentiate the data.

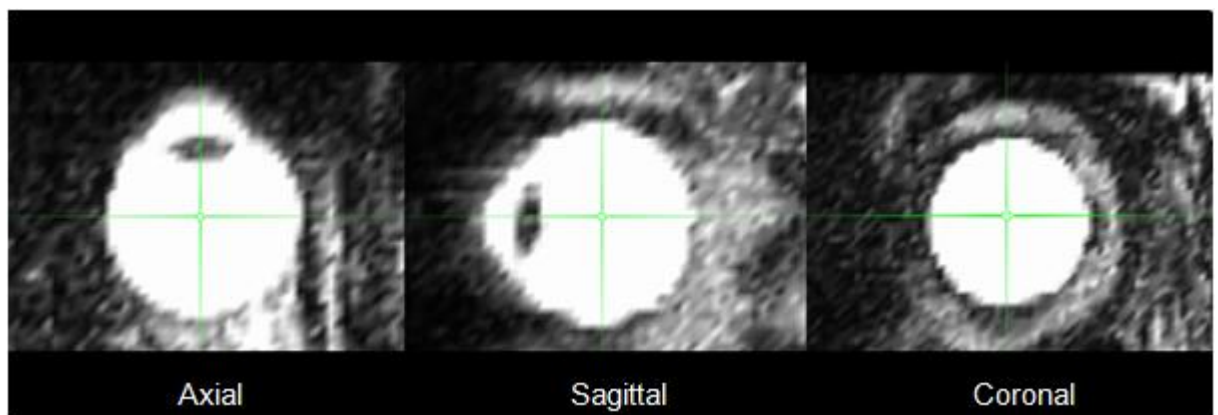


**Figure 25** The three different views presented in mri3dX. Each view shows one slice

#### **9.2.1 Ocular Volume**

For obtaining ocular volume measurements the mri3dX program calculates the number of voxels used to shade each eye and automatically produces a value in  $\text{mm}^3$ . As the flood

filling algorithm shades the fluid ocular areas only; structures such as the lens must be manually shaded to generate volume measurements.

In previous work the described procedure has been used in the calculation of anterior, posterior, and total ocular volumes (see Figure 26). A previous report defined anterior volume as the region from the anterior corneal pole to the posterior lens, and posterior volume to be from the posterior lens to the retinal surface; the sum of these two values was taken as the total ocular volume (Gilmartin et al. 2008).

**Figure 26 The division of anterior and posterior volume measurements is shown by the dashed line (after Gilmartin et al. 2008)**

### **9.2.2 Generation of quadrant and radius band values**

To produce a 3D model using the shaded MR images, a marker within the software is used to manually locate the anterior corneal pole. Although many of the measurements are independent of this manual intervention; the axial length measurement is not. Importantly the positioning of the marker does not have a significant effect on the generation of eye shape through the shrink wrap process (see Figure 27). It is envisaged that subsequent versions of the technique will automate this element of the process.

The marker movements are limited to 1mm increments; therefore in some cases it is only possible to either place the marker too far anterior or too far posterior off the cornea. Using PCI axial length (derived using the *Zeiss IOLMaster*) as gold standard, a maximum error of approximately 1mm (either side of the cornea) is expected. For consistency in this study where there has been doubt over the positioning of the marker the more posterior point has been selected each time.

Following the location of the corneal pole the mri3dX program then produces a spherical mesh which comprises of 32,768 equally distributed triangular polygons. The purpose of the mesh is to completely encapsulate the shaded eye. The sphere diameter is 30mm which ensures even eyes with large axial lengths will be encapsulated by the sphere. The sphere then undergoes a shrink wrap process whereby each of the 32,768 polygons regress towards the geometric centre of the sphere. The point at which the polygon vertices make contact with the shaded voxels is deemed to be the surface of the eye; the polygons are resized and redistributed. 3D vector coordinates are assigned to each of the polygons allowing the position of each to be tracked. The structure produced by the polygons has a corrugated surface; the model then undergoes smoothing by 20 iterations producing a smooth surface model of the eye (see Figure 27). Text files providing data on various parameters, such as radius of curvature and quadrant data are generated and saved.

**Figure 27 Graphic depicting the 3-dimensional MRI process. The first image shows the raw T2 weighted MR image. The second image shows the same scan once shaded using the mri 3dX program. The third image is a representation of the eye once the polygonal envelope has collapsed around the shaded voxels producing a rough corrugated model of the eye (Singh, Logan, & Gilmartin 2006). The final two pictures illustrate 3 dimensional models post smoothing; radius bands (as described in Methods) are visible in the final picture.**

## **Radius bands**

The mri3dX program calculates coronal ‘radius bands’ at each 1% increment along the geometric axis. These radius bands are in fact not the true radius of the eye but the equivalent spherical radius i.e. the closest spherical radius fit at that point along the axis referenced to the geometric centre. Radius bands are calculated using the constant sphere relationship below.

$$r = \frac{A}{2\pi h}$$

Where  $r$  = radius of the sphere

A=Surface area of the segment corresponding to segment width h

h= Segment width (in mm equating to 1% of the axial length)

The radius data text files are imported into Microsoft *Excel* software; data is expressed at each 1% increment of the axial length therefore producing one hundred x and y coordinate data points.

## **Quadrant data**

Data for each quadrant is produced by collapsing the 32,768 data points around the coronal axes which bisect the geometric centre of the eye. This process disregards the difference between the optic and visual axes (see section titled angle  $\alpha$ ). Each ocular quadrant thus comprises approximately 8000 points (see Figure 28).

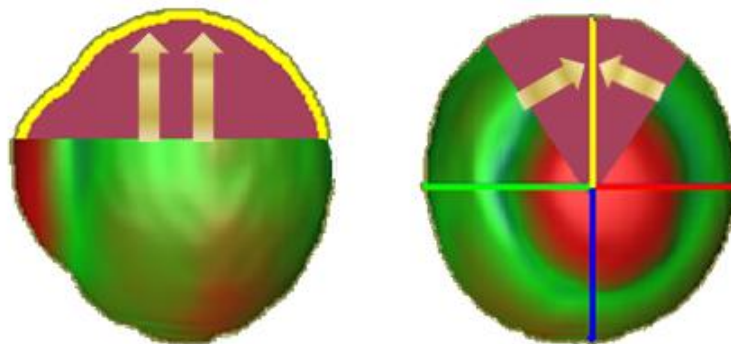


**Figure 28 The direction in which data points are collapsed to generate data for the XQ. The same methodology was applied to the +Q**

The text files are imported into Microsoft *Excel* software in which the quadrant data is reduced from ~8000 points to ~800 points through use of a macro based spreadsheet created by Dr Robert Cubbidge. The purpose of data reduction to ~800 points is to aid data management.

The text files contain data for each quadrant of the eye; the distance along the geometric axis and the distance from the geometric axis to the retinal surface (see Figure 29).

There are two sets of quadrant measurements generated by the program; superior, inferior, nasal and temporal, referred to in this thesis as XQ. The second set is the superior-temporal, superior-nasal, inferior-temporal and inferior-nasal quadrants, referred to as +Q.

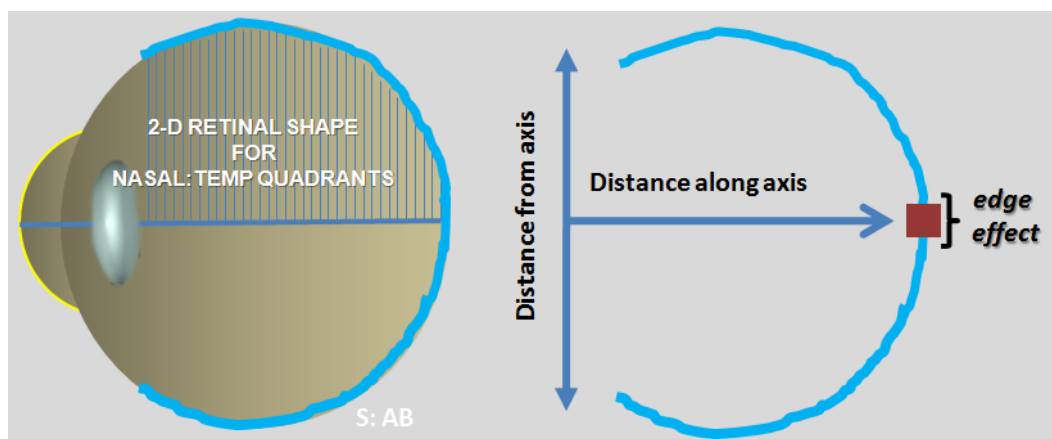


**Figure 29** The diagram shows the conversion of 3D data to 2D. Figure provided c/o Professor Bernard Gilmartin

### 9.2.3 Angle $\alpha$

The 3-dimensional MRI technique detailed above produces quadrant and radius band outputs with reference to the nominal geometric axis of the eye. The difference between the geometric (optic) axis and the visual axis is known as angle  $\alpha$ . There is both a horizontal and to a lesser extent, a vertical element to angle  $\alpha$ .

Angle alpha may be measured through ophthalmophakometry, which is a technique exploiting the positioning of the Purkinje images formed by the cornea and crystalline lens. Horizontally, angle  $\alpha$  is believed to be approximately  $5 \pm 1.2^\circ$  (Dunne et al. 1993) and vertically approximately  $2-3^\circ$  (Tscherning, 1924), however, estimates do vary considerably. Angle  $\alpha$  is difficult to measure and account for exactly. In this study to increase the validity

of measurements a correction was applied to all data; whereby the reference point was shifted from the geometric axis to an adjacent and parallel axis originating from the most posterior location on the retina. Through the period of this study alternative techniques were attempted to derive angle  $\alpha$  prior to the methodology described above being selected. Estimates of angle alpha were made mathematically using data from the Oculus Pentacam, the MRI data sheets and from simple trigonometry. The calculated values showed large variations between techniques; these techniques were rejected in favour of a differentiation method using the second order polynomial coefficients. The data was referenced to the axis running from the most posterior retinal location of the eye.

#### **9.2.4 Previous reports using the Aston University MR scanning protocol**

In 2006 Singh *et al.* detailed their patented technique for obtaining 3-dimensional ocular images and data (International Patent Application number PCT/GB2005/004577: *Method and Apparatus for Imaging the Eye*). Validity of surface measurements was established through use of phantoms, and internal measurements by correlations of MRI derived axial length with PCI derived axial length. In addition to describing the methodology, the paper focused on findings with reference to refractive error. A total of seven subjects underwent the MR imaging; MSE ranged from +4.00D to -16.25D MSE. A chief finding was the high level of inter subject variability. Furthermore nasal and temporal quadrant asymmetries were also noted in some individuals; the temporal quadrant was shown to be more bulbous than the nasal. The same protocol was used in a subsequent series of ARVO Abstracts to describe the radius bands in a cohort of 20 subjects (Gilmartin *et al.* 2007). The radius bands were subdivided into quartiles along the axial length. The anterior aspect of the eye did not show significant differences; the significant change in shape between refractive groups took place at the cusp of the 3<sup>rd</sup> and 4<sup>th</sup> quartiles. The posterior 25% appeared to steepen in myopic subjects and flatten in less myopic or emmetropic/hyperopic subjects. This finding is particularly important as it indicates that although the anterior region of the eye may contribute to the development of myopia, it appears relatively unaffected by myopia itself. The findings were reinforced through examination of ocular volume; whereby anterior ocular volumes were not found to be significantly different amongst refractive groups, however, posterior volume showed larger volumes in myopic subjects and relatively smaller volumes in emmetropic subjects (Gilmartin *et al.* 2008). The original program had allowed only +Q data to be generated; a later software amendment allowed generation of XQ data. To further evaluate nasal *vs.* temporal asymmetry, the data were used to assess differences in

the curvature of XQ and differences in the maximum distance from the presumed visual axis to the ocular surface (Nagra et al. 2009). The data were plotted graphically for each quadrant and fitted with second order polynomials; the  $x^2$  coefficient was taken to be an indicator of curvature or bulbosity. Maximum distance from the presumed visual axis was derived through differentiation of the polynomial coefficients. Due to previous reports of differences in 4<sup>th</sup> quartile ocular shape between refractive groups, this region was examined separately. The chief finding was the relative expansion of the temporal quadrant in the intermediate region of the eye; on average the temporal quadrant was larger in myopic subjects by 0.82mm.

The protocol used for original recordings varied slightly from the protocol used in the current study; initially the voxel size was set at 0.5 x 0.5 x 1.0mm (prior to Oct 2006), this was subsequently amended to 1.0 x 1.0 x 1.0mm to produce more congruent isotropic voxel dimensions.

In summary, the 3-dimensional MR imaging technique provides data on previously inaccessible areas of the eye. Thus far, data have shown significant inter refractive group differences particularly in the posterior 25% of the eye; inter quadrant differences have also been reported. Expansion of cohorts and a wider range of refractive errors will allow accurate ocular models to be constructed for each refractive group.

### **9.3 Purpose**

To evaluate and develop models of eye shape with reference to refractive error using the 3-dimensional ocular MRI techniques developed at Aston University.

### **9.4 Hypothesis**

Based on previous literature it is predicted that myopes will have a larger eye size and myopic eyes will display a prolate or less oblate shape. Posterior ocular volume is hypothesised to increase as a factor of increasing myopia. The calculations of eye size are predicted to be larger in the myopic eyes and exhibit quadrantic differences. Based on previous analysis of a smaller cohort using the same technique it is predicted that the temporal quadrant may show increased stretch in myopic eyes.

### **9.5 Methods**

A total of 76 subjects underwent MR scanning. Subject ages ranged from 18 to 47; approximately 30 males and 46 females. The majority of subjects were of White or British Asian origin; two subjects were East Asian and a further two subjects were of African origin.

Mean Spherical Error (MSE) ranged from -19.76 to +4.38D and refractive error measurements were obtained under cycloplegia using the Shin Nippon SRW-5000. Three subjects were excluded on the basis that their myopia was greater than 15D and therefore were atypical myopes. One of the excluded subjects was under hospital review for possible Marfan's syndrome and another had a known posterior staphyloma. PCI axial length measurements were measured using the Zeiss *IOLMaster* (Carl Zeiss, Germany) and ranged from 21.75 to 28.12mm. Data were analysed with reference to MSE; refractive groups were divided as follows:

High Myopes: Myopia greater than or equal to 6D

Low Myopes: Myopia less than 6D but greater than or equal to 0.75D

Emmetropes: -0.5D to 1.5D

Hyperopes: Hyperopia greater than 1.5D

There were a relatively small number of hyperopes therefore not all analyses include the hyperopic subject group.

<b>Refractive group (<i>n</i>)</b>	<b>Mean MSE <math>\pm</math> SD</b>
High myopes (18)	-8.14 $\pm$ 1.44
Low myopes (22)	-2.93 $\pm$ 1.65
Emmetropes (26)	+0.06 $\pm$ 0.40
Hyperopes (7)	+2.86 $\pm$ 1.18

**Table 3 The distribution of refractive error within the cohort**

Several different aspects of the MR data were investigated; the methodology for each is detailed below.

### **9.5.1 Radius bands**

The original data collated by Gilmartin *et al.* 2007 on radius bands was expanded from 20 to 73 subjects. Data were analysed as a function of refractive group. The previous protocol of examining by quartiles was repeated (see Figure 30).

**Figure 30 Diagrammatical representation of the various parameters of ocular shape measured as part of this study.**

### 9.5.2 Ocular volumes

The original data set of 39 subjects presented by Gilmartin *et al.* 2008 was expanded upon to 73 subjects, both right and left eye volumes were measured. Data for the anterior, posterior and total volume were calculated and analysed (see Figure 26).

Ocular volume for the posterior 25% could not be obtained via the shading technique as there were no definite reference points defining the posterior 25% in the raw MR images. A calculation of the posterior 25% volume was made through graphically plotting the data for each pair of quadrants (nasal-temporal and superior-inferior) for the posterior 25% region, the data were then fitted with a second order polynomial, the curve was integrated and rotated, a total ocular volume for the posterior 25% derived by the addition of the two volume values.

### 9.5.3 Quadrant data

The quadrant data for the right eye (normally the dominant eye) of each individual were plotted graphically; data for the distance along the optic axis was plotted against the data from the axis to the retinal surface. To evaluate the quadrant differences the distance of the chord from the retinal surface to the optic axis was subtracted from the equivalent chord for the opposite quadrant i.e. N-T, S-I, SN-IT, and ST-IN (see Figure 43). For additional details regarding each of the quadrants, the maximum distance from the presumed visual axis to the retinal surface was evaluated. Previous work had shown large refractive group differences in the maximum distances of temporal quadrants; the temporal quadrant was therefore of particular interest (Nagra et al. 2009).

Further evaluations were carried out through fitting data with second order polynomials (see Figure 31). The  $x^2$  coefficient was taken to be an index of curvature or bulbosity and evaluated using a mixed repeated measures ANOVA for both the XQ and the +Q. Subsets of data were plotted from the distance 25%-75% along the presumed visual axis for each quadrant. The data were then plotted for just the posterior 25% of the eye and similarly evaluated. In addition to investigating inter-quadrant, differences between refractive groups with respect to quadrants were made.

To aid analysis of quadrant data a macro based template was developed by Professor Bernard Gilmartin; data was processed via this template and then extracted for various analyses.

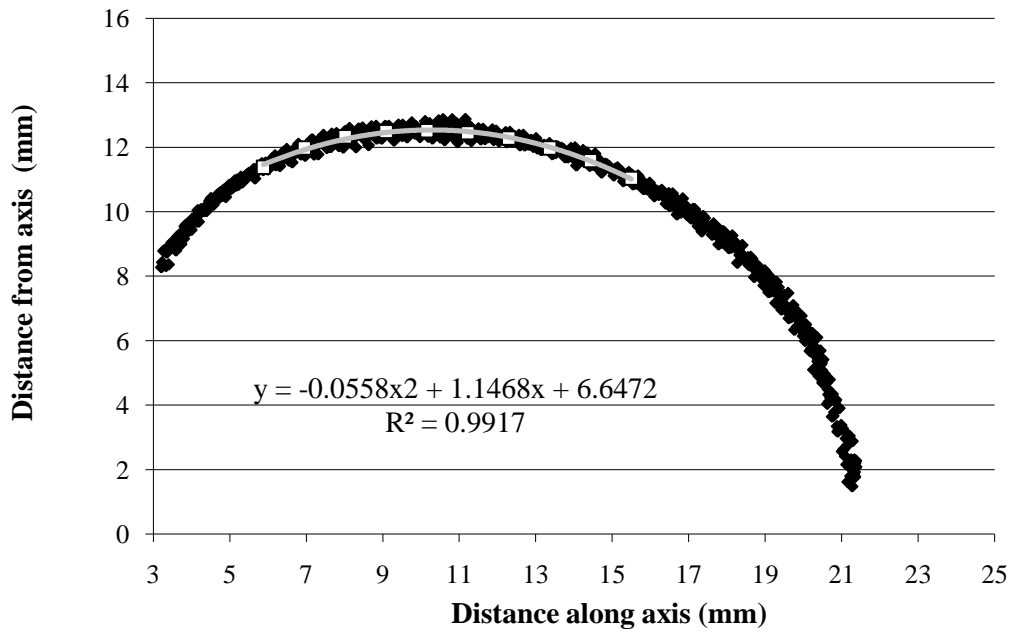


**Figure 31 Data plotted for the region 15-100% along the axis. 2<sup>nd</sup> order polynomial fitted for the region 25-75%.**

#### **9.5.4 Stretch index**

To further examine the consequences of myopic growth, a stretch index was calculated as the ratio of the width of the eye at a given point versus the axial length. This technique was used for examining specific retinal locations; in this thesis the technique was used to evaluate the point 40° temporal to the presumed foveal position (see 14.4).

#### **9.5.5 Interval Variation (IV)**

As a further measure of shape variation the standard deviations of the data comprising the 25-75% region of the eye and separately the posterior 25% of the eye, were derived and interval variance calculated by multiplying standard deviations by a value of 1.96. Interval variation was examined at every 5% increment along the axial length for the 25-75% region and every 2.5% increment in the posterior 25%. The IVs were examined with reference to refractive group and quadrants. The IV values helped evaluate the shape variance across sections of the eye.

### **9.5.6 Surface areas**

The surface area for the posterior 25% of each quadrant was calculated through use of a formula developed by Dr Brian Cox and Professor Bernard Gilmartin, (see chapters 12 and 13 for details).

### **9.5.7 Inter eye differences**

A subset of 18 eyes were examined for inter eye differences; both XQ and +Q were investigated. The data depicting the distance along the axis *vs.* distance to the retinal surface were examined. Also comparisons between ocular volumes were made between right and left eyes.

## **9.6 Results**

### **9.6.1 Radius bands**

The radius bands were plotted graphically; they detailed the equivalent radius of curvature in 1% increments along the geometric axis. For the region approximately 25% along the axis to 75% along the axis, the low myopic and emmetropic groups showed a relatively constant spherical shape. The radius data for the high myopes were flatter compared to other refractive groups, but also maintained a spherical shape in this central region. The hyperopes, although limited in number, showed steeper radius of curvature data compared to other refractive groups in this central region (see Figure 32). A repeated measures ANOVA evaluating the four quarters (0-25%, 25-50%, 50-75%, and 75-92%), showed no significant differences between the 25-50 and 50-75% regions ( $p>0.05$ ). There were significant differences between the posterior 75-92% region and the 25-50 and 50-75% regions ( $p>0.001$ ). The only refractive group difference to reach significance was between hyperopic group *vs.* emmetropic, low myopic, and also high myopic groups.

Posterior eye data were noisy due to eye movements and edge effect artefacts. Previous work at Aston University involved a subject undergoing MR scanning 9 times; these data was used to check repeatability using an ANOVA analysis ( $p>0.05$ ) (Gilmartin et al. 2007).

Examination of the standard deviations for each of the refractive groups showed increased values around the 92% point (the distance 92% along the axis); based on these previous findings all data beyond the 92% region was omitted.

In the posterior region of the eye high myopes and low myopes showed relative steepening of curvature; in contrast the emmetropic subjects showed relative flattening of curvature. The hyperopic group comprised a limited number of subjects; results from the hyperopic group showed relative flattening in the posterior region. Standard deviations were much greater in the anterior 15% of the eye and fell sharply beyond this point. On average the standard deviations in the anterior 15% for emmetropes, low myopes, high myopes and hyperopes were  $\pm 2.92$ , 2.69, 2.96, and 3.65mm respectively. The standard deviations fell to  $\pm 0.61$ , 0.61, 0.86, and 0.87mm for the region beyond 15% along the axis.

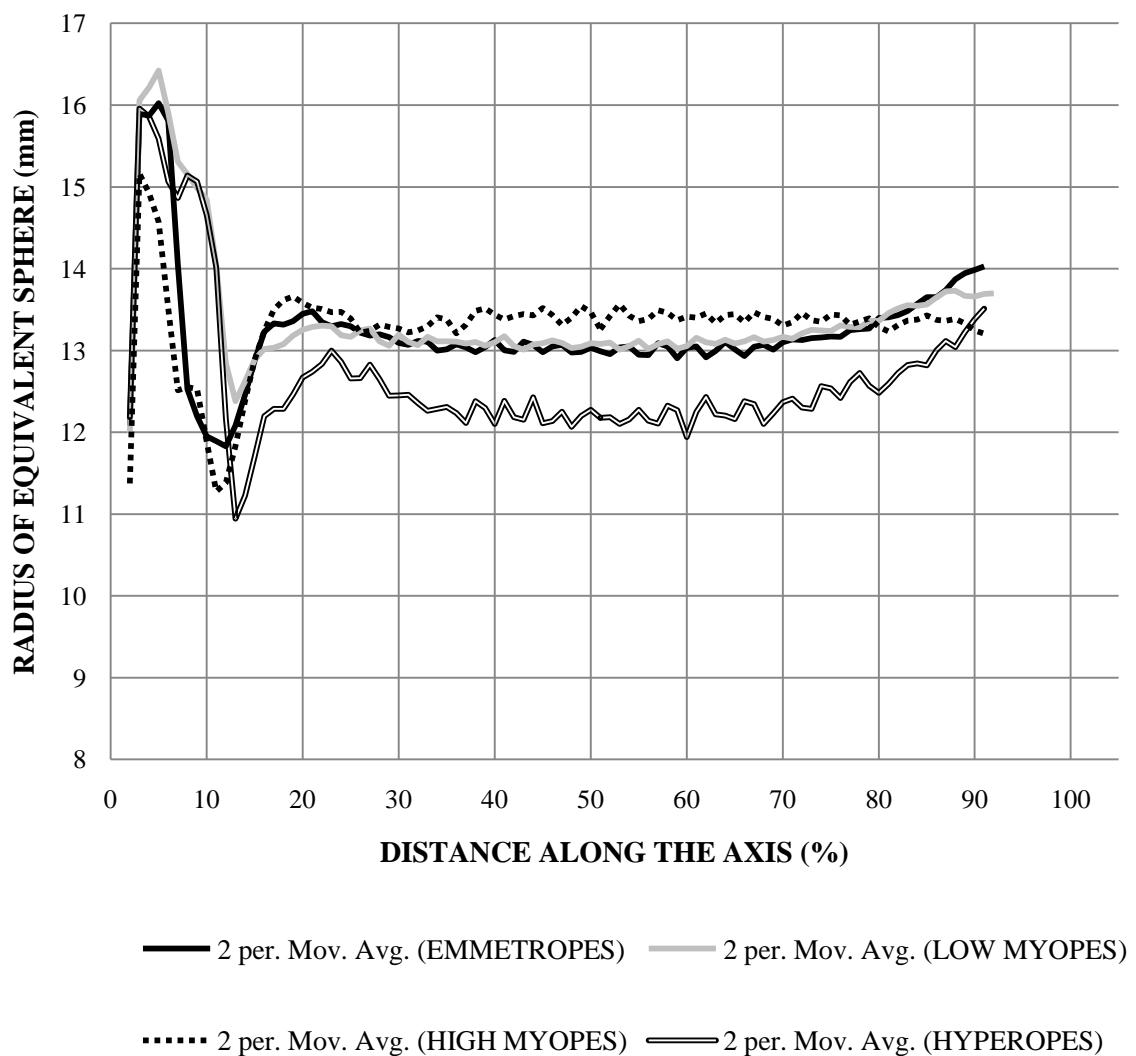


**Figure 32** The equivalent radius of curvature by refractive group. Each data set is fitted with a moving average trendline; averaging every second point

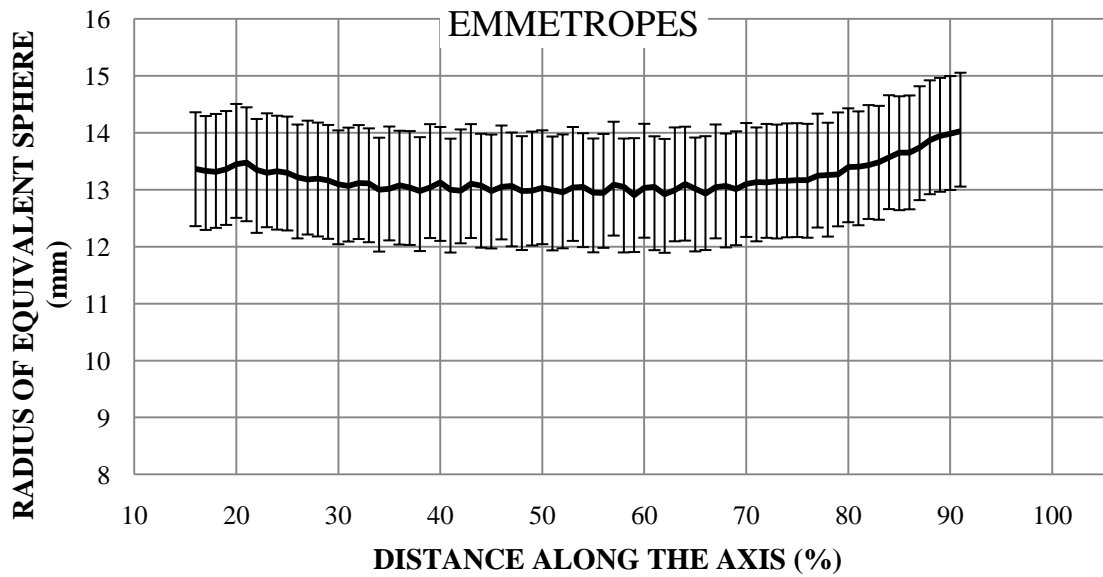


**Figure 33 Shows the standard deviation error bars for the emmetropic refractive group in the region 15-92% along the axis**

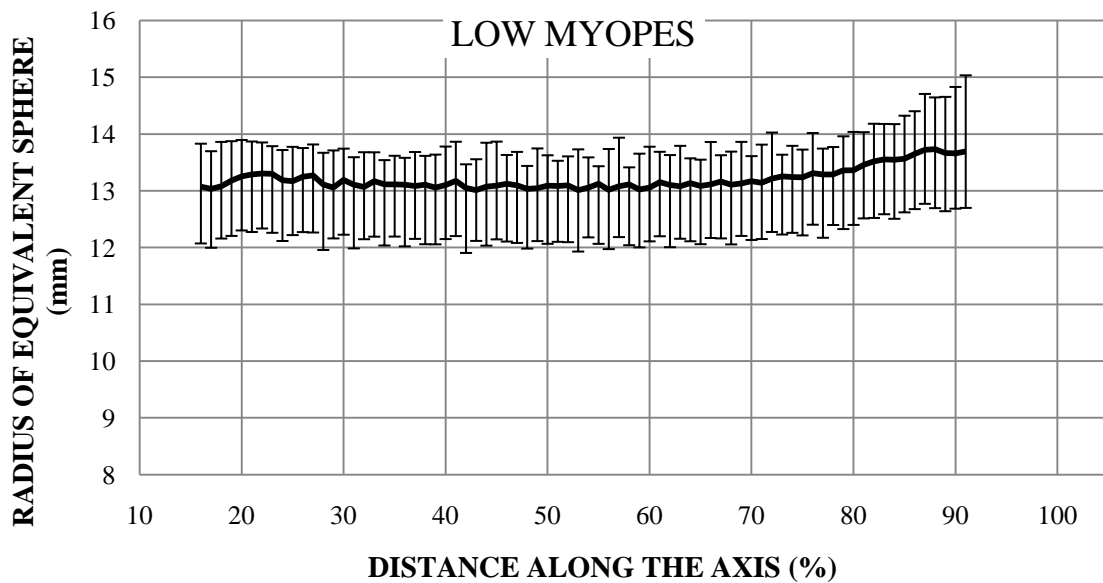


**Figure 34 Shows the standard deviation error bars for the low myopic refractive group in the region 15-92% along the axis**

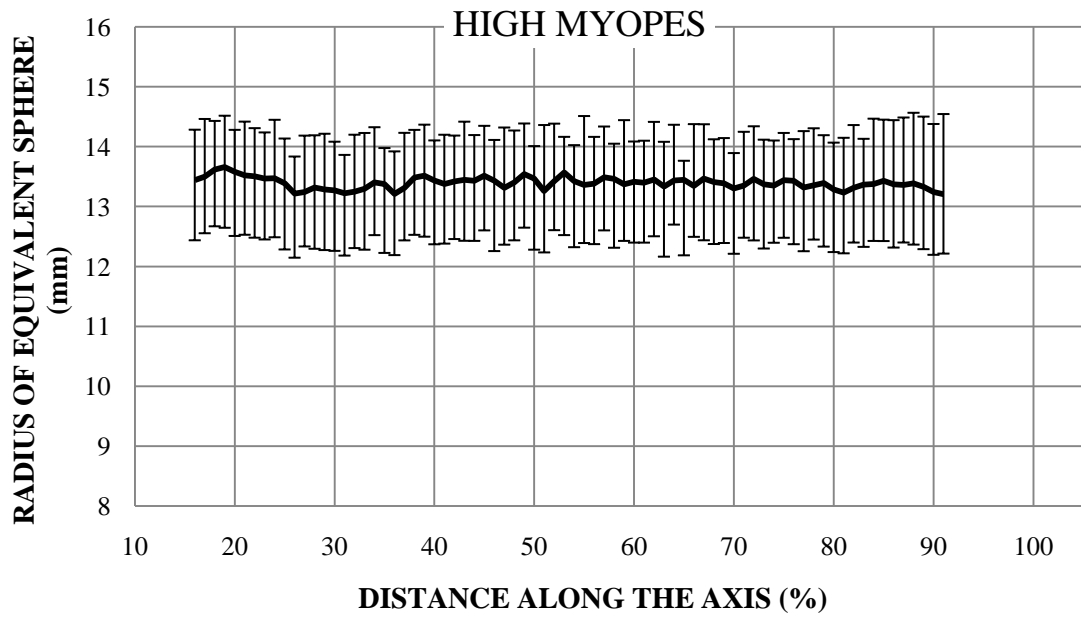


**Figure 35 Shows the standard deviation error bars for the highly myopic refractive group in the region 15-92% along the axis**

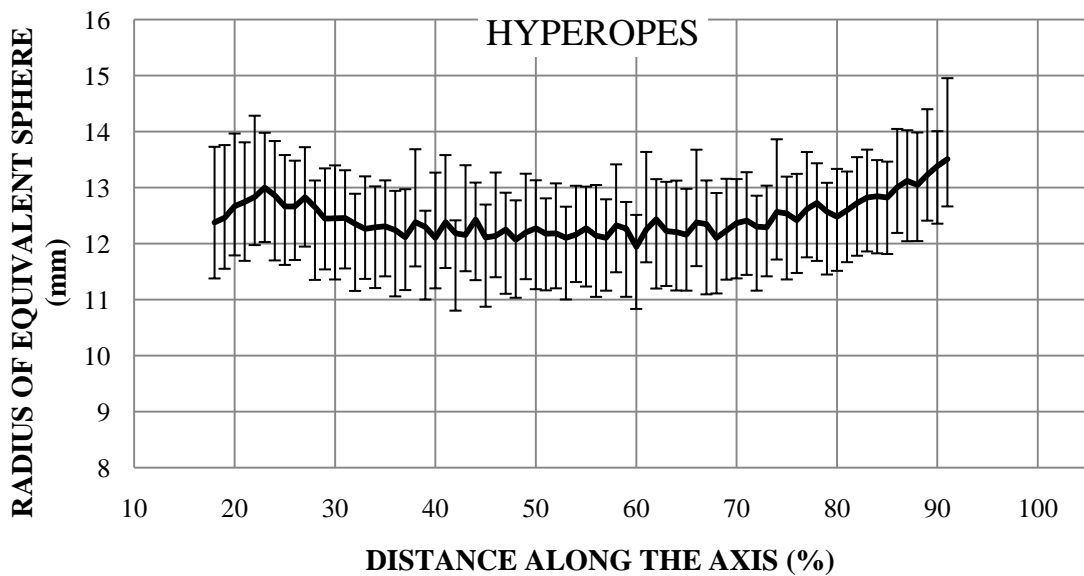


**Figure 36 Shows the standard deviation error bars for the hyperopic refractive group in the region 15-92% along the axis**

To evaluate further the apparent sphericity noted in the central region (~25-75% region) in all refractive groups, each set of data was fitted with higher order polynomials (6<sup>th</sup> order).

Although each refractive group showed a region of sphericity for some part of the central region, variations were evident following through fitting of higher order polynomial curves. The region of sphericity began at a distance approximately 40% along the axis, unlike the previously proposed 25% mark (see 9.6.1). The total region of sphericity was largest for the high myopes and hyperopes. The emmetropes and low myopes showed the greatest amount of variation.

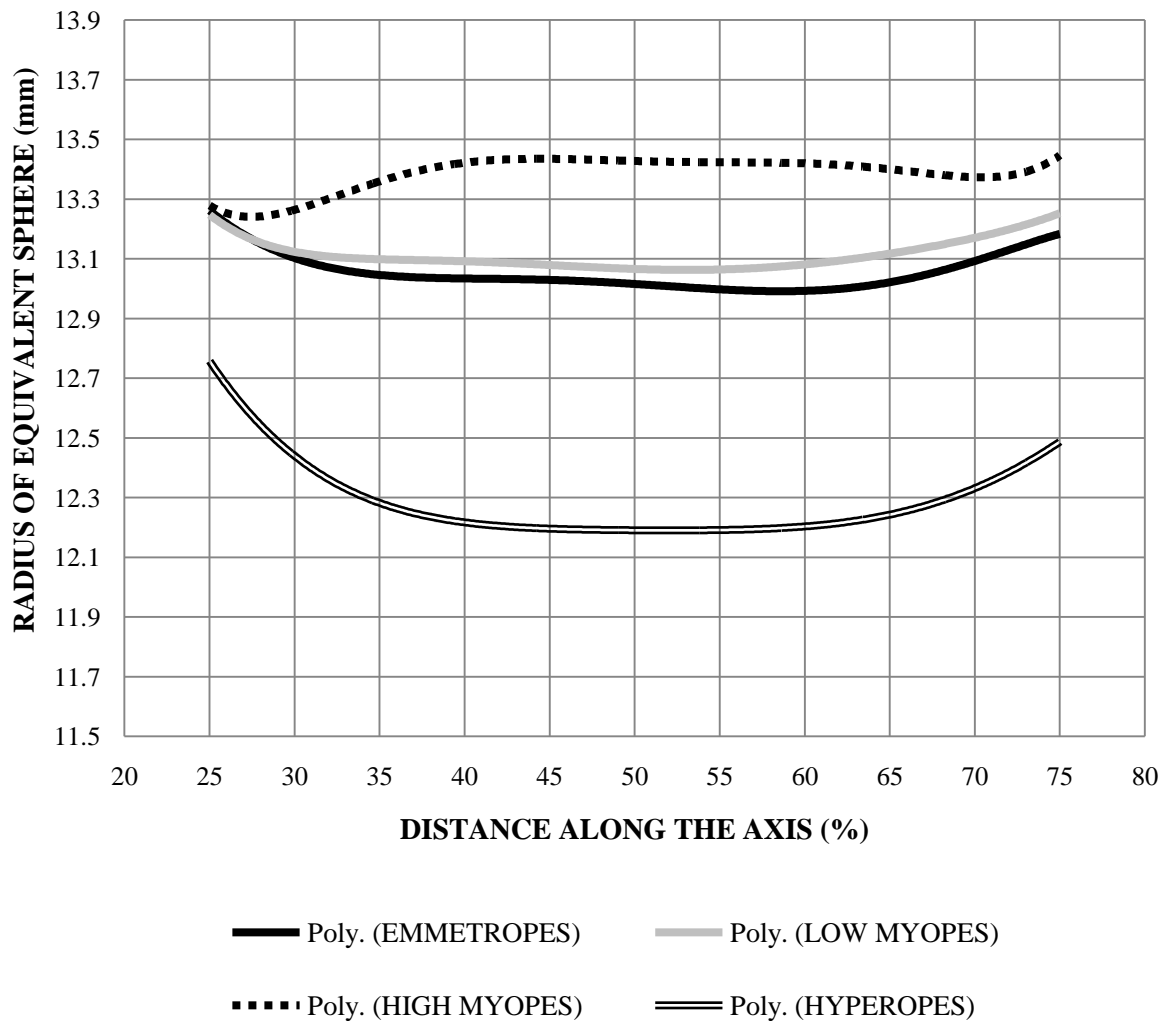


**Figure 37** The equivalent radius data fitted with 6<sup>th</sup> order polynomials to expose subtle changes in shape

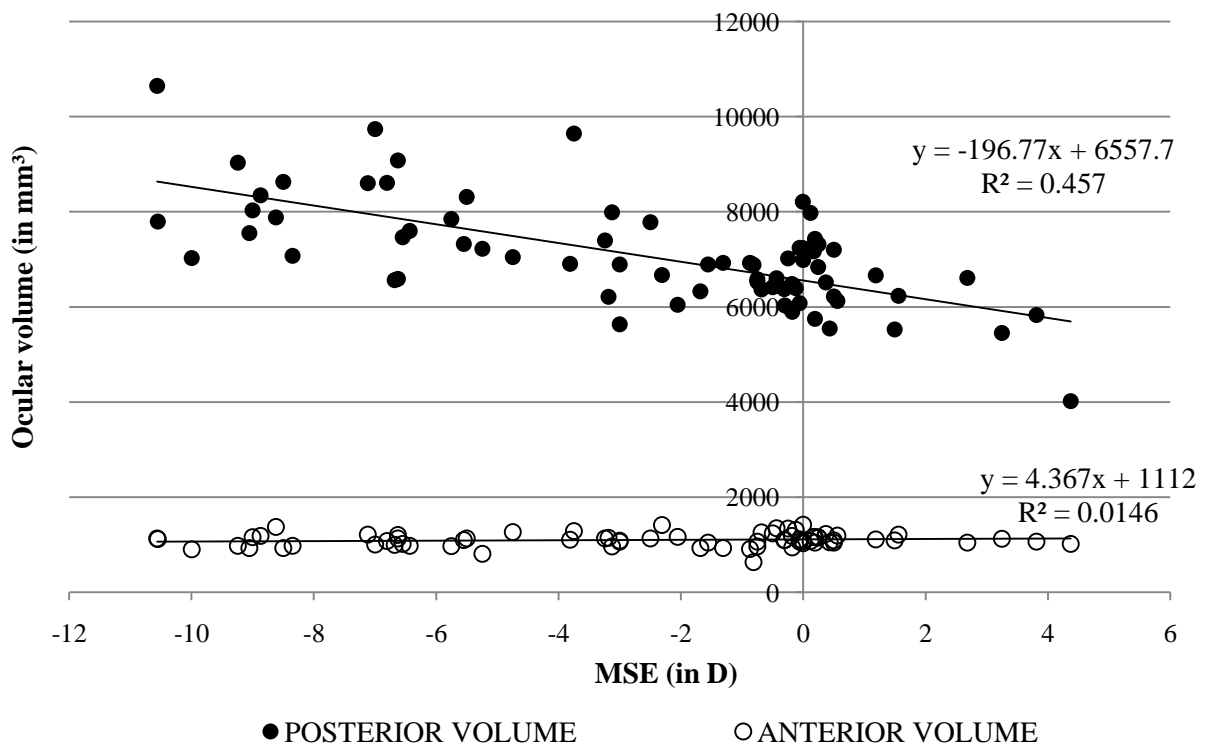
### 9.6.2 Ocular volumes

#### Anterior vs. Posterior volumes

Ocular volumes were calculated using the same methodology as previously reported by Gilmartin *et al.* 2008. Ocular volume for the posterior 25% could not be obtained via the

shading technique due to limitations in determining the reference points defining the posterior 25%; therefore a calculation through integration was used to derive volume in this region.

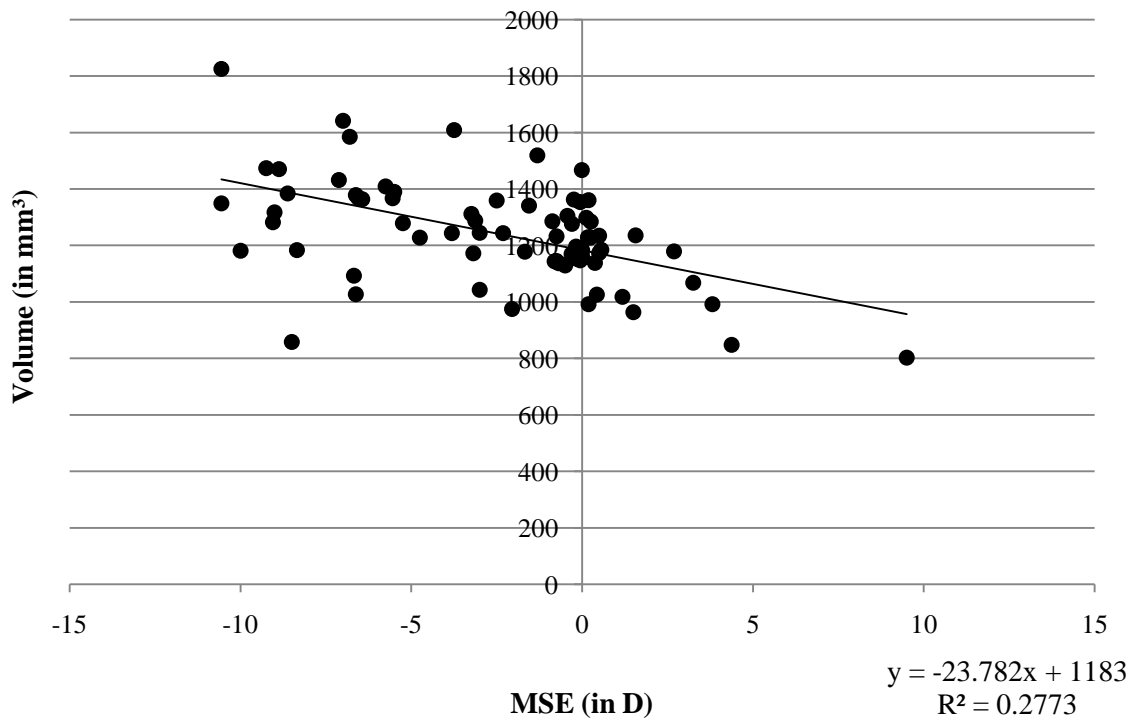
Subject data for the posterior and anterior volumes was plotted as a function of refractive error. The results supported earlier findings which showed the anterior volume was constant across all refractive groups, and posterior volume increased linearly as a function of increasing myopia. Gilmartin *et al.* (2008) reported  $R^2$  values for posterior volume *vs.* MSE of 0.53 and 0.01 for anterior volume *vs.* MSE. The current study showed similar values (see Figure 38). A Pearson's one tailed correlation coefficient showed the posterior volume correlation with MSE to be significant ( $p < 0.01$ ,  $r = -0.676$ ), and as expected there was no significant relationship between anterior volumes and MSE ( $p > 0.05$ ,  $r = 0.121$ ) or between anterior volume and posterior volume ( $p > 0.05$ ). The overall total volume was significantly correlated with MSE ( $p < 0.01$ ).



**Figure 38** The anterior volumes (below in grey) and posterior volumes (above in black) plotted as a function of MSE. Data is shown for RE only ( $n=73$ ).

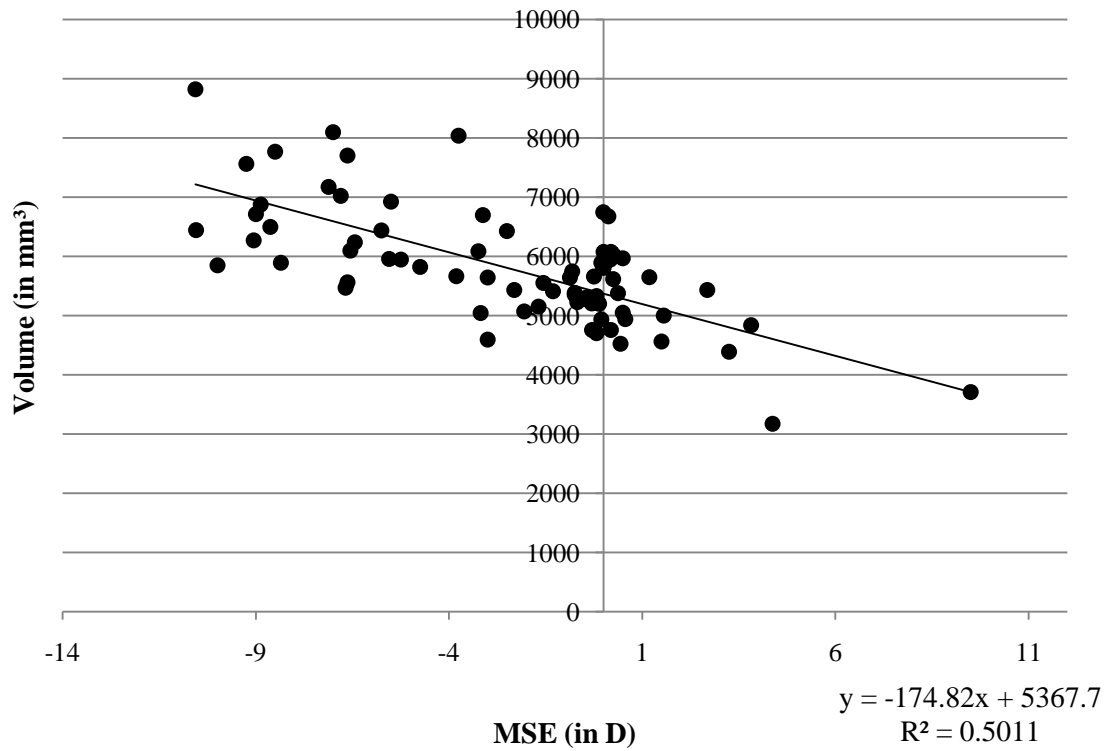
**Posterior 25% cap volume (calculated through integration of polynomial curves)**

The posterior 25% volumes showed an increase in volume which corresponded with an increase in myopia.



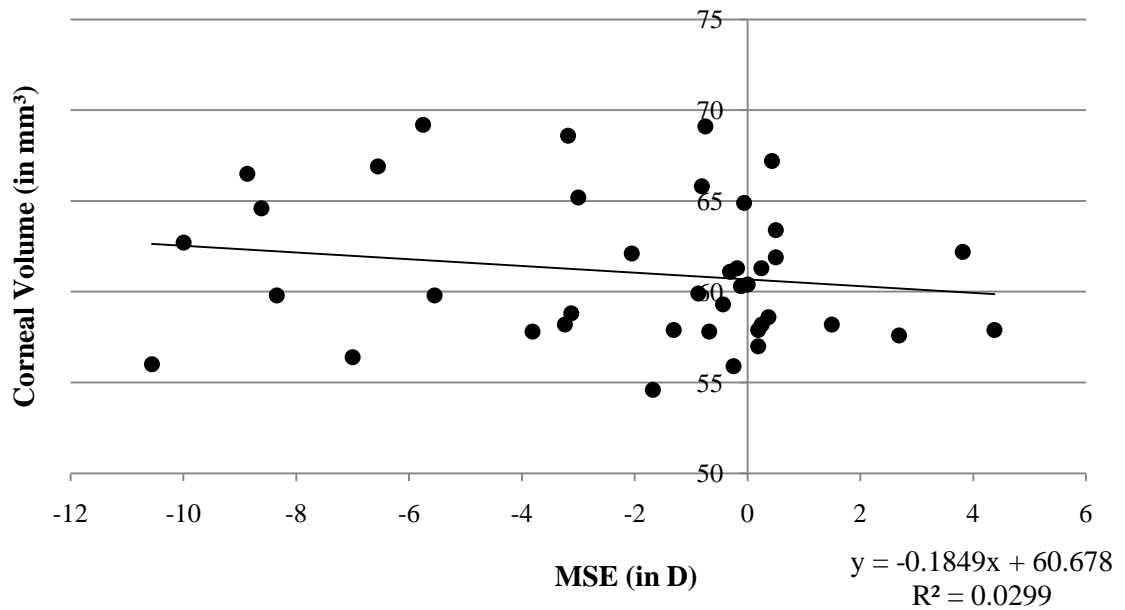
**Figure 39** The volume for the posterior 25% plotted as a function of MSE

The volume for the posterior 25% cap of the eye was then subtracted from the posterior volume defined earlier as the region between the retinal surface and the posterior crystalline lens. The results showed that the posterior 25% volume made little difference to the posterior volume vs. MSE relationship (see Figure 40).



**Figure 40 The posterior volume minus the posterior 25% volume**

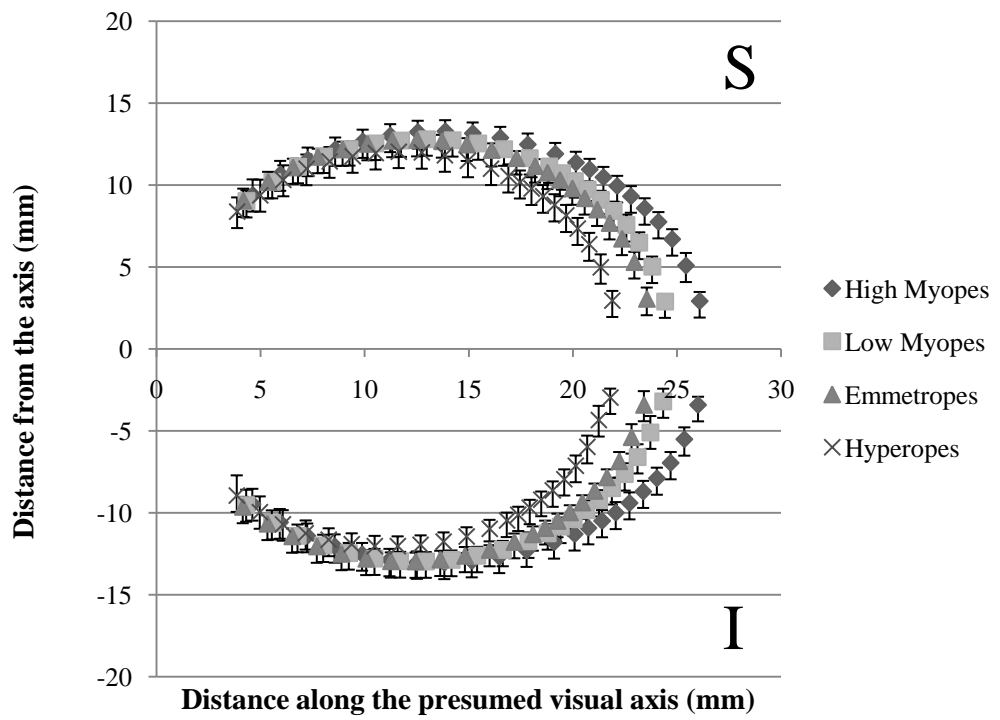
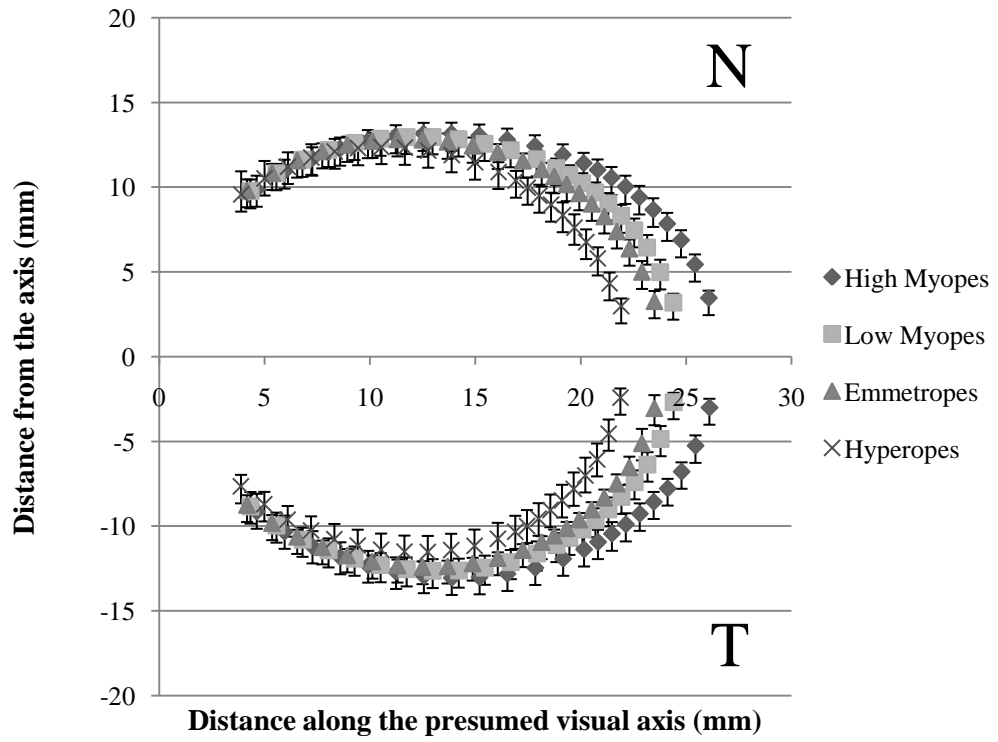
In order to investigate the ocular volume further, corneal volumes were measured using the Oculus Pentacam on a subset of 42 subjects, mean MSE  $-2.05 \pm 3.69D$  (see Figure 41). Corneal volume did not show a significant correlation with MSE, which reaffirms the notion that the volume of the anterior eye is not affected by ocular shape changes present in myopia.



**Figure 41 Corneal volume (via the Oculus Pentacam) vs. MSE (D) ( $p > 0.05$ ,  $r = -0.173$ )**

### 9.6.3 Quadrant data

The data for different quadrants was examined using several methods. The simplest qualitative tool used was plotting the distance along the presumed visual axis against the distance to the retinal surface. The graphs were plotted for each of the meridians; nasal vs. temporal (N-T), superior vs. inferior (S-I), superior-nasal vs. inferior-temporal (SN-IT) and superior-temporal vs. inferior-nasal (ST-IN). Sections of these graphs were then evaluated through polynomial curve fitting and chord measurements. Visual inspection of the graphs for each meridian clearly showed the highly myopic eyes to be largest posteriorly, and hyperopes to be smallest. In general, the plots for the myopic subjects could be described as showing equatorial stretch. Interestingly, the anterior regions showed some overlap between refractive groups, however, discrepancies between the presumed and actual visual axis may have affected the results. It is difficult to quantify how much the discrepancy, angle  $\alpha$ , would have affected the results, but based on previous literature it is expected to be a relatively small amount.



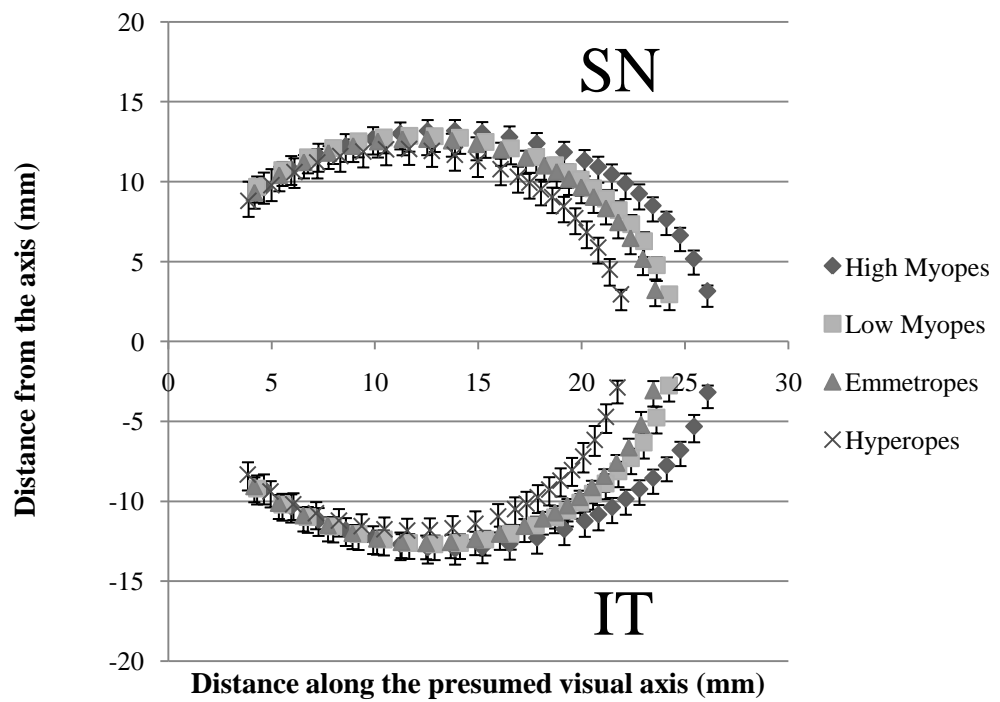
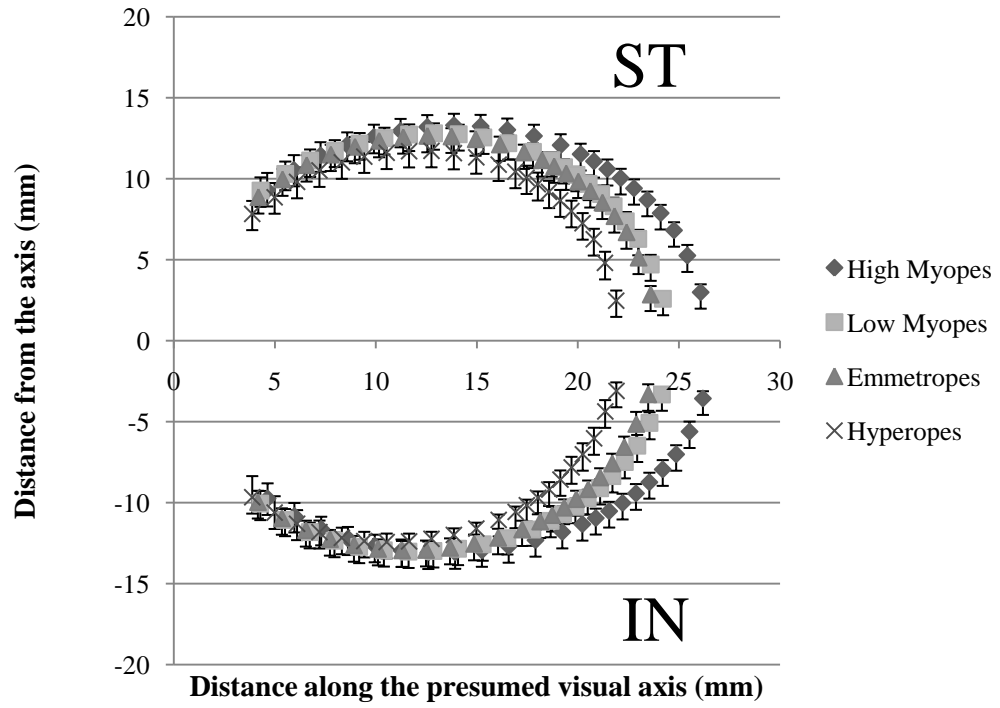
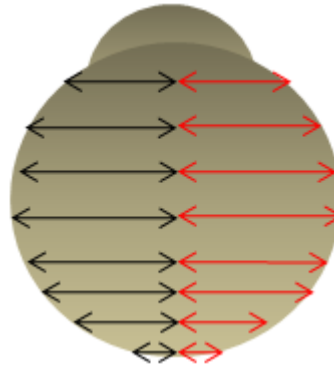


Figure 42 A graphical representation of the retinal contours by quadrant

### **Chord differences**

To evaluate quadrant differences, the chord distances between two parallel quadrants or meridians i.e. N-T, S-I, SN-IT, and ST-IN, were calculated and plotted graphically (see Figure 43).



**Figure 43 Nasal and temporal chord distances. Temporal chord distances were subtracted from nasal and plotted graphically. The same methodology was used for S-I, SN-IT and ST-IN quadrants.**

### **Quadrants: XQ**

The N-T chord differences appeared to follow the same basic pattern for all refractive groups for the region ~15-75% along the optic axis. Interestingly the N-T chord differences in the posterior region appeared to be at similar levels for all refractive groups at approximately 75% along the axis, the difference values between nasal and temporal chords at this cross over point ranged from approximately 0.1-0.05mm. In general the nasal chord was larger than that of the temporal up to the ~75% mark; beyond this point the hyperopes and emmetropes showed the temporal chord to be larger than the nasal (hence the negative values when the temporal chord value is subtracted from the nasal). A repeated measures ANOVA was carried out to compare chord differences up to the 76.25% mark and then beyond the 76.25% mark; 76.25% was selected as it was the closest point to 75% for which values had been derived. For chord differences up to the 76.25% mark results showed significant differences between all refractive groups ( $p < 0.001$ ). Chord differences beyond the 76.25% mark showed significant refractive group differences between all groups ( $p < 0.05$ ) bar the high myopes vs. low myopes, low myopes vs. emmetropes, and emmetropes vs. hyperopes.

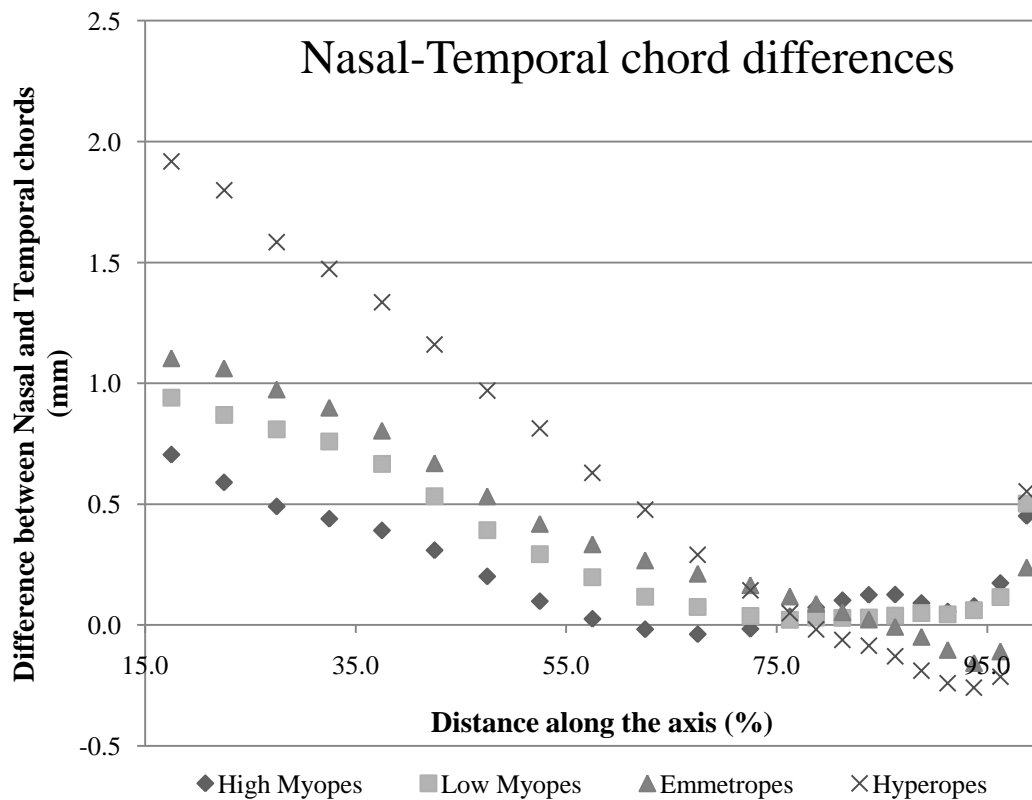


**Figure 44 Differences between the nasal and temporal chords in each refractive group**

A repeated measures ANOVA for superior-inferior chord differences up to the 76.25% mark showed significant refractive group differences between all groups ( $p < 0.05$ ) bar the low myopic vs. hyperopic group. In the posterior region significant refractive group differences were noted for all groups ( $p < 0.05$ ) bar the high myopic vs. low myopic and high myopic vs. emmetropic groups.

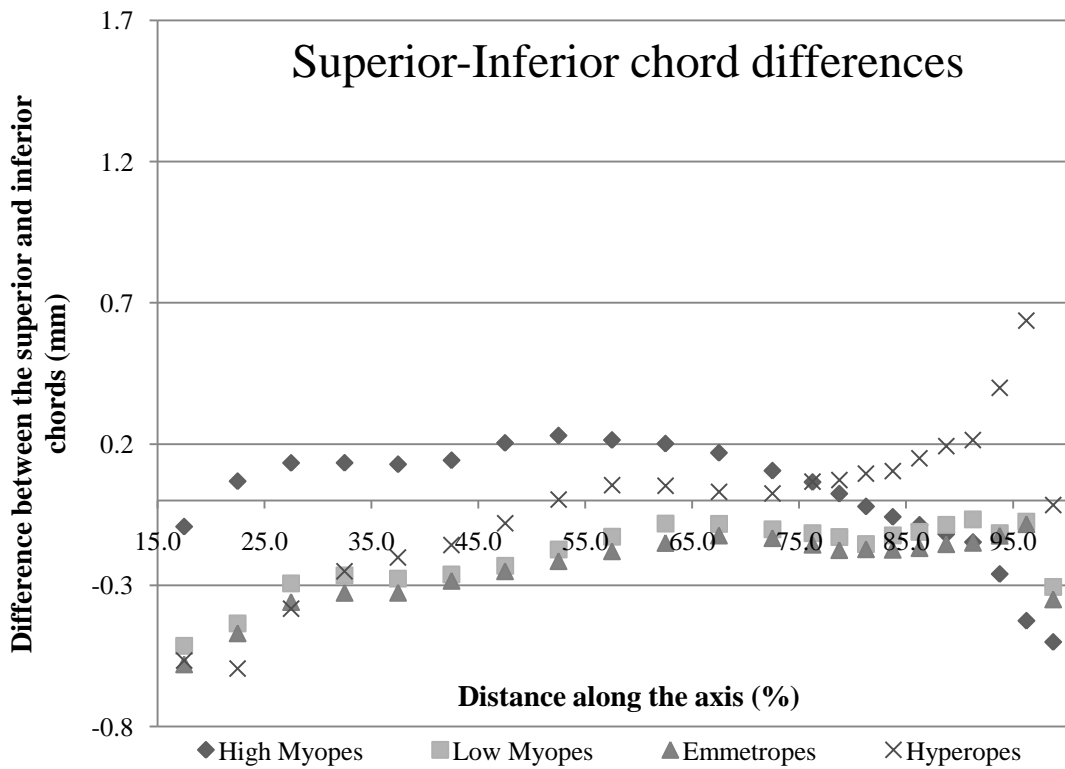


**Figure 45 Differences between the superior and inferior chords in each refractive group**

Examination of standard deviations showed variance to be highest in the anterior and posterior regions of the eyes. Standard deviations were at a minimum at approximately 80% along the presumed visual axis.

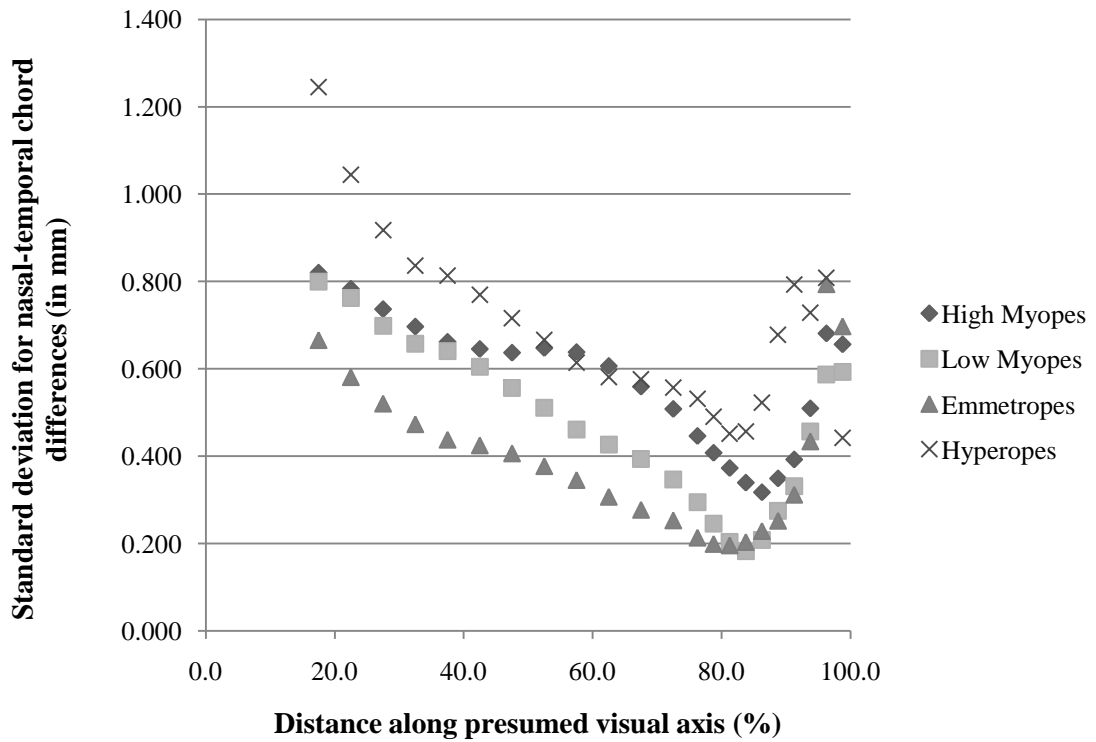


Figure 46 Standard deviations for each refractive group, nasal-temporal quadrants

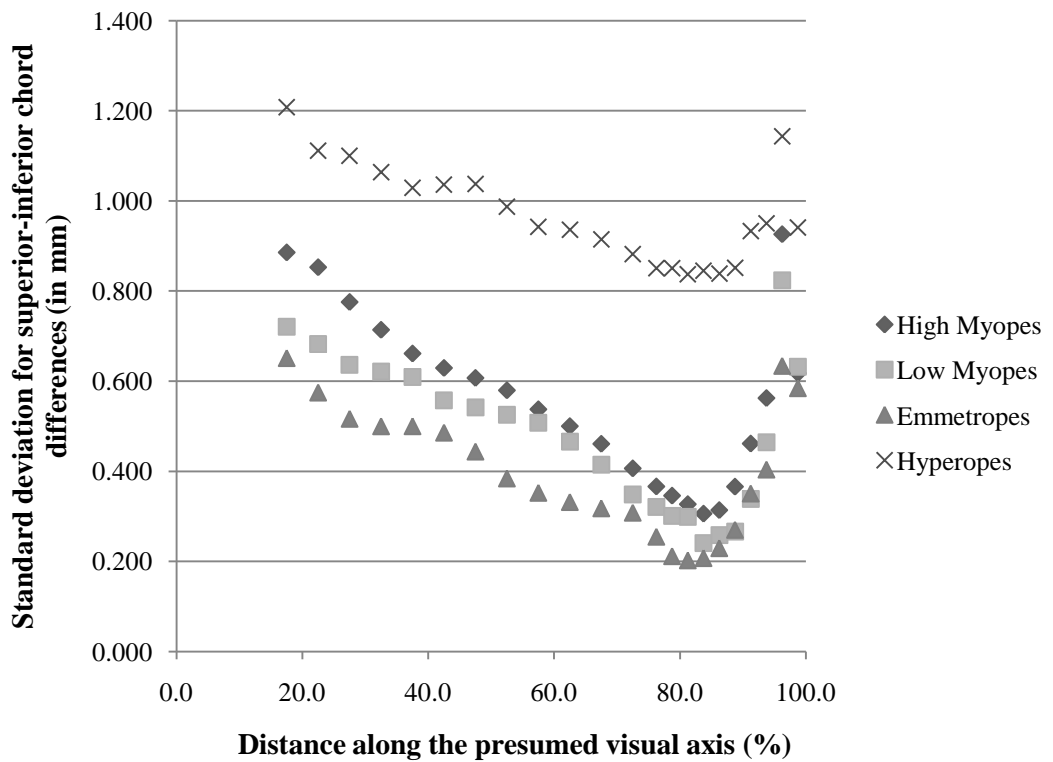
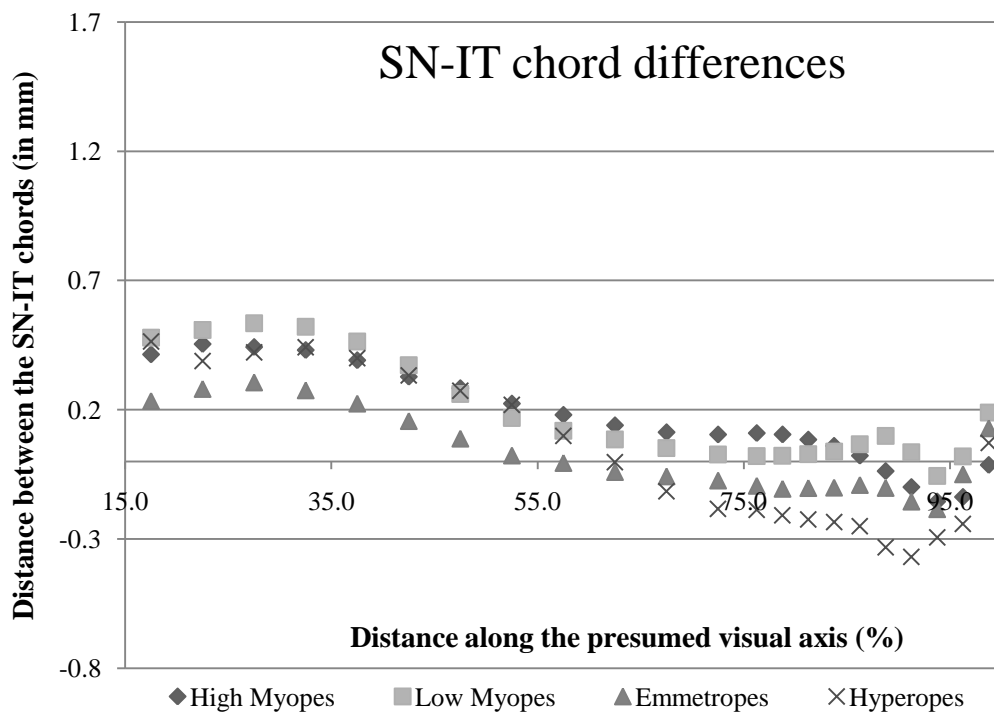


Figure 47 Standard deviations for each refractive group, superior-inferior quadrants

### Quadrants: +Q

A repeated measures ANOVA for the region 17.5-76.25% showed significant refractive group differences between all groups ( $p < 0.05$ ), bar the high myopic vs. low myopic and highly myopic vs. hyperopic groups. Results for the region posterior to the 76.25% mark showed significant refractive group differences for the hyperopic vs. emmetropic, high myopic and low myopic refractive groups. Significant refractive group differences in this region were also noted between the low myopic and emmetropic groups

In general the SN chord appeared to be larger than the IT; however in the posterior region of the eye the SN chord was noticeably smaller than the IT for the hyperopic group.



**Figure 48** The differences between the SN and IT chords for each refractive group

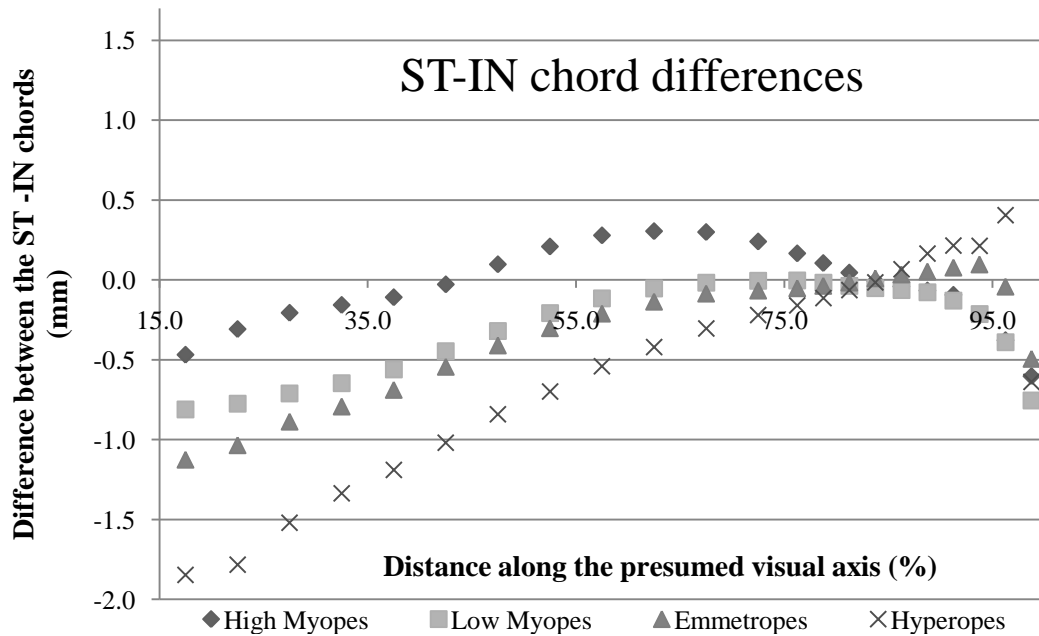


**Figure 49 The differences between the ST and IN chords for each refractive group. NB scaling differences of y axis compared to SN-IT chord differences graph**

The ST-IN chords showed the IN to be larger than the ST, but again changes were noted beyond ~75% (see Figure 49). For the region 17.5-76.25% along the presumed visual axis, a significant refractive group difference was noted for all groups ( $p < 0.01$ ). Beyond the 76.25% mark, refractive group differences failed to reach significance ( $p > 0.05$ )

The standard deviations were plotted for both ST-IN and SN-IT chord differences. Unlike the XQ, the standard deviations for the chord differences did not appear to follow a strict pattern, however for each refractive group at around 80-85% along the presumed axis the standard deviations for chord differences appeared to be at their lowest.

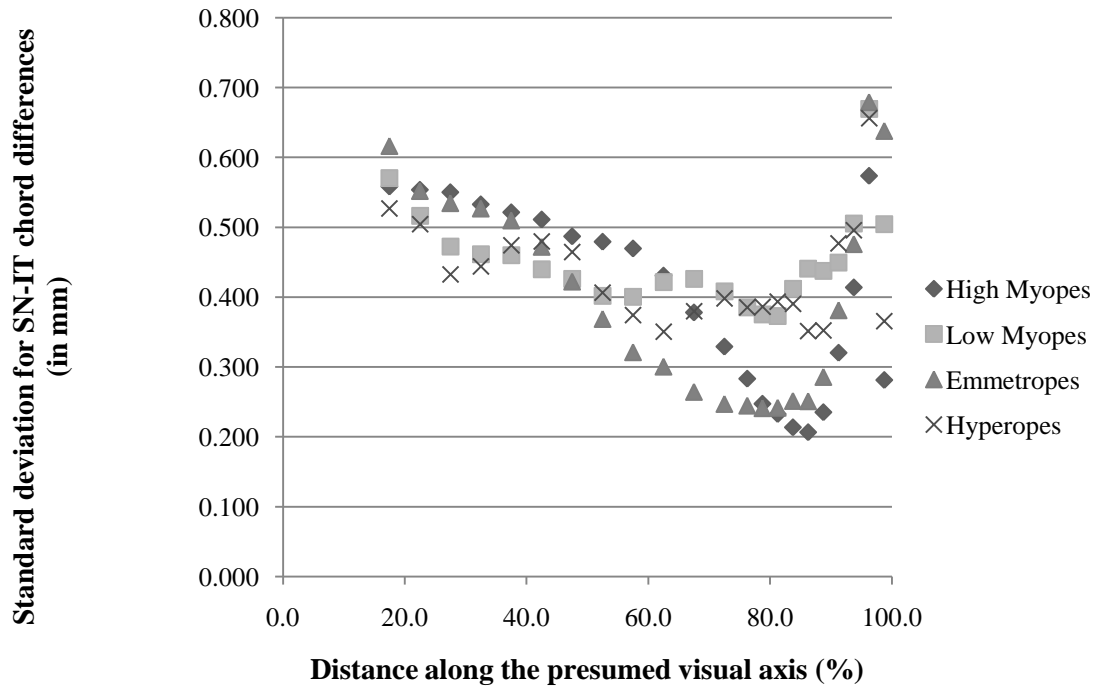


Figure 50 Standard deviations for each of the refractive groups SN-IT quadrants

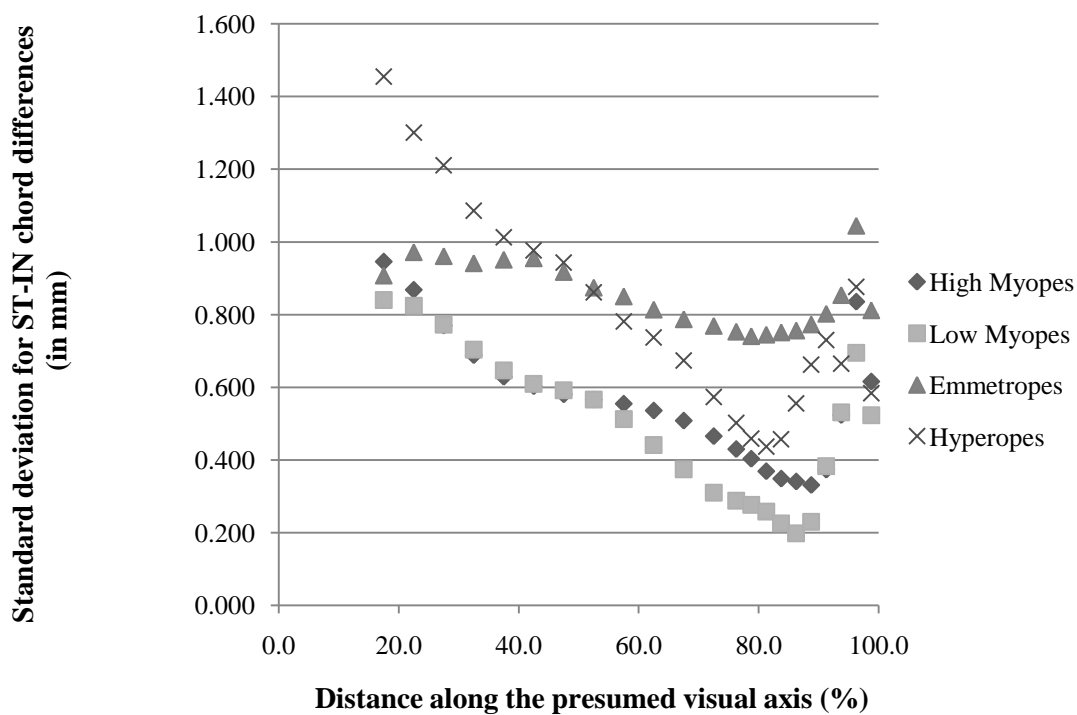


Figure 51 Standard deviations for each of the refractive groups ST-IN quadrants

**Maximum distances**

The maximum distance from the presumed visual axis to the retinal surface was calculated at 5% increments along the axis from 17.5% to 72.5%, and 2.5% increments thereafter. Values were generated for each type of quadrant, XQ and +Q. The maximal values appeared to occur at approximately 47.5-52.5% along the axis.

**Quadrants: XQ**

Table 4 below lists the position along the axis at which the maximal points were noted.

	Nasal	Temp	Sup	Inf
High Myopes	52.5	52.5	52.5	47.5
Low Myopes	47.5	57.5	57.5	52.5
Emmetropes	52.5	52.5	52.5	52.5
Hyperopes	47.5	52.5	52.5	52.5

**Table 4 The mean percentage along the axis at which the maximal point was noted**

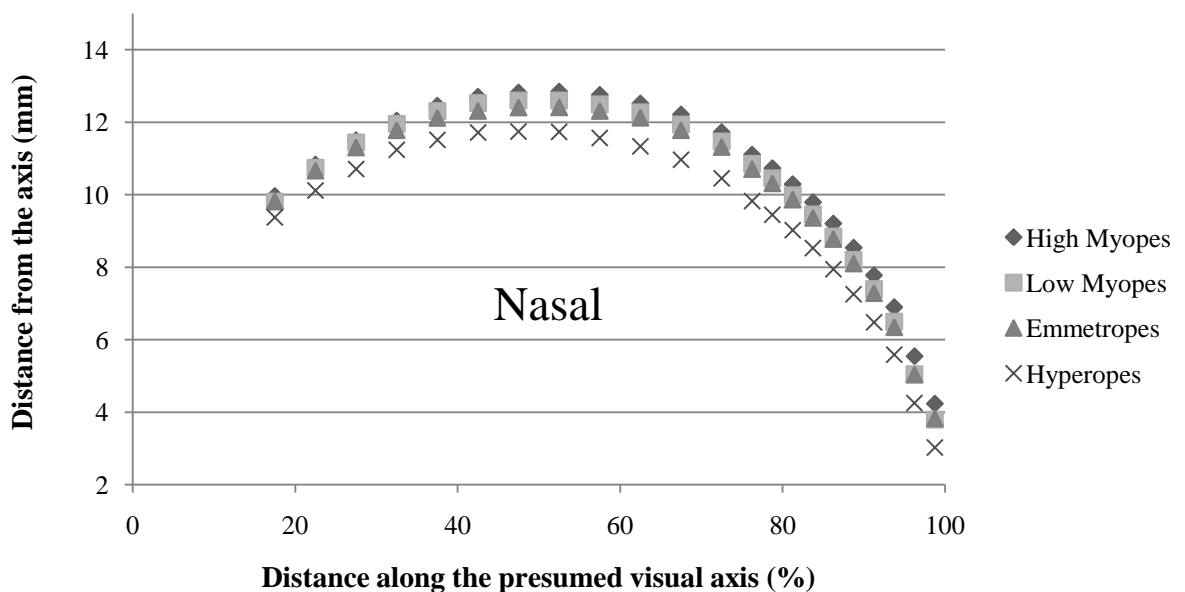


**Figure 52 The maximum distance values at 5% or 2.5% increments along the presumed visual axis**

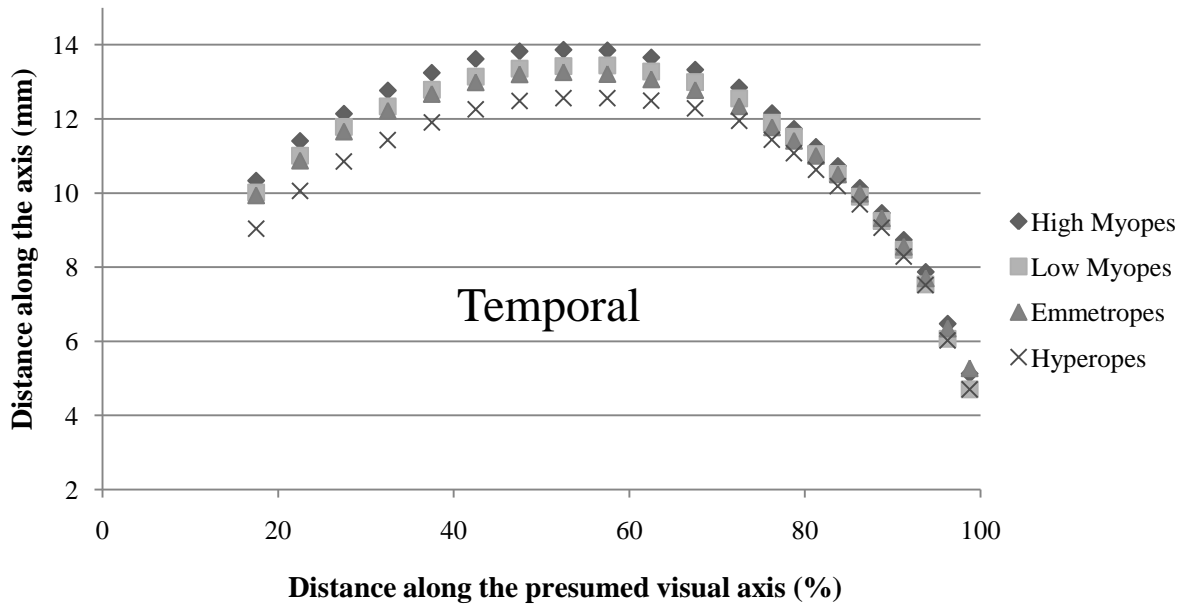


**Figure 53** The maximum distance values at 5% or 2.5% increments along the presumed visual axis

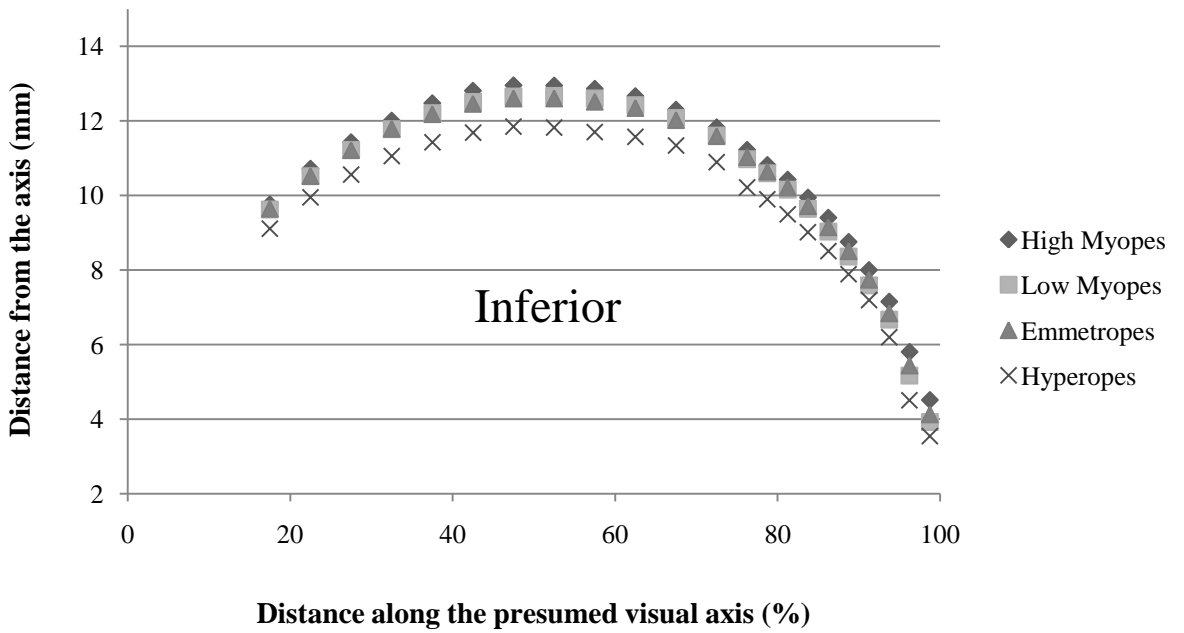


**Figure 54** The maximum distance values at 5% or 2.5% increments along the presumed visual axis

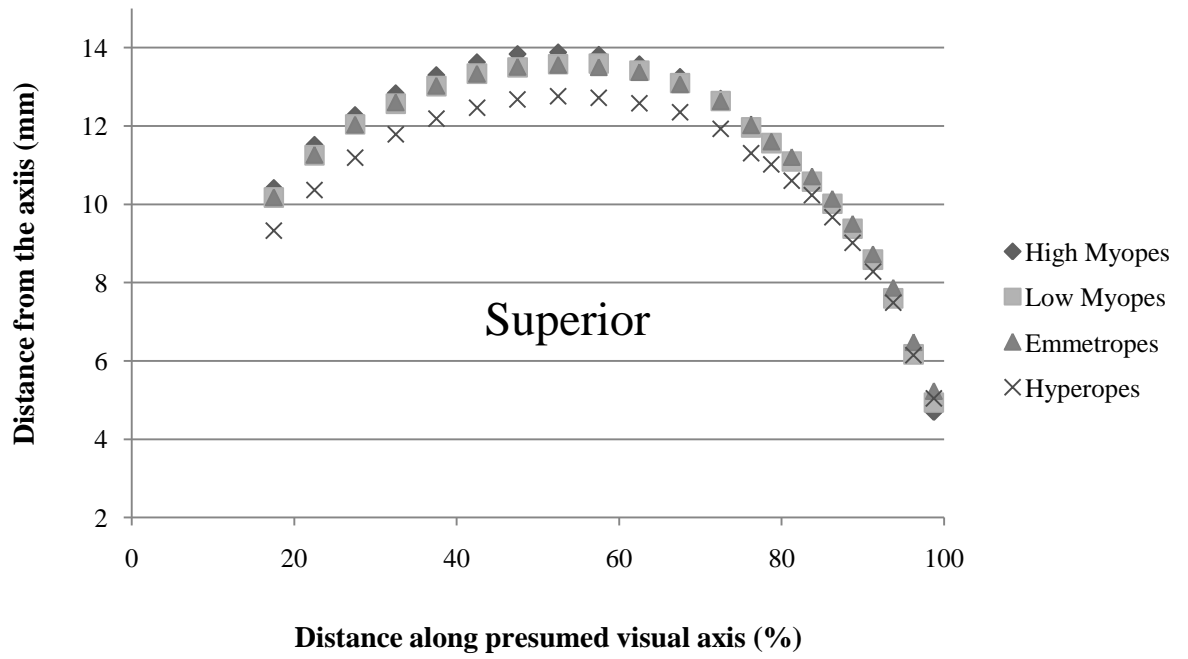


Figure 55 The maximum distance values at 5% or 2.5% increments along the presumed visual axis

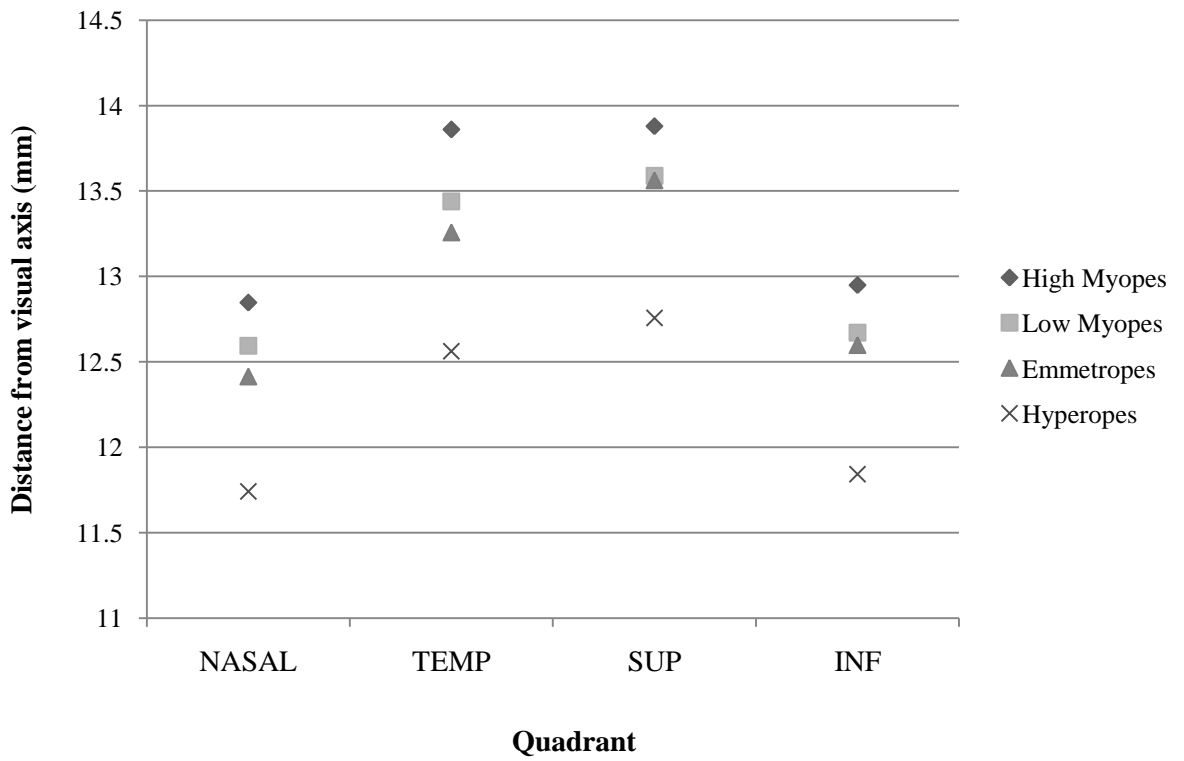


Figure 56 Maximal distance from the presumed visual axis to the retinal surface for each quadrant

A repeated measures ANOVA showed a significant refractive group, and separately, a significant quadrant effect was noted ( $p < 0.01$ ). The maximum distances were largest in the highly myopic subjects and declined as a function of decreasing myopia. The largest maximal distance was noted in the superior quadrant for each refractive group. The smallest maximum distance was noted in the nasal quadrant, this was also the same for each refractive group. All quadrant differences were significant ( $p < 0.05$ ) bar the nasal *vs.* inferior comparison ( $p > 0.05$ ). Refractive group differences were significant between the hyperopic group *vs.* all other refractive groups ( $p < 0.05$ ).

To further describe the differences between refractive groups the mean maximal values between individual quadrants were examined. Of particular interest were the differences between high myopes *vs.* other refractive groups. In line with the previous experiment, the maximum distances of the highly myopic group exceeded other refractive groups for all quadrants; the differences were particularly marked for the temporal quadrant. Comparisons of the mean maximum distances for high myopes with other refractive groups revealed that on average the increases in ascending order were: superior =  $0.58 \pm 0.47$ mm, inferior =  $0.58 \pm 0.46$ mm, nasal =  $0.60 \pm 0.45$ mm, and temporal =  $0.77 \pm 0.46$ mm. The results mirror those of an earlier study conducted using the same techniques where emmetropic and myopic subjects were compared (Nagra et al. 2009). A difference in temporal quadrant maximum distances was also noted in comparisons between the low myopic *vs.* emmetropic group, and between low myopic and hyperopic groups. One anomaly to this pattern was the emmetropic *vs.* hyperopic comparison.

	Nasal max	$\pm$ sd (mm)	Temp max	$\pm$ sd (mm)	Sup max	$\pm$ sd (mm)	Inf max	$\pm$ sd (mm)
High Myopes	12.85	$\pm 0.71$	13.86	$\pm 0.68$	13.88	$\pm 0.68$	12.95	$\pm 0.63$
Low Myopes	12.59	$\pm 0.67$	13.44	$\pm 0.64$	13.59	$\pm 0.55$	12.67	$\pm 0.43$
Emmetropes	12.41	$\pm 0.54$	13.26	$\pm 0.54$	13.56	$\pm 0.46$	12.60	$\pm 0.46$
Hyperopes	11.74	$\pm 0.77$	12.56	$\pm 0.88$	12.76	$\pm 0.75$	11.84	$\pm 0.56$

**Table 5 Mean maximum distance for each quadrant by refractive group. SD indicates the standard deviation of the maximum distance values for each refractive group**

### **Quadrants: +Q**

The results showed a significant refractive group effect, and separately, a significant quadrant effect ( $p < 0.05$ ). All quadrants showed significant differences ( $p < 0.05$ ) except the ST vs. IT comparison. Refractive group differences were significant for all refractive group vs. the hyperopic group, and the highly myopic vs. emmetropic groups ( $p < 0.05$ ).

The table below shows the position at which maximal distances were noted for each of the quadrants by refractive group.

	ST	IN	SN	IT
High Myopes	52.5	52.5	52.5	52.5
Low Myopes	52.5	47.5	52.5	52.5
Emmetropes	52.5	47.5	52.5	52.5
Hyperopes	52.5	47.5	52.5	52.5

**Table 6 Lists the distance in mean percentage along the axis at which the maximal point was noted**

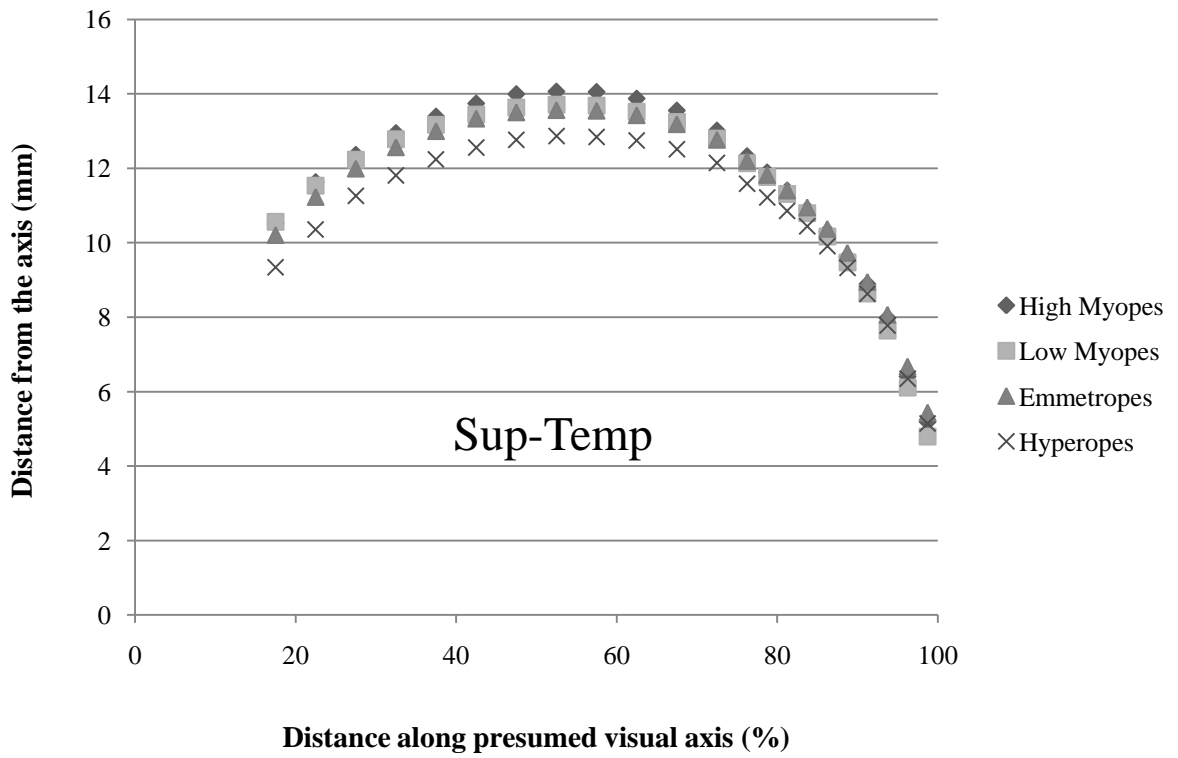


**Figure 57** Maximum distance values at 5% or 2.5% increments along the presumed visual axis

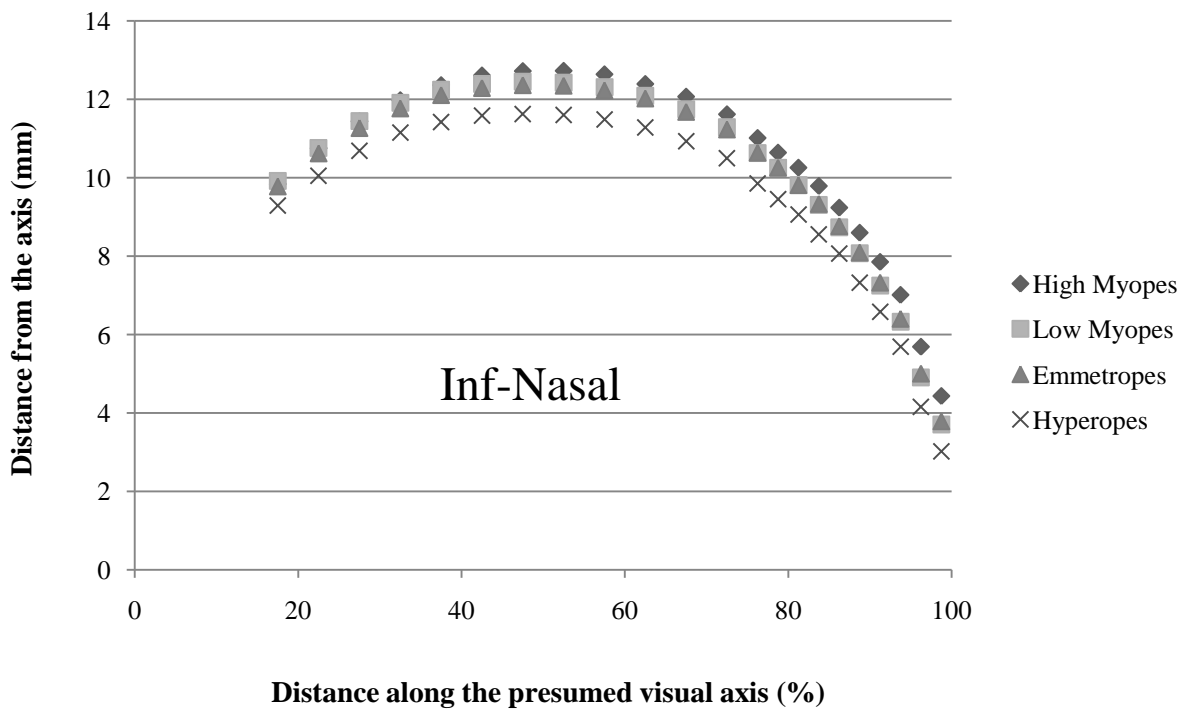


**Figure 58** Maximum distance values at 5% or 2.5% increments along the presumed visual axis

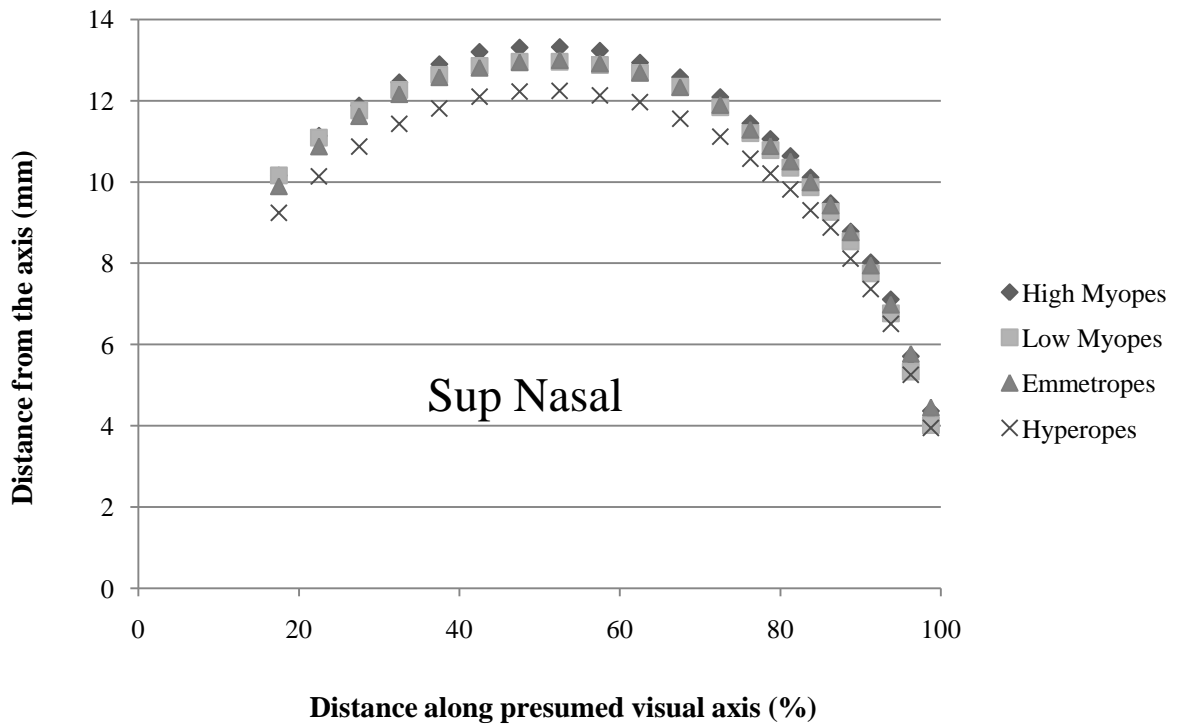


**Figure 59 Maximum distance values at 5% or 2.5% increments along the presumed visual axis**

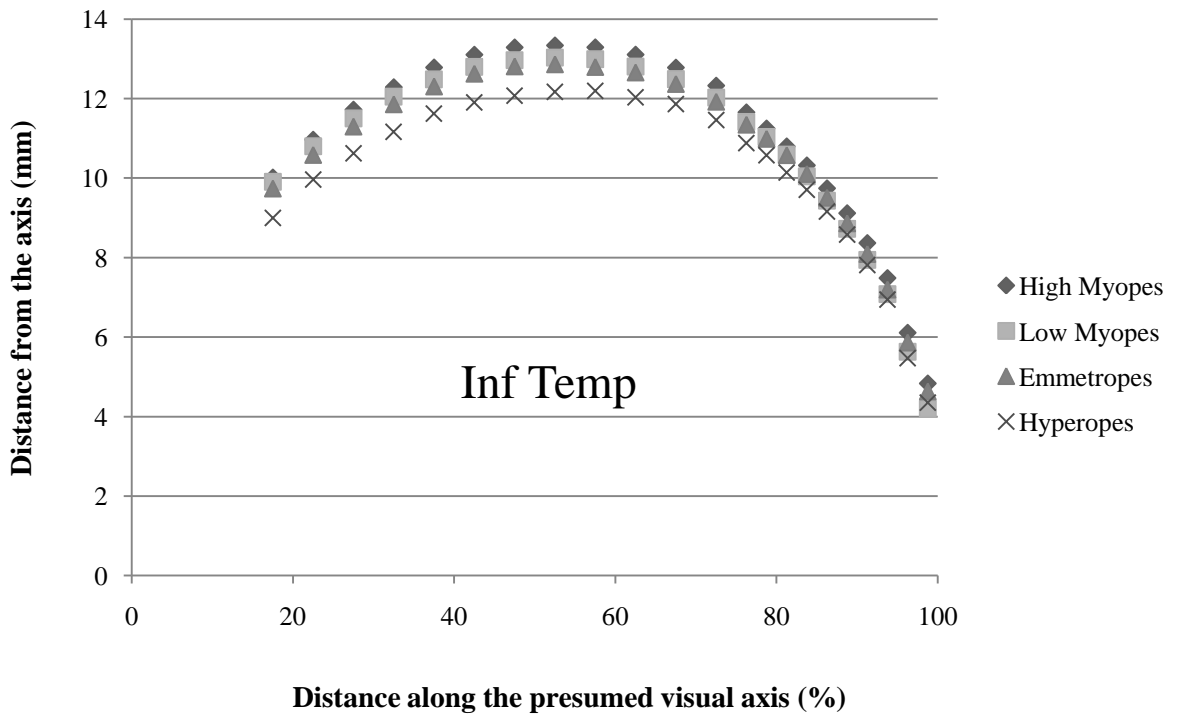


**Figure 60 Maximum distance values at 5% or 2.5% increments along the presumed visual axis**

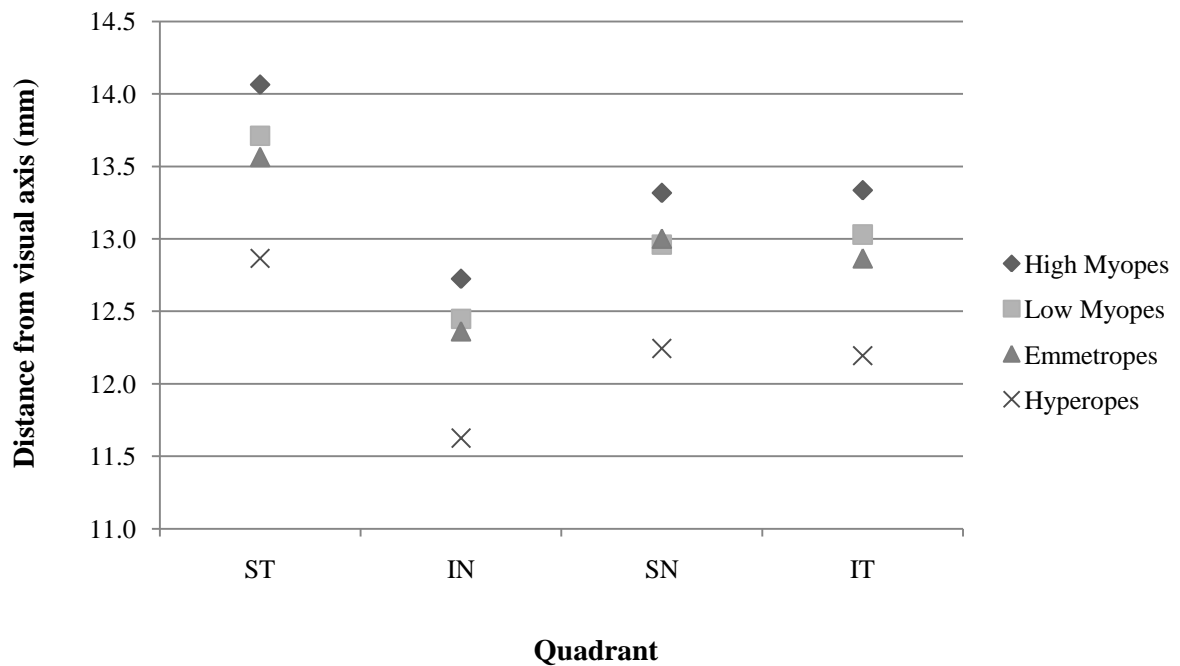


**Figure 61 Maximal distance from the presumed visual axis to the retinal surface for each quadrant**

All refractive groups showed the maximum values in the ST quadrant to be largest and IN to be the smallest (see Figure 61). Comparisons of maximum distance between high myopes and other refractive groups showed the largest differences in the ST quadrants. Using average maximum distance values the ST quadrant was larger in high myopes compared with other refractive groups by  $0.68 \pm 0.45 \text{ mm}$ ; in comparison the IT quadrant was larger by  $0.64 \pm 0.44 \text{ mm}$ , IN by  $0.58 \pm 0.45 \text{ mm}$ , and SN by  $0.58 \pm 0.45 \text{ mm}$ . Maximum distance in low myopes minus maximum distance in hyperopes also showed the ST quadrant differences to be largest. In contrast, other refractive group combinations (i.e. low myopes minus emmetropes, emmetropes minus hyperopes) did not show any clear pattern.

	ST max	$\pm \text{sd}$ (mm)	IN max	$\pm \text{sd}$ (mm)	SN max	$\pm \text{sd}$ (mm)	IT max	$\pm \text{sd}$ (mm)
High Myopes	14.06	$\pm 0.64$	12.73	$\pm 0.66$	13.32	$\pm 0.65$	13.34	$\pm 0.64$
Low Myopes	13.71	$\pm 0.55$	12.45	$\pm 0.54$	12.96	$\pm 0.33$	13.03	$\pm 0.52$
Emmetropes	13.56	$\pm 0.42$	12.36	$\pm 0.38$	13.00	$\pm 0.44$	12.86	$\pm 0.41$
Hyperopes	12.87	$\pm 0.77$	11.63	$\pm 0.54$	12.24	$\pm 0.75$	12.19	$\pm 0.96$

**Table 7 Showing the maximum distance for each quadrant by refractive group. SD indicates the standard deviation**

### **Polynomial equations**

Data for each quadrant was plotted for the region 25-75% along the presumed visual axis; data were fitted with second order polynomials using Microsoft Excel and the  $x^2$  coefficient of the polynomial equation analysed in order to assess bulbosity.

### **Quadrants: XQ**

The  $x^2$  coefficients for each of the quadrants were examined with reference to refractive group. A 2-way mixed repeated measures ANOVA showed that although the between-subject effects of refractive error were significant ( $p < 0.01$ ) and the differences in quadrants within subjects were also significant ( $p < 0.01$ ), the quadrant: refractive group interaction was not significant ( $p > 0.05$ ). The significant refractive group differences were principally differences between the hyperopic group and other refractive groups ( $p < 0.01$ ). Within-subject quadrant effects showed all interactions bar the nasal vs. superior (0.229) and inferior vs. temporal ( $p = 0.279$ ) to be significant ( $p < 0.01$ ).

Visual inspection of the graphs showed that in general the inferior quadrant appeared to be most bulbous; however in hyperopic subjects the superior quadrant was most bulbous. The least bulbous quadrant varied depending on refractive group; the emmetropes and low myopes showed the least bulbous quadrant to be the nasal quadrant; the high myopes and hyperopes showed the least bulbous quadrant to be the temporal quadrant.

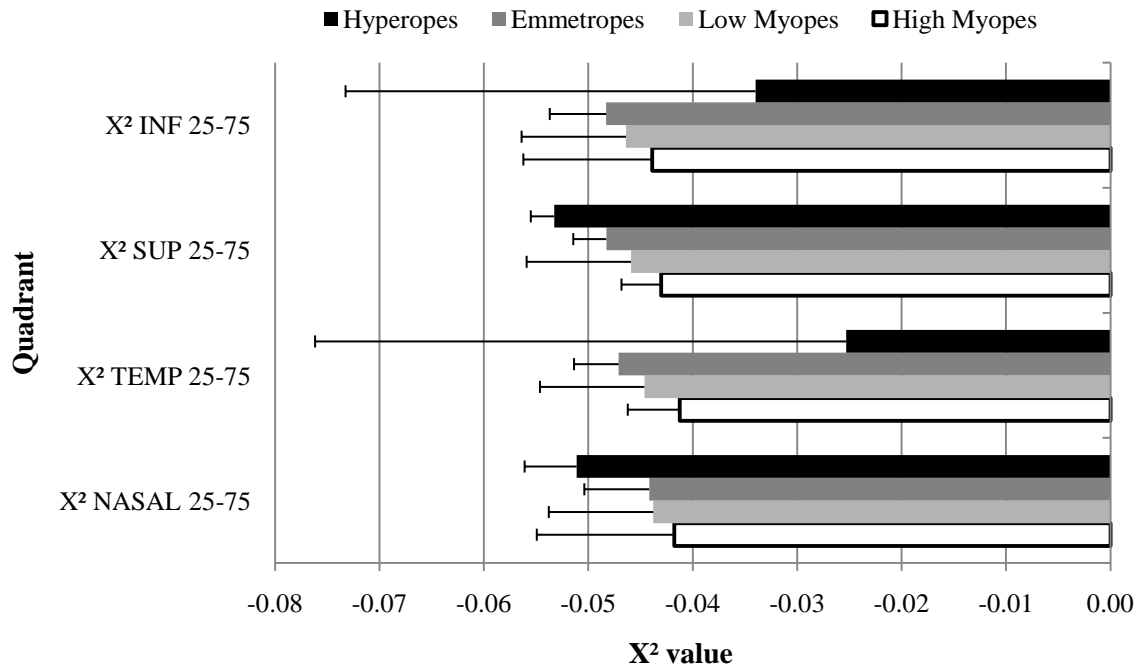


**Figure 62** The mean  $x^2$  coefficient values for each quadrant divided further by refractive group

The  $x^2$  coefficient corresponding to data comprising the posterior 25% cap of the eye was examined for the N-T meridian and the S-I meridian. Visual inspection of the data showed the N-T meridian to be more bulbous than the I-N for all refractive groups, bar the high myopes.

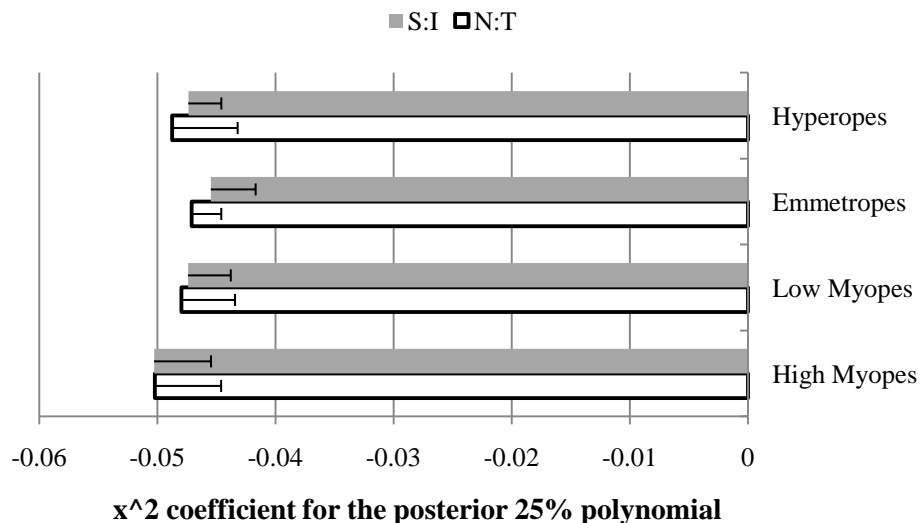


**Figure 63** The mean  $x^2$  coefficient values for the polynomial curves fitted to data representing the posterior 25% cap of the eye. Data are separated by refractive group

A repeated measures ANOVA showed the meridian differences were not significant ( $p=0.072$ ). Furthermore the meridian: refractive group difference was also not significant ( $p=0.457$ ). A significant between-subjects refractive error effect was noted ( $p = 0.011$ ); *post hoc* tests revealed the refractive group differences to lie between the high myopes and emmetropes ( $p = <0.01$ ).

**Quadrants: +Q**

The  $\chi^2$  coefficient for +Q was then examined using the same methodology described above. Unlike the XQ, a 2-way mixed repeated measures ANOVA showed the between subjects effect of refractive error was not significant.

Similar to the XQ the quadrant: refractive group interaction was not significant whilst the within subjects quadrant effect was significant ( $p<0.01$ ).

Quadrant pairwise interaction were significant for all combinations except the ST vs. SN and IN vs. IT. The results for the 25-75% along the axis region showed the least bulbous quadrant to be the IN; this was the case for all refractive groups. There was no clear pattern regarding which was the most bulbous quadrant.

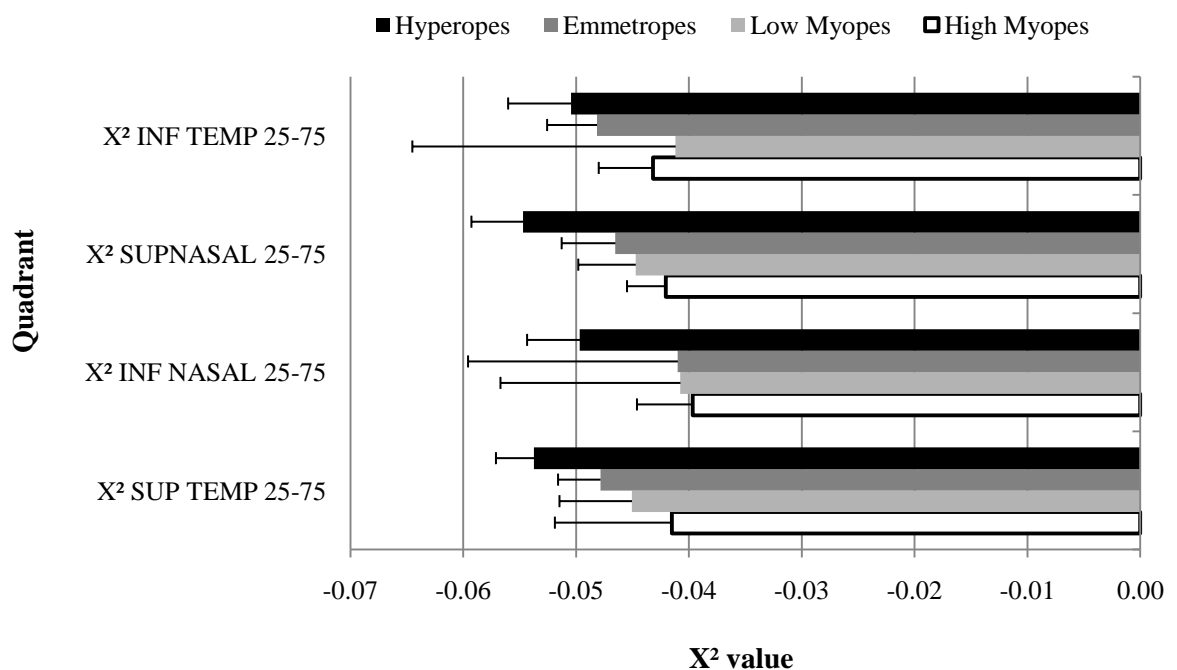


**Figure 64** The mean  $\chi^2$  coefficient values for each quadrant divided further by refractive group

For the posterior 25%, the meridians SN-IT were compared with the ST-IN. Each refractive group showed the SN-IT meridian to be more bulbous than the ST-IN. A repeated measures ANOVA showed a significant meridian effect ( $p < 0.01$ ) and also a significant refractive group effect ( $p = 0.036$ ), however the meridian: refractive group interaction was not significant ( $p = 0.916$ ). The refractive group differences lay between the high myopic and emmetropic groups, which was in line with the results for the XQ.

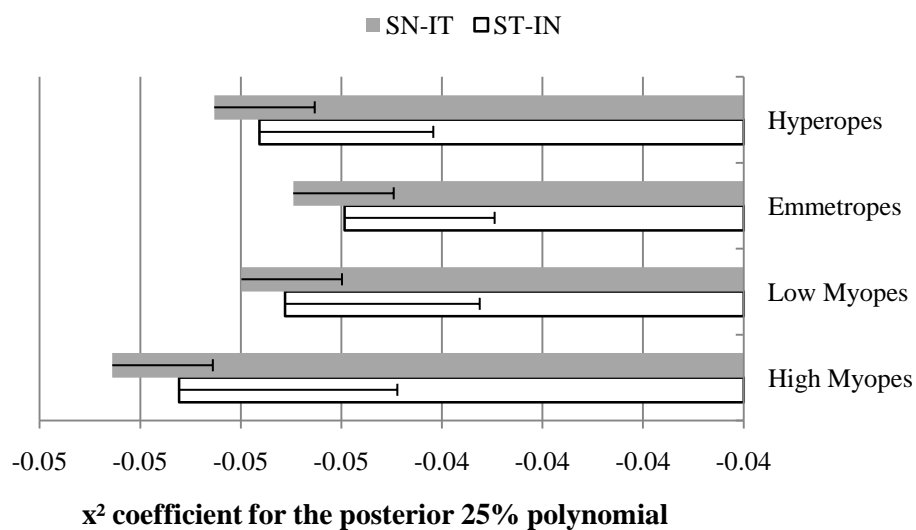


**Figure 65** The mean  $x^2$  coefficient values for the polynomial curves fitted to data representing the posterior 25% cap of the eye. Data are separated by refractive group

### Interval Variation (IV)

#### Interval variance in the XQ

The interval variations were calculated for the region 25-75% along the presumed visual axis by quadrant, and then for the posterior 25% cap. A 2 way mixed repeated measures ANOVA showed a significant within subjects effect for IV ( $p < 0.01$ ) and also a significant between subjects refractive group interaction ( $p < 0.01$ ). The IV:refractive group effect failed to reach significance ( $p = 0.078$ ).

The significant refractive group differences appeared to exist between the hyperopic groups and other refractive groups ( $p < 0.016$ ). The quadrant differences were significant for all combinations ( $p < 0.01$ ) bar the temporal vs. superior ( $p = 0.435$ ) and inferior vs. superior quadrants ( $p = 0.093$ ).

The results showed the IV for the nasal quadrant was smallest in all refractive groups; the largest quadrant was the temporal in all subjects bar the high myopes who showed the superior quadrant to be marginally greater than the temporal (by 0.01mm).

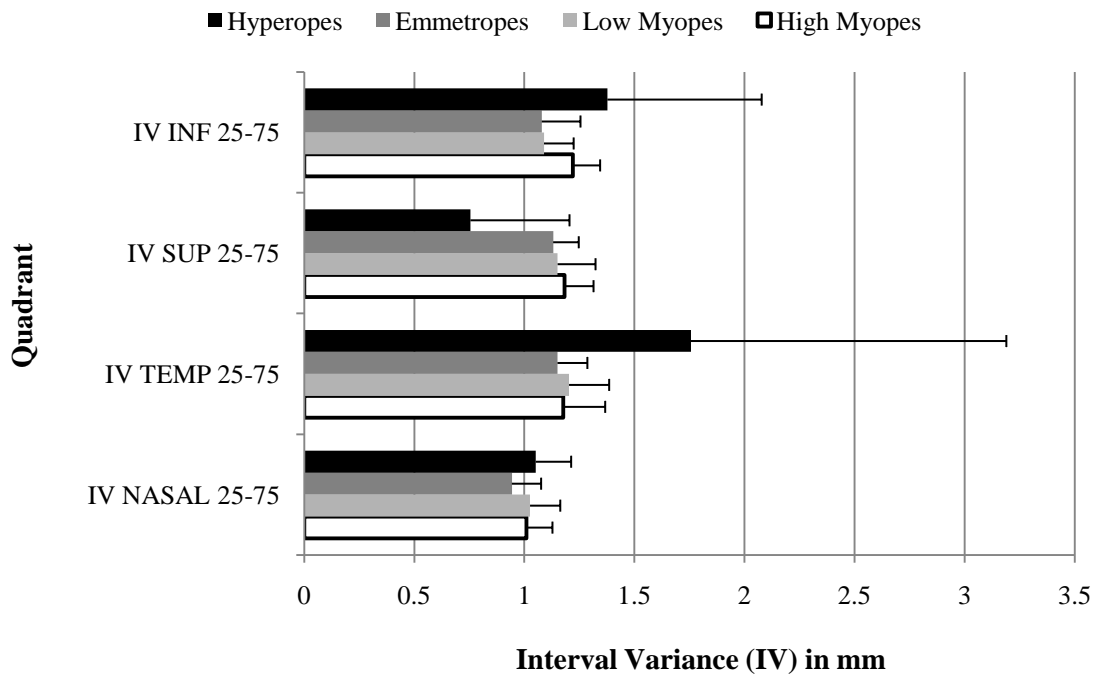


**Figure 66 The mean Interval Variance (IV) shown for the XQ**

Results for the posterior 25% were calculated in the N-T meridian and the S-I meridian. A repeated measures ANOVA showed the meridian effect to be significant ( $p=0.021$ ). The meridian: refractive group interaction and between subjects refractive group effects were not significant ( $p=<0.01$ ). Overall the results indicated that although there were significant quadrant differences they were largely unaffected by refractive group.

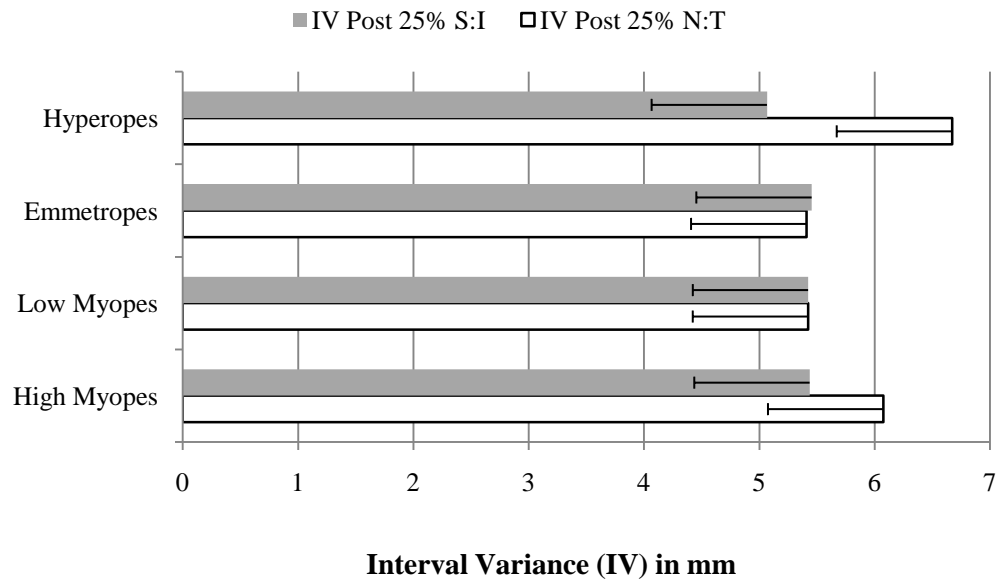


**Figure 67 The mean Interval Variance (IV) for the XQ meridians**

**Interval variance in the +Q**

The IV values were then generated for the +Q. A mixed repeated measures ANOVA did not show a significant within subjects effect for quadrants, quadrant: refractive group, or a between subjects effect for refractive error ( $p = <0.05$ ). Visual inspection of the graphs showed that in general the ST quadrant was the most bulbous for all refractive groups bar the low myopes. The least bulbous appeared to be the IN quadrant except in the emmetropic group.

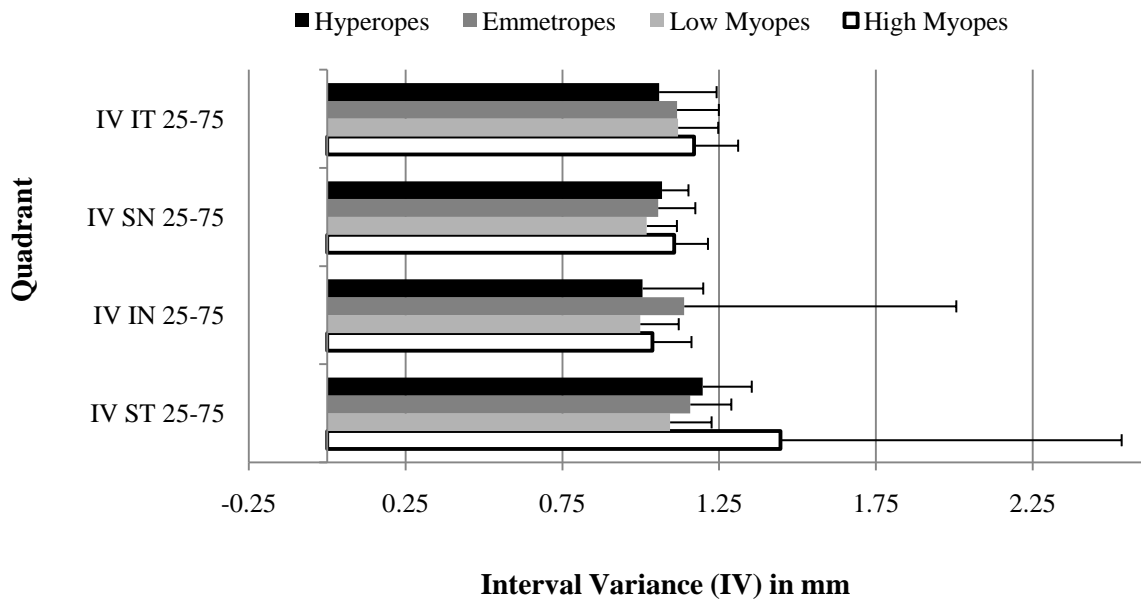


**Figure 68 The mean Interval Variance (IV) for the +Q in the 25-75% region**

The meridians SN-IT and ST-IN in the posterior 25% did not show significant differences for meridian or refractive group effects ( $p > 0.05$ ). Similarly, the meridian: refractive group interaction was not significant ( $p = 0.923$ ).

Overall, unlike the XQ, the +Q showed little difference between quadrants; refractive group differences were not noted either.

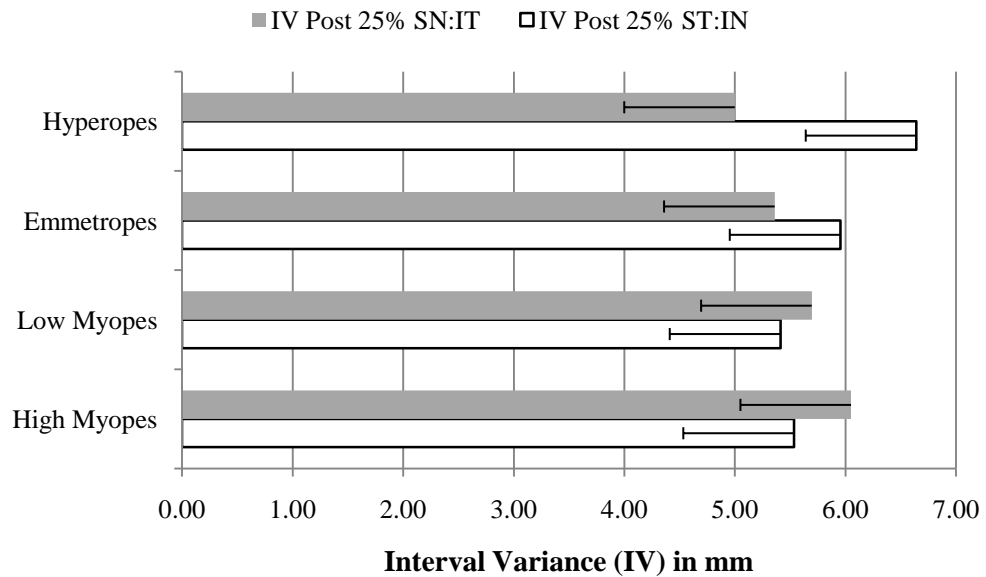


**Figure 69 The mean Interval Variance (IV) for +Q meridians**

#### 9.6.4 Inter eye differences

The differences between the right and left eyes of 18 subjects were evaluated; all subjects had anisometropia of less than or equal to 1D between eyes except one subject with anisometropia of 1.38D. The selection of subjects was based upon subjects who had taken part in the multifocal electroretinogram study, thus analysis of left MR data had been carried out and also this group of 18 subjects was known to comprise of a similar number of emmetropes and hyperopes. The subjects were divided into two groups according to refractive error: emmetropic or myopic.

Eye and refractive group,	MSE in D ± standard deviation	Axial length in mm ± standard deviation
RE Myopes	4.99±3.16D	25.60±1.15
LE Myopes	5.20±3.31D	25.85±1.38
RE Emmetropes	0.06±0.38D	23.87±0.76
LE Emmetropes	0.02±0.32D	24.24±1.00

**Table 8 The refractive errors of the 18 subjects for whom right and left eyes were compared. Axial length are taken from MR data**

## Quadrants: XQ

The inter eye differences in distance to the retinal surface from the presumed visual axis were calculated for both emmetropic and myopic eyes by quadrant. The differences in values were plotted against the distance along the presumed visual axis. Results for the nasal and temporal quadrants showed that the right and left eyes differed most in the anterior region of the eye. The superior and inferior quadrants showed dissimilar patterns of inter eye differences between the refractive groups unlike the nasal and temporal quadrants where patterns were largely similar between both quadrants and refractive groups. In general, nasal and temporal inter eye differences were larger than the superior and inferior. In order to reduce the effects of angle alpha, statistical analysis was carried out for the N-T and S-I meridians rather than individual quadrants. Both the emmetropic and myopic refractive groups showed significant inter eye differences for the N-T meridians ( $p < 0.01$ ). For the superior-inferior regions only myopic eyes showed significant inter eye differences ( $p < 0.01$ ).

The graphs which follow show differences of left eyes values minus right eyes values.

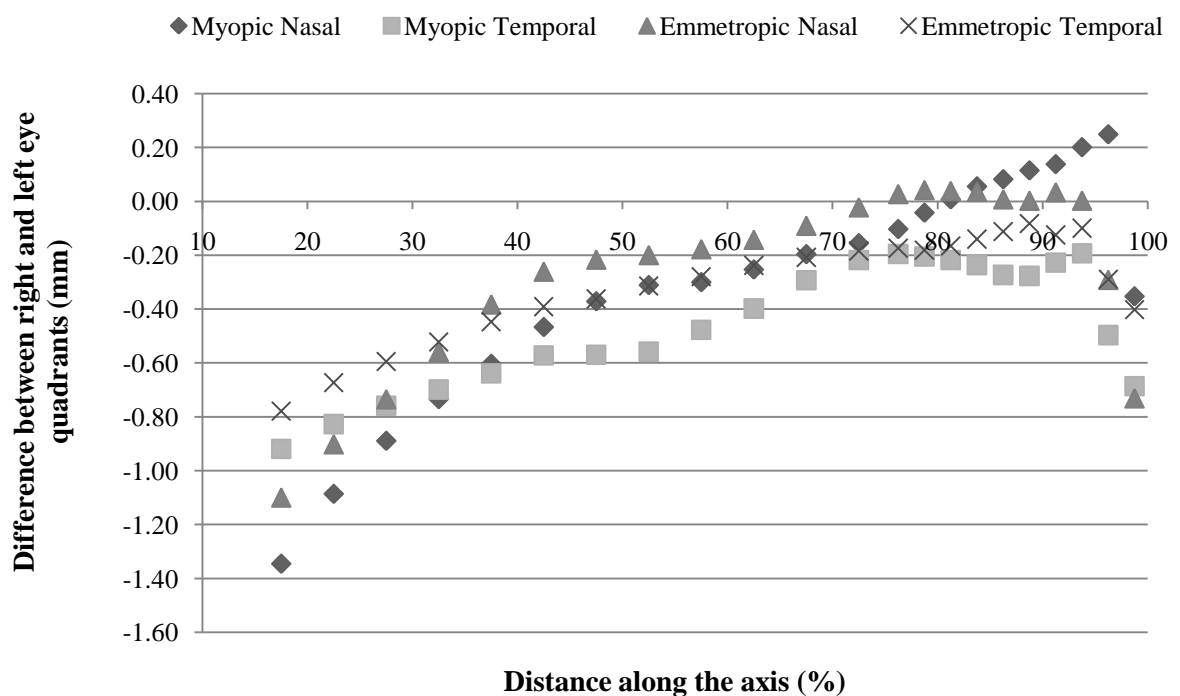


**Figure 70** The mean differences between the right and left eyes of emmetropic and myopic refractive groups for the nasal and temporal quadrants.

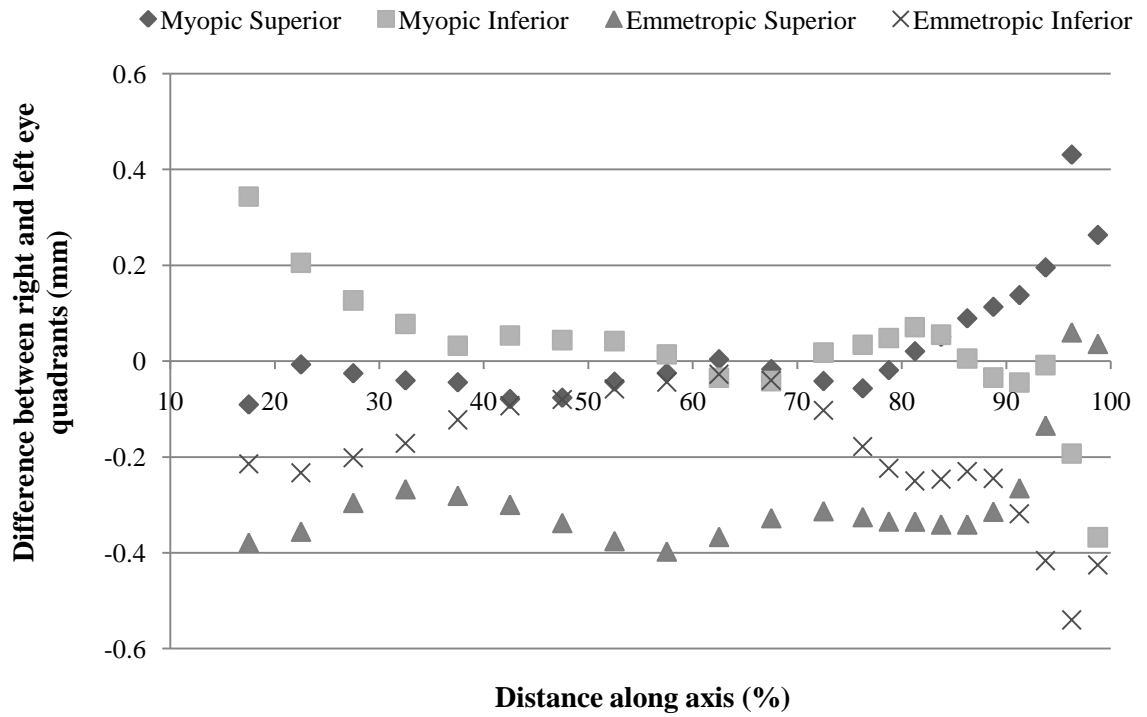


**Figure 71 The mean difference between the right and left eyes of emmetropic and myopic refractive groups for the superior and inferior quadrants**

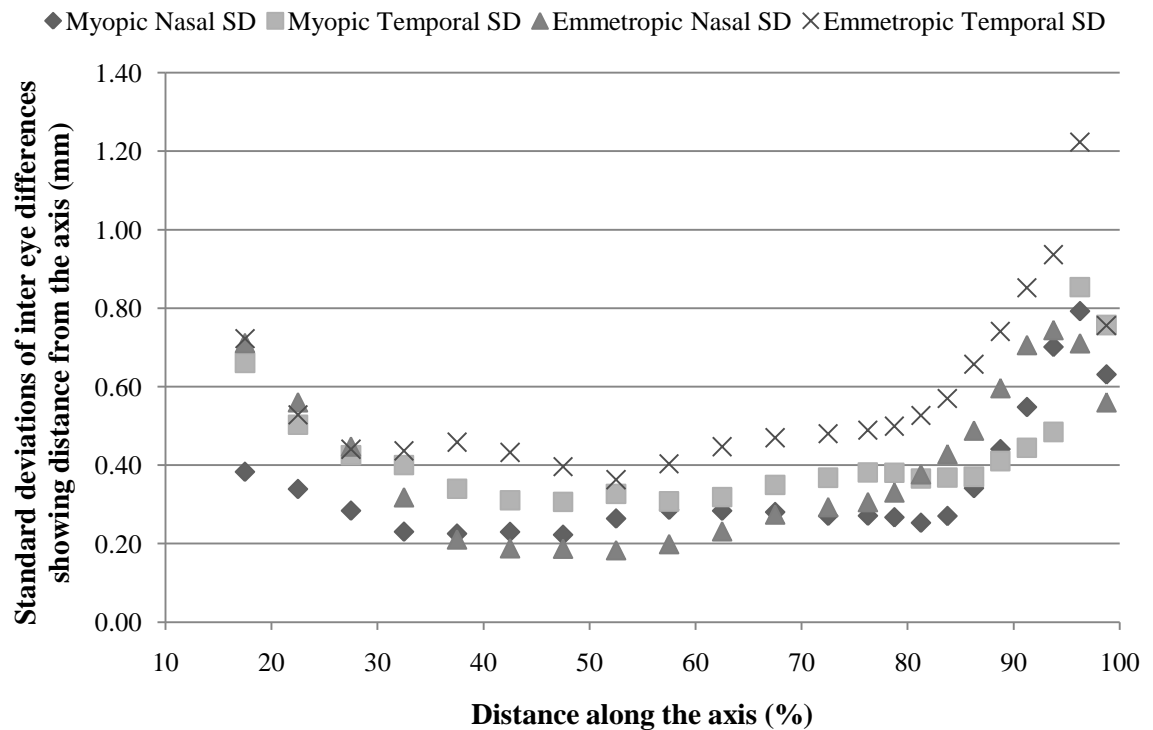


**Figure 72 Standard deviations (SD) for the nasal and temporal inter eye differences**

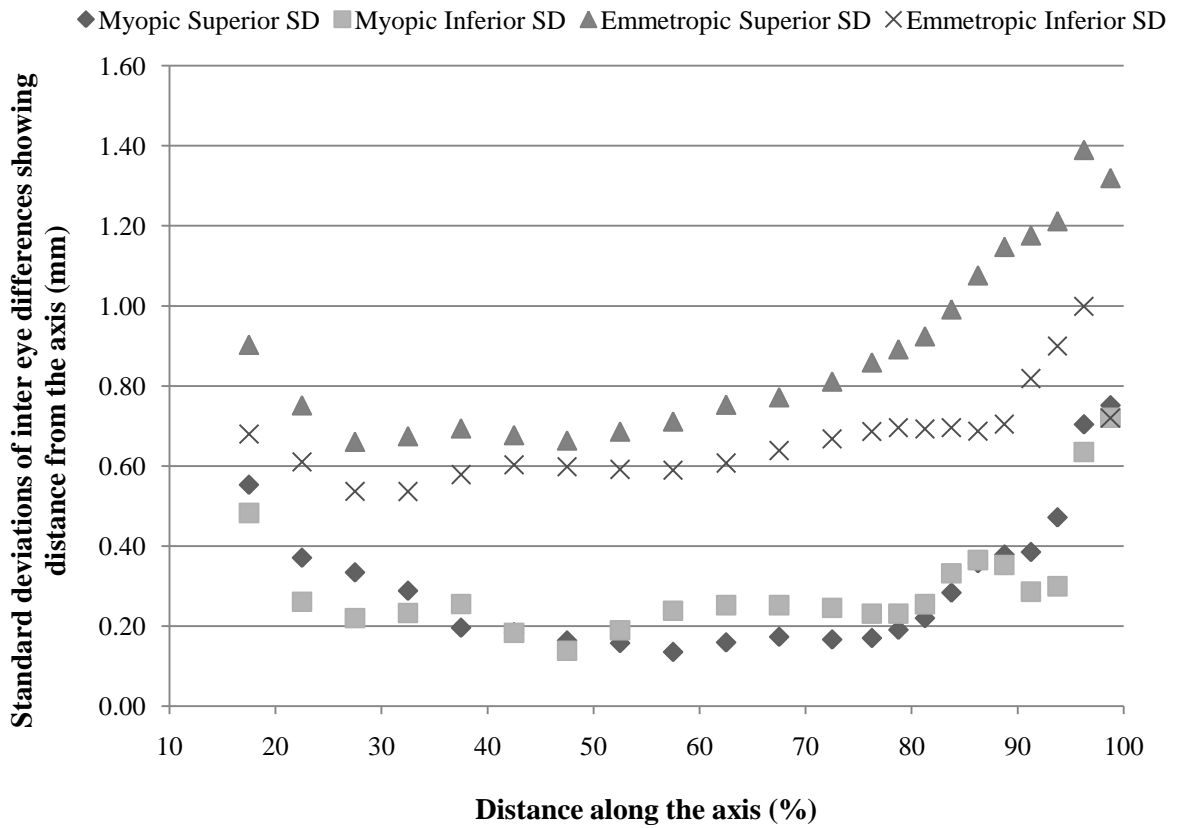


**Figure 73 Standard deviations (SD) for the superior and inferior inter eye differences**

**Quadrants: +Q**

Statistical analysis showed significant inter eye differences for both the myopic and emmetropic groups ( $p < 0.01$ ) for the SN-IT and ST-IN meridians. Visual inspection of the graphs showed differences between the right and left eyes to be generally larger in the more anterior aspects of the eye, but gradually decreasing up to the mid section of the eye (approximately 50-70% along the axis), before gradually increasing again.

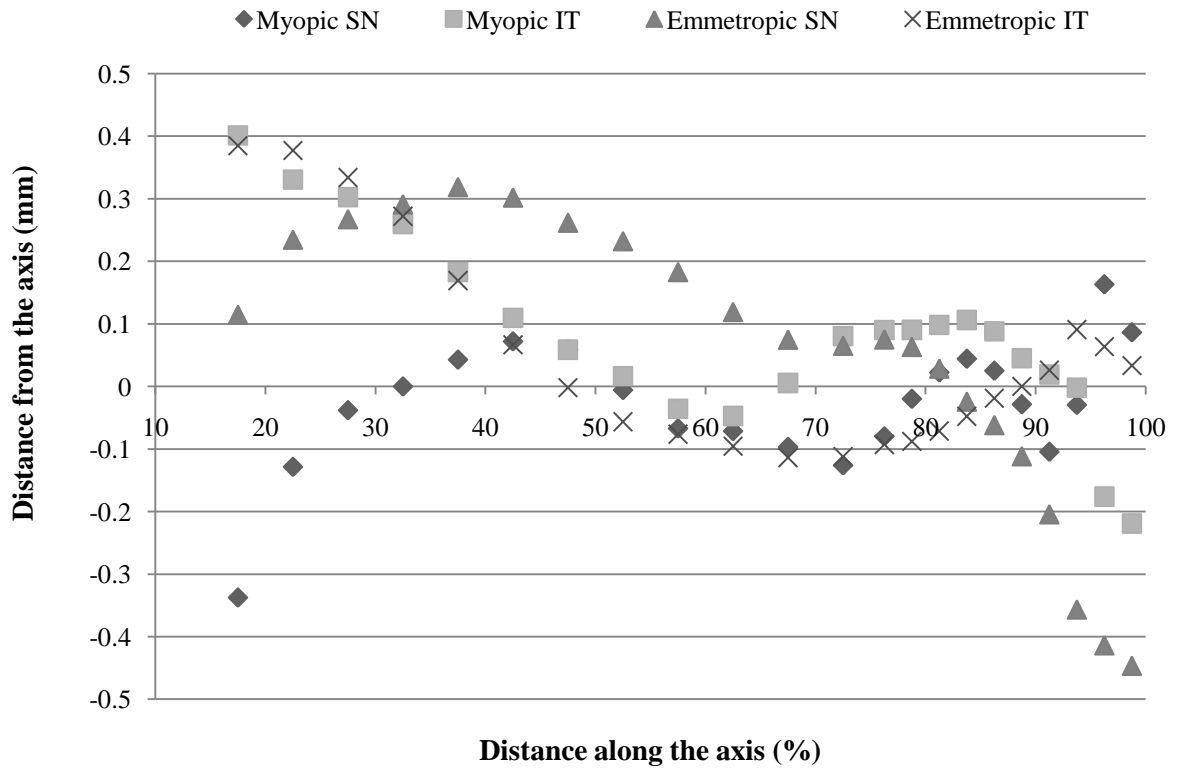


**Figure 74** The mean difference between the right and left eyes of emmetropic and myopic refractive groups for the SN and IT quadrants

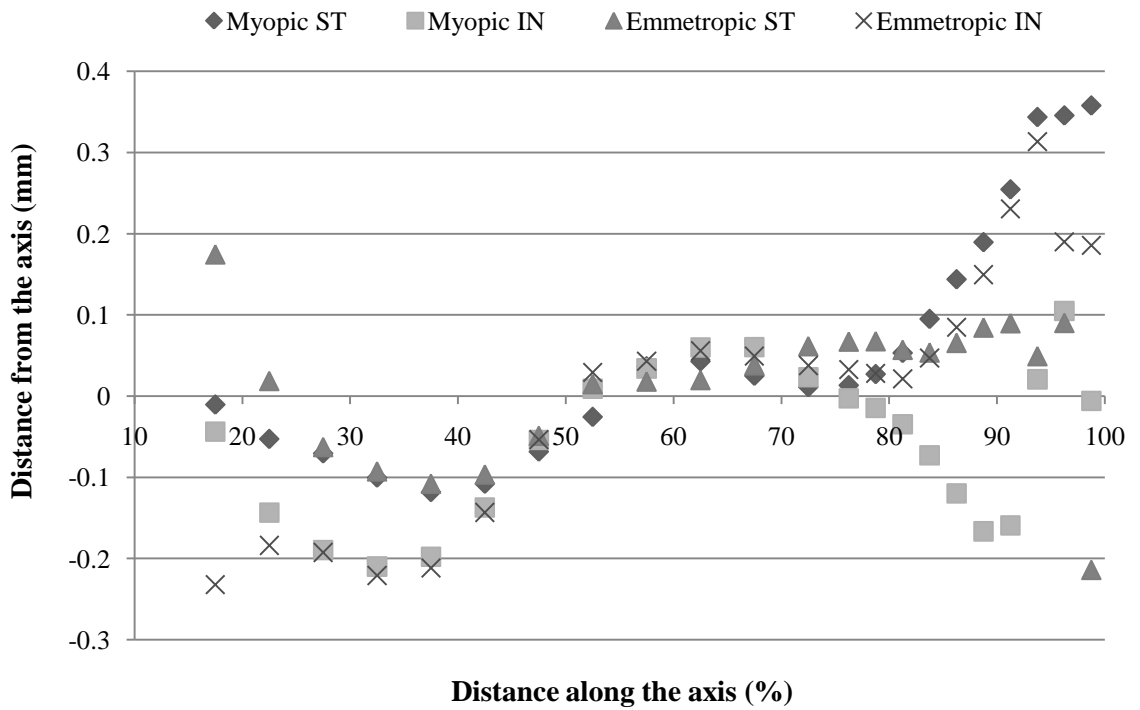


**Figure 75** The mean difference between the right and left eyes of emmetropic and myopic refractive groups for the ST and IN quadrants

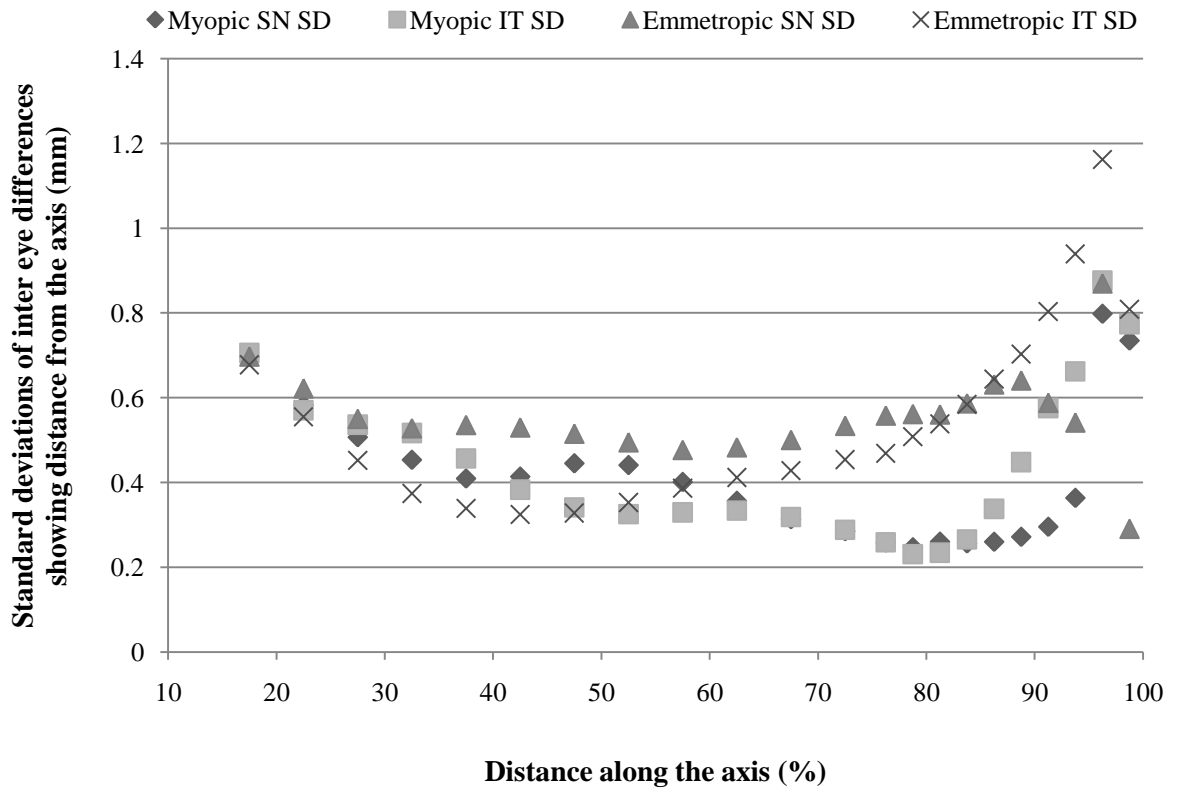


Figure 76 Standard deviations (SD) for the SN and IT inter eye differences

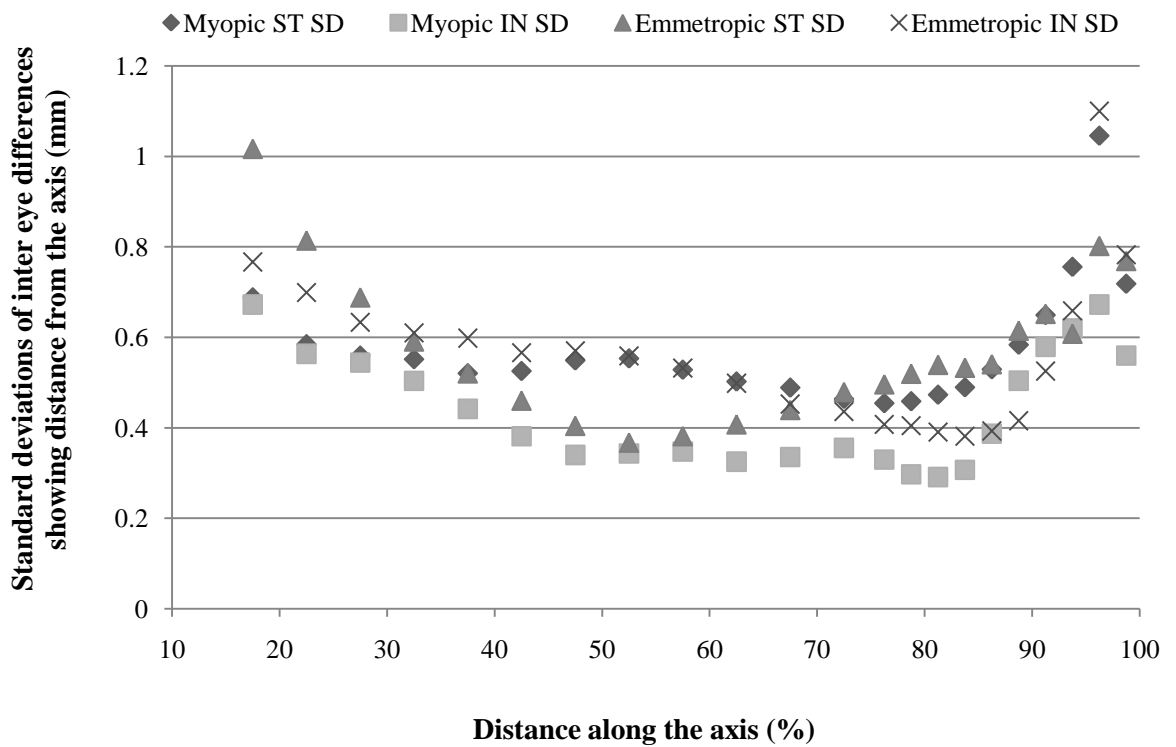
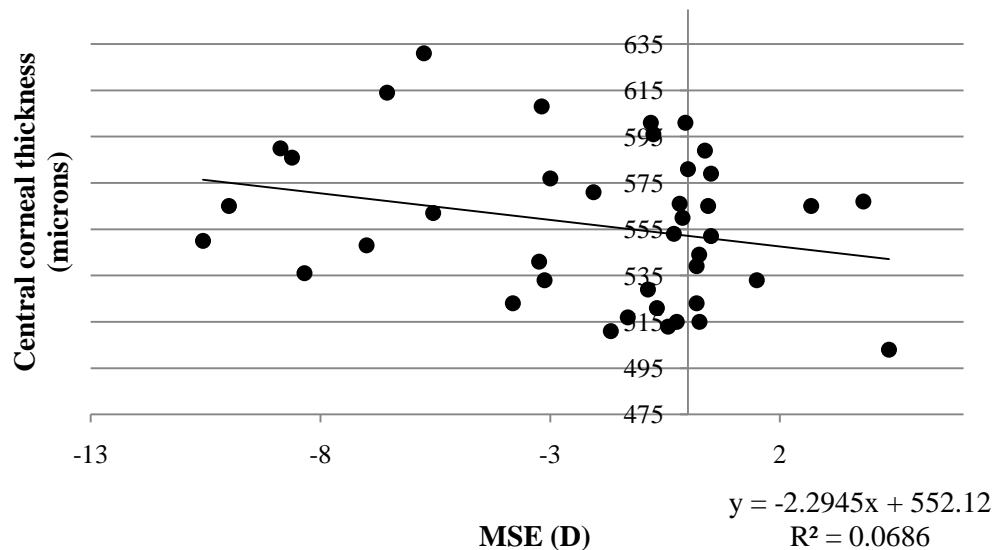


Figure 77 Standard deviations (SD) for the ST and IN inter eye differences

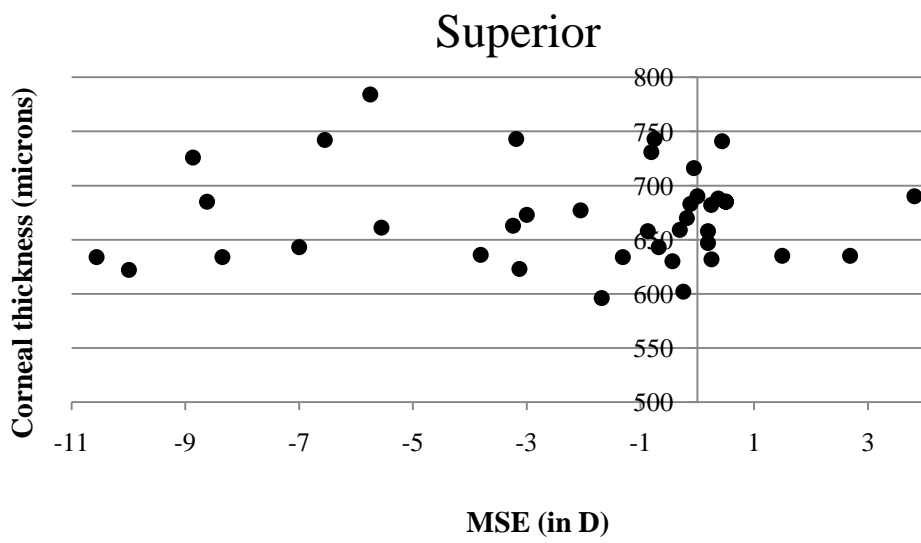
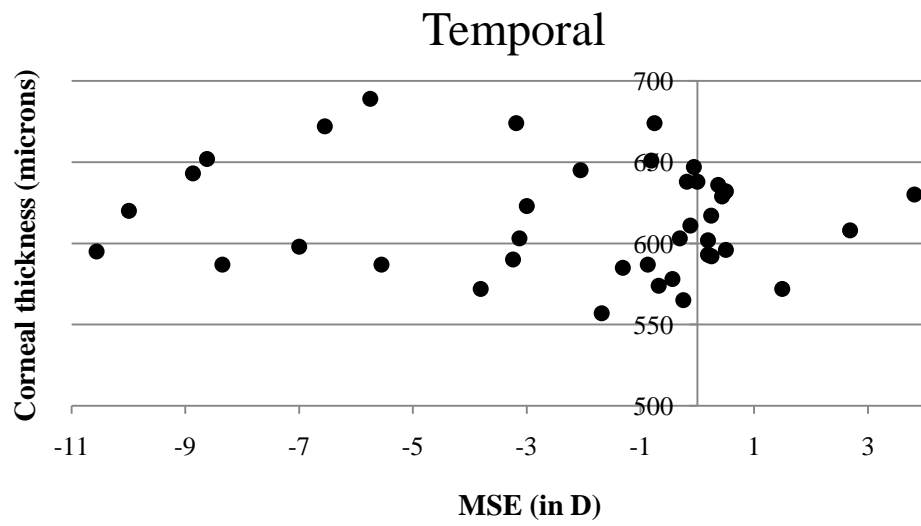
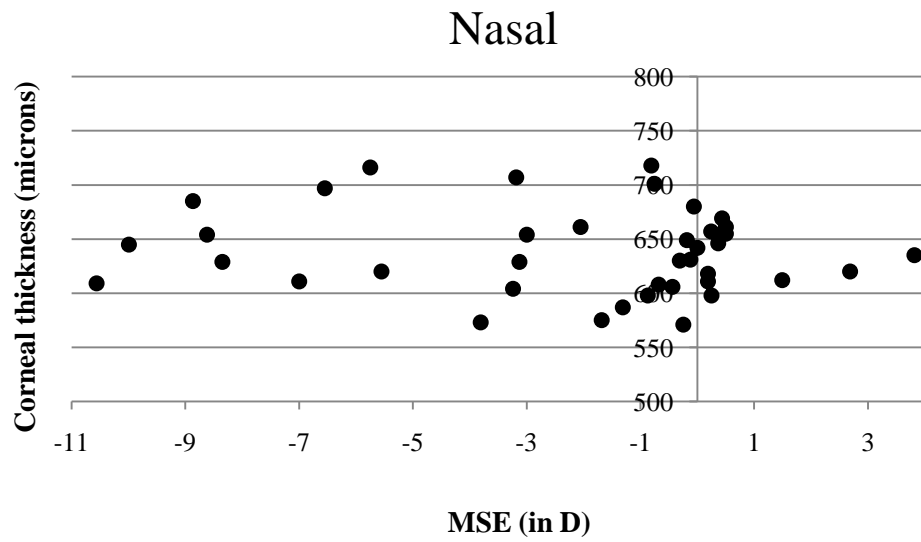
### Anterior eye changes

To further investigate the changes noted in the anterior region of the eye pachymetry data collected using the Oculus Pentacam was examined. Pachymetry measurements at a distance of 3mm from the central cornea for the XQ were examined, and separately, central corneal pachymetry values were also examined. Pachymetry values were plotted as a function of MSE (see Figure 78).



**Figure 78 Central corneal thickness versus MSE (in D) as measured by the Oculus Pentacam (n=42). All subjects from the MRI subject group were invited for Pentacam readings to be taken, results are shown for subjects who responded (p= 0.051, r= -0.262).**

Results showed an increase in central corneal thickness with increasing myopia, although this relationship was not significant (p=0.051). Examination of the corneal thickness for the XQ also showed interesting results, although the change in thickness with refractive error was not significant for any of the quadrants (p<0.05); there were marked differences in the thickness of each quadrant (p<0.01). The superior cornea was thickest and the temporal the thinnest. Further evidence for characterising anterior vs. posterior myopic growth can be sought from examining maximum distances; comparisons of emmetropic and myopic eyes showed the temporal retina to be most affected by myopic growth and the superior quadrant to be least affected.



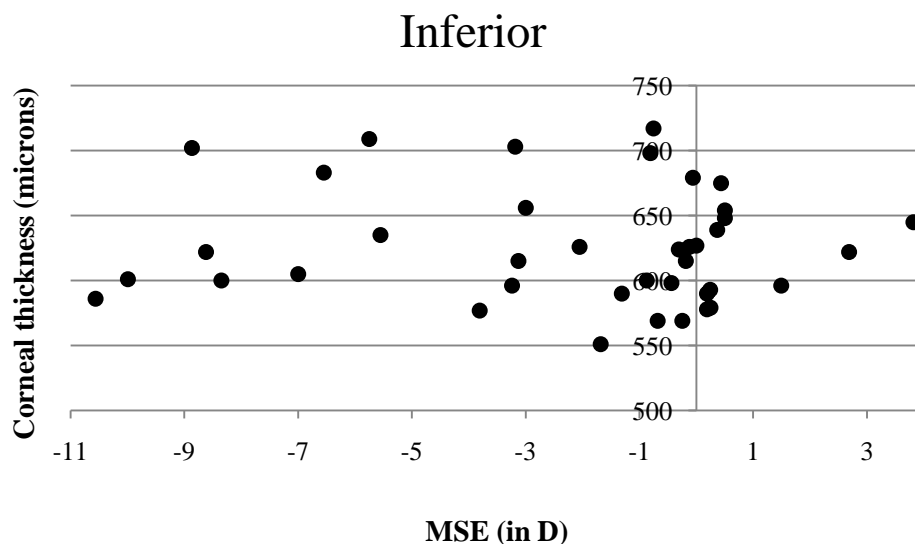


**Figure 79 Corneal thickness values (in microns) for the XQ, obtained using the Oculus Pentacam ( $n=40$ )**

### 9.7 Discussion and conclusions

Initially the findings placed focus on the inter-refractive group differences in the posterior 25% of the eye. The myopes showed gradual steepening of radius of curvature in the posterior regions; in contrast both emmetropes and hyperopes displayed relative flattening. The shape characteristics noted in the posterior eye agree with previous reports of a more prolate, or less oblate, eye shape in myopes compared to emmetropes (Atchison et al. 2005; 2004; Logan et al. 2004). Of particular note is the area preceding the posterior changes, where a more spherical shape was found. Greater irregularity in eye shape was also noted in both low myope and emmetrope subject groups compared to high myopes. Irregularities in eye shape have been previously noted in data collected using peripheral refraction techniques (Taberero & Schaeffel 2009).

The anterior eye was found to be similar between refractive groups in terms of radius of curvature and ocular volume. The ocular volume results mirrored those of an earlier study carried out using the same technique (Gilmartin et al. 2008). Corneal volume was measured using the Oculus Pentacam and was also found to be similar between refractive groups.

To examine ocular shape in further detail, retinal quadrant shape differences were evaluated. Initially chord differences between quadrants were examined. The results showed a great deal of asymmetry in the anterior regions of the eye; a region which had thus far been

regarded as homogenous across refractive groups. Anteriorly, the nasal chord was larger than the temporal (at a position approximately 15% along the distance of the presumed visual axis). The quadrant asymmetries reduced up to the 75% mark, beyond which increased disparity between quadrant chord lengths recommenced. In the vertical meridian the inferior chord, in general, was larger than the superior. At the 75% mark there was a larger dissimilarity between the superior and inferior chords for both myopic and hyperopic eyes. These findings would suggest that despite the presence of many inter refractive group similarities for the anterior ocular shape, pronounced quadrant dissimilarities exist. The results will be affected, to a small degree, by the discrepancies between the visual and optic axes. At the 75% mark all the differences in chord length appeared to be at a similar level between refractive groups i.e. the graphs show the data from each refractive group intersect in this region. The apparent similarity between refractive groups at the 75% mark once again highlights the 75% region as a critical site in refractive error development.

Using a modification of an earlier experiment (Nagra et al. 2009) the maximal distances from the presumed visual axis to the retinal surface were measured for each of the quadrants. The largest maximum distance was noted in the superior quadrant (XQ) and ST (+Q); this was the case for all refractive groups. Maximum distance values for the nasal quadrant were noted as being the smallest for all refractive groups. Comparisons of maximum values in high myopes *vs.* all other refractive groups showed particular enlargement of the temporal quadrant, however, these findings did not reach statistical significance. The differences in temporal growth compared to less myopic groups are noted in even low myopes. Multiple reports have cited the temporal retina as being the most common site for retinal degenerations associated with myopia e.g. retinal detachments and retinal holes (Shukla et al. 1986). It is speculated that the temporal quadrant may possess some form of structurally or sensory driven weakness, which ultimately exposes the temporal retina as a vulnerable site for mechanical myopic stretch.

After establishing that there were both anterior and posterior inter refractive group differences in eye shape, the study focused on the curvature, or bulbosity, of quadrants. The  $\chi^2$  coefficient for the 25-75% region revealed few refractive group differences, there were however significant quadrant differences. The results demonstrated that although quadrants were different in shape, this was not generally a consequence of refractive error. Greatest variations were expected in the posterior 25% cap, however it was considered that 2<sup>nd</sup> order polynomial curve fits would not be able to accurately represent the data in this region,

therefore as an alternative respective meridians were examined (N-T, S-N, SN-IT, and ST-IN). The meridional differences were not found to be significant across refractive groups; it is acknowledged that combining two quadrants to produce a meridian may have masked quadrant differences.

Inter eye differences produced interesting results showing differences in both the anterior and posterior regions of right and left eyes and specific quadrant differences. While some quadrants were noted as being different between eyes other quadrants were far more homogenous. These differences can either indicate a physiological difference between the right and left eyes or indicate a natural variation between eyes of the same individual.

Previous literature has described three models of eye shape; global expansion, equatorial growth, and posterior pole elongation (Atchison et al. 2004; 2005; Strang et al. 1998). The results from the current study indicate that a combination of these models best describes the data. Posterior pole elongation has been associated with increasing myopia and the results clearly indicate that myopic eyes are larger in size. Many reports have shown that myopic eyes tend to have prolate, or less oblate, shaped eyes compared to emmetropes (Atchison et al. 2005; Stone & Flitcroft 2004). The posterior pole model illustrates the relative steepening of myopic eyes in the posterior region and the radius band findings are in agreement with this model. The variations in the more anterior region of the eye suggest that global expansion models are not applicable to this region. Subtle quadrant differences in eye shape are overlooked by these simplistic models. Additionally, further evaluation of the data is required to assess the anterior regions of myopic eyes; MRI can be used in conjunction with data collected with the Oculus Pentacam to provide more accurate descriptions of anterior eye shape. Measures of anterior structures such as the crystalline lens and anterior chamber will provide further understanding and help create models of the more anterior regions of the eye in myopia.

## **9.8 Summary**

In conclusion, there are significant differences in the size of myopic, emmetropic and hyperopic eyes. Eye shape in the anterior sections of the eye is similar between refractive groups, although subtle quadrant differences have been noted. In the posterior eye meridional differences are not significant between refractive groups. Quantifying the differences between quadrants in the posterior eye is challenging due to the discrepancies in

the optic and visual axes. The maximum distances for the superior-temporal and the superior quadrants are largest relative to other quadrants for all refractive groups, and the temporal quadrant appears to be most affected by myopic growth (see Figure 61). It is envisaged that future analysis of the data will use engineering techniques such as finite element analysis and mathematical modelling in order to quantify the change between emmetropic eyes and myopic eyes.

Pages 137 and 138 have been removed for copyright restrictions.

## 11 PERIPHERAL REFRACTION AND OCULAR SHAPE

### 11.1 Introduction

Research in the field of peripheral refractive error has enjoyed renewed interest in recent years due to the proposal that the peripheral retina mediates central structural development of the eye (Wallman & Winawer 2004). In the 1970s a series of major studies concluded that emmetropic subjects who subsequently developed myopia had been shown to possess peripheral refractive errors which were hyperopic relative to the central refractive error (Rempt et al 1971). The finding of a hyperopic periphery, relative to the fovea, in myopia has been reported many times since (Seidemann et al 2002; Logan et al 2004; Calver et al. 2007).

The reasons why myopic development takes place in the presence of a hyperopic periphery have been less well explored. In animal studies, occlusion of an eye generally causes enlargement of the globe and thus myopia, that is, form deprivation myopia. It has been suggested that as the eye cannot 'see' a blurred image in front of the retina, the eye assumes the image must lie behind it i.e. the eye believes it is too small and has a hyperopic refractive error; the eye consequently grows to compensate for the presumed refractive error and can be thought of as 'searching' for a clearer image (Wallman & Winawer 2004). The compensatory growth can also be shown through the use of negative powered lenses which defocus the image and move it to a position behind the retina. Evidence for this reactive growth in animals can be gained from measuring the changes in choroidal thickness in form deprived animal eyes, where the introduction of a positive lens moves the images anterior to the retina, and in an attempt to slow down growth the choroid thickens moving the retina to a more anterior position. Conversely, the introduction of a negative powered lens moves the image posterior to the retina, and the choroid becomes thinner in an attempt to move closer to the image (Wallman & Winawer 2004).

Form deprivation can also lead to ocular enlargement in humans (O'Leary & Millodot 1979; Twomey et al. 1990). The eye is unable, however, to exercise exact homeostatic control and prevent myopia from developing in otherwise healthy eyes. There has been a suggestion that perhaps each individual has their own specific default refractive error setting which acts as a 'STOP signal' to growth, i.e. an individual with a default setting of -3 dioptres may regulate growth about this level of defocus, not allowing the eye to become more myopic or

emmetropic. The STOP signals may be cellular, biochemical or molecular based (Morgan & Megaw 2004).

The theory that a hyperopic periphery drives myopic growth is explained in similar terms to the reasons explaining form deprivation myopic growth. The relatively hyperopic region is believed to send growth signals to the relatively myopic centre and stimulate axial growth (Wallman & Winawer 2004). Therefore a relatively hyperopic peripheral refraction may act as a predictor of future myopia onset and development (Rempt et al 1971).

## **11.2 Peripheral astigmatism**

Ferree and Rand (1933) stated that it may be possible to calculate retinal contour from peripheral refraction. With increasing eccentricity from the visual axis there is a simultaneous variation in low level off axis aberrations; particularly peripheral astigmatism. Consequently a peripheral refraction measurement cannot be directly converted into its equivalent dioptric length in order to represent ocular shape and size; all refractive components must be taken into account. Peripheral astigmatism and refractive error has been modelled in schematic eyes in an attempt to derive retinal contour (Dunne et al. 1987). Dunne *et al.* (1995) devised a computational approach for calculating retinal contour from peripheral refraction taking account of crystalline lens thickness, corneal curvature, anterior chamber depth and axial length. The program has been well established and has been used to measure retinal contour in a number of studies (Dunne et al 1995; Logan et al 2004).

Although peripheral refraction techniques can provide a useful tool for retinal contour calculation, their validity has been questioned (Stone & Flitcroft 2004). As the posterior globe is particularly vulnerable to structural changes in myopia, it is imperative to the understanding of myopic development that accurate assessments of eye shape in this region can be made.

Three-dimensional MR imaging of the eye is a relatively new technique (Singh et al. 2006) which has thus far not been compared to peripheral refractive techniques used to derive eye shape. To evaluate whether the two techniques are comparable and interchangeable, the current study sets out to compare data from subjects who have undergone both procedures. If peripheral refraction is found to be an accurate and precise measure of retinal contour it will possess several advantages over the MRI method. Costs of carrying out peripheral refraction are much lower than MRI; a trained technician is able to carry out peripheral

autorefraction, whereas MRI requires qualified radiographers. Equipment and scan costs are significantly greater for MRI scanning than autorefraction. Additionally, there are many possible reasons why a subject may be unable to undergo MRI scanning; e.g. dental work, metal implants or claustrophobia. In contrast, the autorefractor has very few procedural limitations.

### **11.3 Purpose**

The purpose of this study is to evaluate the differences between using the peripheral refraction technique to derive retinal contour and contour derived from 3 dimensional ocular MRI.

### **11.4 Hypothesis**

It is hypothesised that measurements of retinal contour derived from peripheral refraction will be contiguous with those found using MR imaging of ocular shape

### **11.5 Instrumentation**

The Shin Nippon SRW 5000 IR binocular free space autorefractor was used to take peripheral refractive measurements at 5° intervals up to a maximum of ±30° nasal and temporal. Measurements were taken to the nearest 0.12D at a vertex distance of 12mm. The Shin Nippon has been used extensively in peripheral refraction research. It has shown to be highly repeatable and demonstrated a high level of accuracy through correlation with subjective refraction (Mallen et al. 2001). A more comprehensive review of the Shin Nippon autorefractor is detailed in the Chapter 7.

### **11.6 Methods**

Forty two unpaid volunteers with refractive errors ranging from -10.56D to +4.38D underwent peripheral refractive measurements, which were taken at 5° intervals up to a maximum of 30° in the horizontal meridian. Subjects with astigmatic error greater than -2.00D were excluded. The majority of subjects were either undergraduate Optometry students or qualified optometrists, with ages ranging from 18 years to 40 years. Subjects comprised of 30 females and 12 males. All subjects (bar one) had previously undergone the ocular MRI. In addition to peripheral refractive and MR measurements, ocular biometric components were measured using the Zeiss *IOL Master* (see section 7.3). Keratometry, axial length measurements and anterior chamber depth recordings were used to facilitate the calculation of retinal contour. Lens thickness was derived from the regression equation reported by Smith et al. 2009. Informed consent was obtained from all volunteers prior to the study.

To minimise the effect of accommodation 1 drop of 1% tropicamide ophthalmic solution (*Minims*<sup>®</sup>, Bausch and Lomb Limited, Surrey, U.K) was instilled into each eye approximately 25 minutes prior to autorefractometry. The tropicamide also helped facilitate the peripheral refraction readings by increasing the pupil size and enabling the measurement of more peripheral readings, however some subjects responded less well to the dilating effects of tropicamide and thus more peripheral measurements were difficult to obtain. Intraocular pressures were measured before and after the experiment with non contact tonometry, and verbal advice given in case of ocular adverse reactions to the tropicamide.

Subjects were positioned on the Shin Nippon autorefractor by use of an adjustable chin rest and head rest. A custom designed and built extendable arm with a fixation target was affixed to the autorefractor (see 7.2). The subject was then asked to fixate on a target at a distance of approximately 1m, and a minimum of four readings at each angle were attempted. The Shin Nippon autorefractor relies upon a focused image of the corneal mires in order to take a measurement; for the more extreme peripheral measurements, corneal curvature and pupil size restricted the number of readings. In some subjects measurements up to 30° were not achievable.

## 11.7 Results

The spherical-cylindrical outputs from the autorefractor were converted into vector components through use of equations developed by Thibos *et al.* (1997), these equations have also been used by Atchison *et al.* 2006 and Calver *et al.* 2007 in their respective analyses of peripheral refraction data.

The first equation calculates mean spherical error (MSE) using the standard equation:

$$\text{MSE} = \text{Sph} + \left( \frac{\text{Cyl}}{2} \right)$$

Where MSE =Mean Spherical Error

Sph = Spherical error

Cyl = Cylindrical error

The second equation calculates the vector component  $J_{180}$  which is astigmatic error with an axis between  $90^{\circ}$ - $180^{\circ}$ :

$$J_{180} = \frac{-Cyl \cos(2\theta)}{2}$$

The third equation calculates the astigmatic vector component  $J_{45}$  which is astigmatic error with an axis that lies between  $45^{\circ}$ - $135^{\circ}$ :

$$J_{45} = \frac{-Cyl \sin(2\theta)}{2}$$

Calver *et al.* 2007 discuss a fourth equation to help recover the magnitude of astigmatism; which takes the mean value of the three previous equations:

$$C' = 2\sqrt{(J_{45}^2 + J_{180}^2)}$$

Consistent with previous studies the reading  $15^{\circ}$  temporal to the fovea was removed as it is the likely location of the optic disc (Atchison, 2006). Subject data were grouped according to central mean MSE group. MSE results for each eccentricity were then compared between refractive groups. Polynomial fits of  $J_{180}$  and linear fits of  $J_{45}$  helped describe the relationship between refractive groups and the orientation of the astigmatism. Measures of  $J_{180}$  and  $J_{45}$  were then used to calculate the cylindrical component ( $C'$ ).

Retinal contour was then derived by use of the computational program by Dunne *et al.* (1995), *RetinaFit*. The program calculates retinal contour using formulae derived from schematic eyes. There are three separate sections to the program; calculating tangential corneal radius, sagittal refractive error and the interval of Sturm; then entering data for each eccentricity into the main retinal contour program. The program adjusts the corneal conic constant values until they match the peripheral astigmatic value. The calculated sagittal refractive value is then adjusted to match the measured value. Both adjustments require manual manipulation. For each angle of eccentricity *RetinaFit* generates X and Y coordinates. X and Y<sup>2</sup> coordinates are then used to derive curve fit estimates using a statistical software package (SPSS version 16). From the quadratic curvature estimates, values for the apical radius (r) and conic constants (p) are generated using the formula:

$$Y=AX+BX^2$$

where  $r = A/2$

and  $p= -B$  (Dunne 1995).

The values  $r$  and  $p$  are inputted into the equation:

$$y^2 = 2rx - px^2$$

Previous literature cites fixed  $x$  values which correspond to each field angle (Dunne, 1995). These values for  $x$  were inputted into the equation to calculate values for  $y$ . These figures are based on schematic eyes and thus introduce a level of error for actual field angle being tested (see Table 9); however the objective of the study was to compare the two techniques so for this reason fixed values of  $x$  were used for both peripheral refraction and MRI techniques to produce a direct comparison of techniques. For comparison purposes, the same methodology was used on the MRI data to calculate  $r$  and  $p$  values. Again fixed  $x$  values were used for the MR data to derive the  $y$  coordinate using the equation above.

<b>X coordinate</b>	<b>Field angle (°)</b>
0.35	10
1.38	20
2.99	30
5.05	40
7.37	50
9.75	60

**Table 9 The approximate distance from the fovea towards the anterior eye in millimetres which would correspond to each field angle using a schematic eye (after Dunne, 1995)**

The program is not significantly affected by inherent ocular errors such as crystalline lens asphericity or changes in lens gradient index (Dunne 1995).

The differences between the MRI calculated  $y$  values and *RetinaFit* technique derived  $y$  values were taken at each of the tested eccentricities. The mean differences for each subject were plotted graphically to display the disparity between the two techniques.

In the current study the primary interests were:

- I. The presence of relative peripheral hyperopia in myopic eyes
- II. The correlation of retinal contour based on peripheral refraction with that based on MRI.

For these reasons results from  $J_{180}$ ,  $J_{45}$ , and  $C'$  data is included for completeness only, and not explored in depth.

### **MSE**

Subjects were placed into one of three groups based on MSE:

High myopes (greater than 6D myopia)

Low myopes (myopia between -6D and -0.5D)

Emmetropes ( $>-0.5 \leq +1.75$ D).

Hyperopic subjects were excluded from this study due to insufficient subject numbers ( $n=2$ ).

A summary of the average refractive errors and standard deviations are shown in Table 10 below. Right and left eyes were examined separately.

Refractive group	Eye	Average MSE	Standard deviation
High myopes ( $n=6$ )	Right	-8.42	$\pm 1.33$
High myopes ( $n=7$ )	Left	-7.45	$\pm 1.13$
Low myopes ( $n=13$ )	Right	-2.39	$\pm 1.53$
Low myopes ( $n=13$ )	Left	-1.82	$\pm 1.23$
Emmetropes ( $n=22$ )	Right	+0.19	$\pm 0.60$
Emmetropes ( $n=20$ )	Left	+0.20	$\pm 0.51$

**Table 10 The average MSE in dioptres (D) and standard deviations for each refractive category, right and left eyes**

The average MSE and corresponding standard deviations for each eccentricity are listed in Table 11 for right and left eyes.

Eccentricity	High myopes	Low myopes	Emmetropes
30n	$-6.17 \pm 3.78$	$-1.02 \pm 1.84$	$-0.01 \pm 1.32$
25n	$-7.07 \pm 3.02$	$-1.85 \pm 2.19$	$0.22 \pm 1.04$
20n	$-8.08 \pm 2.18$	$-2.09 \pm 2.11$	$0.29 \pm 0.77$
15n	$-8.37 \pm 2.23$	$-2.43 \pm 2.02$	$0.16 \pm 0.89$
10n	$-8.48 \pm 1.42$	$-2.49 \pm 1.82$	$0.23 \pm 0.65$

5n	-8.37±1.58	-2.48±1.94	0.20±0.69
0	-8.42±1.33	-2.39±1.53	0.19±0.59
5t	-8.24±1.59	-2.54±1.57	0.18±0.56
10t	-8.15±1.87	-2.60±1.56	0.09±0.57
20t	-7.38±2.18	-2.50±1.93	-0.25±0.92
25t	-5.71±2.66	-2.33±1.68	0.12±1.13
30t	-2.90±0.57	-0.61±1.30	-0.13±0.89

**Table 11 Mean MSE at each eccentricity for right eyes, for each refractive group ± standard deviations (*n*= nasal retina, *t*= temporal retina). Results for eccentricity 15 degrees temporal were omitted due to effect of the optic nerve head.**

In general, most data were not normally distributed in accordance with the Kolmogorov-Smirnov and Shapiro-Wilks tests of normality, therefore non parametric tests were employed throughout.

The Kruskal Wallis test showed the three refractive groups were significantly different in MSE at each eccentricity ( $p < 0.001$ ), except the temporal 30°. The lack of significance at temporal 30° may be due to the limited number of readings taken at this point; results for this eccentricity should therefore be treated with caution.

*Post hoc* tests were carried out using Mann Whitney U tests to compare peripheral MSE at each eccentricity with central MSE. Critical values of significance were therefore reduced to  $0.05/3 = 0.0167$  (i.e. Bonferroni correction). Differences between emmetropes and low myopes were significant at all eccentricities ( $p \leq 0.002$ ), bar the temporal 30 and nasal 30 degrees. Differences between emmetropes and high myopes were significant at all eccentricities ( $p \leq 0.001$ ) bar temporal 30 degrees. Differences between low and high myopes were significant at all eccentricities ( $p \leq 0.008$ ) bar temporal 30 and temporal 25 degrees.

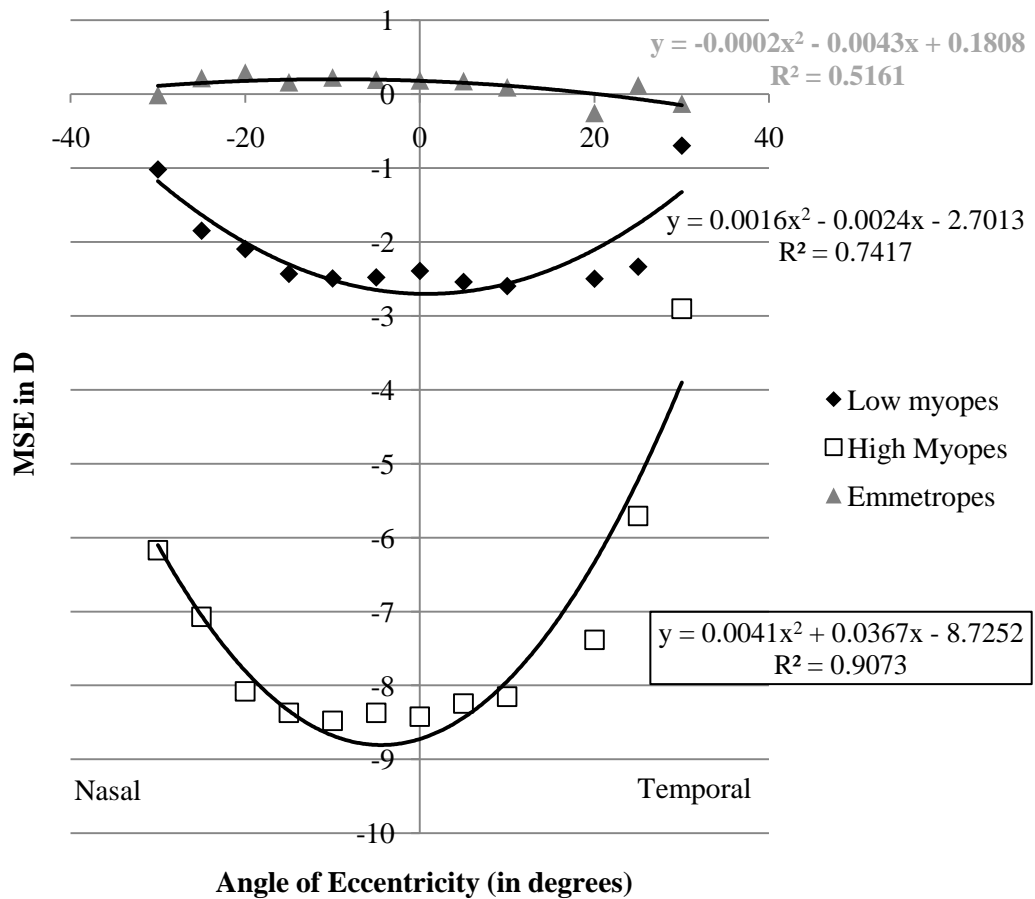


**Figure 80 Graph of the mean uncorrected peripheral refractive error for right eyes fitted with 2<sup>nd</sup> order polynomial curves (references to nasal and temporal refer to retinal not field locations,  $n=42$ )**

### Relative difference in peripheral MSE compared to central MSE

To assess the amounts of relative hyperopia or myopia in the peripheral retina for each group, the difference between the central MSE and MSE at each eccentricity for each individual was calculated. The mean values for each refractive group were compared.

Eccentricity	High myopes	Low myopes	Emmetropes
30n	2.61±2.60	1.12±1.45	-0.27±1.48
25n	1.63±1.97	0.67±1.27	0.03±1.10
20n	0.34±1.11	-0.30±1.11	0.10±0.64
15n	0.05±1.10	-0.04 ±0.79	-0.03±0.59
10n	0.06±0.53	-0.10±0.74	0.04±0.30
5n	0.05±0.55	-0.09±0.56	0.01±0.29
5t	0.18±0.56	-0.15±0.41	-0.01±0.25

10t	0.27±0.58	-0.28±0.68	-0.09±0.35
20t	2.27±2.57	-0.18±1.12	-0.46±0.92
25t	2.99±2.06	-0.19±1.41	-0.08±1.18
30t	4.81±1.50	+1.53±2.50	-0.06±1.06

**Table 12 Mean difference in MSE between central and peripheral locations, right eyes**

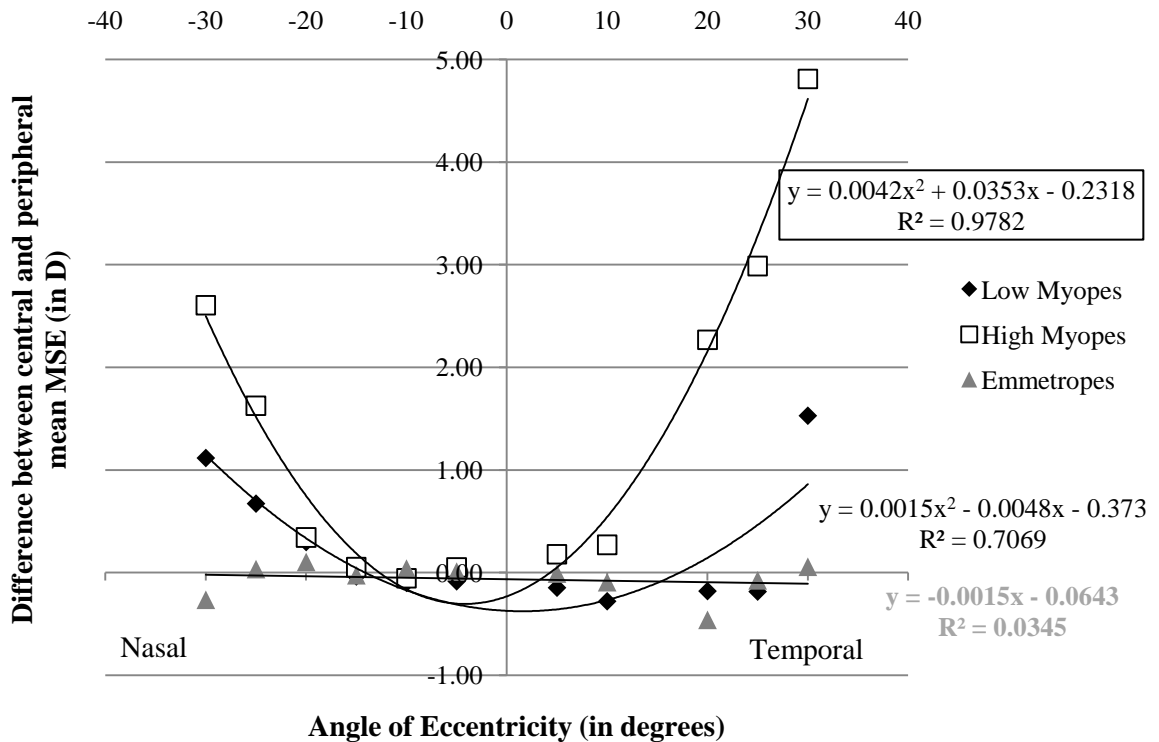


**Figure 81 Graphical representation of the mean difference in MSE between central and peripheral locations, right eyes (linear fit used for emmetropic group, 2<sup>nd</sup> order polynomials for myopic groups)**

Wilcoxon signed ranks test was used to compare the difference in MSE at each eccentricity to the centre. The low myopic group showed a significant increase in hyperopia at nasal 30 degrees. High myopia showed significant differences in the temporal 20 and 25 degrees in MSE relative to the central MSE. In emmetropic subjects, the only significant difference between the central MSE and peripheral MSE was for temporal 30 degrees ( $p \leq 0.05$ ).

Overall between groups there was a significant effect (found using the Kruskal Wallis test) at temporal 20, 25 degrees and nasal 30 degrees which on *post hoc* testing (Mann Whitney U) showed differences between the emmetropes and high myopes at all three eccentricities and between low and high myopes at 25 degrees. There were no significant differences

between emmetropes and low myopes in the degree of relative hyperopic or myopic defocus in the periphery.

## Astigmatism

MSE estimates the mean spherical error, which can be a useful approximation of central refractive error. With increasing eccentricity from the fovea peripheral astigmatism can comprise a large part of the refractive error, it is therefore expedient to examine the cylindrical component as a separate entity. Although the implication of peripheral astigmatism in myopic development is unclear, values for the astigmatic vector components  $J_{180}$  and  $J_{45}$  are included for completeness.

### **$J_{180}$**

Eccentricity	High myopes	Low myopes	Emmetropes
30n	0.82±0.55	-0.13±1.55	-0.69±0.87
25n	0.72±0.71	0.16±1.22	0.45±0.49
20n	0.30±0.47	0.13±0.91	-0.24±0.39
15n	0.18±0.36	0.26±0.65	-0.12±0.33
10n	0.20±0.48	0.36±0.53	-0.01±0.22
5n	0.19±0.27	0.30±0.34	-0.06±0.16
0	-0.01±0.33	0.14±0.35	-0.09±0.24
5t	-0.17±0.38	0.08±0.50	-0.16±0.25
10t	-0.53±0.35	-0.22±0.42	-0.30±0.28
20t	-0.31±0.29	-0.82±0.86	-0.79±0.67
25t	0.43±0.76	-0.87±1.16	0.86±0.72
30t	0.92±0.11	-0.12±0.67	-0.81±0.00

**Table 13 Mean  $J_{180}$  values right eye listed by angle of eccentricity and refractive group**

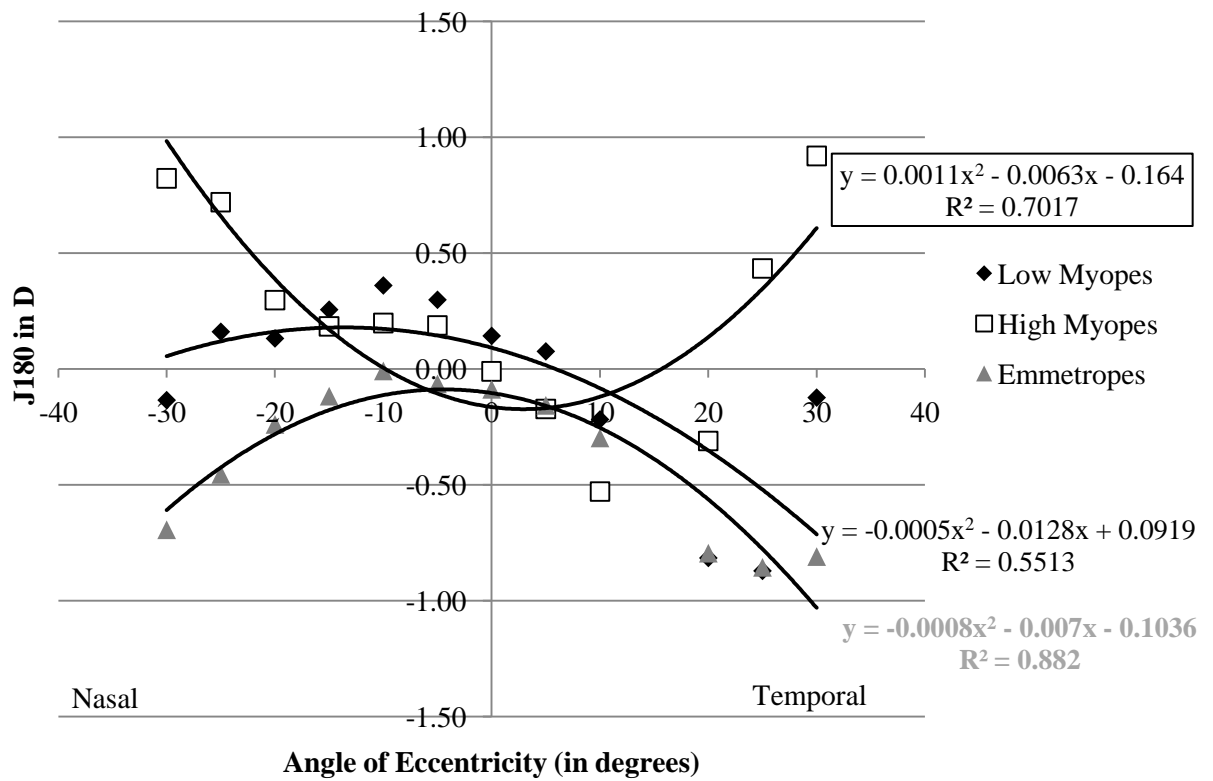


**Figure 82 Mean  $J_{180}$  values for right eyes, fitted with 2<sup>nd</sup> order polynomial curves**

Although not the main part of the study;  $J_{180}$  values were plotted for each refractive group as a function of eccentricity (see Figure 82). The emmetropic and low myopic groups displayed some nasal-temporal asymmetries; appearing to show higher levels of astigmatic error in the temporal retina.

**J<sub>45</sub>**

Eccentricity	High myopes	Low myopes	Emmetropes
30n	-0.13±0.37	-0.08±0.56	-0.23±0.42
25n	-0.26±0.64	-0.08±0.42	-0.13±0.36
20n	0.01±0.62	0.01±0.33	0.16±0.35
15n	-0.04±0.80	0.01±0.42	-0.02±0.36
10n	0.04±0.47	-0.17±0.36	-0.01±0.24
5n	0.03±0.29	0.01±0.42	-0.04±0.14
0	0.02±0.42	-0.07±0.32	0.01±0.10
5t	0.04±0.41	0.03±0.42	0.06±0.15
10t	0.29±0.74	-0.13±0.31	0.10±0.18
20t	0.34±0.64	-0.04±0.39	0.18±0.31
25t	0.38±0.94	0.06±0.54	0.22±0.34
30t	0.22±0.27	-0.08±0.39	-0.78±0.00

**Table 14 J<sub>45</sub> right eye, listed by angle of eccentricity and refractive group**

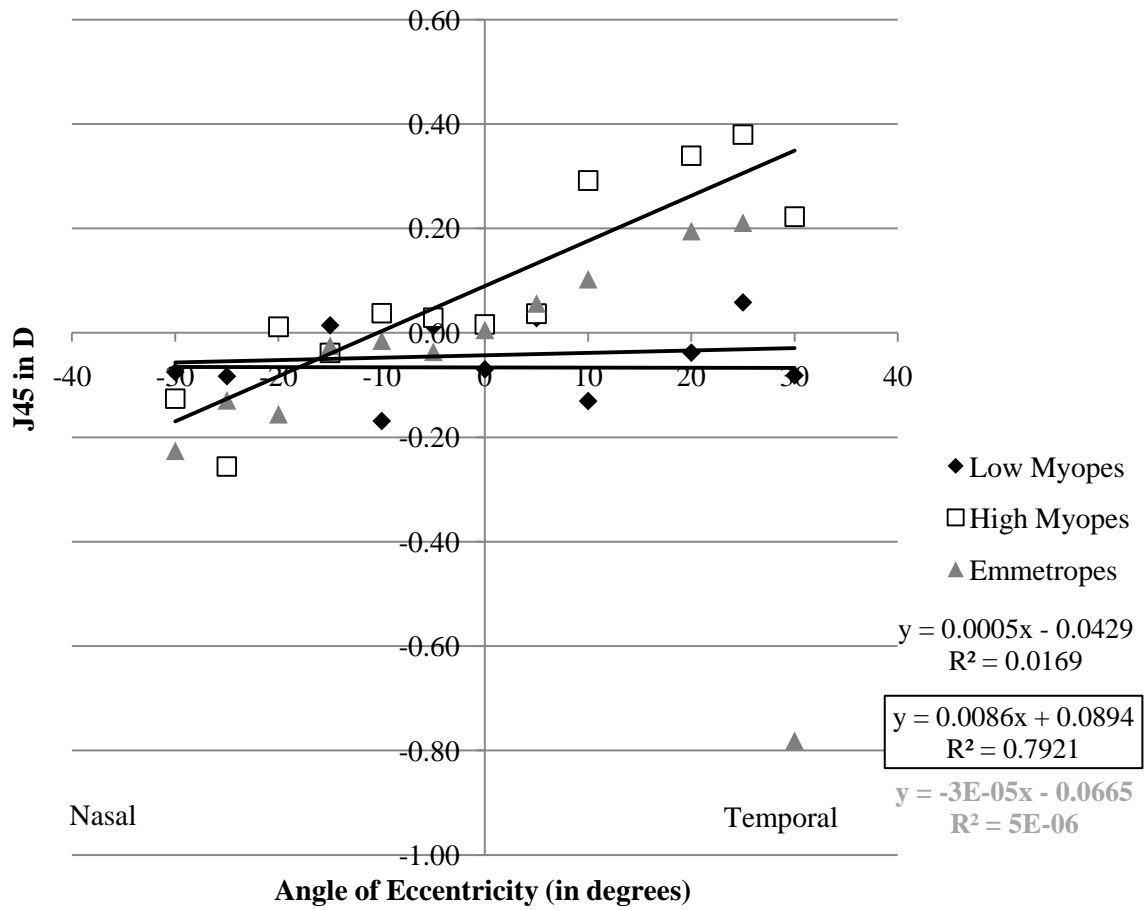


**Figure 83 Mean  $J_{45}$  values for right eyes, fitted with linear trend lines**

Consistent with previous reports the nasal retina tended to show a greater degree of  $J_{45}$  astigmatism (Calver et al. 2007).

## Cylindrical component

The cylindrical component was derived as a measure of the magnitude of astigmatism at each of the eccentricities. The cylindrical component is considered to be more useful than  $J_{180}$  and  $J_{45}$  vector analysis as it provides information on magnitude of astigmatism rather than reducing astigmatism into separate components and describing them separately (Thibos et al 1997; Calver et al 2007).

Eccentricity	High myopes	Low myopes	Emmetropes
30n	-1.84±0.97	-2.84±1.41	-2.11±1.11
25n	-1.95±1.37	-2.22±1.20	-1.35±0.70
20n	-1.33±0.85	-1.65±0.92	-1.03±0.59
15n	-1.46±0.86	-1.54±0.60	-0.85±0.50
10n	-1.17±0.62	-1.37±0.53	-0.57±0.32
5n	-0.71±0.47	-1.06±0.59	-0.40±0.20
0	-0.89±0.44	-0.80±0.57	-0.45±0.30
5t	-1.04±0.31	-0.97±0.85	-0.56±0.37
10t	-1.73±0.93	-0.95±0.64	-0.80±0.42
20t	-1.42±0.71	-1.94±1.55	-1.93±1.05
25t	-2.22±1.16	-2.37±1.93	-1.75±1.33
30t	-1.94±0.09	-1.27±0.69	-2.25±0.00

**Table 15 Cylindrical component as calculated from vector components  $J_{180}$  and  $J_{45}$ , right eyes**

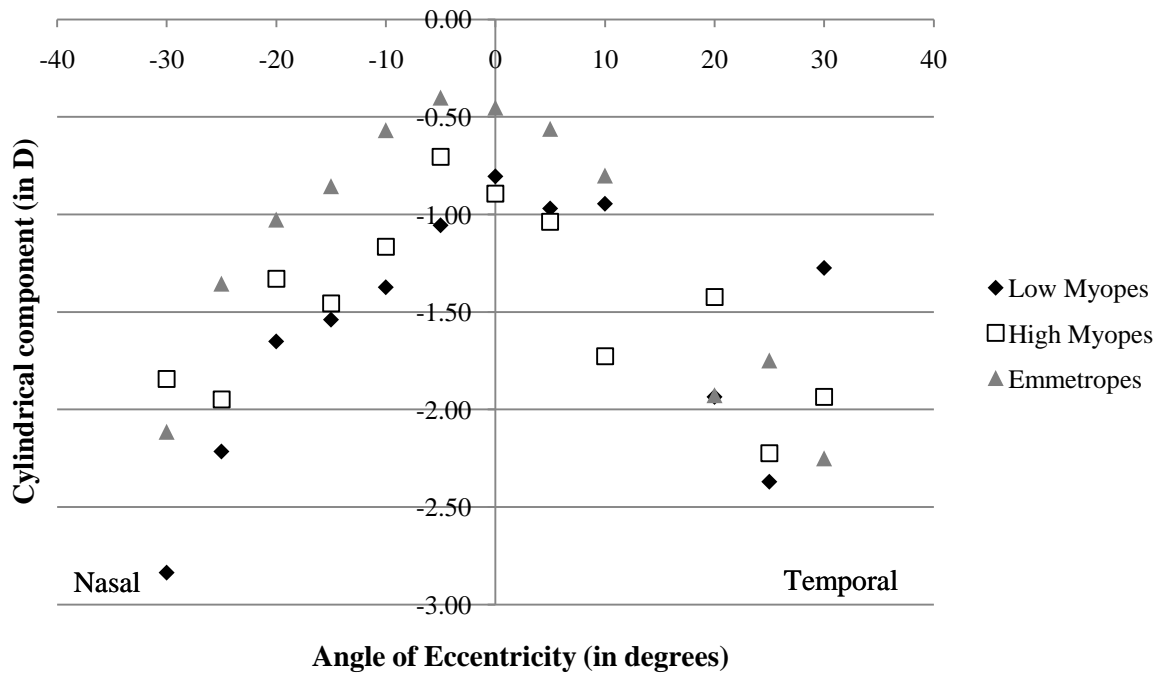


**Figure 84 Graphical representation of cylindrical component, for right eyes only**

Each of the refractive groups showed clear nasal-temporal asymmetry. The magnitude of astigmatism varied significantly between groups in the central  $\sim 15^\circ$  ( $p = < 0.05$ , Kruskal Wallis test), interestingly beyond this eccentricity there was not a significant difference in amount of astigmatism between the three refractive groups.

### Retinal contour calculation through *RetinaFit*

Each subject's peripheral refractive measurements were inputted into the *RetinaFit* program as described above, alongside their individual ocular biometric measurements. The difference in the y coordinates was examined.

Each individual subject's MRI data was also analysed in the horizontal meridian. The data for the distance 3mm either side of the fovea (nasal and temporal) was taken and plotted (see Table 9). The distance along the axis was subtracted from the calculated total axial length to derive a new set of axial length corrected values; these were then corrected to ensure 3mm either side of the presumed foveal location was used. As with the *RetinaFit* procedure the calculated x values and the  $y^2$  values were inputted into a statistical package and quadratic curve fit estimations derived; from this r and p values were calculated (see Methods). Assuming the same x fixed values previously indicated the y coordinate was derived. The difference between MRI and *RetinaFit* y values was taken and represented graphically (see Figure 85).

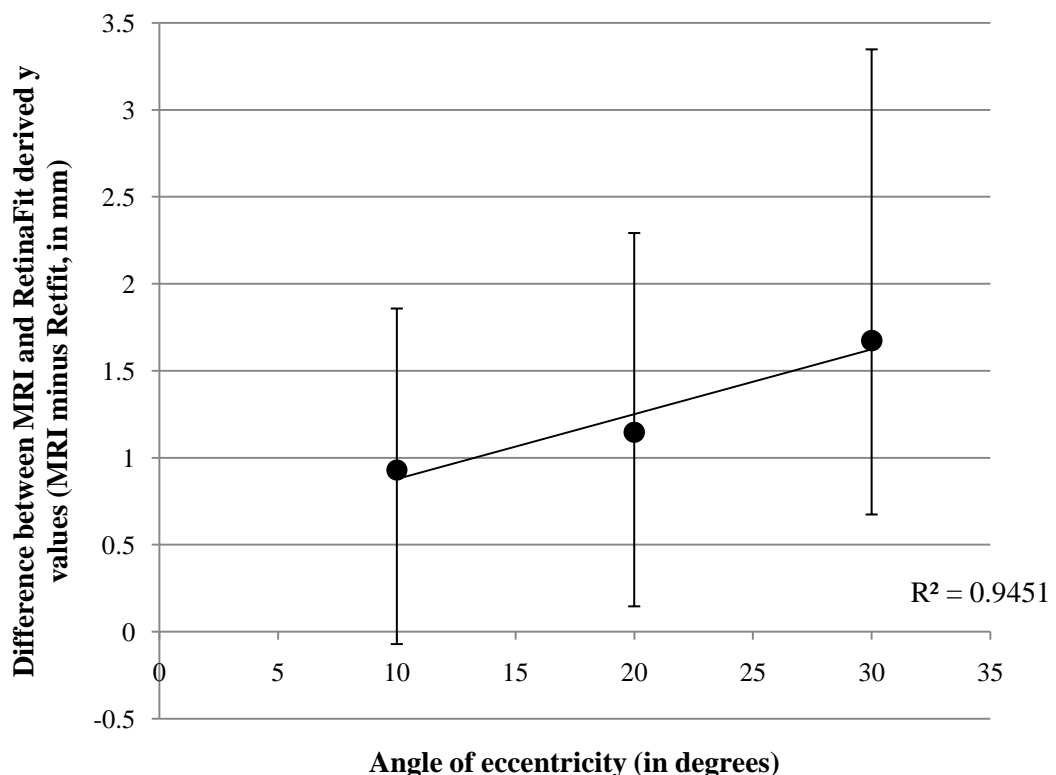


**Figure 85** The difference in retinal contour data as derived by MRI and RetinaFit by field angle (combined average of  $n=41$ )

As results were not normally distributed (as found by the Kolmogorov-Smirnov test of normality), the non parametric Wilcoxon test was used. A significant difference between the MRI and *RetinaFit* techniques was found at each of the tested eccentricities ( $p < 0.001$ ). The MRI measurements recorded a slightly flatter ocular shape. The differences enlarged as a function of increasing angle of eccentricity from the line of sight. At  $10^\circ$  eccentricity there was approximately 0.59mm difference in y values calculated between the *RetinaFit* and MR techniques, at  $20^\circ$  this increased to 0.67mm and at  $30^\circ$  to 0.78mm. Based on the results it can be understood that there was an average increase in disparity between the MRI and *RetinaFit* techniques of 0.1mm with every  $10^\circ$  increase from a field angle of  $10^\circ$  (which itself had a disparity of 0.59mm).

	Angle of eccentricity (in degrees)		
	10	20	30
Average (mm)	0.59	1.27	2.04
Standard deviation	$\pm 0.93$	$\pm 1.15$	$\pm 1.67$
Average difference in RetFit and MRI derived y values with respect to increasing field angle		0.68	0.77

**Table 16 The relative differences between the two techniques at different field angles**

When the data are grouped and examined by refractive error a clear difference of a 0.1mm increment is not visible. All three refractive groups show an increase in disparity between the MRI and *RetinaFit* calculated y values with increasing field angle. The magnitude of discrepancy between the two techniques appears to be greater with increasing levels of myopia.

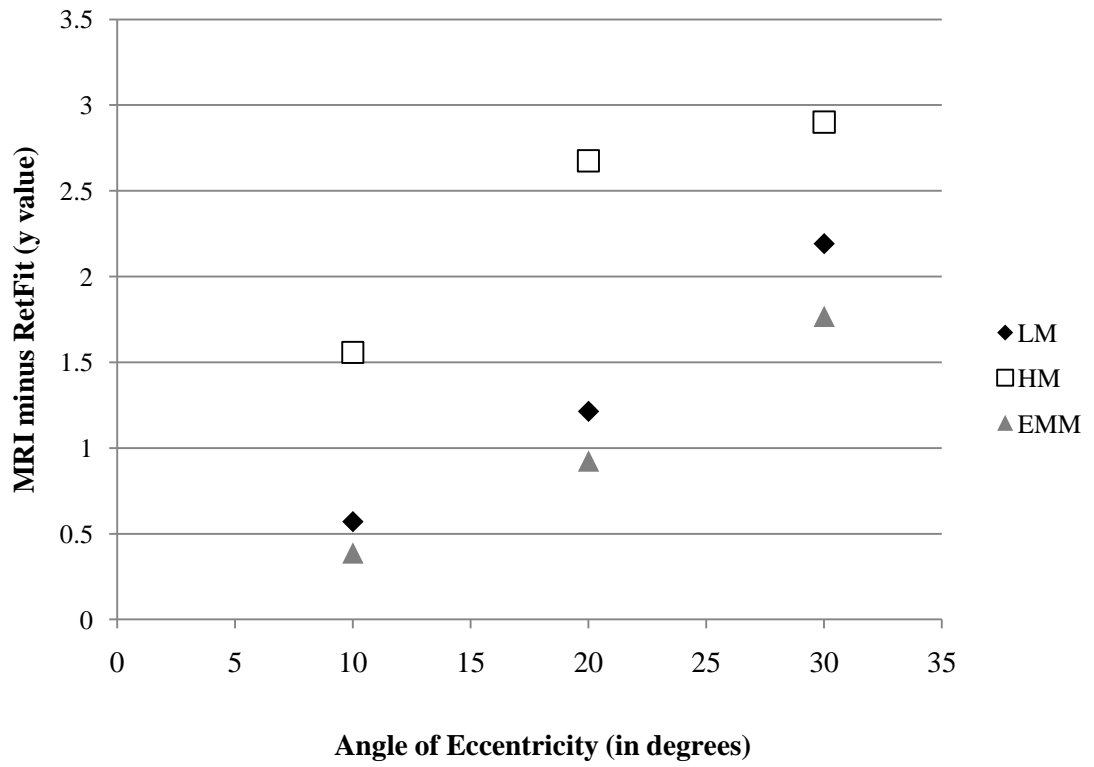


**Figure 86 Mean difference for y values between the MRI and RetinaFit techniques, with reference to refractive error**

Refractive group	Angle of Eccentricity (in degrees)		
	10	20	30
Low Myopes	0.57±0.34	1.21±0.06	2.19±1.69
High Myopes	1.56±1.00	2.68±0.84	2.9±1.07
Emmetropes	0.39±1.31	0.92±1.56	1.77±0.10

**Table 17 Mean differences in y values between the MR data and RetinaFit program values (in mm)**

## **11.8 Discussion and conclusions**

### **MSE and astigmatic components**

Results for MSE and the astigmatic representations of the peripheral refraction data were generally in line with previous reports (Calver et al. 2007; Atchison et al. 2006). Myopic eyes generally showed hyperopic defocus at field angles away from the fovea; the hyperopia appeared to increase with increasing eccentricity. The levels of hyperopic defocus only became significant at more peripheral locations (i.e. 25° and beyond) compared to the central MSE. Emmetropic eyes showed relative myopia in the periphery, but the disparity between central and peripheral MSE was less pronounced compared with myopes. Furthermore the highly myopic group appeared to show a more exaggerated effect i.e. more relative hyperopia in the periphery, than the low myopes.

Consistent with previous reports  $J_{180}$  and  $J_{45}$  components appeared to show astigmatic error for  $J_{180}$  to be greater in the temporal retina than nasal, and  $J_{45}$  to be greater in the nasal retina (Calver et al 2007; Atchison et al. 2006). Also consistent with previous reports, the differences between nasal and temporal retinae are more marked for the  $J_{180}$  component than  $J_{45}$ .

The magnitude of astigmatism varied between the nasal and temporal hemi-fields. In general, the temporal retina showing greater astigmatism than the nasal. Similar nasal-temporal asymmetries in astigmatism have been reported previously, (Seidemann et al 2002; Dunne et al 1993).

Interestingly, the amount of astigmatism for the three refractive groups only varied significantly in approximately the central 15°. Beyond the central region there were no significant differences in the magnitude of astigmatism; this places further focus on the spherical element of the Rx.

### **RetinaFit and MRI correlation**

A unique aspect of this study was the correlation of the retinal contour generated from peripheral refraction with the MRI ocular shape data. Results showed consistent differences between the two techniques as a function of increasing field angle. Due to technical difficulties with the program, which could not be resolved within the time scale of the

current study, a maximum retinal area of 30° only was covered. Once these technical difficulties are resolved, the extent of the retina examined will depend upon the angles at which peripheral refraction was measurable by the investigator. Overall, the MRI technique estimated retinal contour to be flatter than the *RetinaFit*. The disparities between the results increased as a function of increasing field angle. The relationship between the field angle and error appeared to be linear when the cohort was not split by refractive group; increasing at a rate of 0.1mm for every 10° increase in angle beyond 10°. Thus this error can be used to develop a correction within the *RetinaFit* program. Examining the differences between MR data and the *RetinaFit* program by refractive error did not show the same level of error; therefore a 0.1mm correction factor would introduce its own level of error.

The present study has shown that laboratories using peripheral refraction methods as a means of estimating retinal contour should treat peripheral field angle results with caution owing to the discrepancies noted with increasing field angle.

There could be several causes for the differences in results derived from the two techniques; in peripheral refraction the location of the line of sight is easily located through use of the Shin Nippon autorefractor. In MR imaging, locating the visual axis is more problematic (see 9.2.3). The difference between the optic axis (geometric axis) and visual axis is termed angle  $\alpha$ . There is both a horizontal, and of less significance, vertical element to angle  $\alpha$ . MRI images are taken along the nominal optic axis.

Additionally, MR imaging is not affected by optical refractive components, whereas peripheral refraction is vulnerable to refractive component properties such as changes in refractive index, curvature of refractive components and errors in autorefractor measurements. Although lens tilt and optical component displacement do not significantly affect the *RetinaFit* program, it is likely that other aberrations will affect the results.

As the differences between the y values calculated from MRI data and *RetinaFit* appear to be linear for refractive groups as a whole, a correction could be applied to the *RetinaFit* program to make values comparable to MR data. However, it must be stressed that differences in the MR data and *RetinaFit* discrepancy exist as a function of refractive group.

Peripheral refraction possesses several advantages over the MRI technique, the main being cost. MRI also potentially poses significant risk to volunteer subjects and a stringent set of criteria must be met before subjects can undergo MR scanning. Furthermore retinal contour

measures derived through peripheral refraction are especially advantageous in paediatric ocular research, as the requirement for good fixation for MR scanning can be overcome.

### **11.9 Summary**

In conclusion, the results from the MSE,  $J_{180}$ ,  $J_{45}$  measures are consistent with those reported previously. The study has examined a unique application of peripheral refraction derived retinal contour by correlating it with MRI derived retinal contour. The results indicate that there is some scope for transforming *RetinaFit* data to generate retinal contours that match approximately those generated by MRI.

## 12 VISUAL FIELD SENSITIVITY AND OCULAR SHAPE

### 12.1 Introduction

Visual field testing is a commonly used technique by practitioners to assess peripheral visual function in clinical optometric practice and hospital settings. The test involves determining sensitivity to light at multiple locations in both the central and peripheral retina; the responses are derived from the cone photoreceptor pathway. Visual field testing has shown reduced sensitivity in myopic subjects (Martin-Boglund, 1991; Aung et al. 2001; Rudnicka and Edgar 1995). Loss in sensitivity may occur at levels of myopia as low as  $-2D \pm 1D$  (Czepita and Chmielewska, 2004). In particular the superior temporal field (inferior nasal retina) has been reported to show reduced sensitivity (see 4.4). Although the source of a reduced sensitivity is unclear, there are several possibilities. Decreased retinal luminance due to a longer axial length; changes in the photoreceptor cells; decreased photoreceptor density as a consequence of ocular expansion (Rudnicka and Edgar, 1995); misdirection or misalignment of photoreceptors caused by an increased in axial length, or pathological fundus changes may all contribute to a reduction in visual field sensitivity.

To further explore the theory that ocular shape may affect the light sensitivity threshold, specific indices of retinal curvature and shape derived from MR imaging analysis are correlated with mean visual field thresholds from the corresponding retinal regions. It is envisaged that in general larger eye sizes will correlate with reduced visual field sensitivity.

## **12.2 Purpose**

The purpose of this study is to determine the relationship between retinal shape, specifically the posterior 25% cap of the eye, with visual field sensitivity, using subjects from a range of refractive error and age groups.

## **12.3 Hypothesis**

Based upon the current literature, it is proposed that ocular expansion produces reduced visual field responses possibly as a consequence of reduced photoreceptor density. It is hypothesised that retinal quadrants which show greater expansion, as determined through surface area and interval variance (IV) measurements, will correlate with a reduction in visual field response.

## **12.4 Instrumentation**

The commercially available and widely used automated Humphrey Visual Fields Analyser (HFA) was used to test visual field sensitivity (see 7.4). The SITA-Standard threshold program within the HFA was used as an alternative to a full threshold fields program, due to its ability to yield results comparable to full threshold testing in a fraction of the time. The SITA Standard program also helped simulate a typical clinical setting and aided in combating the effects of fatigue by providing a shorter test time. Previous studies of automated perimetry in myopic subjects have shown the 30-2 single threshold test on the Humphrey Visual Field Analyser as sufficient for screening purposes for pathology affecting visual fields (Rudnicka and Edgar, 1995).

Two program settings were used: the 30-2 program, which tests locations within the central 60° field at 6° intervals and on a smaller subset of subjects; the central 10-2 program which tests the central 20° field at 1° intervals. The 10-2 fields program improves the ability to detect smaller areas of focal loss in the central field.

## **12.5 Methods**

The cohort comprised of 40 young adult subjects for whom 3-dimensional ocular MR images had been previously acquired. Ages ranged from 18-40 years old. Mean spherical error (MSE) for the group ranged from -9.31D to +4.19D, and respective axial lengths from

27.64mm to 21.84mm. Subject refractive errors were obtained by use of the Shin Nippon 5000 autorefractor and axial length measurements were recorded using the *Zeiss IOL Master* (see 7.2 and 7.3). Full refractive corrections were worn throughout all recordings, only subjects with astigmatism under 2.00DC were included in the study to ensure most ametropia was of spherical origin.

All subjects underwent central 30-2 SITA standard visual fields testing on the Humphrey Visual Fields Analyser. Subjects were invited back to attend for a 10-2 SITA threshold fields program test however response was poor with only 9 subjects returning. Ethical consent was sought and all subjects were unpaid.

Monocular tests were carried out: right eyes were tested first, followed by the left eye. The same order was maintained throughout the experiment, but for the purposes of analysis only right eye data is presented. There were no significant differences between right and left eye sensitivities (TD and MS) as determined by a paired student t-test.

Subjects were given a break for approximately ten minutes between each test; breaks were also provided at the subject's request. Throughout the visual fields tests, subject fixation was monitored via a fixation video monitor and also by the Humphrey machine's built in Heijl-Krakau method of fixation monitoring. All tests with fixation losses above 20% were rejected.

Mean maximum sensitivity (MS) values for each quadrant of the visual field were obtained through averaging results using the orthogonal axes provided on the visual fields plot for XQ quadrants (as defined in Chapter 9). For the +Q quadrants the plots were divided at 45° to the orthogonal axes. To maximise inclusion of data, any point lying on the XQ axis was included into the quadrant which lay directly anticlockwise (right eyes). The method is detailed in the Figure 87.



Further measures of visual field function were obtained through use of age corrected total deviation (TD) plots. The TD quadrant averages were obtained using the same method as the numeric MS plots.

In order to compare visual field sensitivity values for each quadrant with ocular shape, interval variance measurements (IV) were obtained by calculating the standard deviations for the MR data comprising the posterior 25% of each quadrant and deriving the 95% IV (i.e. 1.96 \* standard deviation). Further indices of shape were calculated by deriving the surface area (SA) for each quadrant. The mean 2-dimensional data for the posterior 25% of each quadrant were plotted graphically and fitted with second order polynomials (see 9.5). The polynomial equations were then inputted into formulae for the calculation of surface area (derived by Dr Bill Cox and Professor Bernard Gilmartin):

$$S = \frac{\pi}{6a^2} [(1+4a^2r^2)^{3/2} - 1]$$

S = surface area of posterior 25% cap

a = the 'a' coefficient in  $y = ax^2 + c$  (from fitting the posterior 25% data for each quadrant with a second order polynomial curve)

r = the x coefficient of the polynomial equation

Analysis was carried out through repeated measures ANOVAS, and ANCOVAS with age as a covariate. Further investigations were carried out using linear correlations.

## 12.6 Results

### Refractive error vs. axial length

Pearson's correlation coefficient showed refractive error to be correlated significantly with axial length; the  $R^2$  value was consistent with previous studies.

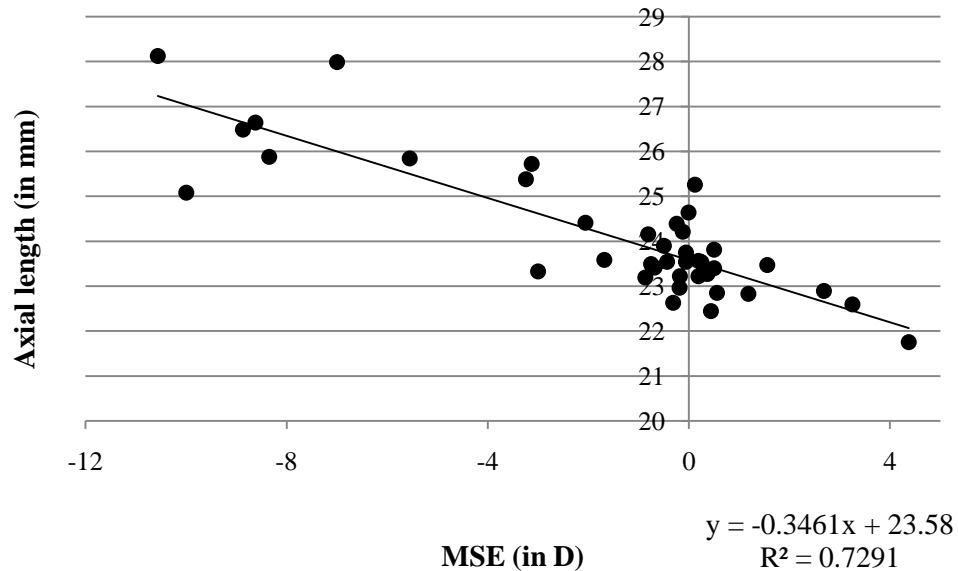


**Figure 88 The significant relationship between axial length (in mm) and mean spherical error (MSE in D,  $n=40$ ) (one tailed Pearson's correlation coefficient  $p<0.001$ ,  $r = -0.854$ )**

Mean spherical error (MSE) ranged from +4.185D to -9.31D and axial lengths ranged from 21.84mm to 27.24mm.

### Age vs. Visual fields sensitivity

As expected increasing age was significantly correlated with a decline in mean visual field sensitivity (one-tailed Pearson's correlation coefficient  $p<0.05$ ,  $r=-0.267$ ).

### Visual field sensitivity by quadrant

#### **Maximum Sensitivity (dB)**

Mean MS values for each quadrant are shown in Table 18.

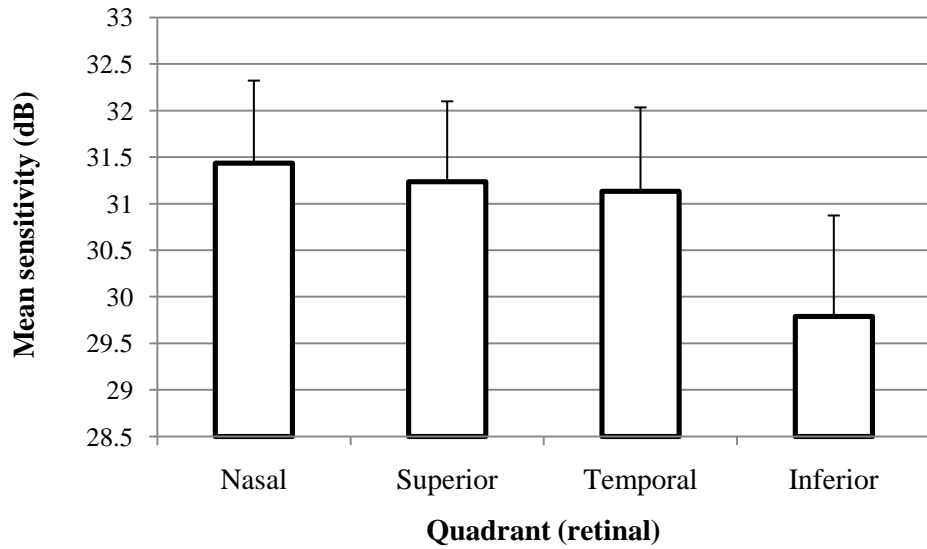


**Figure 89** Graph showing the mean sensitivity for each of the XQ quadrants, error bars show standard deviations

Repeated measures ANCOVA, with age as a covariate, showed significant differences between the inferior vs. temporal, nasal and superior quadrants ( $p < 0.01$ ).

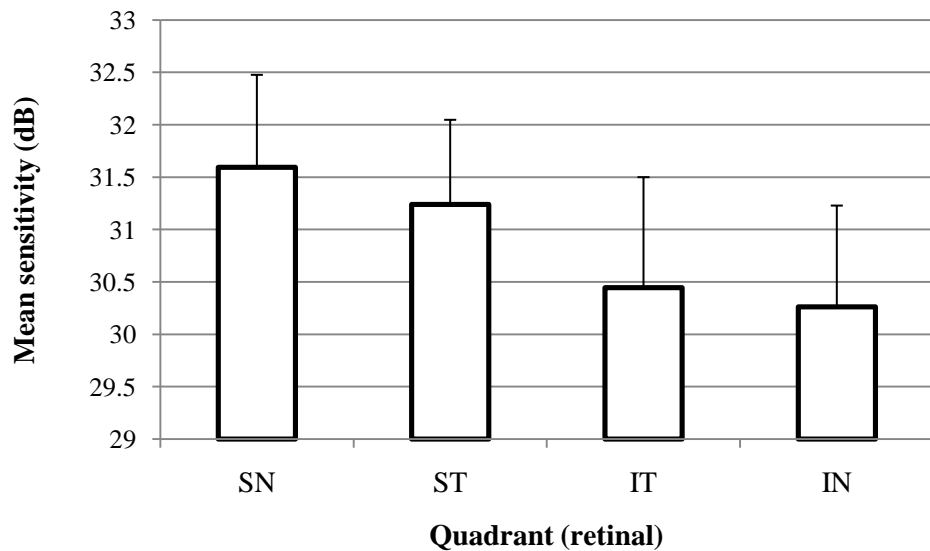


**Figure 90** Graph showing the mean MS response for each of the +Q quadrants, error bars show standard deviations

Repeated measures ANCOVA controlling for age showed significant differences between all quadrants ( $p < 0.01$ ) bar inferior nasal vs. inferior temporal.

Quadrant	Nasal	Sup	Temp	Inf	SN	ST	IT	IN
Mean MS (dB)	31.46	31.27	31.18	29.82	31.62	31.28	30.49	30.28
Standard deviation	0.89	0.85	0.86	1.08	0.88	0.78	1.02	0.97

**Table 18 Mean MS response for each quadrant**

**Total Deviation**

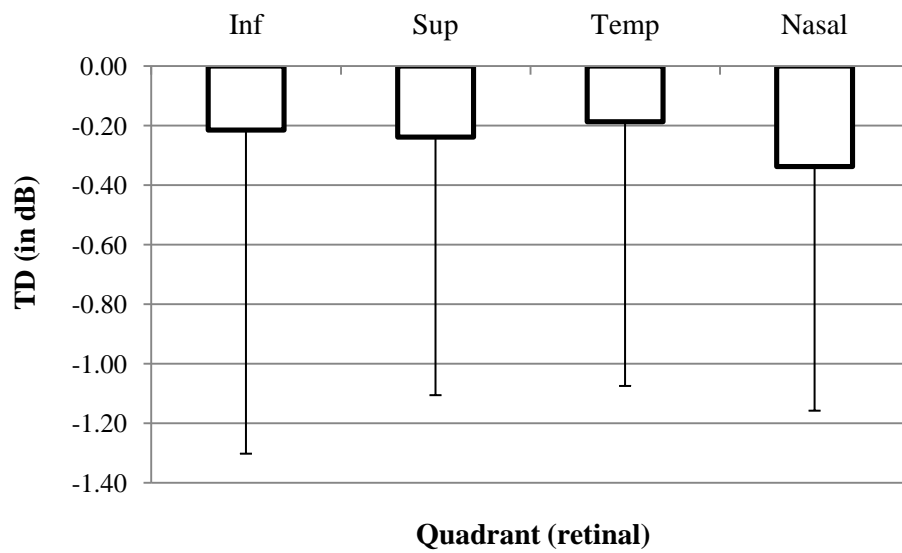


**Figure 91 Mean TD per XQ quadrant, error bars show standard deviations**

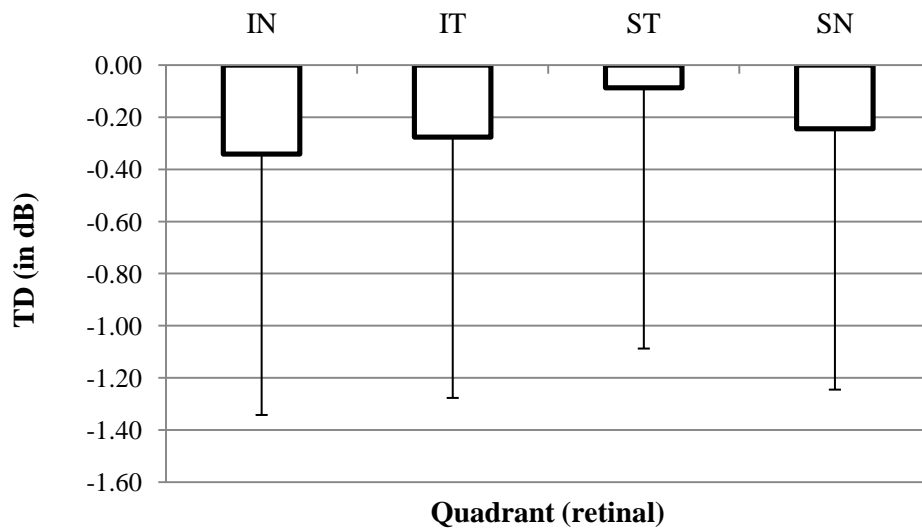


**Figure 92 Mean TD per +Q quadrant, error bars show standard deviations**

Repeated measures ANOVA showed there to be no significant differences between quadrants for both XQ and +Q ( $p = <0.05$ ).

Quadrant	Temp	Inf	Sup	Nasal
Mean TD (dB)	-0.19	-0.22	-0.24	-0.34
Standard deviation	0.89	1.09	0.87	0.82

**Table 19 Mean TD of responses for each XQ quadrant**

Quadrant	ST	SN	IT	IN
Mean TD (dB)	-0.09	-0.24	-0.28	-0.34
Standard deviation	0.79	0.80	1.01	0.99

**Table 20 Mean TD of responses for each +Q quadrant**

### **Axial length**

Axial length was tested for correlation with MS, using a semi-partial correlation which controlled for age. Axial length was not significantly correlated with MS responses for any quadrant. TD was also checked for correlations with axial length using Pearson's correlation coefficient; but no significant correlations were noted for any of the quadrants ( $p = <0.05$ ).

## Retinal surface area

Mean retinal surface area for each quadrant, XQ and +Q are shown in the figures below:

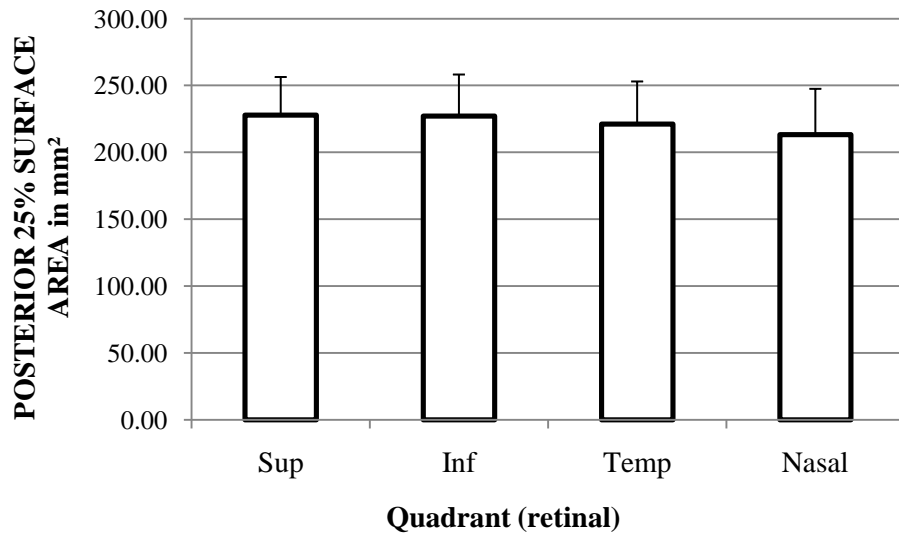


**Figure 93 Mean surface areas for each XQ quadrant are shown for the posterior 25% cap of the eye. Error bars show standard deviations**

Repeated measures ANOVA showed significant differences between the surface areas of the nasal vs. superior and nasal vs. inferior quadrants ( $p=0.013$  for both).

A semi-partial correlation with age as a covariate did not show a significant relationship between MS and SA of corresponding quadrants (XQ) ( $p= <0.05$ ).

Pearson's correlation coefficient did not show a significant relationship between TD and SA (XQ).

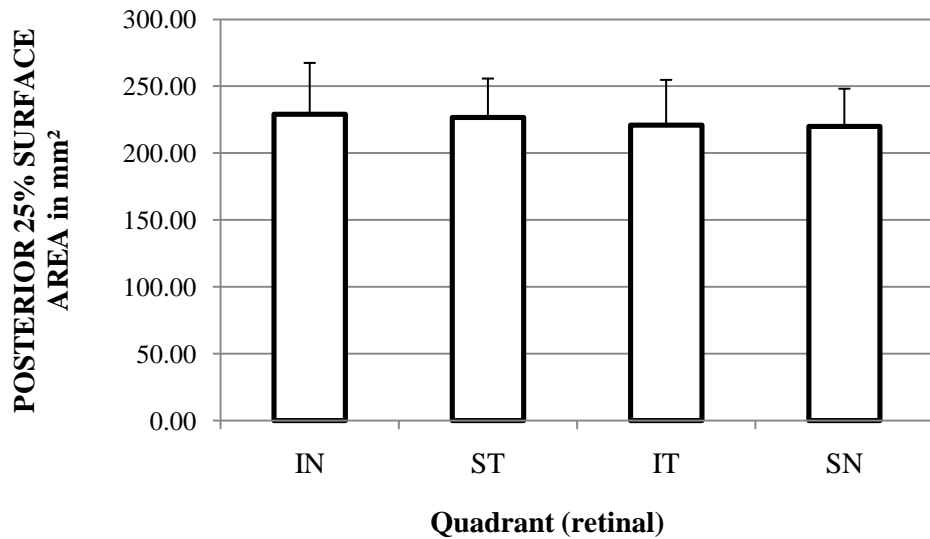


**Figure 94** Mean surface areas for each +Q quadrant are shown for the posterior 25% cap of the eye. Error bars show standard deviations

Repeated measures ANOVA did not show significant differences between surface areas of +Q quadrants. A semi-partial correlation (controlled for age) did not show a significant relationship between MS and SA of corresponding quadrants (+Q) ( $p < 0.05$ ).

Quadrant	Nasal	Temporal	Superior	Inferior	Sup-temp	Inf-nasal	Sup-nasal	Inf-temp
<b>Average (mm<sup>2</sup>)</b>	213.15	221.25	227.89	227.04	226.77	229.09	220.03	220.86
<b>Standard deviation</b>	34.26	31.68	28.37	31.09	29.11	38.48	28.27	34.02

**Table 21** Surface area values and standard deviations for each quadrant

### Interval Variance (IV)

Mean retinal IV values are shown for each quadrant in Table 22.

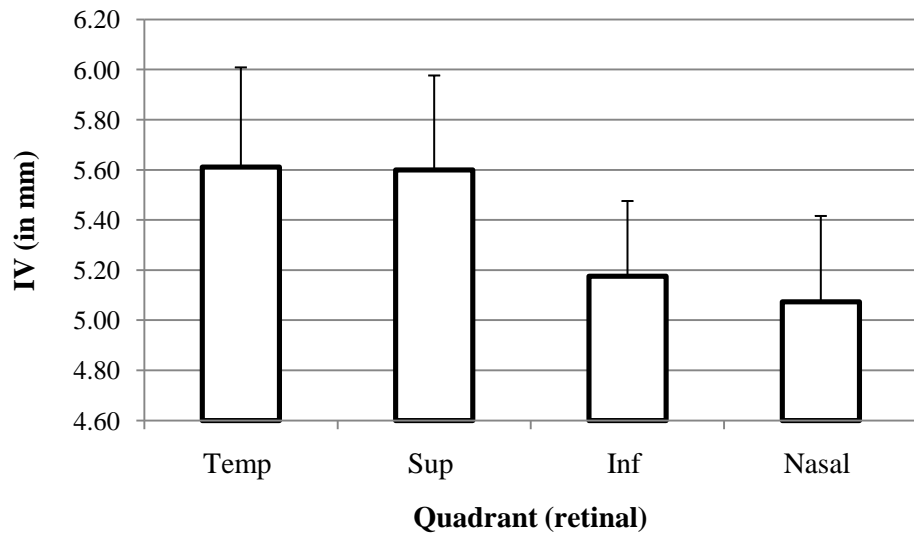


**Figure 95 IV indices per retinal quadrant, error bars show standard deviations**

One way repeated measures ANOVA showed significant differences between all quadrants ( $p < 0.01$ ) bar the nasal vs. inferior and temporal vs. superior.

A semi-partial correlation (controlling for age) showed a significant relationship between the superior quadrant IV and MS ( $p = 0.022$ ,  $r = -0.365$ ), although by using a Bonferroni correction for four quadrants this would no longer be significant.

Pearson's correlation of TD and IV showed a significant relationship for the superior quadrant ( $p = < 0.001$ ,  $r = -0.498$ ).

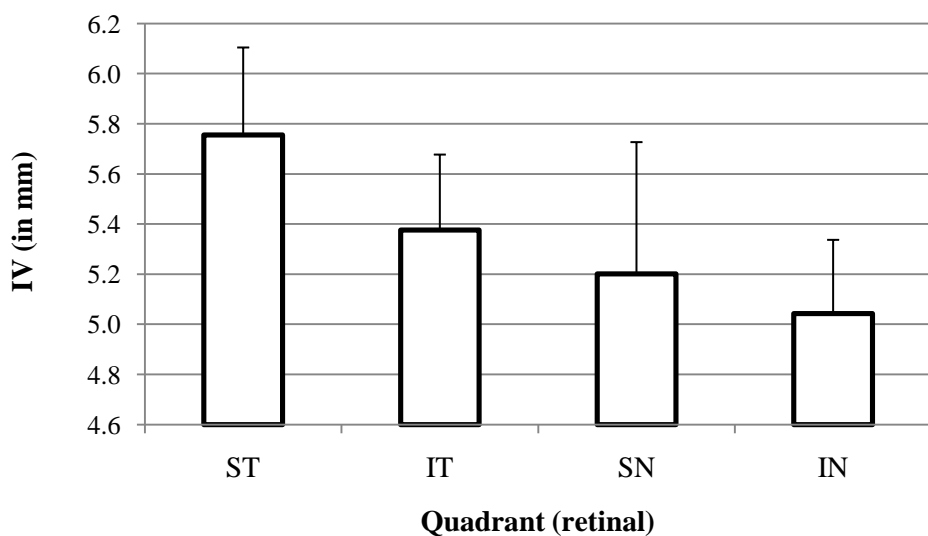


**Figure 96 IV per retinal quadrant, error bars show standard deviations**

Repeated measures ANOVA showed significant differences between all quadrants ( $p < 0.01$ ), bar inferior-nasal vs. superior-nasal and superior-nasal vs. inferior-temporal.

A semi-partial correlation (controlling for age) showed a correlation between MS and IV for the superior temporal quadrant ( $p = 0.005$ ,  $r = -0.445$ ).

Pearson's correlation of TD and IV showed a significant relationship for the superior temporal quadrant ( $p = 0.002$ ,  $r = -0.478$ ).

Quadrant	Nasal	Temporal	Superior	Inferior	Sup-temp	Inf-nasal	Sup-nasal	Inf-temp
Average (mm)	5.07	5.61	5.60	5.18	5.76	5.04	5.20	5.38
Standard deviation	0.34	0.40	0.38	0.30	0.35	0.29	0.53	0.30

**Table 22 Mean IV values for each quadrant, based on MRI data for the posterior 25% of the eye**

### 12.6.1 Discussion and conclusions

Reduced photoreceptor density created by ocular expansion has been suggested as a cause of reduced visual field sensitivity in myopic subjects. To investigate the effect of ocular shape on visual field sensitivity, shape indices derived from magnetic resonance imaging data were correlated with visual field sensitivity from corresponding retinal quadrants. Both maximum sensitivity (MS) and total deviation (TD) plots were correlated with surface areas and interval variance (IV). Correlations of surface areas with TD and MS failed to reach significance; IV, however, was correlated with visual field sensitivity. Notably the superior and superior-temporal TD and the superior-temporal MS were correlated with the IV. Based on the results of the current study the relationship between ocular shape and visual field sensitivity appears to be limited to the superior and superior-temporal quadrants only; interestingly the superior-temporal quadrant has been widely implicated in myopia as a site of myopic retinal damage. Retinal degenerations associated with myopic enlargement are known to occur most frequently in the superior-temporal quadrant (Hyams et al. 1975; Shukla and Ahuja, 1983).

The present study shows that although the significant correlations between eye shape and visual field sensitivity are limited to just the superior-temporal and superior quadrants, a well established inter quadrant variance exists. The inferior quadrant MS response was significantly reduced compared to the nasal, superior and temporal quadrants. Furthermore the inferior hemifields also showed reduced visual field sensitivity in the +Q.

Although the purpose of the experiment was to investigate ocular shape with reference to visual field sensitivity, isolating the effect of shape alone is difficult. There are several factors associated with shape: surface area, curvature, stretch, and photoreceptor distribution and density. To accurately evaluate the relationship between ocular shape and visual field sensitivity, determination of all the factors is required.

### **12.7 Summary**

Although two quadrants did show a significant correlation between visual field sensitivity and indices of ocular shape, in general it can be concluded that visual fields sensitivity and ocular shape are not correlated.

## 13 MULTIFOCAL ELECTRORETINOGRAM AND OCULAR SHAPE

### 13.1 Introduction

Electrophysiological testing provides an objective method of quantifying the functional changes in the retina. Most recently the multifocal electroretinogram (mfERG) has been used to compare responses from myopic and emmetropic eyes; mfERG helps to provide information about specific locations over the central 50° of the retina (see Figure 99). A number of sources have cited the decline in mfERG response with a longer axial length (Chan & Mohidin 2003), whilst others have attributed the reduced response to myopic refractive error. As the two conditions often coexist it is difficult to control for the effects of each, however, through use of ANCOVA analyses it has been suggested that axial length may only be responsible for approximately 15% of the decline in response and refractive error for 27% (Chen et al. 2006a). The remaining decline in response has been attributed to numerous factors such as increased retinal cell spacing with myopic retinal stretch (Kawabata & chi-Usami 1997) or damage to retinal cells as a consequence of retinal expansion. Reports of mfERG investigation with reference to axial length and refractive error have not been consistent; although the amplitudes or implicit times may be reduced in myopic eyes there is still variation in the retinal location producing the reduced response. Some reports have suggested loss originating from a central location whereas others a more central and peripheral location (Kawabata & chi-Usami 1997). Additionally the reductions in mfERG response appear to be limited to progressing myopes or high myopes; stable myopes and emmetropes have been reported to produce similar responses (Chen et al. 2006a). In part the lack of consistency may originate from individual variations in cell topography, but also differences in the protocols used by different laboratories. The differences in protocols arise most frequently in the type of mfERG component analysed and the type of stimulus. The mfERG produces a waveform response, and most often researchers concentrate on the amplitude of the first peak (P1) and its implicit time (also referred to as latency). Another widely assessed component is the amplitude and implicit time of the first trough: N1. Additionally, further components of the mfERG waveform response may be examined; investigations of the second trough (N2) and other smaller secondary aspects of the response waveform have also been reported (Chen et al. 2006b).

Differences between laboratories have also arisen in the type of stimulus used. The stimulus comprises a hexagonal pattern and there are three levels of stimulus: 61, 103, or 241 hexagons. If a smaller number of hexagons are used as a stimulus, a larger region of the

retina is represented by each hexagon. For detecting small retinal differences, a larger number of hexagons is considered more favourable. The advantage of a larger number of hexagons can be offset by the inaccuracies produced by fixation losses; if a small number of hexagons are used, with each covering a larger retinal region, small eye movements could be accommodated without loss of accuracy. For the purpose of this study a stimulus array of 103 hexagons is used to enable a small reduction in response to be detected without the detrimental effects of small eye movements

Multifocal ERG is a difficult measurement to obtain; the signal is highly susceptible to contamination from nearby electrical sources, blinking, movement or jaw clenching. As subjects are required to fixate on a screen which displays a flashing stimulus for extended periods of time, the probability of contamination through blinking is particularly high. To reduce the commonly encountered artefacts many labs use software to 'smooth' the data by averaging the response with neighbouring hexagons. The use of this smoothing tool is warned against by the International Society for Clinical Electrophysiology of Vision in their standards for mfERG recordings as loss of information may occur. In the current study subjects with high levels of contaminated data which were deemed unreliable were rejected; therefore no smoothing was required.

Although the mfERG has been studied in reference to refractive error and axial length, thus far results are inconsistent. It is unclear whether the mfERG response of myopic eyes is affected by the retinal shape. In the present study in addition to carrying out analyses with refractive error and axial length, analysis will also be carried out with reference to specific indices of ocular shape namely Interval Variance (IV) and surface areas (see 9.5.5).

## 13.2 Purpose

To evaluate the relationship between ocular shape and multifocal electroretinogram responses.

## 13.3 Methods and instrumentation

Twenty three young adult subjects of good ocular health underwent standard mfERG recordings. Subjects were divided by refractive error; the cohort comprised of 12 myopes and 11 emmetropes. Mean refractive errors were  $-4.63 \pm 3.2D$  for the myopes and  $-0.03 \pm 0.31D$  for the emmetropes, mean PCI axial length measurements were  $25.32 \pm 1.20mm$  for myopes and  $23.48 \pm 0.45mm$  for emmetropes. The left eyes of each subject were examined. Left eyes were selected on the basis that the preliminary data had shown the right eyes to possess greater signal contamination and interference (possibly due to the positioning of electrical equipment in the lab). Informed consent was obtained from all subjects and all undergraduate subjects were paid a small fee for attendance. All recordings were carried out with the advice and guidance of experienced electrophysiologists, Andrea Scott and Dr Ian Fawcett.

Left eye monocular multifocal recordings were carried out using the VERIS System (VERIS Electro-Diagnostic Imaging, Inc.CA, USA), the right eye was occluded. All recordings were repeated in order to obtain an average of two readings, in 2 cases a repeat was not possible owing to either poor fixation, subject discomfort or machine error. A Dawson-Trick-Litzkow (DTL) thread electrode was used to detect the response. DTL fibres provide increased comfort compared to contact lens electrodes (Dawson et al 1979) and are therefore less likely to produce blink artefacts. Intraocular pressure readings and anterior chamber readings were obtained prior to the instillation of 1% tropicamide ophthalmic solution (*Minims*<sup>®</sup>, Bausch and Lomb U.K Limited, Surrey, U.K). Intraocular pressures were also measured post dilation, using a standard commercially available non contact tonometer. All subjects were given advice regarding the side effects of tropicamide.

An abrasive paste was used to clean subjects skin in preparation for the grounding and active electrodes. The cleaning helped minimise skin oils which may otherwise have disturbed the transmission of signals and recordings. In addition to the corneal electrode, gold cup electrodes were attached on the left ear lobe and forehead. Conductive gel (NuPrep<sup>®</sup> gel, Weaver and Company) was used in the gold cup electrodes to allow improved transmission of the signal.

The subject was then positioned in front of the stimulus monitor with the aid of a chin and forehead rest. Subjects were asked to manually focus the stimulus through use of the machine's eyepiece; this helped compensate for refractive blur. A small fixation cross was used to aid reduce eye movements. Fixation was monitored through the VERIS software and through a video fixation monitor (see Figure 97).

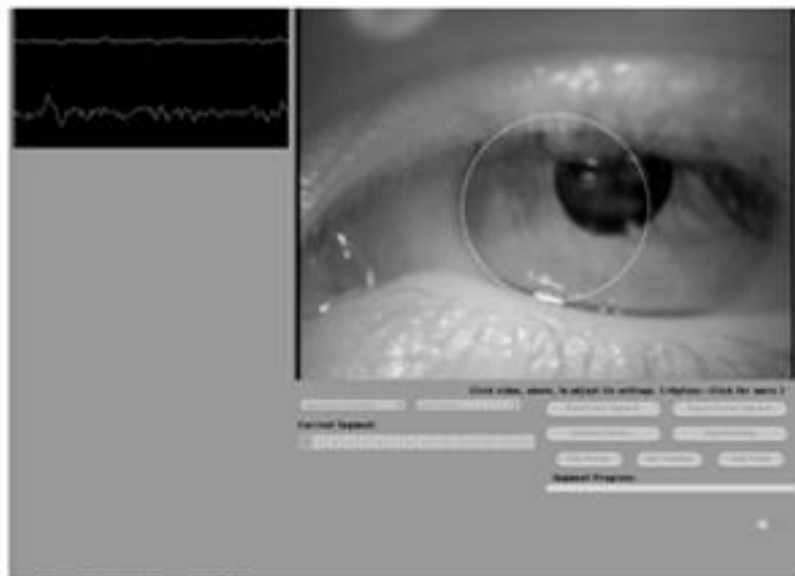


**Figure 97** The fixation monitor visible to the investigator, the top left shows the signal recorded

The stimulus consisted of a standard 103 black and white hexagonal pattern, 16 segments of 13.65 seconds each were used. The time between samples (i.e. the stimulus flashes) was 0.83ms, producing a total testing time of 3 minutes and 38 seconds. Frame rate was set at 75Hz. The stimulus measured 29cm in height and 38cm in width. The stimulus was displayed on a black and white CRT monitor which had a screen resolution of 1024x768 pixels. The electrical signal was amplified through use of a GRASS Quad amplifier; amplification was set at 50K throughout and preamplifier electric cut offs set at 10 to 300Hz.

Blinking contaminates results therefore shorter recording times were used to allow subjects to maintain better fixation for the duration of the segment. Breaks were provided periodically or when the subject requested.

Average N1 and P1 amplitudes and implicit times were examined by the standard concentric ring formats and then again by quadrants (+Q and XQ, as previously defined in Chapter 9, also see Figure 98).

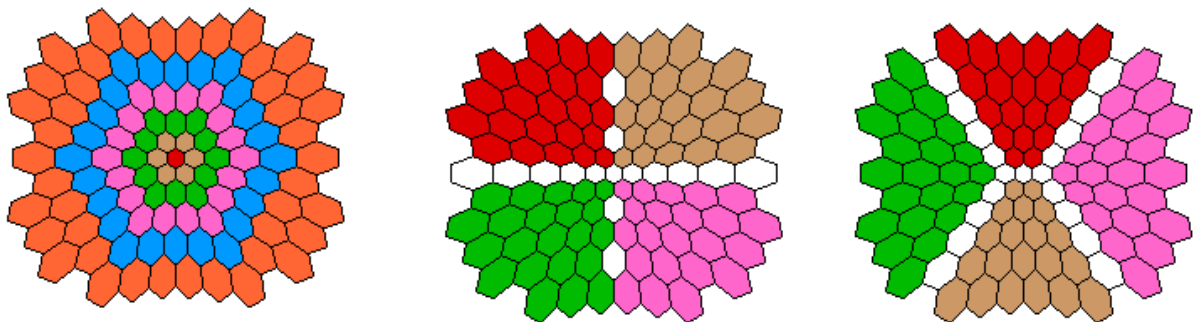


**Figure 98 The method by which mfERG rings and quadrants configurations were divided before responses from each region were averaged and analysed**

The N1 and P1 amplitudes and implicit times for the concentric ring averages were investigated with reference to axial length and also refractive error. The N1 and P1 amplitudes and implicit times for the quadrant averages were investigated with reference to axial length, refractive error and indices of shape derived from MR imaging.

Refractive error measurements were made using the Shin Nippon 5000 autorefractor; measurements were made under cycloplegia. Axial length measurements were made using the Zeiss *IOL Master* (see 7.2 and 7.3).

Twenty-one of the 23 subjects underwent MR scanning and from these data calculations of IV were made for each quadrant; the CIs were then compared to each of the mfERG responses (N1 amplitude, N1 implicit time, P1 amplitude, and P1 implicit time).

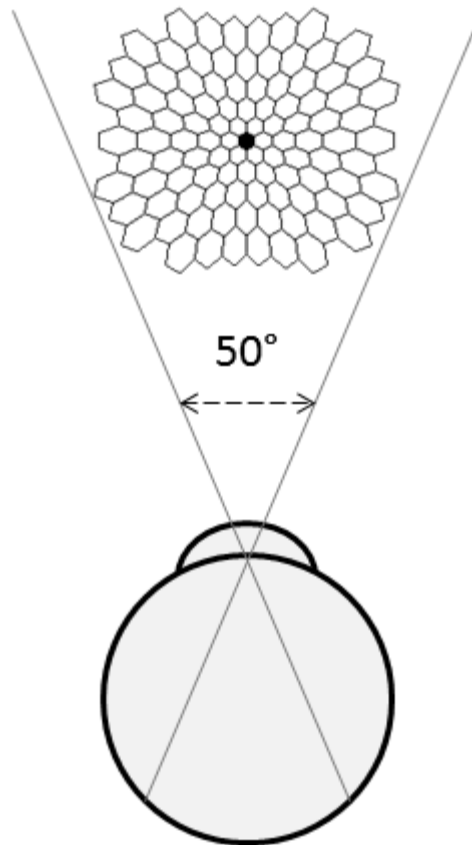


**Figure 99** Schematic representation of the angular subtense by the mfERG stimulus (NB not to scale)

### **13.4 Results**

A Pearson's correlation coefficient showed a longer axial length to be strongly correlated with a greater myopic mean left spherical refractive error ( $r = -0.9417$ ,  $p < 0.001$ ).

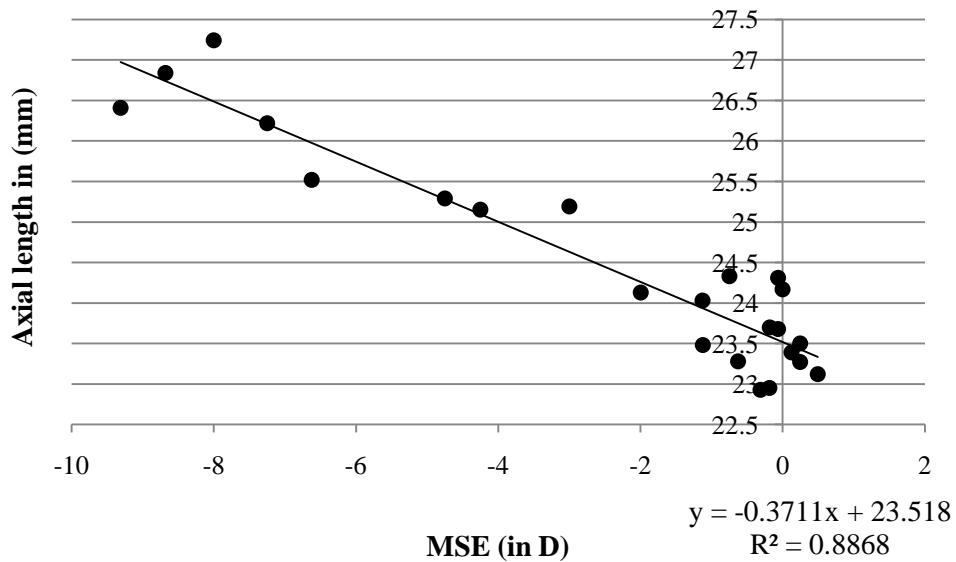


**Figure 100** The PCI axial length against the mean spherical error (MSE) as measured by the Shin Nippon autorefractor ( $n=23$ , left eye data)

**Ring Configuration**

The standard mfERG concentric ring configurations were analysed. Central refers to the hexagon corresponding with the foveal response, and R5 corresponds to the peripheral retinal response.

As expected the N1 and P1 amplitudes declined significantly with increasing retinal eccentricity ( $p<0.01$ ) in line with a decrease cell density (see Figure 101 and Figure 102).

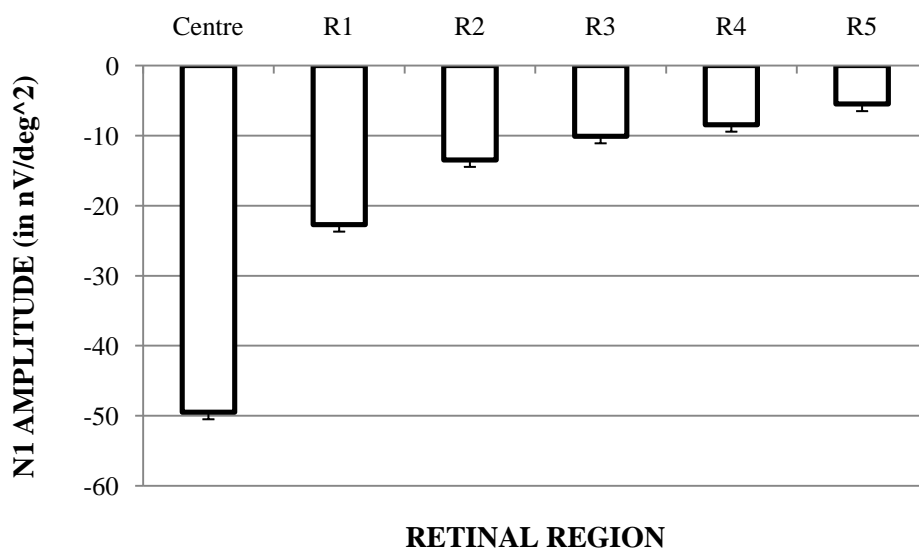


**Figure 101** N1 amplitudes shown as a function of retinal eccentricity (R5 indicates the ring furthest from the fovea). Error bars show standard deviation of the dataset

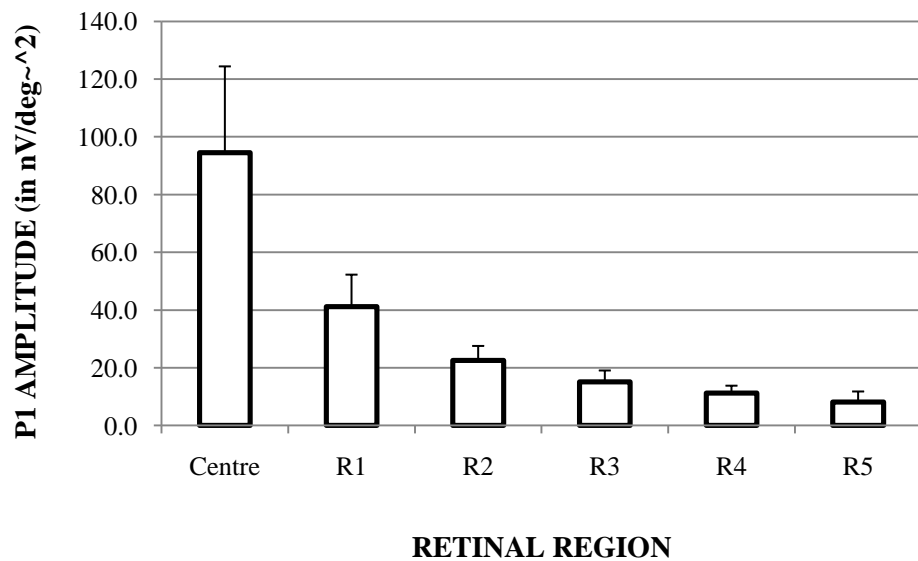


**Figure 102 P1 amplitudes shown as function of retinal eccentricity. Error bars show standard deviation of the dataset**

A Pearson's two tailed linear correlation coefficient was used to evaluate the effect of axial length, and separately, refractive error on four components of the response waveform: N1 implicit times, N1 amplitudes, P1 implicit times, P1 amplitudes. Each of the four responses were evaluated by the retinal region as defined by the rings; a Bonferroni correction was used as there were six retinal regions in total, thus a critical p value of  $0.05/6=0.0083$  was used. Results showed neither axial length nor refractive error correlated significantly with each of the four responses for any of the six regions.

To investigate further potential differences between emmetropic and myopic mfERG responses a 2-way mixed ANOVA was used to evaluate the responses from the four types of response (i.e. N1 and P1 implicit times and amplitudes) for each of the six ring retinal regions. The four responses did not show a significant difference between the two refractive groups ( $p<0.05$ ).

### Quadrants: +Q

To evaluate the effect of refractive error on quadrant responses a repeated measures 2-way mixed ANOVA was used to examine each type of response for the +Q quadrants. For the four responses there were no significant differences between the two refractive groups. There were however significant differences between quadrants (see Figure 103 and Figure 104).

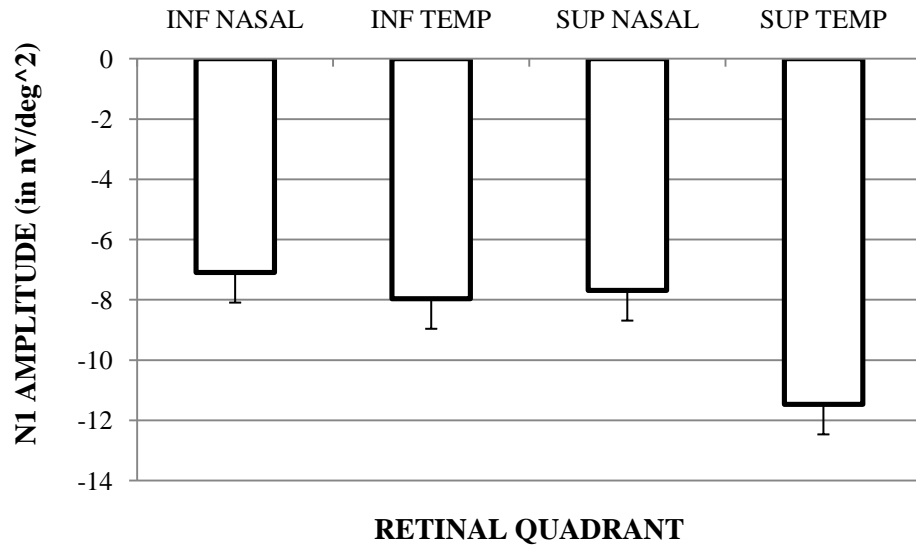


Figure 103 The N1 response amplitudes for +Q (LE data). Error bars show standard deviation of the dataset

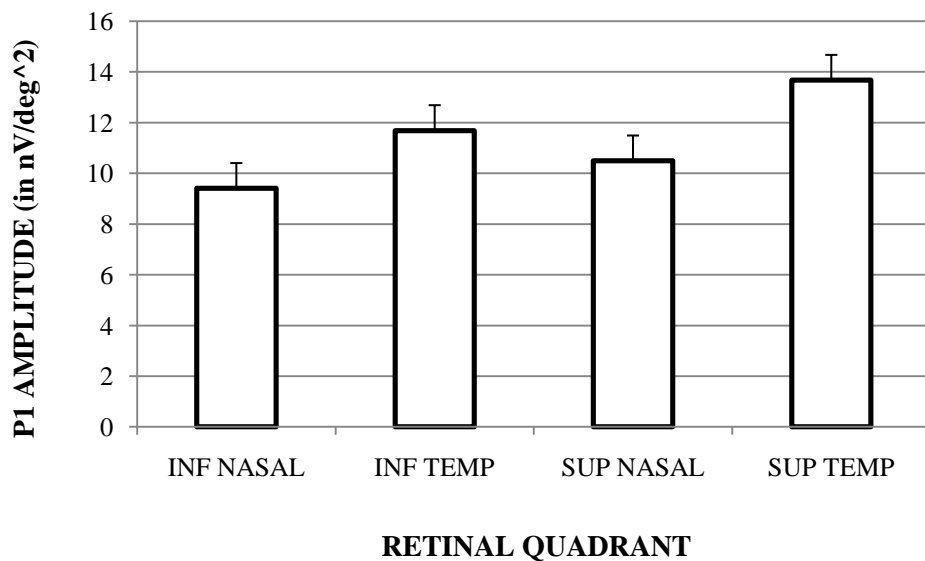
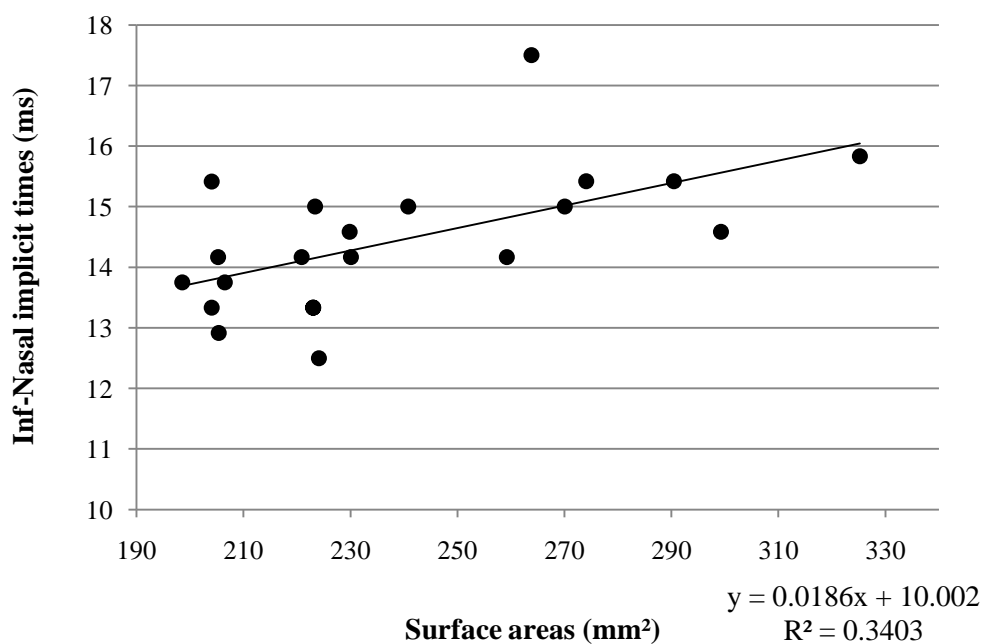


Figure 104 The P1 response amplitudes for +Q (LE data). Error bars show standard deviation of the dataset

The N1 amplitudes showed significant differences across all quadrants ( $p < 0.01$ ) bar the inferior-nasal vs. superior-nasal and also the inferior-temporal vs. superior-nasal. Significant differences were noted across all P1 amplitude quadrant responses. The superior-temporal quadrant showed the highest amplitude and the inferior-nasal quadrant was found to have the lowest amplitude.

There were no significant differences between the implicit times of quadrants. Linear correlations through use of Pearson's correlation coefficient showed that all four types of mfERG response failed to correlate with refractive error or axial length.

The four types of response did not correlate with the IV for any quadrant. Surface areas showed a significant correlation with N1 implicit times for the inferior-nasal quadrant only ( $p = 0.006$ ,  $r = 0.583$ ); all other combinations of +Q surface areas and mfERG responses failed to show significant correlations (see Figure 105).



**Figure 105 Surface areas and implicit times for the inferior-nasal retinal quadrant**

### Quadrants: XQ

To evaluate the effect of refractive error on mfERG responses from each quadrant a repeated measures 2-way mixed ANOVA was used to examine each type of response for the XQ quadrants. For the four responses there were no significant differences between the two refractive groups. There were however significant inter-quadrant differences (see Figure 106).

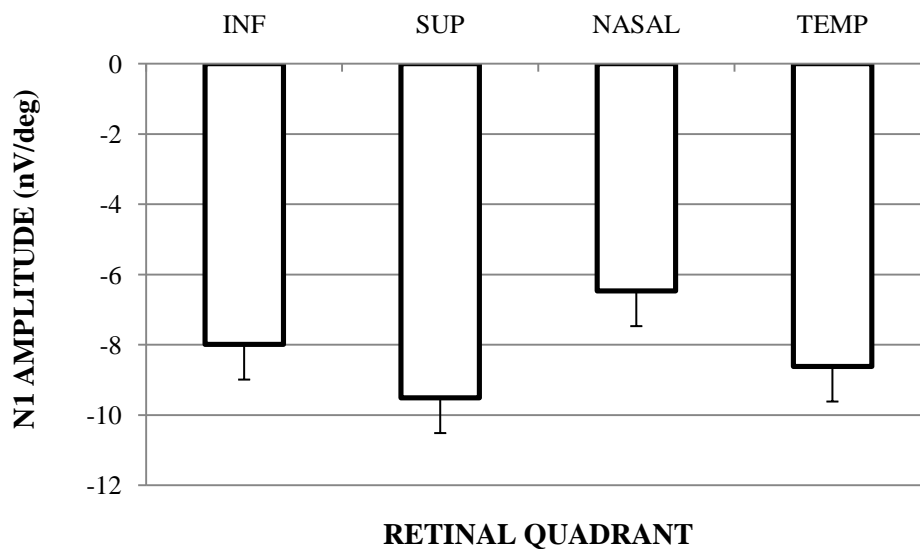


**Figure 106 Shows the N1 response amplitudes for XQ (LE data)**

Significant differences were present between the N1 amplitude responses of all quadrants ( $p < 0.01$ , except inferior vs. temporal). There were no significant differences in N1 implicit times between quadrants.

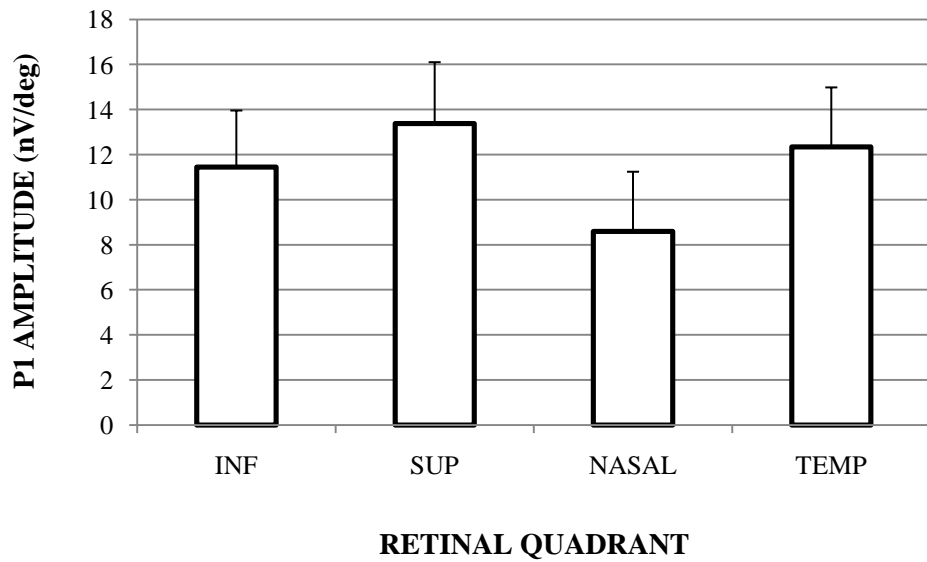


**Figure 107 The P1 response amplitudes for the XQ (LE data). Error bars indicate the standard deviation**

There were significant differences noted between the P1 amplitude responses of all quadrants ( $p < 0.01$ ) bar the inferior vs. temporal and superior vs. temporal (see Figure 107).

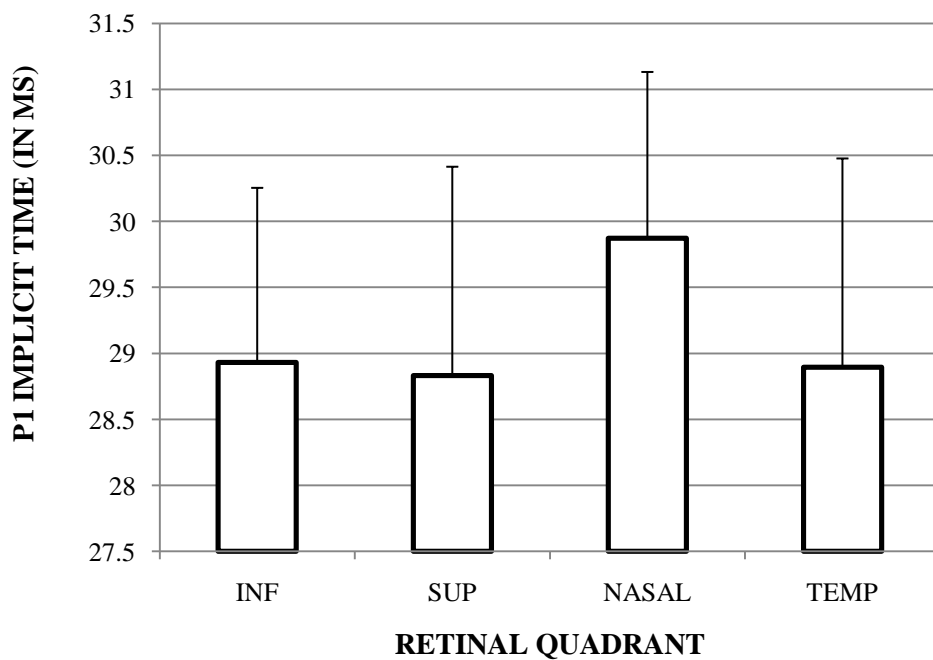


**Figure 108 Shows P1 Implicit times for the XQ (LE data). Error bars indicate the standard deviations**

There were significant differences between the P1 implicit times of all quadrants ( $p < 0.05$ ) bar the inferior vs. temporal and superior vs. temporal (see Figure 108). Two tailed Pearson's correlations for each of the four responses failed to show significant correlations with refractive error, axial length, and IV. Surface areas and N1 implicit times for the inferior quadrant were significantly correlated ( $p = 0.004$ ,  $r = 0.599$ ).

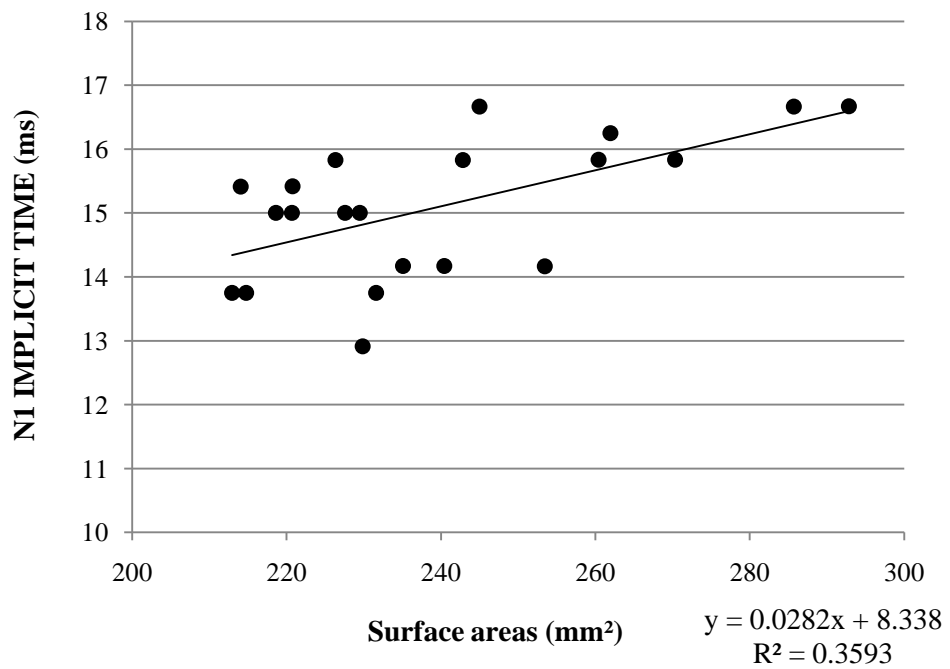


**Figure 109 Surface areas and N1 implicit times for the inferior retinal quadrant**

### **13.5 Discussion and conclusions**

The first negative (N1) and first positive (P1) components of the mfERG response waveform were assessed; the response of these components originates mainly from the cone receptors and bipolar cells. As expected the response amplitudes, for both N1 and P1, declined with increasing retinal eccentricity. The decline with increasing eccentricity has been well documented and is believed to relate to the concomitant decline in cone photoreceptors. Inspection of standard deviations showed inter subject variability to be greatest in the foveal region, this has also been noted previously (Nagatomo et al 1998). The variability in the foveal region has often been attributed to the differences in the retinal cell topography between individuals (Curcio et al. 1990).

In the current study refractive error did not correlate with mfERG responses to a significant level for either ring or quadrant formats. Responses also failed to correlate with axial length. Additionally, correlations with IV did not reveal significant relationships. There were two correlations with surface areas; the implicit times of the N1 component correlated significantly for the inferior and the inferior-nasal retina.

For this particular subject group it can be concluded that refractive error was not related to mfERG responses. Specific aspects of ocular shape correlate with N1 implicit times for some quadrants only. In general the relationship between ocular shape and mfERG responses is weak.

#### **Quadrant differences**

A surprisingly few number of studies have examined the link between quadrant variations in mfERG with refractive error. In the current study both +Q and XQ quadrants were examined. Although refractive error did not correlate with quadrants, inter quadrant differences were observed. The +Q quadrants showed significant differences in both the N1 and P1 amplitudes; highest amplitudes were noted in the superior-temporal retina and lowest in the inferior-nasal retina. Reduced amplitudes with normal implicit times may indicate damage to the cone photoreceptors (Hood et al. 2002).

For the XQ quadrants the nasal retina showed significantly reduced amplitudes and significant delays in implicit time. This combination of responses indicates damage to the cone receptors and the ON bipolar cells. If these responses are considered in the context of retinal cell distribution then cone photoreceptor density is actually far greater in the nasal

retina than the temporal (Curcio et al. 1991), which is inconsistent with the results found. However, the reduced nasal retinal response may be attributable to the optic nerve head (ONH). In visual fields research the area represented by the ONH is removed from data analysis. In the case of mfERG it can be difficult to isolate the hexagon representing the optic nerve head and in some cases may not be possible at all. The reduced response in the nasal quadrant may represent the ONH and although it would confirm that subjects were properly fixating throughout the recording, an unfortunate consequence would be that direct comparisons of quadrants would be rendered invalid.

In the current study highest amplitudes and shortest implicit times for the XQ quadrants were noted in the superior retina. Similar findings have been reported in studies of hemifield responses which have compared responses for the superior vs. inferior regions. The superior retina is frequently reported to produce better responses than the inferior (Kawabata & chi-Usami 1997)

### **Absence of a shape or refractive error effect on mfERG responses**

Previous literature has reported on the reduction of mfERG responses in myopic subjects. It is often the responses of progressing myopes or high myopes, not stable myopes, which are found to be significantly different to emmetropes. In the current study all the myopes were believed to be stable and only 5 of the 23 subjects exceeded levels of myopia which would normally be classed as high myopia (i.e. greater than -6D MSE), therefore a reduced response would not necessarily be expected. Furthermore the differences previously reported in progressing or high myopes do not appear to display a clear or definite pattern of reduced response. Examination of previous literature shows that no systematic variation with refractive error has been reported. Previously it has been suggested that ocular shape may be responsible for variations in mfERG response (Kawabata & chi-Usami 1997), however the results from the present study are in disagreement with this view as the majority of shape indices have not correlated with mfERG responses.

Unlike a number of previous studies of mfERG and myopia, spatial averaging was not applied to the results. A strict criterion of rejecting noisy data was applied by experienced electrophysiologists (Andrea Scott and Dr Ian Fawcett).

The current study would be extended through inclusion of subjects with progressive and high myopia. Based on previous reports (Chen et al. 2006a) and the current study it is

hypothesised that the mfERG responses of progressive and high myopes will significantly differ from that of emmetropes and stable myopes.

### **13.6 Summary**

The mfERG response is known to vary greatly between individuals. Previous reports of reduced mfERG responses in myopic subjects are not supported by the current study; however, this may be due to the type and level of myopia tested. This study shows that indices of ocular shape based on MRI data do not correlate well with mfERG responses, except in the inferior and inferior-nasal quadrants. The evidence suggests that there is limited support for a relationship between ocular shape and mfERG response. In general stable myopic subjects retained mfERG response levels similar to those measured in emmetropic subjects.

## 14 INVESTIGATION OF GANGLION CELL DENSITY WITH REFERENCE TO OCULAR SHAPE

### 14.1 Introduction

Beyond the central foveal region the numbers of cone receptors rapidly decrease (Curcio et al. 1990). The peripheral retinal regions are therefore poor at resolving detailed high spatial resolution images. The ganglion and rod cells dominate these peripheral regions with a minority number of cone cells.

The sampling theorem dictates that for a sinusoidal grating to be detected and reconstructed accurately, two sampling points are required for each cycle of the waveform. The limit of the sampling frequency is referred to as the Nyquist limit. If the drifting sinusoidal grating is spatially undersampled, its direction of motion will reverse. In consequence, performance will fall below 50% correct (e.g. See Figures 1-4 in Anderson et al. 1995).

Previous reports have suggested that the increase in ocular size, synonymous with myopia, can lead to an increase in the distance between ganglion cells (Chui et al. 2004) which may cause the resolution ability of the ganglion cells to be reduced (Thibos et al. 1987). Conversely, predicted models of myopic eye shape correlated with calculations of ganglion cell density have failed to explain reductions in peripheral visual acuity (Strang et al. 1998). Until recently acquisition of accurate parameters of eye shape were limited to one dimensional longitudinal measurements. The introduction of three dimensional ocular Magnetic Resonance Imaging MRI (Singh et al. 2006) allows ocular shape to be investigated in substantially more detail allowing direct associations to be made between ocular shape and ocular function.

The methodology for measuring ganglion cells density *in vivo*, through psychophysical methods has been well established (Thibos et al. 1987; Anderson et al. 1992; Anderson et al. 1995). The current study uses a modification of a protocol developed and reported by Anderson *et al.* 1995 to investigate the relationship between ocular shape and ganglion cell density (see Methods section). This study is the first attempt at correlating structural data from ocular MRI with psychophysical estimates of ganglion cell density. The aim is to construct a more informed report to determine whether eye shape affects retinal receptor density or function.

## 14.2 Purpose

To evaluate the effects of myopic ocular expansion on ganglion cell density.

## 14.3 Hypothesis

The degree of myopia is significantly correlated with longitudinal axial length and eye size (Singh et al. 2006). Previous work has shown ganglion cell density to be reduced in myopia (Chui et al. 2004). It is hypothesised that subjects with myopic refractive errors and hence relatively larger eyes will have poorer detection ability; as a consequence these subjects will show an aliasing or distortion of the visual signal at lower spatial frequencies than emmetropic subjects.

## 14.4 Methods

There are two main methods available to measure ganglion cell density in humans. The most direct technique is through *in vitro* examination of retinal histological samples. In contrast, *in vivo* ganglion cell sampling can be achieved through the use of psychophysical techniques. The protocol used was adapted from a study by Anderson *et al.* (1995).

Four young adult female subjects (aged between 26-29 years) with good ocular health acted as subjects. All subjects had previously undergone ocular MR scanning and a range of ocular biometric measurements taken prior to the experiment. All volunteers were unpaid. Informed consent was obtained from the four subjects.

Each of the four subjects (two emmetropes and two myopes) were tested monocularly through natural pupils. The non-cycloplegic peripheral refractive error of the right (test) eye as determined by retinoscopy at 40° eccentricity to the fovea in the temporal retina was corrected by use of full aperture trial lenses (see Table 23). The contralateral eye was occluded through use of an eye patch.

All subjects were postgraduate optometrists, accustomed to visually demanding tests for research purposes and known to possess accurate fixation and concentration. Subjects were seated so that the stimulus was in line with the primary direction of gaze. Fixation was well controlled through vocal prompting and repeatedly checking subjects' eyes. Tests were repeated a minimum of 25 times at each spatial frequency. Regular breaks were offered at each spatial frequency change and taken by all subjects as required.

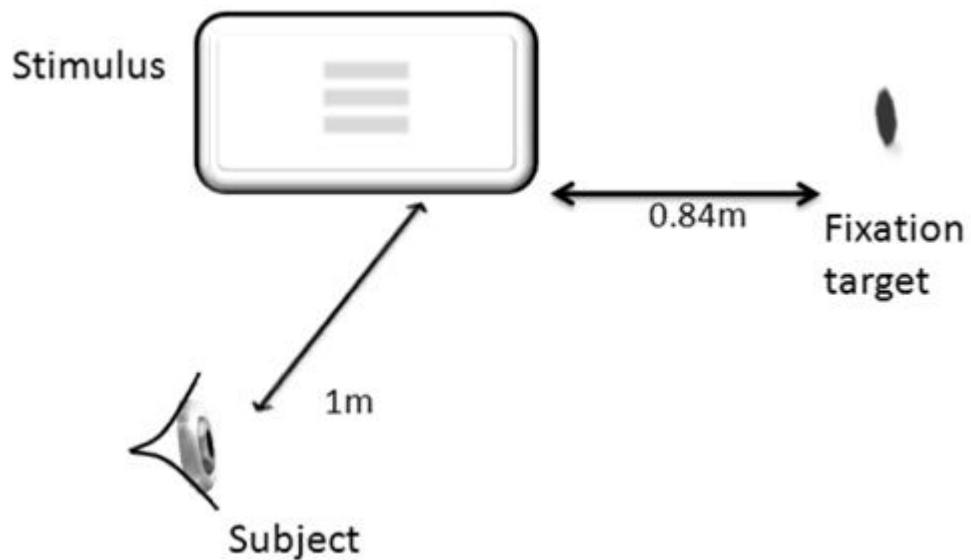


**Figure 110 Diagram showing the experimental setup (not to scale)**

The experiment was divided into two parts; sensitivity to (a) stimulus detection and (b) stimulus direction discrimination.

Subject	Refractive error, D	Central error (MSE D)	Peripheral error (D)
Subject OH	-8.12/-1.00 x 85	-8.62D	-5.00/-0.50 x 70
Subject MN	-3.00DS	-3.00	-2.12/-0.75 x 42
Subject AS	+0.75/-0.50 x 180	+0.50	+0.50/-4.00 x 80
Subject JA	+0.50/-0.62 x 118	+0.19	-3.00/-2.25 x 180

**Table 23 Central and peripheral refractions (at ~40° temporal to fovea) of subjects corrected with full trial aperture lenses (right eyes)**

Subject	Axial length (mm) (from MRI measurements for consistency with ocular stretch index-see results)	Central corneal radii (mm) (from the Zeiss <i>IOL Master</i> )
Subject OH	25.96	7.62/7.5
Subject MN	25.67	7.89/7.84
Subject AS	23.78	8.06/7.87
Subject JA	23.68	8.06/7.98

**Table 24 Biometric data of subjects**

Axial lengths were consistent with the well established relationship between a longer axial length and higher degrees of myopia.

## **14.5 Instrumentation**

In order to exploit the on/off centre arrangement of the ganglion cells a sinusoidal grating stimulus was presented on a 21 inch Sony GDM-F520 Trinitron CRT monitor with 100Hz frame rate, in a dimly lit room. Screen resolution was 1024 x 768 pixels. Stimulus size was approximately 9.7cm wide and 9.5cm in height. Subjects had a viewing distance of 1m. The edges of the stimulus were blurred to limit edge detection and accommodative responses, by use of translucent paper. A fixation target was located 84cm from the stimulus, at a viewing angle of 40° relative to the primary line of sight.

Peripheral refractions at 40° eccentricity of the temporal retina were carried out using a Keeler streak retinoscope by an experienced practitioner, and refractive errors corrected using full aperture lenses to limit refractive blur. Lenses were secured by use of a standard *Oculus* trial frame, at a back vertex distance of approximately 11mm.

### **14.5.1 Stimulus detection**

A two alternative forced choice experimental protocol was employed, through use of a subject controlled keypad. The experiment was commenced, and could be paused, by the subject's keypad.

Twenty five pairs of stimulus intervals were shown on the screen; each pair presented either a horizontal sinusoidal grating or a blank screen. Subjects were asked to indicate in which of the two randomly ordered presentations the stimulus was present.

Subjects repeated this procedure a minimum of 25 times for each spatial frequency. Spatial frequencies ranged from 1 to 7 c/deg (cycles per degree) in steps of 1 c/deg, or 0.5 c/deg when required. After 25 runs at a given spatial frequency the computer program produced a score expressed as a percentage of correct responses. The upper limit of spatial frequencies was largely dependent on the point at which a subject was unable to achieve a score above 50%. Responses at 50% were assumed to be the point at which aliasing took place. A Michelson contrast of 80% for the sinusoidal stimulus was maintained throughout by use of

the computer program settings. Subjects were encouraged to take regular breaks to minimise the influence of fatigue between recordings of each spatial frequency.

#### 14.5.2 Stimulus direction discrimination

The same protocol was used as that for detection with the exception of the blank screen i.e. a stimulus was shown in both presentations. The stimulus grating moved in either an upwards or downwards direction. Subjects were asked to identify in which presentation, the first or second, the grating appeared to be moving upwards.

#### 14.5.3 Validity

The validity of the technique is well established. Psychophysical techniques have proven to be sensitive and valid predictors of ganglion cell density through comparisons to histological data (Anderson et al. 1992; Curcio et al 1990). The protocol used in the current study matches that of a similar experiment by Anderson *et al.* 1995. The computer program for the above procedure was written and developed by Professor SJ Anderson, Aston University.

### 14.6 Results

Right eye results for discrimination and detection experiments:

#### 14.6.1 Detection and direction discrimination experiments

As expected all subjects demonstrated a decline in stimulus detection as spatial frequency increased.

AVERAGE OF % CORRECT		
Spatial Frequency (c/deg)	Subject OH	Subject MN
1	98±2.83	100
2	100	96
3	86.67±10.07	88
4	76±26.23	81.33±14.05
5	69.33±8.33	84±5.66
6	45.33±10.07	52
7		48

<b>AVERAGE OF % CORRECT</b>		
<b>Spatial Frequency (c/deg)</b>	<b>Subject AS</b>	<b>Subject JA</b>
1	88	98±2.83
2	82±2.83	92±6.93
3	82±2.83	72±5.66
3.5		68±11.31
4	60±11.31	50±2.83
5	54±2.83	42±8.49
6	54	
7	46±2.83	

**Table 25 Detection task results (mean values with standard deviations where repeat runs were carried out). Blank cells indicate that either the subject was unable to complete the test at a particular spatial frequency or correct responses had fallen to below 50% and thus there was no need for further measurements.**

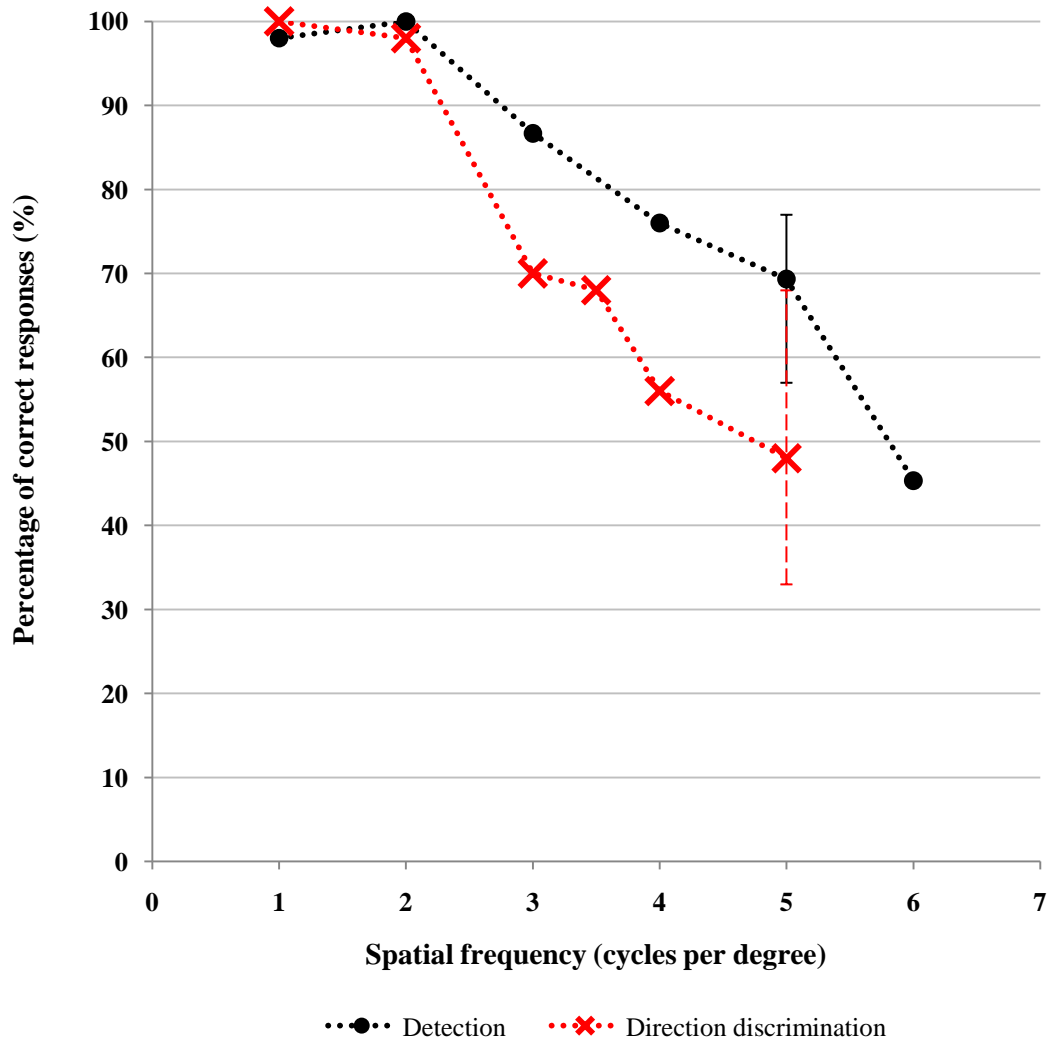


**Figure 111 Subject OH, MSE: -8.62D. Vertical lines express 95% confidence limits, solid lines show confidence limits for the detection function and dashed line for the direction discrimination**

### Subject OH

Subject OH was the most myopic of the 4 subjects. Detection ability fell to below chance between 5-6 c/deg. Direction discrimination fell to below chance (correct responses  $\leq 50\%$ ) at 5-6 c/deg also.

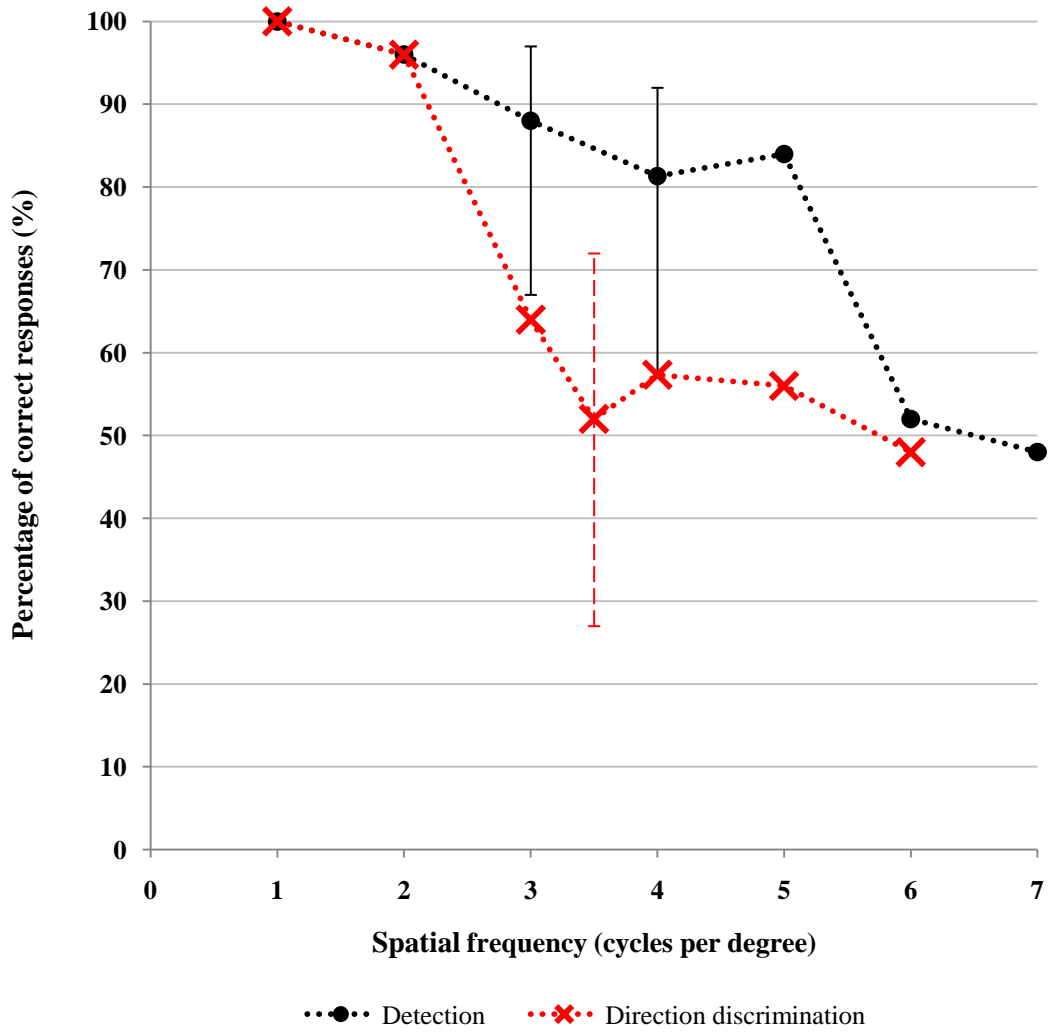


**Figure 112 Subject MN, MSE: -3.00D**

### Subject MN

Subject MN showed detection performance to fall below chance at 6-7 c/deg. Direction discrimination fell below chance at 6-7 c/deg. Subject MN's results showed motion reversal at 6 c/deg.

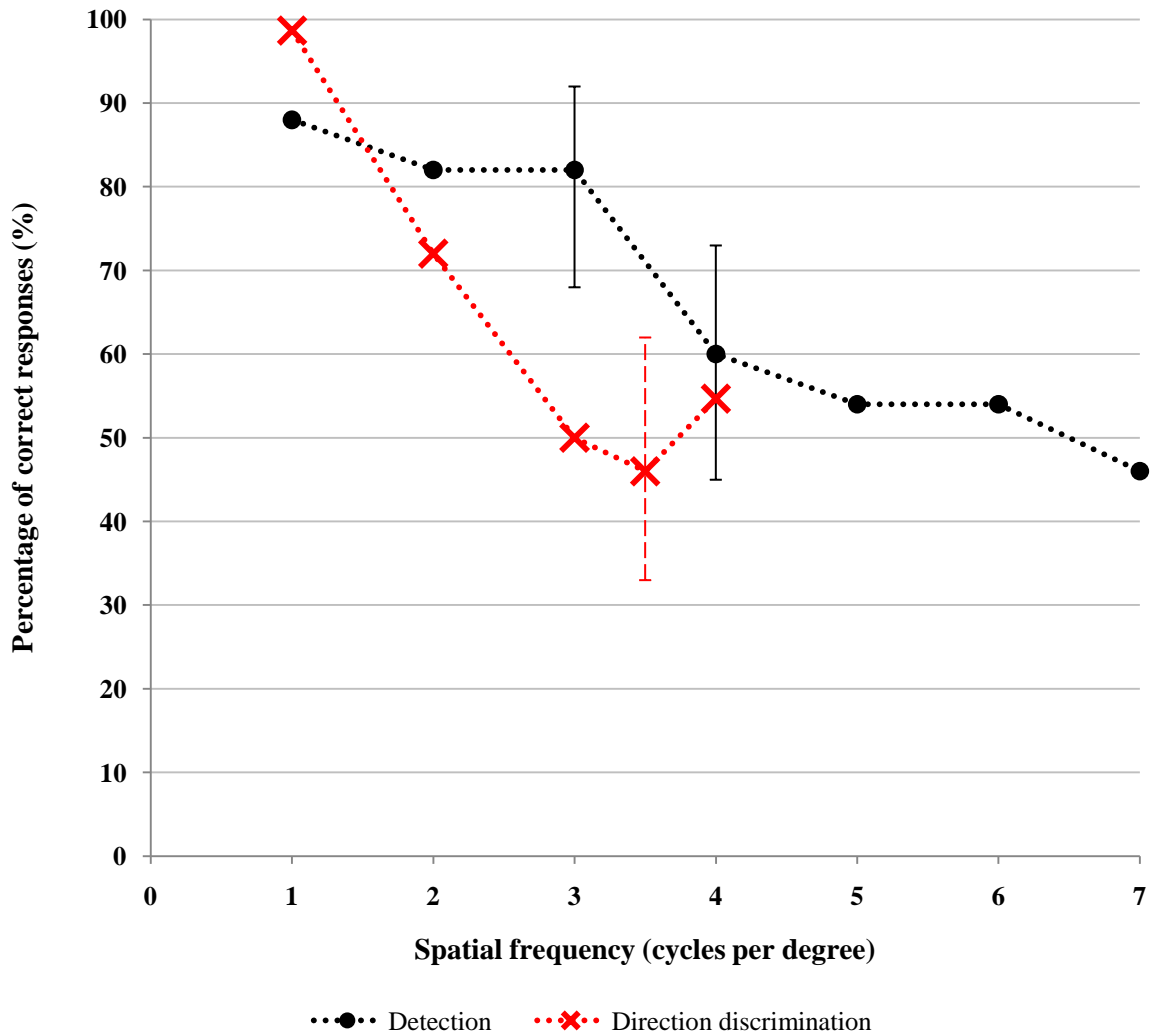


**Figure 113 Subject AS, MSE: +0.50D**

### Subject AS

Subject AS showed detection ability to decline to below chance at 6-7 c/deg; direction discrimination fell to below chance at 3 c/deg. Subject AS also displayed motion reversal (evidence of aliasing); this was noted at 5 c/deg.

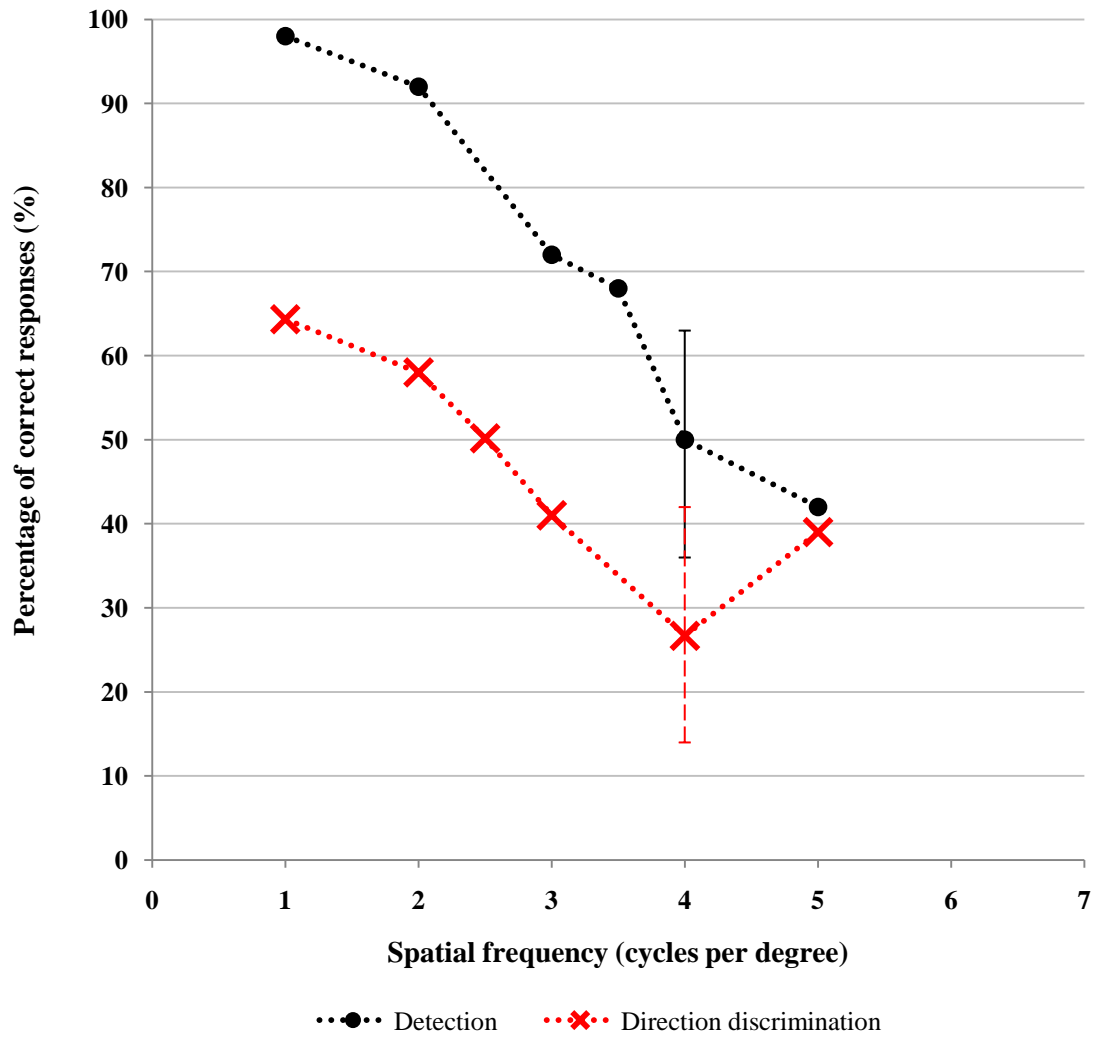


**Figure 114 Subject JA, MSE: +0.19D**

### Subject JA

Detection ability fell below chance at only 4 c/deg; the lowest of the four subjects. Direction discrimination ability fell below chance at 3 c/deg. Subject JA also displayed motion reversal at 5 c/deg.

	AVERAGE OF % CORRECT	
Spatial Frequency	Subject OH	Subject MN
1	100	100
2	98±2.83	96
3	70±2.83	64
3.5	68	52
4	56±11.31	57.33±6.11
5	48	56
6		48
	AVERAGE OF % CORRECT	
Spatial Frequency	Subject AS	Subject JA
1	98.67	64.33±5.66
2	72	58±8.49
2.5		50.17±2.83
3	50	41±5.66
3.5	46	
4	54.67	26.67±2.83
5		39

**Table 26 Direction discrimination task results (mean values with standard deviations where repeat runs were carried out)**

All subjects bar subject OH (the most myopic subject) showed motion reversal, which is clear evidence of signal aliasing. In many of the experiments (75%) the Nyquist limit fell between two spatial frequencies. Linear interpolation was used to gauge a more accurate estimate of the Nyquist limit. All subjects bar Subject MN showed the direction discrimination threshold to be lower than the detection threshold. The difference for Subject MN was minimal (0.3 c/deg).

#### **14.6.2 The effect of eye conformation on ganglion cell receptors**

To study the relationship between eye shape on the two experimental protocols detection and direction discrimination, previously acquired ocular MR scans for each subject were analysed. In order to quantify retinal stretch, a ratio for the index of stretch was calculated; additionally surface area for the temporal retinal quadrant strip which lay 60-80% along the

visual axis was calculated. There were several other indices which may have been used, however the chosen index of stretch was considered most useful due to its specificity to the region 40° temporal to the fovea; surface area could also be localised to the retinal area tested in ganglion cell density measurements and therefore provided a valuable measurement for comparison to detection and discrimination thresholds.

### **Index of stretch**

The chord distance from the location 40° temporal to the fovea to the corresponding point on the nasal retina was expressed as a fraction of the total axial length. Graphical representations of the data were used to locate the point 40° temporal to the fovea; this was generally found to be around 72.5% along the visual axis. The stretch index was calculated for each individual subject.

### **Surface area**

Surface area was calculated for the region 60-80% along the visual axis, for the temporal quadrant strip only (see Figure 115). The region for the temporal quadrant of the right eye 60-80% along the presumed visual axis was plotted graphically and fitted with a second order polynomial. Calculations were made using a formula developed in collaboration Dr Bill Cox, Aston University.

$$S = \frac{\pi}{32a^2} \left[ t\sqrt{1+t^2} \left( 2t^2 + 4(4ac - b^2) \right) + (4(4ac - b^2) - 1) \ln \left( t + \sqrt{t^2 + 1} \right) \right]_{t_1}^{t_2}$$

Where  $t_1 = b + 2al_1$  and  $t_2 = b + 2al_2$  and S represents surface area.

The values a, b and c correspond to the polynomial coefficient values of  $y = ax^2 + bx + c$ .

The values  $l_1$  and  $l_2$  (in mm) correspond to the respective 60 and 80 percent x-axis values

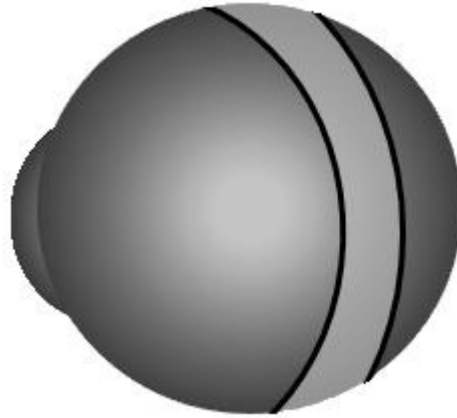


**Figure 115 Diagrammatical representation of the surface area calculation of the ocular surface. The grey band represents the 60-80% region for which area was calculated (not to scale)**

<b>Subject</b>	<b>Detection NL</b>	<b>Direction Discrimination NL</b>	<b>Index of stretch (%)</b>	<b>Surface area (mm<sup>2</sup>)</b>
Subject O.H	6.8	4.8	93	112.95
Subject M.N	6.5	6.8	91	97.82
Subject A.S	6.5	3	99	95.02
Subject J.A	4	2.5	92	85.03

**Table 27 Calculated index of ocular stretch and Nyquist limit (NL) estimates calculated for each subject (in %). NB a higher % for index of stretch indicates a smaller eye**

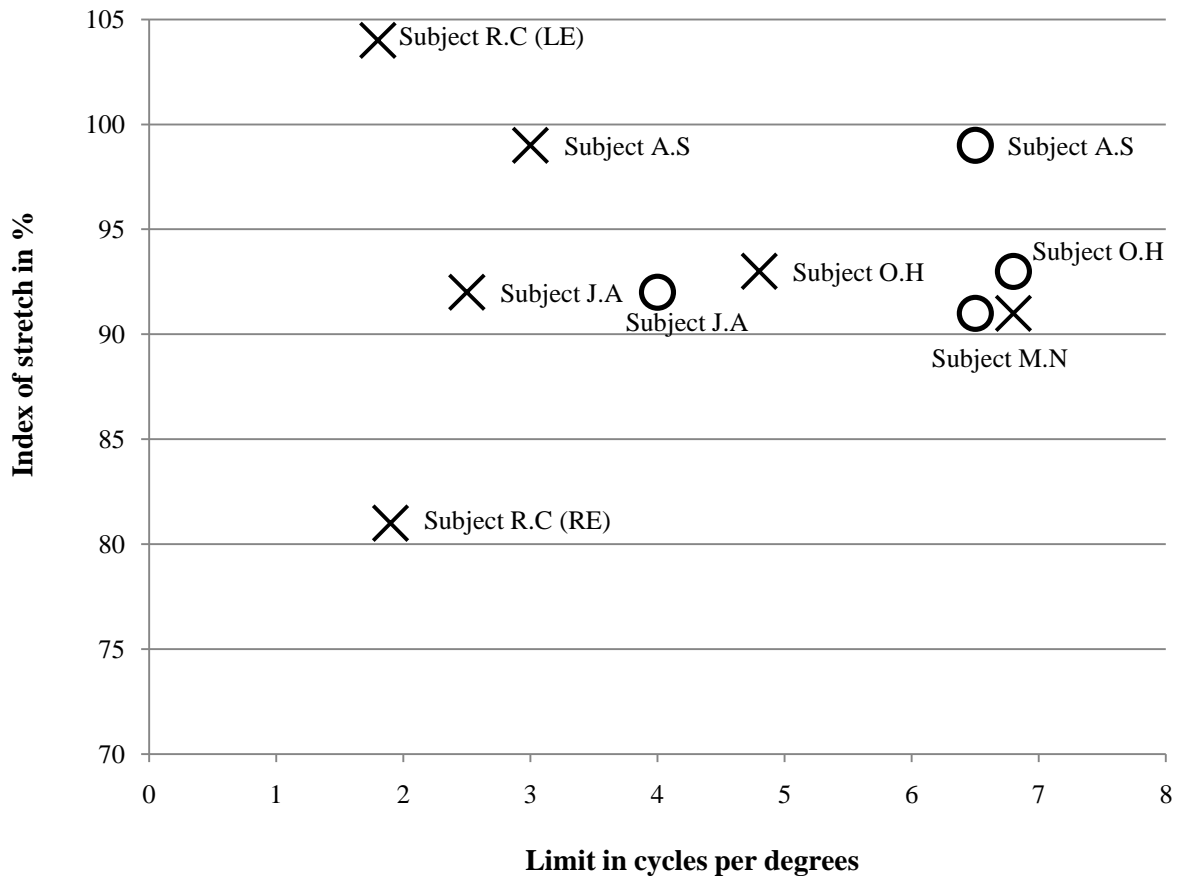


**Figure 116 Graphical representation of the spatial frequencies at which 50% of responses are correct, plotted as a function of stretch index. Circles denote detection and stars indicate direction discrimination. Case study RC is also included (see below).**

From the four subjects in the main study myopic subjects OH and MN had the highest index of stretch. The index of stretch was correlated with the threshold values for each subject in each of the experiments. The estimate of the spatial frequency at which correct subject responses were at the 50% level is shown in the table above. The ocular stretch did not correlate with either detection threshold or direction discrimination threshold. Surface area was calculated and shown to be larger in the myopic subjects OH and MN, however, variation in surface area had no systematic effect on either detection or discrimination tasks.

It can be seen from the calculated indices of ocular stretch that there is much variation between individual eye shape and variations may not occur as a function of refractive error.

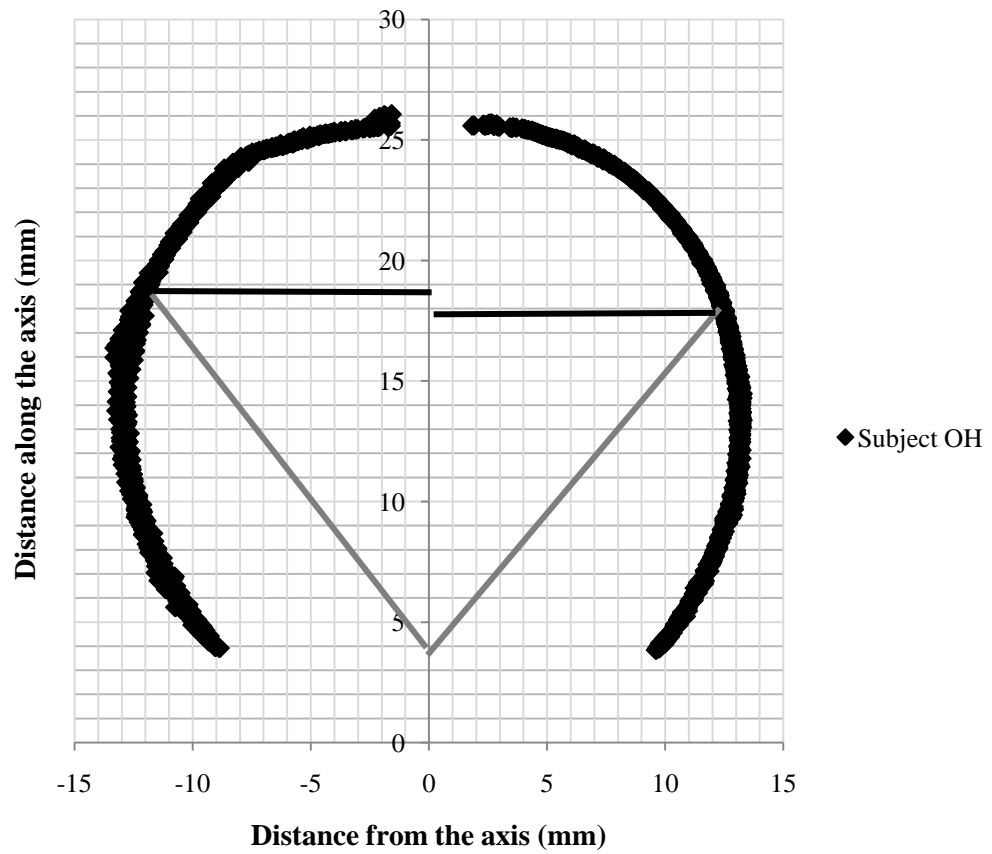


**Figure 117** Calculated index of stretch for subject OH: 93%. The graph shows the point situated  $40^\circ$  from the presumed foveal location; the horizontal lines denote the distance from the  $40^\circ$  location to the presumed visual axis (RE) Negative values denote the temporal region and positive numbers denote the nasal.

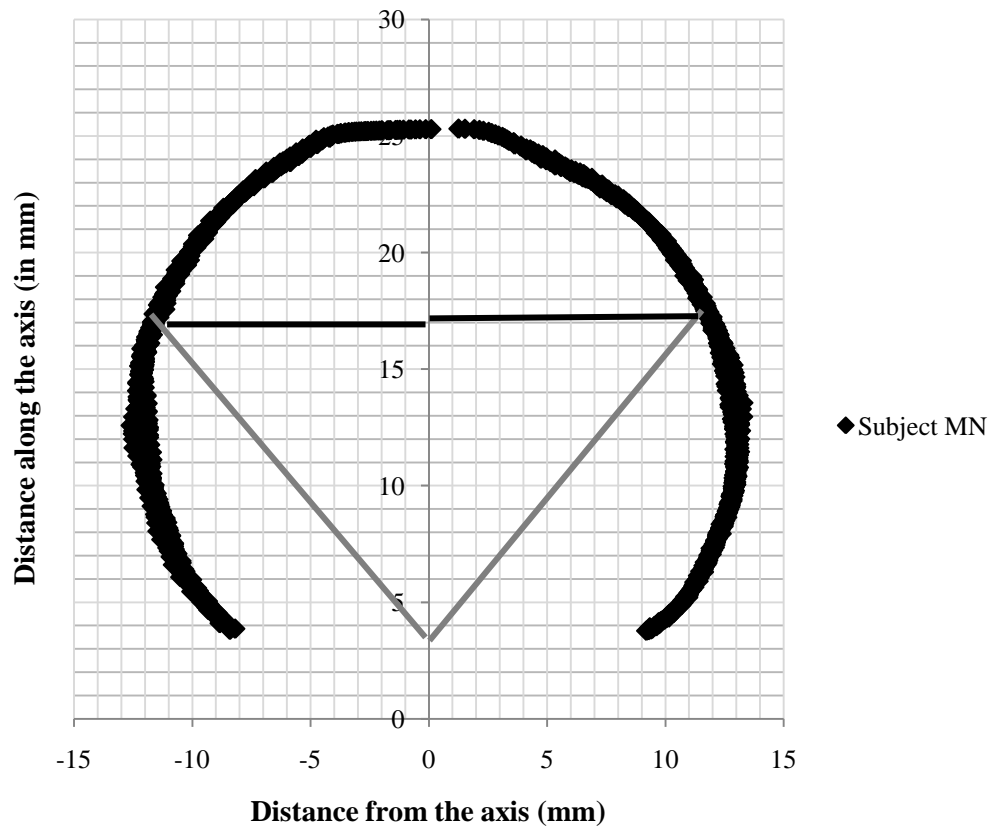


**Figure 118** Calculated index of stretch for subject MN: 91% (RE). Negative values denote the temporal region and positive numbers denote the nasal

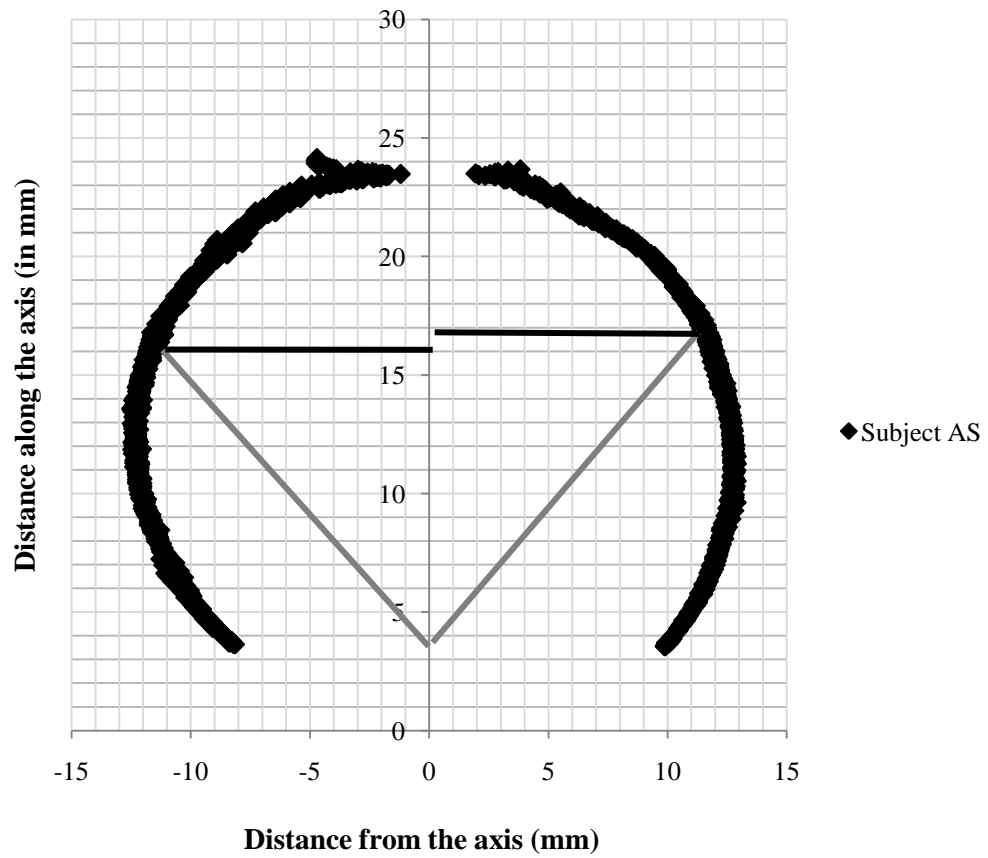


**Figure 119** Calculated index of stretch for subject AS: 99% (RE). Negative values denote the temporal region and positive numbers denote the nasal

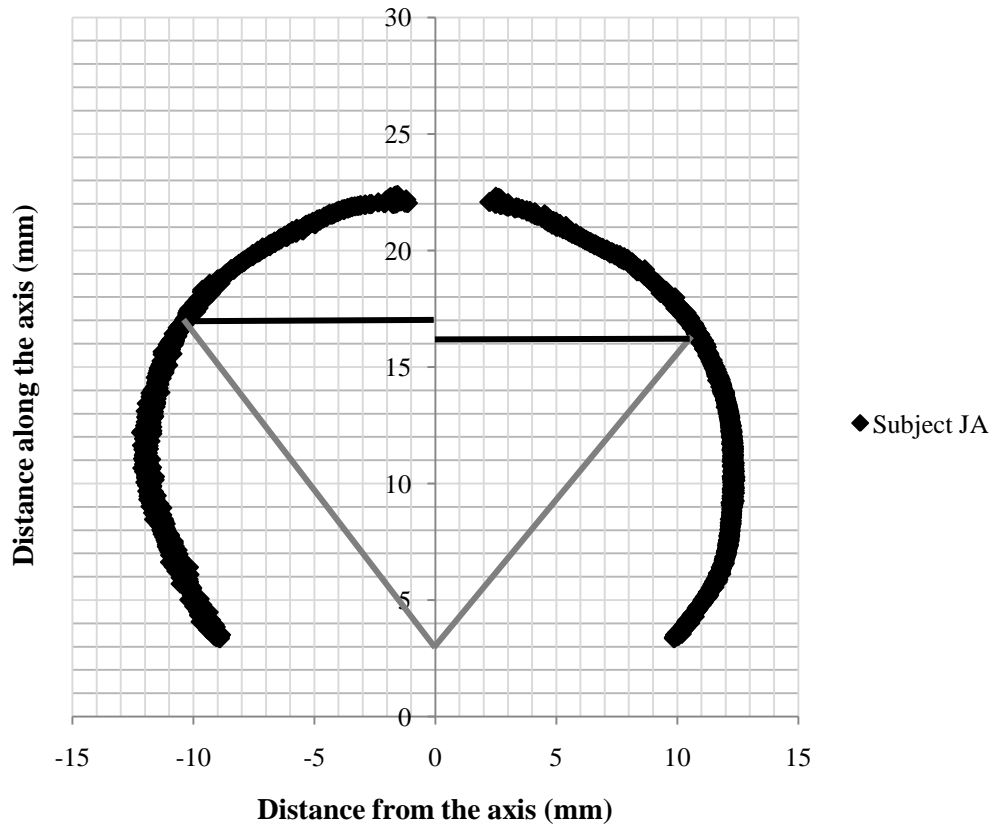


**Figure 120** Calculated index of stretch for subject JA: 92% (RE). Negative values denote the temporal region and positive numbers denote the nasal

#### 14.7 Case study

The four subjects above did not show a significant relationship between ganglion cell density and the calculated ocular index of stretch. For a more robust comparison of the effect of myopia a case study of a highly anisomyopic subject was carried out. The high level of anisomyopia allowed the less myopic eye to act as a control.

Case study subject RC, a 45 year old male anisomyope underwent the same experimental protocols for detection and direction discrimination, however both right and left temporal retinae were tested.

Eye	Central MSE (D)	Refractive error at ~ 40° temporal to fovea (D)	Axial length (from MRI, in mm)	Corneal curvature (from Zeiss IOL Master, in mm)
Right	-19.76	-8.00/-2.50 x 90	27.87	7.32/7.29
Left	-2.75	-3.50/-1.50 x 90	21.93	7.38/ 7.12

**Table 28** Refractive and ocular biometric data for subject R.C

Results showed that an increase in spatial frequency led to a reduction in detection ability. Detection ability was retained at a similar level in both the highly myopic right and the less myopic (control) left eye, detection ability was still retained above 50% with stimuli of 6 c/deg. Direction discrimination fell below chance between 1.5-2 c/deg in both eyes. Linear interpolation showed a reduction in direction discrimination ability for both eyes at 1.9 c/deg, despite a large difference in ocular stretch and surface area.

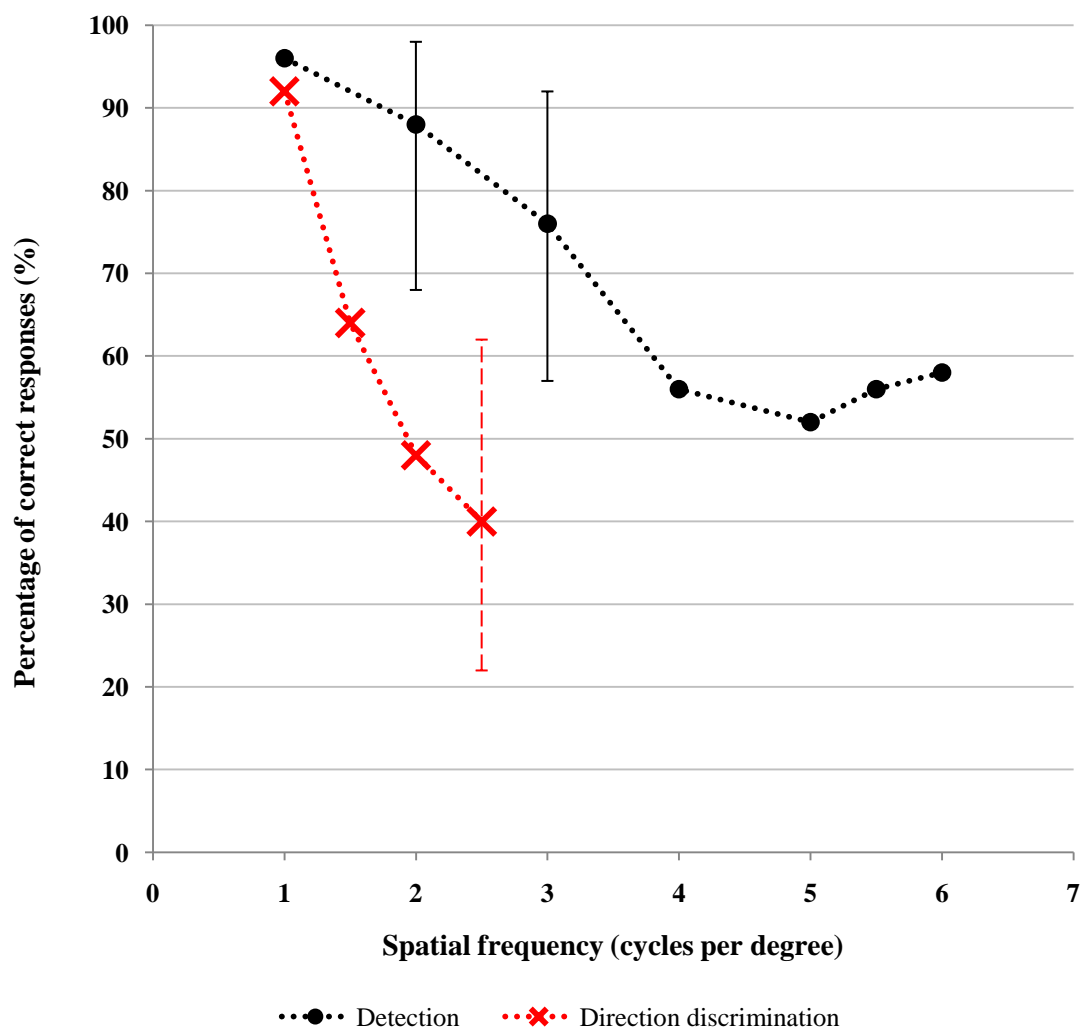


**Figure 121 Case study: RC right eye**

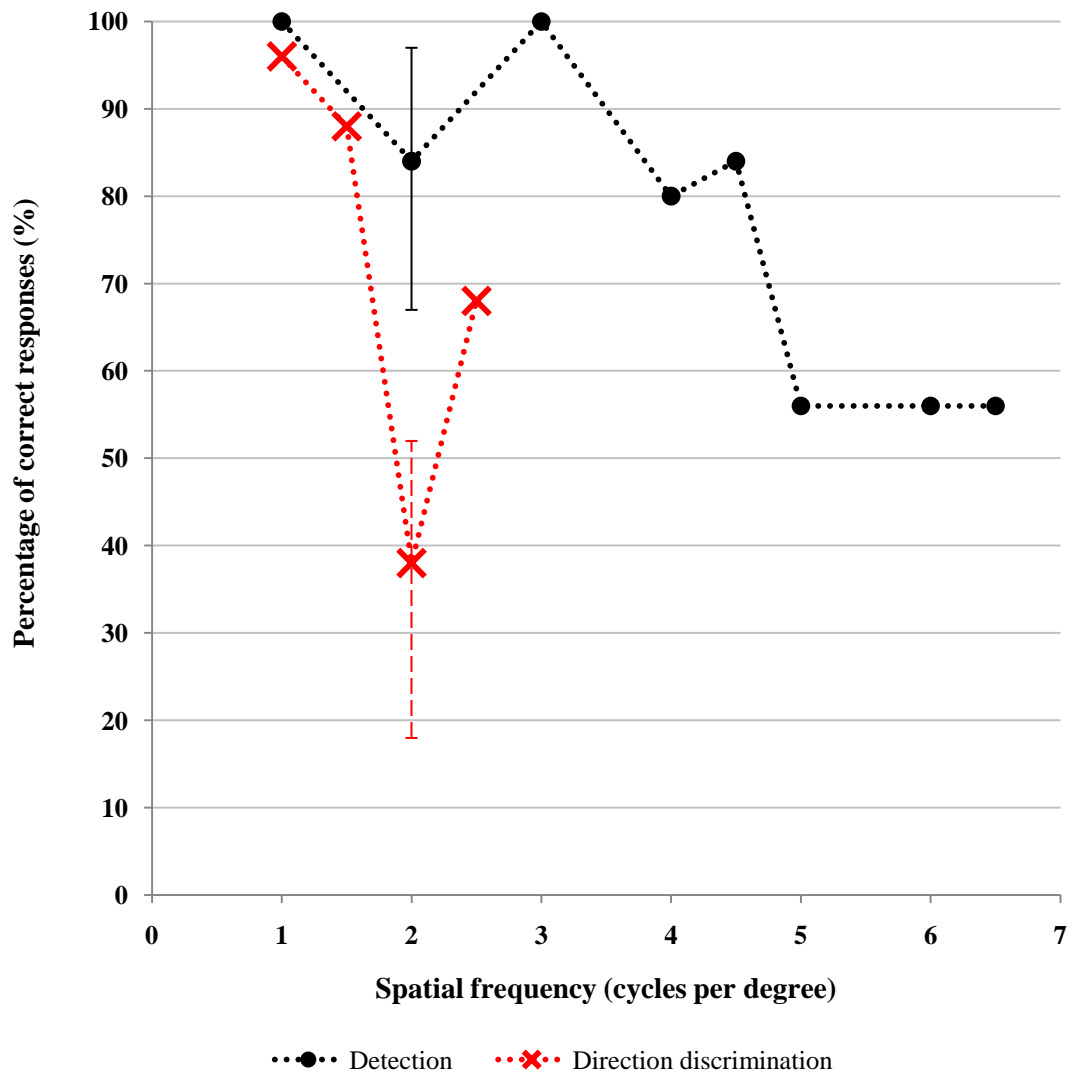
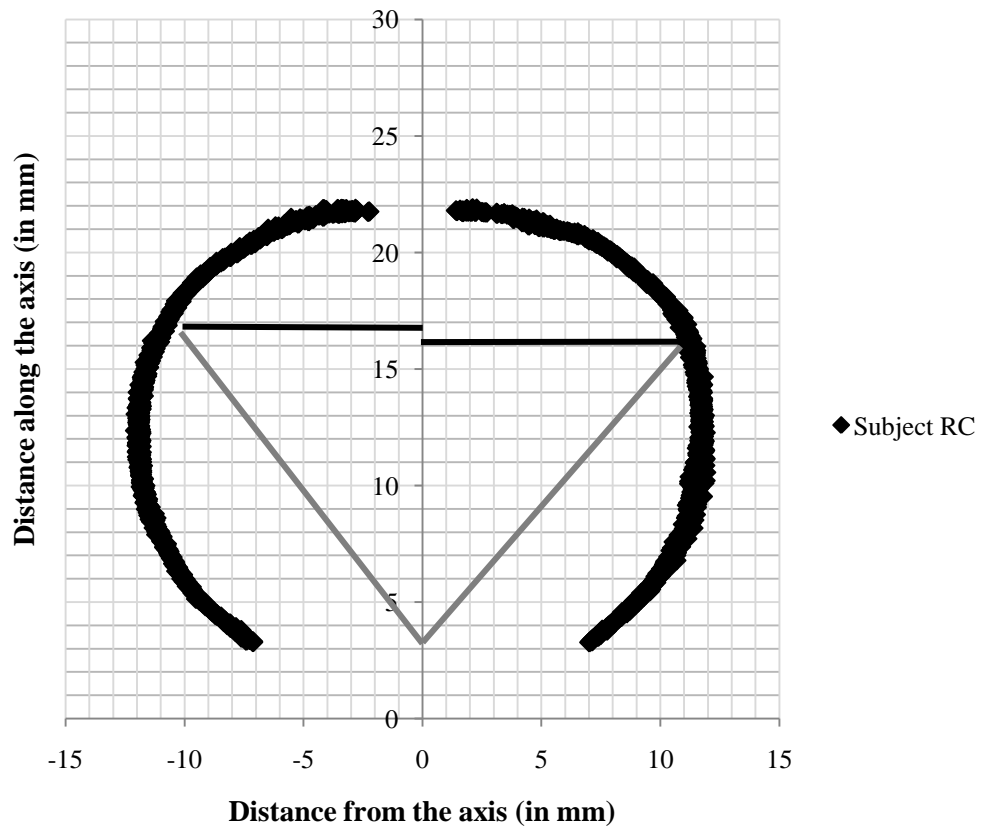


Figure 122 Case study: RC left eye

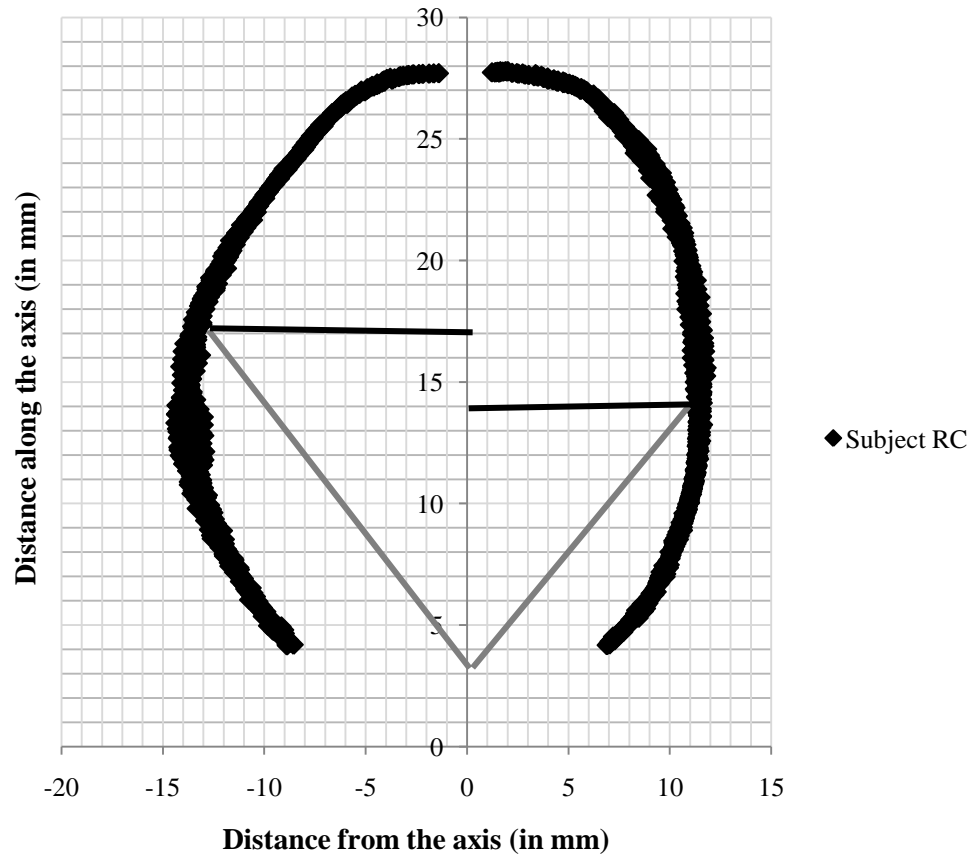
Eye	Direction discrimination threshold	Index of stretch	Surface area (mm <sup>2</sup> )
Right	1.9	81%	123.37
Left	1.8	104%	83.33

Table 29 Estimates of threshold values and indices of ocular stretch

Detection failed to fall below 50% in both right and left eyes, consequently the comparison to ocular shape was excluded for this experiment. However the overall responses were similar for both eyes; detection fell to 56% correct responses at approximately 6 c/deg.



**Figure 123** Calculated index of stretch, subject RC, left eye: 104%. Negative values denote the temporal region and positive numbers denote the nasal



**Figure 124** Calculated index of stretch, subject RC, right eye: 81%. Negative values denote the temporal region and positive numbers denote the nasal

#### 14.7.1 Discussion and conclusions

The relationship between estimated ganglion cell density and stimulus detection has been well documented: if the spacing of the ganglion cells is too large then the visual stimulus will be undersampled, consequently aliasing (or misinterpretation) of the stimulus will occur (Thibos et al. 1987). In myopic subjects reduced ganglion cell density has been reported (Chui et al. 2004). This has been attributed to ocular expansion and subsequent retinal stretch, both synonymous with high myopia. The numbers of psychophysical studies reporting ganglion cell density in different refractive groups are limited. Current knowledge is also limited by the little knowledge of ganglion cell density data through histological analysis of eyes from a range of refractive groups.

The aim of the current investigation was to evaluate the effect of eye conformation on ganglion cell density. Based on previous literature, an adverse effect i.e. increased ganglion cell spacing was predicted in larger eyes (Chui et al. 2004; Vera-Diaz et al. 2005). Although a previous attempt at correlating myopic stretch with ganglion cell density and visual acuity

has been made, the study was based on theoretical assumptions of ganglion cell density and models of myopic growth (Strang et al. 1998). In the present study the ocular shape was determined through MR imaging, by a recently introduced technique which enables accurate depictions of the 3D conformations of myopic eyes. Indices of retinal stretch and retinal surface area were calculated based on the MR data; these parameters were subsequently compared to the Nyquist limits for each individual subject. In the case of the highly anisomyopic subject RC, a difference of approximately 22% in the index of stretch and 32% in surface area was noted between the right and left temporal retinae. Consequently, the direction discrimination of the right eye would be expected to lie in the range of 1.2-1.4c/deg (based on the left eye threshold of 1.8c/deg), however, the right eye showed a direction discrimination threshold of 1.9c/deg. Ganglion cell density failed to vary as a function of both ocular stretch and surface area. The results would indicate that any decreases in estimated ganglion cell density noted previously in the peripheral myopic retina are independent of ocular shape.

#### **14.7.2 Possible causes for the absence of a relationship between ganglion cell density and ocular shape**

Previous studies have reported reduced peripheral visual function or reduced ganglion cell density as a consequence of ocular expansion; however these studies have investigated much smaller eccentricities of 15° (Vera-Diaz et al. 2005) and 0, 5° and 15° (Chui et al. 2004) from the fovea. Others have constructed theoretical models of myopic eye shape and attempted to correlate these with calculated values of ganglion cell density. The current study is unique as an accurate depiction of the retinal shape in the region tested has been obtained through MR imaging. The findings have been correlated for psychophysical estimates of ganglion cell density at 40° eccentricity; this was the location at which Anderson *et al.* (1995) carried out their study as preliminary trials had shown it to be an optimal location for demonstrating motion reversal. Furthermore this point is approximately coincident with the retinal area reported to show significant changes in retinal shape as a function of refractive error (Gilmartin et al. 2007). The absence of a decline in response with increasing myopia suggests that ganglion cell density is not reduced as a function of shape. The findings cannot establish whether myopia and ganglion cell function are independent factors.

The mechanical stretching of the retina is complex, furthermore the effect of ocular expansion on retinal cells is difficult to ascertain. The ocular expansion in myopic eyes has been presumed to affect retinal cells by increasing spacing between cells; this was not shown in the current study. The view that stretching a tissue would lead to its components, the cells, separating may be an overly simplistic view. It may be possible that if ocular stretch is taking place perhaps the cells themselves also stretch, either as a consequence or part of the myopic development process. This would imply that the ganglion cell receptive field becomes larger allowing images of low spatial frequency to be detected, but would not explain detection of high spatial frequencies. Damage to cells in individuals may also be explained through cell stretch.

Secondly the impact of mechanical stress on each individual retinal layer in myopic growth is unclear (Wolsley et al. 2008). Estimates of the magnitude of impact may be inferred from measurements of retinal thickness. Retinal thickness measured by optical coherence tomography (OCT) have shown the perifoveal regions in myopic subjects to be significantly thinner particularly in the temporal retina (Coletta et al. 2008) and the central foveal region to be thicker (Lam et al. 2007). Retinal thinning occurs most notably in the choroid located in the outer segment next to the pigment epithelium (Ikuno & Tano 2009).

Often the reasons cited for reduced functional response in myopia relate to the decreased retinal cell density or retinal cell damage (Jaworski et al. 2006; Chen et al. 2006; Atchison et al. 2006). Cell damage or misalignment is particularly relevant in the outer retina where photoreceptors are direction specific and misalignment may lead to cessation of function (Stiles & Crawford, 1934). To explain the lack of impact of ocular expansion on the ganglion cell layer it is speculated that outer retinal layers may not be able to withstand mechanical pressure as well as the inner retinal layers. The effect of stretch is likely to be dependent on mechanical characteristics such as tensile strength and thickness of each individual retinal layer (Wolsley et al. 2008).

Histological studies calculating the density of ganglion cells in retinal tissue samples for a range of refractive errors would provide further insight into the effect of ocular expansion on ganglion cells. Mechanical stress caused by myopia could be further explored by measurement of individual retinal layer thickness, which would help demonstrate the impact of myopic stretch on each retinal layer.

For the index of stretch considered and for retinal surface areas, ganglion cell density does not correlate significantly. The finding is highlighted in the case of a highly anisometric

subject. The results are contrary to previous findings of ganglion cell density with reference to refractive error (Chui et al. 2004). It is hypothesised that individual retinal layers are affected separately by the mechanical stress of myopic growth or in a way not yet established. Ganglion cell density information through histological and retinal thickness studies would help explain these results further.

#### **14.8 Summary**

In the two experimental protocols, detection and direction discrimination the level of ocular expansion was unrelated to the point at which aliasing occurred. Owing to individual variation in ganglion cell density, the comparison between emmetropic and isomyopic thresholds are of limited value and therefore the case study of a highly anisomyopic subject RC has been described.

Despite a large difference in the refractive error and index of expansion between the two eyes, the Nyquist limit values for subject RC were similar for both eyes. The results suggest that ganglion cell density does not reduce as a function of ocular stretch in myopia. Histological analysis of individual retinal layers in eyes from a range of refractive errors would provide further insight into the mechanical effects of myopia on retinal cells.

## **15 GENERAL DISCUSSION**

### **15.1 Introduction**

The principle aim of this thesis was to evaluate the relationship between ocular shape and visual function. Previous works have identified both structural and sensory factors as potential precipitants of myopic development. It was envisaged that this thesis could help characterise the structural effects of myopia and subsequently facilitate the development of future therapies for myopia prevention. In this thesis a unique application of a recently introduced MR ocular imaging technique has been used to investigate ocular shape. The evaluation of visual function has been made through several vehicles, enabling multiple strata of the retina to be examined.

The thesis assesses direct comparisons of a popularly used technique to derive retinal contour, peripheral refraction, with 3-dimensional MR imaging. The thesis reports on previously unidentified structural variations in eye shape, some of which are independent of refractive error and others which are not. Specifically quadrant variations in eye shape have been described in detail. Furthermore, previously unknown variations in visual function have been identified; the functional ability of the eye has been further explored with reference to refractive error and eye shape.

The findings are of direct clinical relevance to optometrists and the evaluations of visual function can contribute significantly to the management of the myopic eye. The findings from the experimental work have the potential to lead to further research initiatives and larger scale studies (see 15.4).

### **15.2 Eye shape and its role in myopia**

In the 1970s a series of well known studies attributed the development of myopia in adults to a relatively hyperopic peripheral image shell in comparison to the central refraction (Rempt et al. 1971). The principal technique used to investigate this theory was peripheral refraction. Peripheral refraction is not directly indicative of ocular shape; peripheral refraction data require transformation before ocular shape may be inferred. Previously, transformation of peripheral refraction data has shown myopic eyes to be relatively prolate, or less oblate than their emmetropic counterparts. The ocular shape findings from peripheral refraction data have been supported by measurements taken through ocular MR imaging

(Atchison et al. 2004; 2005). Until recently a significant proportion of the eye has remained inaccessible to measurements; the advent of 3D MRI has allowed greater access to the eye *in vivo*.

The results from the 3D MRI have shown multiple variations in eye shape some of which are present irrespective of refractive error magnitude and others which are highly dependent on refractive error. The variations which are independent of refractive state may be attributed to natural or biological variations present in most subjects. Although these variations do not necessarily help explain myopia, they do help in the understanding of ocular growth in general.

Variations dependent on refractive state are most evident in the general size of the eye; eye size increases as a function of increasing myopia. In all eyes there is a more spherical region in the mid section of the eye (which begins approximately 40% along the optic axis); although quadrant shape variations also exist. The irregularities noted within this apparently spherical region led to the conclusion that a more irregular eye shape is present in the eyes of both low myopic and emmetropic subjects in comparison to high myopes. The greater shape regularity in the high myopic group could be attributed to ocular stretch.

Of particular note was the exaggerated growth of the temporal quadrant in myopia as indexed by calculations of the maximum distances from the retinal surface to the presumed visual axis. Although the temporal quadrant differences failed to reach statistical significance they are still of interest as the temporal and superior quadrants are frequently cited as the locations most affected by myopic degenerations which can in part be explained by the tissue stress caused by the rapid myopic growth in these regions. The rationale for why myopic changes manifest themselves in the temporal quadrant is unclear. Asymmetric growth could be stimulated by several factors; asymmetric sensory input into the eye (e.g. through ocular aberrations or extent of the visual field), structural factors (e.g. ocular muscle action), or innate retinal tissue vulnerabilities which predispose specific quadrants to growth in myopia.

A distinctive feature of this thesis is the comparison made between the two major techniques of ocular imaging; MRI and transformed peripheral refraction data. The results showed that retinal curvature readings obtained using the ocular 3D MRI were consistently flatter than those using peripheral refraction. It was suggested that although a general correction factor could be applied to the data in order to make the two techniques more comparable, the presence of refractive group variations would compromise the accuracy of the correction

factor. It can be concluded that although peripheral refraction and MRI techniques produce similar conclusions of eye shape measurements, the two techniques are not comparable.

In summary, some parameters of ocular shape are specifically variants of refractive error (e.g. posterior ocular volume, posterior radius bands); other variations are unrelated to refractive error (e.g. anterior volume, specific intra quadrant differences). The asymmetries unrelated to refractive error could stem from the extra ocular muscles insertions, sensory factors or anthropologic reasons.

### 15.3 Visual Function and ocular shape

Visual functionality of the human eye is affected by many factors. In addition to refractive error, factors such as accommodative state, aberrations, visual experience, binocular status and ocular pathology may all affect visual information received by the retinal receptors. It has been suggested that sensory visual experience can mediate ocular growth and development of refractive error; in this study several tests of visual functionality were correlated with specific indices of ocular shape. The responses for each of the tests originated from different layers of the retina. The purpose of this type of design was two-fold; firstly by examining the function *vs.* shape relationship it can be elicited whether or not ocular shape does affect functionality and indeed if special considerations or correction factors should be taken into consideration when examining myopic eyes in a clinical situation. Secondly, by using tests examining specific retinal layers the study was able to draw out which retinal layers may be most affected by myopic stretch.

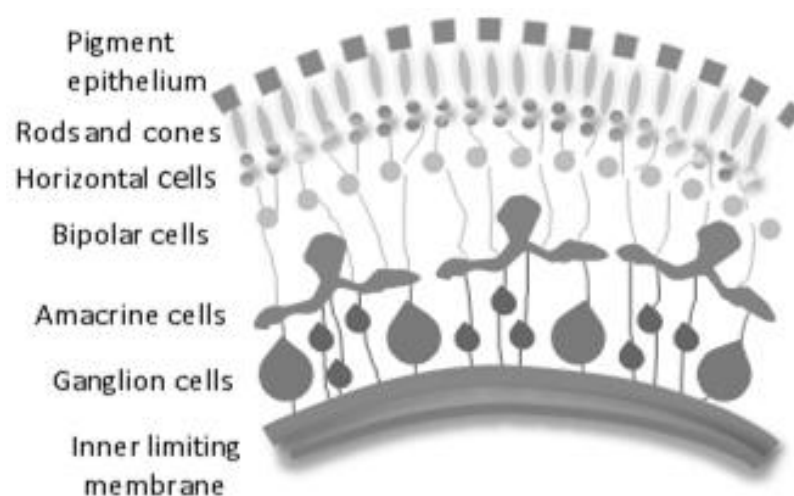


**Figure 125 Schematic illustration of the retinal layers of the human eye**

Visual field sensitivity is representative of the cone receptor response which originates from the outer retina. The responses showed the superior and superior-temporal quadrants to be correlated with eye shape. The inferior retinal quadrant response was significantly reduced relative to the superior, nasal and temporal quadrants.

The responses from the mfERG originate largely from the bipolar cells and responses correlated with shape indices in only the inferior and inferior-nasal quadrants. Highest amplitudes were noted in the superior-temporal retina and lowest in the inferior-nasal retina. The nasal retina showed significantly reduced amplitudes and significant delays in implicit time.

In general, tests of visual function showed the superior retina to perform better than the inferior; this was true of both mfERG and visual field tests. The nasal –temporal asymmetries showed less consistency between mfERG and visual fields testing. Chord distances from the MRI data showed the superior chords to be smaller than the inferior. If chord distance is used as a representative of ocular stretch it can be theorised that increased stretch may create a reduced functional response. For the MR indices which were correlated with functional test results (i.e. surface areas and interval variance) there were very few significant correlations.

Surface area in the visual fields and mfERG groups showed superior *vs.* inferior asymmetry: the inferior surface area was larger than the superior. This would indicate that the inferior quadrant is further from the presumed visual axis and has a larger surface area i.e. it is enlarged. From these results we may form the hypothesis that the retinal receptors are further stretched and subsequently produce reduced functional response in the inferior retina.

The ganglion cell density was tested through psychophysical methods. It was expected that the ganglion cell density would decline as a function of increasing myopia. Of particular interest was a case study examining the eyes of a highly anisomyopic individual; the results showed little difference in the responses of the two eyes. The results led to the conclusion that despite a large refractive difference and a large difference in eye shape the ganglion cell density was retained at similar levels.

## **15.4 Further work**

### **15.4.1 Orbital size versus ocular size**

All aspects of the experimental work allow scope for further development of the subject area. With reference to ocular shape, there have been theories presented proposing that the exaggerated axial growth in myopia is due to minimal restriction to longitudinal growth by the posterior aspect of the globe. Vertical and horizontal restrictions to growth are imposed by the orbital walls. This theory has thus far only been explored, and subsequently disproved, in the eyes of Far Eastern subjects (Chau et al. 2004), who are well known to have different shaped eyes to White-Caucasian subjects (Logan et al. 2004). As part of the MRI experimental work in this thesis an attempt was made to compare orbital and ocular size, however, the resolution of the images was not sufficient to allow accurate measurements. Recently, the introduction of 7-tesla MRI has allowed high resolution images to be obtained (Richdale et al. 2009). Examination of subjects who have undergone this type of scanning may help explore this theory further.

### **15.4.2 Advanced data analysis and development of myopia treatments**

The use of more advanced analysis techniques on the current data set is required. In particular more recent research advocates the use of finite element analysis for analysing biological tissues. In order to quantify the impact of myopic stretch and growth, the emmetropic eye may be used as a reference, or undeformed state, and the myopic eye as a state of deformation. Using this approach the quantification of changes may allow more accurate preventative treatments for myopia to be developed. The findings may also be used in conjunction with peripheral refraction findings. Currently, peripheral refraction data is being used to develop contact lens treatments to inhibit myopic development.

### **15.4.3 Extending peripheral refraction work**

Although not detailed in the main body of this thesis, a case study was carried out on a highly myopic subject, whereby peripheral refractive measures were obtained under a cycloplegic state and then with contact lenses in situ (see appendices, Figure 132). The case study demonstrated the significant amount of peripheral hyperopic defocus; leading to the conclusion that contact lens wear may in fact stimulate myopic growth. A study calculating

the image shells of subjects with and without their contact lenses in situ may help quantify the level of peripheral hyperopic defocus and perhaps identify which contact lens design is most suitable for use in myopes.

The development of a peripheral refractive device for measurement of multiple meridians would greatly aid the development of more accurate contact lens designs in the prevention of myopia.

A further aspect of the peripheral refraction dataset could be examined to determine whether or not a 'mirror-effect' exists between the right and left eyes, i.e. the temporal readings of the left and right eyes are similar, and the nasal readings of the left and right eyes are similar. Previously a mirror-effect has been noted through peripheral refraction measurements (Seidemann et al. 2002). Interestingly the current cohort showed inter eye differences in eye shape as determined by MR imaging, it would be interesting to quantify the inter eye discrepancies between the two techniques.

#### **15.4.4 Identifying high risk cases of myopia**

One key finding has been the excessive growth of the temporal quadrant in myopia. Although the finding did not reach statistical significance it is still particularly interesting as the temporal retina has frequently been identified as a site of myopic degeneration. A larger cohort study in combination with a longitudinal study of myopic fundus changes would help identify at which level of myopia significant fundus changes occur, whether the changes in ocular shape precede the visible fundus changes, and perhaps most importantly, at which level of myopic refractive error is the risk of developing a visible fundus change increased. A visible myopic degeneration is highly correlated with the development of retinal detachments which can lead to ocular morbidity. The findings could be used to review the current criteria for NHS eye tests for myopic patients and also the frequency at which patients are reviewed.

#### **15.4.5 Anterior eye biometric and functional investigations**

A further interesting finding of this thesis was concerning the structural characteristics of the anterior eye. The findings from the MRI and Oculus Pentacam data showed a spectrum of changes in the anterior eye; for some parameters such as ocular volume the anterior eye measurements remain homogenous across all refractive error groups, but for other measures

such as chord differences and pachymetry there are notably asymmetries between quadrants. As yet it is unclear whether the anterior eye plays a homeostatic regulatory role in preventing myopia or is in fact a contributor to myopic development. The cornea itself is known to possess homeostatic qualities in the regulation of epithelial cells, noted in studies examining post surgery wound healing (Wilson et al. 2003). Further analysis of both the current data set and additional anterior eye biometric measures will help further characterise the role of the anterior eye.

#### **15.4.6 Histological studies**

The functional aspect of the project has drawn interesting conclusions revealing the presence of multiple variations in the retinal responses of the different retinal quadrants. In general, highly myopic eyes are expected to show increased cell spacing and thus reduced visual function, however, the results from this thesis have not substantiated these claims. Many of the functional changes were present irrespective of refractive error and eye shape.

The findings from this thesis provide a basis for further research, in particular histological studies which examine the retinal receptor cell spacing in cohorts with a range of ametropia. Additionally histological studies of the anterior eye, namely the cornea may be beneficial in identifying the corneal layer most affected in ametropia through both cell density and thickness.

#### **15.5 Summary**

In conclusion, this investigation of ocular shape has described a variety of previously unknown variations in eye shape, some of which are present irrespective of refractive error. The structural changes which occur as a consequence of myopia have been noted and discussed. The posterior eye appears most affected by myopia although it is unclear whether the changes are a consequence or precipitant of myopia. The potential role of the anterior eye has been discussed and briefly investigated. Many parameters remain unchanged in the myopic anterior eyes, others act contrary to hypotheses. It is unclear whether the anterior eye plays either a regulatory role in myopic development or is a contributory factor itself. The question of why homeostatic regulations fail remains unanswered, although genetic structural vulnerabilities could play a role in addition to environmental sensory stresses such as near work.

The study provides scope for further investigations, including further analysis of the existing dataset. It is envisaged that engineering methodologies such as finite element analysis will enable the construction of more accurate myopic models of eye shape which may be used in the development of myopic preventative therapies namely in the form of contact lenses.

## REFERENCES

- Anderson, S. J., Mullen, K. T., & Hess, R. F. 1991, "Human peripheral spatial resolution for achromatic and chromatic stimuli: limits imposed by optical and retinal factors", *J Physiol*, vol. 442, pp. 47-64.
- Anderson, R. S., Wilkinson, M. O., & Thibos, L. N. 1992, "Psychophysical localization of the human visual streak", *Optom.Vis.Sci.*, vol. 69, no. 3, pp. 171-174.
- Anderson, S. J., Drasdo, N., & Thompson, C. M. 1995, "Parvocellular neurons limit motion acuity in human peripheral vision", *Proc.Biol.Sci.*, vol. 261, no. 1360, pp. 129-138.
- Atchison, D. A., Jones, C. E., Schmid, K. L., Pritchard, N., Pope, J. M., Strugnell, W. E., & Riley, R. A. 2004, "Eye shape in emmetropia and myopia", *Invest Ophthalmol.Vis.Sci.*, vol. 45, no. 10, pp. 3380-3386.
- Atchison, D. A. & Smith, G. "Possible errors in determining axial length changes during accommodation with the IOLMaster", *Optom.Vis.Sci.*, vol. 81, no. 4, pp. 283-6
- Atchison, D. A., Pritchard, N., Schmid, K. L., Scott, D. H., Jones, C. E., & Pope, J. M. 2005, "Shape of the retinal surface in emmetropia and myopia", *Invest Ophthalmol.Vis.Sci.*, vol. 46, no. 8, pp. 2698-2707.
- Atchison, D. A., Pritchard, N., & Schmid, K. L. 2006, "Peripheral refraction along the horizontal and vertical visual fields in myopia", *Vision Res.*, vol. 46, no. 8-9, pp. 1450-1458.
- Aung, T., Foster, P. J., Seah, S. K., Chan, S. P., Lim, W. K., Wu, H. M., Lim, A. T., Lee, L. L., & Chew, S. J. 2001, "Automated static perimetry: the influence of myopia and its method of correction", *Ophthalmology*, vol. 108, no. 2, pp. 290-295.
- Bar, D. Y., Levin, A., Morad, Y., Grotto, I., Ben-David, R., Goldberg, A., Onn, E., Avni, I., Levi, Y., & Benyamini, O. G. 2005, "The changing prevalence of myopia in young adults: a 13-year series of population-based prevalence surveys", *Invest Ophthalmol.Vis.Sci.*, vol. 46, no. 8, pp. 2760-2765.
- Bartlett, J. D., Niemann, K., Houde, B., Allred, T., Edmondson, M. J., & Crockett, R. S. 2003, "A tolerability study of pirenzepine ophthalmic gel in myopic children", *J.Ocul.Pharmacol.Ther.*, vol. 19, no. 3, pp. 271-279.
- Bayramlar, H., Cekic, O., & Hepsen, I. F. 1999, "Does convergence, not accommodation, cause axial-length elongation at near? A biometric study in teens", *Ophthalmic Res.*, vol. 31, no. 4, pp. 304-308.
- Bharatah Anil, 2009, *Introductory Medical Imaging*. Morgan & Claypool Publishers
- Benjamin, B., Davey, J. B., Sheridan, M., Sorsby, A., & Tanner, J. M. 1957, "Emmetropia and its aberrations; a study in the correlation of the optical components of the eye", *Spec.Rep.Ser.Med.Res.Counc.(G.B)*, vol. 11, no. 293, pp. 1-69.
- Blach, R. K., Jay, B., & Kolb, H. 1966, "Electrical activity of the eye in high myopia", *Br.J.Ophthalmol.*, vol. 50, no. 11, pp. 629-641.

- Bullimore, M. A., Gilmartin, B., & Royston, J. M. 1992, "Steady-State Accommodation and Ocular Biometry in Late-Onset Myopia", *Documenta Ophthalmologica*, vol. 80, no. 2, pp. 143-155.
- Calver R., Radhakrishnan H., Osuobeni E., O'Leary D., 2007, "Peripheral refraction for distance and near vision in emmetropes and myopes", *Ophthalmic Physiol Opt.*, vol. 27, no. 6, pp. 584–593.
- Carney, L. G., Mainstone, J. C., & Henderson, B. A. 1997, "Corneal topography and myopia - A cross-sectional study", *Invest Ophthalmol. Vis. Sci.*, vol. 38, no. 2, pp. 311-320.
- Chan, H. L. & Mohidin, N. 2003, "Variation of multifocal electroretinogram with axial length", *Ophthalmic Physiol Opt.*, vol. 23, no. 2, pp. 133-140.
- Chandra, S., Thomas, J. N., Madhavi, L., Joseph, J., Thanga, P., Anil, K. M., & Santosh, G. H., 2000, "Sensitivity of Swedish interactive threshold algorithm compared with standard full threshold algorithm in Humphrey visual field testing". *Ophthalmology.*, vol. 107, no. 7, pp. 1303-1308.
- Chang, S. W., Tsai, I. L., Hu, F. R., Lin, L. L. K., & Shih, Y. F. 2001, "The cornea in young myopic adults", *Br.J.Ophthalmol.*, vol. 85, no. 8, pp. 916-920.
- Chat, S. W. & Edwards, M. H. 2001, "Clinical evaluation of the Shin-Nippon SRW-5000 autorefractor in children", *Ophthalmic Physiol Opt.*, vol. 21, no. 2, pp. 87-100.
- Chau, A., Fung, K., Pak, K., & Yap, M. 2004, "Is eye size related to orbit size in human subjects?", *Ophthalmic Physiol Opt.*, vol. 24, no. 1, pp. 35-40.
- Chen, J. F., Elsner, A. E., Burns, S. A., Hansen, R. M., Lou, P. L., Kwong, K. K., & Fulton, A. B. 1992, "The Effect of Eye Shape on Retinal Responses", *Clinical Vision Sciences*, vol. 7, no. 6, pp. 521.
- Chen, J. C., Brown, B., & Schmid, K. L. 2006a, "Delayed mfERG responses in myopia", *Vision Res.*, vol. 46, no. 8-9, pp. 1221-1229.
- Chen, J. C., Brown, B., & Schmid, K. L. 2006b, "Evaluation of inner retinal function in myopia using oscillatory potentials of the multifocal electroretinogram", *Vision Res.*, vol. 46, no. 24, pp. 4096-4103.
- Chen, J. C., Brown, B., & Schmid, K. L. 2006c, "Retinal adaptation responses revealed by global flash multifocal electroretinogram are dependent on the degree of myopic refractive error", *Vision Res.*, vol. 46, no. 20, pp. 3413-3421.
- Chen, J. C., Brown, B., & Schmid, K. L. 2006d, "Slow flash multifocal electroretinogram in myopia", *Vision Res.*, vol. 46, no. 18, pp. 2869-2876.
- Chen, X., Sankaridurg, P., Donovan, L., Lin, Z., Li, L., Martinez, A., Holden, B., & Ge, J. 2010, "Characteristics of peripheral refractive errors of myopic and non-myopic Chinese eyes", *Vision Res.*, vol. 50, no. 1, pp. 31-35.
- Cheng, H.M., Singh, O.S., Kwong, K.K., Xiong, J., Woods, B.T., Brady, T.J. 1992. "Shape of the Myopic Eye as Seen with High-Resolution Magnetic Resonance Imaging", *Optom. Vis. Sci.*, vol. 69, no. 9, pp. 698-701.

Choplin & Edwards, 1998, Visual fields. SLACK Int

Chui, T. Y., Song, H., & Burns, S. A. 2008, "Individual variations in human cone photoreceptor packing density: variations with refractive error", *Invest Ophthalmol.Vis.Sci.*, vol. 49, no. 10, pp. 4679-4687.

Chui, Y., Yap, M., Chan, H., & Thibos, L. 2004, "Retinal stretching limits visual acuity in myopic eyes", *ARVO Meeting Abstracts*, vol. 45, no. 5, p. 2773.

Chui, T. Y., Yap, M. K., Chan, H. H., & Thibos, L. N. 2005, "Retinal stretching limits peripheral visual acuity in myopia", *Vision Res.*, vol. 45, no. 5, pp. 593-605.

Chui, Y., Yap, M., & Chan, H. 2002, "The Retinal Ganglion Cell Density and Nerve Fiber Layer Thickness in the Human Myopic Eye", *Invest Ophthalmol.Vis.Sci*, vol. 43, no. 12, p. 183.

Coletta, N. J., Raghuram, A., Rondon, M., & Johnson, L. 2008, "Foveal and perifoveal thickness in myopia measured with a Fourier-Domain OCT", *Journal of Vision*, vol. 8, no. 17, p. 49.

Curcio, C. A. & Allen, K. A. 1990, "Topography of ganglion cells in human retina", *J.Comp Neurol.*, vol. 300, no. 1, pp. 5-25.

Curcio, C. A., Sloan, K. R., Kalina, R. E., & Hendrickson, A. E. 1990, "Human photoreceptor topography", *J.Comp Neurol.*, vol. 292, no. 4, pp. 497-523.

Czepita, D. & Chmielewska, I. 2004, "Changes in the static visual field of patients with low and medium myopia", *Ann.Acad.Med.Stetin.*, vol. 50, no. 1, pp. 21-24.

De Monasterio, F. M. & Gouras, P. 1975, "Functional properties of ganglion cells of the rhesus monkey retina", *The Journal of Physiology*, vol. 251, no. 1, pp. 167-195.

Dirani, M., Chamberlain, M., Shekar, S. N., Islam, A. F. M., Garoufalos, P., Chen, C. Y., Guymer, R. H., & Baird, P. N. 2006, "Heritability of refractive error and ocular biometrics: The Genes in Myopia Twin Study", *Invest Ophthalmol.Vis.Sci*, vol. 47, no. 11, pp. 4756-4761.

Drexler, W., Findl, O., Menapace, R., Rainer, G., Vass, C., Hitzenberger, C. K., & Fercher, A. F. 1998, "Partial coherence interferometry: a novel approach to biometry in cataract surgery", *American Journal of Ophthalmology*, vol. 126, no. 4, pp. 524-534.

Dunne, M. C. & Barnes, D. A. 1987, "Schematic modelling of peripheral astigmatism in real eyes", *Ophthalmic Physiol Opt.*, vol. 7, no. 3, pp. 235-239.

Dunne M.C.M, Misson G.P, White E.K, Barnes DA., 1993, "Peripheral astigmatic asymmetry and angle alpha", *Ophthalmic Physiol Opt.*, vol. 13, no. 3, pp. 303-305.

Dunne, M. C. 1995, "A computing scheme for determination of retinal contour from peripheral refraction, keratometry and A-scan ultrasonography", *Ophthalmic Physiol Opt.*, vol. 15, no. 2, pp. 133-143.

Edwards, M. H. & Lam, C. S. 2004, "The epidemiology of myopia in Hong Kong", *Ann.Acad.Med.Singapore*, vol. 33, no. 1, pp. 34-38.

- Enroth-Cugell, C. & Robson, J. G. 1966, "The contrast sensitivity of retinal ganglion cells of the cat", *J.Physiol*, vol. 187, no. 3, pp. 517-552.
- Farbrother, J. E., Kirov, G., Owen, M. J., Pong-Wong, R., Haley, C. S., & Guggenheim, J. A. 2004, "Linkage analysis of the genetic loci for high myopia on 18p, 12q, and 17q in 51 UK families", *Invest Ophthalmol.Vis.Sci*, vol. 45, no. 9, pp. 2879-2885.
- Fedtko, C., Ehrmann, K., & Holden, B. A. 2009, "A review of peripheral refraction techniques", *Optom.Vis.Sci.*, vol. 86, no. 5, pp. 429-446.
- Ferree, C. E. & Rand, G. 1933, "Interpretation of refractive conditions in the peripheral field of vision: a further study", *Archives of Ophthalmology*, vol. 9, no. 6, pp. 925-938.
- Ferree, C. E., Rand, G., & Hardy, C. 1931, "Refraction for the peripheral field of vision", *Archives of Ophthalmology*, vol. 5, no. 5, pp. 717-731.
- Galvin, S. J., Williams, D. R., & Coletta, N. J. 1996, "The Spatial Grain of Motion Perception in Human Peripheral Vision", *Vision Res.*, vol. 36, no. 15, pp. 2283-2295.
- Garner, L. F., Stewart, A. W., Owens, H., Kinnear, R. F., & Frith, M. J. 2006, "The Nepal Longitudinal Study: Biometric characteristics of developing eyes", *Optom.Vis.Sci.*, vol. 83, no. 5, pp. 274-280.
- Gilmartin, B. 2004, "Myopia: precedents for research in the twenty-first century", *Clin.Experiment.Ophthalmol.*, vol. 32, no. 3, pp. 305-324.
- Gilmartin, B., Logan, N. S., & Singh, K. D. 2007, "Determining Regional Variations in Globe Conformation Using 3-D Ocular MRI", *Invest Ophthalmol.Vis.Sci*, vol. 48, no. 5, p. 1215.
- Gilmartin, B., Logan, N. S., & Singh, K. D. 2008, "In vivo Comparison of Anterior and Posterior Ocular Volume in Human Ametropia", *Invest Ophthalmol.Vis.Sci.*, vol. 49, no. 5, p. 3582.
- Goel, S., Chua, C., Butcher, M., Jones, C. A., Bagga, P., & Kotta, S. 2004, "Laser vs ultrasound biometry a study of intra- and interobserver variability", *Eye*, vol. 18, no. 5, pp. 514-518.
- Goss, D. A. & Erickson, P. 1990, "Effects of Changes in Anterior-Chamber Depth on Refractive Error of the Human Eye", *Clinical Vision Sciences*, vol. 5, no. 2, pp. 197-201.
- Goss, D. A., VanVeen, H. G., Rainey, B. B., & Feng, B. 1997, "Ocular components measured by keratometry, phakometry, and ultrasonography in emmetropic and myopic optometry students", *Optom.Vis.Sci.*, vol. 74, no. 7, pp. 489-495.
- Grosvenor, T. 1988, "High Axial Length Corneal Radius Ratio As A Risk Factor in the Development of Myopia", *American Journal of Optometry and Physiological Optics*, vol. 65, no. 9, pp. 689-696.
- Grosvenor, T. & Goss, D. A. 1998, "Role of the cornea in emmetropia and myopia", *Optom.Vis.Sci.*, vol. 75, no. 2, pp. 132-145.

- Gwiazda, J., Marsh-Tootle, W. L., Hyman, L., Hussein, M., & Norton, T. T. 2002, "Baseline refractive and ocular component measures of children enrolled in the Correction of Myopia Evaluation Trial (COMET)", *Invest Ophthalmol.Vis.Sci*, vol. 43, no. 2, pp. 314-321.
- Hamilton, K. E., Pye, D. C., Aggarwala, S., Evian, S., Khosla, J., & Perera, R. 2007, "Diurnal variation of central corneal thickness and Goldmann applanation tonometry estimates of intraocular pressure", *Journal of Glaucoma*, vol. 16, no. 1, pp. 29-35.
- Hashemi H., Yazdani K., Mehravaran S., Fotouhi A., 2005, "Anterior chamber depth measurement with a-scan ultrasonography, Orbscan II, and IOLMaster", *Optom.Vis.Sci.*, vol. 82, no. 10, pp. 900-904.
- Hebel, R. & Hollander, H. 1983, "Size and distribution of ganglion cells in the human retina", *Anat.Embryol.(Berl)*, vol. 168, no. 1, pp. 125-136.
- Heijl, A. & Krakau, C. E. 1975, "An automatic static perimeter, design and pilot study", *Acta Ophthalmol.(Copenh)*, vol. 53, no. 3, pp. 293-310.
- Hood D.C, 2000, "Assessing retinal function with the multifocal technique", *Progress in Retinal and Eye Res.*, vol. 19, no.5, pp. 607-646.
- Hood, D. C., Frishman, L. J., Saszik, S., & Viswanathan, S. 2002, "Retinal origins of the primate multifocal ERG: Implications for the human response", *Invest Ophthalmol.Vis.Sci*, vol. 43, no. 5, pp. 1673-1685.
- Hood, D. C., Odel, J. G., Chen, C. S., & Winn, B. J. 2003, "The multifocal electroretinogram", *Journal of Neuro-Ophthalmology*, vol. 23, no. 3, pp. 225-235.
- Hood, D. C., Bach, M., Brigell, M., Keating, D., Kondo, M., Lyons, J. S., & Palmowski-Wolfe, A. M. 2008, "ISCEV guidelines for clinical multifocal electroretinography (2007 edition)", *Doc.Ophthalmol.*, vol. 116, no. 1, pp. 1-11.
- Hoogerheide, J., Rempt, F., & Hoogenboom, W. P. 1971, "Acquired myopia in young pilots", *Ophthalmologica*, vol. 163, no. 4, pp. 209-215.
- Hyams, S.W., Neumann, E., Friedman, Z. 1975, "Myopia-aphakia. II. Vitreous and peripheral retina", *Br J Ophthalmol*;; vol. 59, pp. 483-485.
- Ikuno, Y. & Tano, Y. 2009, "Retinal and Choroidal Biometry in Highly Myopic Eyes with Spectral-Domain Optical Coherence Tomography", *Investigative Ophthalmology Visual Science*, vol. 50, no. 8, pp. 3876-3880.
- Jaworski, A., Gentle, A., Zele, A. J., Vingrys, A. J., & McBrien, N. A. 2006, "Altered visual sensitivity in axial high myopia: a local postreceptor phenomenon?", *Investigative Ophthalmology Visual Science.*, vol. 47, no. 8, pp. 3695-3702.
- Jiang, B. C. & Woessner, W. M. 1996, "Vitreous chamber elongation is responsible for myopia development in a young adult", *Optom.Vis.Sci.*, vol. 73, no. 4, pp. 231-234.
- Jonas, J. B., Schneider, U., & Naumann, G. O. 1992, "Count and density of human retinal photoreceptors", *Graefes Arch.Clin.Exp.Ophthalmol.*, vol. 230, no. 6, pp. 505-510.

- Kawabata, H. & chi-Usami, E. 1997, "Multifocal electroretinogram in myopia", *Invest Ophthalmol.Vis.Sci.*, vol. 38, no. 13, pp. 2844-2851.
- Khoramnia, R., Rabsilber, T. M., & Auffarth, G. U. 2007, "Central and peripheral pachymetry measurements according to age using the Pentacam rotating Scheimpflug camera", *Journal of Cataract and Refractive Surgery*, vol. 33, no. 5, pp. 830-836.
- Kitaguchi, Y., Bessho, K., Yamaguchi, T., Nakazawa, N., Mihashi, T., & Fujikado, T. 2007, "In vivo measurements of cone photoreceptor spacing in myopic eyes from images obtained by an adaptive optics fundus camera", *Jpn.J.Ophthalmol.*, vol. 51, no. 6, pp. 456-461.
- Koller, G., Haas, A., Zulauf, M., Koerner, F., & Mojon, D. 2001, "Influence of refractive correction on peripheral visual field in static perimetry", *Graefes Arch Clin.Exp.Ophthalmol.*, vol. 239, no. 10, pp. 759-762.
- Kuffler, S. W. 1953, "Discharge patterns and functional organization of mammalian retina", *J.Neurophysiol.*, vol. 16, no. 1, pp. 37-68.
- Lackner B., Schmidinger G., Skorpik C., 2005, "Validity and Repeatability of Anterior Chamber Depth Measurements with Pentacam and Orbscan", *Optom.Vis.Sci.*, vol. 82, no. 9, pp. 858-861.
- Lam A.K.C, Chan R, Pang P.C.K., 2001, "The repeatability and accuracy of axial length and anterior chamber depth measurements from the IOLMaster", *Ophthalmic Physiol Opt.* vol. 21, no. 6, pp. 477-483.
- Lam, D. S. C., Leung, K. S., Mohamed, S., Chan, W. m., Palanivelu, M. S., Cheung, C. Y. L., Li, E. Y. M., Lai, R. Y. K., & Leung, C. K. 2007, "Regional Variations in the Relationship between Macular Thickness Measurements and Myopia", *Investigative Ophthalmology Visual Science*, vol. 48, no. 1, pp. 376-382.
- Lee, K. E., Klein, B. E. K., & Klein, R. 1999, "Changes in refractive error over a 5-year interval in the Beaver Dam Eye Study" *Invest Ophthalmol.Vis.Sci*, vol. 40, no. 8, pp. 1645-1649.
- Liang, C. L., Yen, E., Su, J. Y., Liu, C., Chang, T. Y., Park, N., Wu, M. J., Lee, S., Flynn, J. T., & Juo, S. H. H. 2004, "Impact of family history of high myopia on level and onset of myopia", *Invest Ophthalmol.Vis.Sci*, vol. 45, no. 10, pp. 3446-3452.
- Liu, J. H. K. & Farid, H. 1998, "Twenty-four-hour change in axial length in the rabbit eye", *Invest Ophthalmol.Vis.Sci*, vol. 39, no. 13, pp. 2796-2799.
- Logan, N., Davies, L. N., Mallen, E. A. H., & Gilmartin, B. 2005, "Ametropia and ocular biometry in a UK university student population", *Optom.Vis.Sci.*, vol. 82, no. 4, pp. 261-266.
- Logan, N. S., Gilmartin, B., Wildsoet, C. F., & Dunne, M. C. 2004, "Posterior retinal contour in adult human anisomyopia", *Investigative Ophthalmology Visual Science.*, vol. 45, no. 7, pp. 2152-2162.
- Logan, N. S., Singh, K. D., & Gilmartin, B. 2005, "3D Conformation of Human Eye Shape Using MRI", *Invest Ophthalmol.Vis.Sci*, vol. 46, no. 5, p. 4266.
- Lotmar, W. & Lotmar, T. 1974, "Peripheral astigmatism in the human eye: experimental data and theoretical model predictions", *J.Opt.Soc.Am.*, vol. 64, no. 4, pp. 510-513.

- Luu, C. D., Foulds, W. S., & Tan, D. T. H. 2007, "Features of the multifocal electroretinogram may predict the rate of myopia progression in children, *Ophthalmology*, vol. 114, no. 8, pp. 1433-1438.
- Mallen, E. A. & Kashyap, P. 2007, "Technical note: measurement of retinal contour and supine axial length using the Zeiss IOLMaster", *Ophthalmic Physiol Opt.*, vol. 27, no. 4, pp. 404-411.
- Mallen, E. A., Wolffsohn, J. S., Gilmartin, B., & Tsujimura, S. 2001, "Clinical evaluation of the Shin-Nippon SRW-5000 autorefractor in adults", *Ophthalmic Physiol Opt.*, vol. 21, no. 2, pp. 101-107.
- Mallen, E. A. H., Kashyap, P., & Hampson, K. M. 2006, "Transient axial length change during the accommodation response in young adults", *Invest Ophthalmol. Vis. Sci.*, vol. 47, no. 3, pp. 1251-1254.
- Marmor, M. F., Hood, D. C., Keating, D., Kondo, M., Seeliger, M. W., & Miyake, Y. 2003, "Guidelines for basic multifocal electroretinography (mfERG)", *Documenta Ophthalmologica*, vol. 106, no. 2, pp. 105-115.
- Marsich, M. W. & Bullimore, M. A. 2000, "The repeatability of corneal thickness measures", *Cornea*, vol. 19, no. 6, pp. 792-795.
- Martin, D. K. & Holden, B. A. 1982, "A new method for measuring the diameter of the in vivo human cornea", *Am.J.Optom. Physiol Opt.*, vol. 59, no. 5, pp. 436-441.
- Martin-Boglund, L. 1991, "High-pass resolution perimetry in uncomplicated myopia", *Acta Ophthalmol.(Copenh)*, vol. 69, no. 4, pp. 516-520.
- McBrien, N. A. & Adams, D. W. 1997, "A longitudinal investigation of adult-onset and adult-progression of myopia in an occupational group - Refractive and biometric findings", *Invest Ophthalmol. Vis. Sci.*, vol. 38, no. 2, pp. 321-333.
- McBrien, N. A. & Millodot, M. 1987, "A biometric investigation of late onset myopic eyes", *Acta Ophthalmologica*, vol. 65, no. 4, pp. 461-468.
- McBrien, N. A., Young, T. L., Pang, C. P., Hammond, C., Baird, P., Saw, S. M., Morgan, I. G., Mutti, D. O., Rose, K. A., Wallman, J., Gentle, A., Wildsoet, C. F., Gwiazda, J., Schmid, K. L., Smith, E., III, Troilo, D., Summers-Rada, J., Norton, T. T., Schaeffel, F., Megaw, P., Beuerman, R. W., & McFadden, S. A. 2008, "Myopia: Recent advances in molecular Studies; prevalence, progression and risk factors; emmetropization; therapies; optical links; peripheral refraction; sclera and ocular growth; signalling cascades; and animal models", *Optom. Vis. Sci.*
- McCarthy, C. S., Megaw, P., Devadas, M., & Morgan, I. G. 2007, "Dopaminergic agents affect the ability of brief periods of normal vision to prevent form-deprivation myopia", *Exp. Eye Res.*, vol. 84, no. 1, pp. 100-107.
- McRobbie, Moore, Graves. 2003, "MRI from picture to proton". Cambridge University Press
- Miller, J. M., Wildsoet, C. F., Guan, H., Limbo, M., & Demer, J. L. 2004, "Refractive Error and Eye Shape by MRI", *Invest Ophthalmol. Vis. Sci.*, vol. 45, no. 5, p. 2388.

- Millodot, M. 1981, "Effect of ametropia on peripheral refraction", *Am.J.Optom.Physiol Opt.*, vol. 58, no. 9, pp. 691-695.
- Morgan, I. & Megaw, P. 2004, "Using natural STOP growth signals to prevent excessive axial elongation and the development of myopia", *Ann.Acad.Med.Singapore*, vol. 33, no. 1, pp. 16-20.
- Mutti, D. O., Sholtz, R. I., Friedman, N. E., & Zadnik, K. 2000, "Peripheral refraction and ocular shape in children", *Invest Ophthalmol.Vis.Sci.*, vol. 41, no. 5, pp. 1022-1030.
- Mutti, D.O., Hayes, J.R., Mitchell, G.L., Jones, L.A., Moeschberger, M.L., Zadnik, K., Cotter, S.A., Kleinstein, R.N., Manny, R.E., & Twelker, J.D. 2005, "The effect of ethnicity on axial length and ocular shape before and after the onset of myopia", *ARVO Meeting Abstracts*, 46, (5) 4623.
- Nagatomo A, Nao-i N, Maruiwa F, Arai M, Sawada A., 1998, "Multifocal electroretinograms in normal subjects", *Jpn J Ophthalmol.*, vol. 42, no. 2, pp. 129-135.
- Németh. J., Orsolya, F., & Norbert, P., 2003, "Optical and ultrasound measurement of axial length and anterior chamber depth for intraocular lens power calculation", *Journal of cataract and refractive surgery*, vol. 29, no. 1, pp.85-88.
- Nagra, M., Gilmartin, B., Logan, N. S., Furlong, P., Wilkinson, E., & Singh, K. 2009, "Conformation of Sagittal and Axial Meridians in Human Myopia", *Invest Ophthalmol.Vis.Sci.*, vol. 50, no. 5, p. 3941.
- O'Donoghue, L., Saunders, K. J., & Anderson, R. S. 2005, "Effect of Accommodation on Axial Length Measurement in Myopes and Emmetropes", *ARVO Meeting Abstracts*, vol. 46, no. 5, p. 5591.
- O'Leary, D. J. & Millodot, M. 1979, "Eyelid closure causes myopia in humans", *Cellular and Molecular Life Sciences*, vol. 35, no. 11, pp. 1478-1479.
- Ojaimi, E., Rose, K. A., Morgan, I. G., Smith, W., Martin, F. J., Kifley, A., Robaei, D., & Mitchell, P. 2005, "Distribution of ocular biometric parameters and refraction in a population-based study of Australian children", *Invest Ophthalmol.Vis.Sci.*, vol. 46, no. 8, pp. 2748-2754.
- Pardhan S and Rae S. 2009 "Variation in Nasal-Temporal Asymmetry in Refractive Error Groups" 12<sup>th</sup> International Myopia Conference, Queensland Australia , July 2008.
- Perlman, I., Meyer, E., Haim, T., & Zonis, S. 1984, "Retinal function in high refractive error assessed electroretinographically", *Br.J.Ophthalmol.*, vol. 68, no. 2, pp. 79-84.
- Popovic, Z. & Sjöstrand, J. 2005, "The relation between resolution measurements and numbers of retinal ganglion cells in the same human subjects", *Vision Res.*, vol. 45, no. 17, pp. 2331-2338.
- Pruett, R. C. 1988, "Progressive myopia and intraocular pressure: what is the linkage? A literature review", *Acta Ophthalmol.Suppl*, vol. 185, pp. 117-127.

- Reddy, A. R., Pande, M. V., Finn, P., & El-Gogary, H. 2004, "Comparative estimation of anterior chamber depth by ultrasonography, Orbscan II, and IOLMaster", *J.Cataract Refract.Surg.*, vol. 30, no. 6, pp. 1268-1271.
- Rempt F., Hoogerheide J., Hoogenboom W.P., 1971, "Peripheral retinoscopy and the skiagrams", *Ophthalmologica.*, vol. 162, no. 1, pp. 1-10.
- Richdale, K., Wassenaar, P., Teal, B. K., Abduljalil, A., Christoforidis, J. A., Lanz, T., Knopp, M. V., & Schmalbrock, P. 2009, "7 Tesla MR imaging of the human eye in vivo", *J.Magn Reson.Imaging*, vol. 30, no. 5, pp. 924-932.
- Rose, K. A., Morgan, I. G., Ip, J., Kifley, A., Huynh, S., Smith, W., & Mitchell, P. 2008, "Outdoor activity reduces the prevalence of myopia in children", *Ophthalmology*, vol. 115, no. 8, pp. 1279-1285.
- Rudnicka, A. R. & Edgar, D. F. 1995, "Automated static perimetry in myopes with peripapillary crescents--Part I", *Ophthalmic Physiol Opt.*, vol. 15, no. 5, pp. 409-412.
- Rudnicka, A. R. & Edgar, D. F. 1996, "Automated static perimetry in myopes with peripapillary crescents--Part II", *Ophthalmic Physiol Opt.*, vol. 16, no. 5, pp. 416-429.
- Santodomingo-Rubido, J., Mullen, E. A. H., Gilmartin, B., & Wolffsohn, J. S. 2002, "A new non-contact optical device for ocular biometry", *Br.J.Ophthalmol.*, vol. 86, no. 4, pp. 458-462.
- Saw, S. M., Chua, W. H., Hong, C. Y., Wu, H. M., Chia, K. S., Stone, R. A., & Tan, D. 2002, "Height and its relationship to refraction and biometry parameters in Singapore Chinese children", *Invest Ophthalmol.Vis.Sci*, vol. 43, no. 5, pp. 1408-1413.
- Schiller, P. H. & Malpeli, J. G. 1977, "Properties and tectal projections of monkey retinal ganglion cells", *Journal of Neurophysiology*, vol. 40, no. 2, pp. 428-445.
- Schmid, G. F. 2003, "Variability of retinal steepness at the posterior pole in children 7-15 years of age", *Current Eye Research*, vol. 27, no. 1, pp. 61-68.
- Seidemann, A., Schaeffel, F., Guirao, A., Lopez-Gil, N., & Artal, P. 2002, "Peripheral refractive errors in myopic, emmetropic, and hyperopic young subjects", *Journal of the Optical Society of America A-Optics Image Science and Vision*, vol. 19, no. 12, pp. 2363-2373.
- Sheng, H. U. A. N., Bottjer, C. A., & Bullimore, M. A. 2004, "Ocular component measurement using the Zeiss IOLMaster", *Optom.Vis.Sci.*, vol. 81, no. 1.
- Siatkowski, R. M., Cotter, S., Miller, J. M., Scher, C. A., Crockett, R. S., & Novack, G. D. 2004, "Safety and efficacy of 2% pirenzepine ophthalmic gel in children with myopia: a 1-year, multicenter, double-masked, placebo-controlled parallel study", *Arch.Ophthalmol*, vol. 122, no. 11, pp. 1667-1674.
- Singh, K. D., Logan, N. S., & Gilmartin, B. 2006, "Three-dimensional modeling of the human eye based on magnetic resonance imaging", *Invest Ophthalmol.Vis.Sci*, vol. 47, no. 6, pp. 2272-2279.

- Shukla, M. & Ahuja, O.P., 1983, "Peripheral retina in myopia", *Indian Journal of Ophthalmology*, vol. 31, no. 6, pp. 719-722.
- Shukla M, Ahuja OP, Jamal N., 1986, "Traumatic retinal detachment", *Indian J Ophthalmol.*, vol. 34, no. 1, pp. 29-32.
- Sjöstrand, J., Olsson, V., Popovic, Z., & Conradi, N. 1999, "Quantitative estimations of foveal and extra-foveal retinal circuitry in humans", *Vision Res.*, vol. 39, no. 18, pp. 2987-2998.
- Smith, E. L., III, Ramamirtham, R., Qiao-Grider, Y., Hung, L. F., Huang, J., Kee, C. S., Coats, D., & Paysse, E. 2007, "Effects of foveal ablation on emmetropization and form-deprivation myopia", *Invest Ophthalmol. Vis. Sci.*, vol. 48, no. 9, pp. 3914-3922.
- Smith, G., Atchison, D. A., Robert Iskander, D., Jones, C. E., & Pope, J. M. 2009, "Mathematical models for describing the shape of the in vitro unstretched human crystalline lens", *Vision Res.*, vol. 49, no. 20, pp. 2442-2452.
- Sorsby, A. & Leary, G. A. 1969, "A longitudinal study of refraction and its components during growth", *Spec. Rep. Ser. Med. Res. Counc. (G.B)*, vol. 309, pp. 1-41.
- Spiers A.S, Calne D.B., 1969, "Action of dopamine on the human iris", *Br Med J.*, vol. 4 no. 5679, pp. 333-335.
- Stenstrom, S. 1948, "Investigation of the variation and the correlation of the optical elements of human eyes", *Am. J. Optom. Arch. Acad. Optom.*, vol. 58, pp. 1-71.
- Stiles W. S. and Crawford B. H. 1934. "The Liminal Brightness Increment for White Light for Different Conditions of the Foveal and Parafoveal Retina", *Proceedings of the Royal Society of London Series B, Biological Sciences.*, vol. 116, no. 796, pp. 55-102
- Stone, R. A. & Flitcroft, D. I. 2004, "Ocular shape and myopia", *Annals Academy of Medicine Singapore*, vol. 33, no. 1, pp. 7-15.
- Strang, N. C., Winn, B., & Bradley, A. 1998, "The role of neural and optical factors in limiting visual resolution in myopia", *Vision Res.*, vol. 38, no. 11, pp. 1713-1721.
- Sutter, E. E. & Tran, D. 1992, "The field topography of ERG components in man--I. The photopic luminance response", *Vision Res.*, vol. 32, no. 3, pp. 433-446.
- Tabernero, J. & Schaeffel, F. 2009, "More irregular eye shape in low myopia than in emmetropia", *Invest Ophthalmol. Vis. Sci.*, vol. 50, no. 9, pp. 4516-4522.
- Tate, G. W., & Lynn, J. R. 1977. *Principles of quantitative perimetry: testing and interpreting the visual field*. New York, Grune & Stratton.
- Tay, E., Seah, S. K., Chan, S. P., Lim, A. T., Chew, S. J., Foster, P. J., & Aung, T. 2005, "Optic disk ovality as an index of tilt and its relationship to myopia and perimetry", *Am. J. Ophthalmol.*, vol. 139, no. 2, pp. 247-252.
- Thibos, L. N., Walsh, D. J., & Cheney, F. E. 1987, "Vision beyond the resolution limit: Aliasing in the periphery", *Vision Res.*, vol. 27, no. 12, pp. 2193-2197.

- Thibos, L. N., Wheeler, W., Horner, D. 1997, "Power vectors: an application of Fourier analysis to the description and statistical analysis of refractive error", *Optometry & Vision Science*, vol.74, no. 6, pp.367-375.
- Tomlinson, A. & Phillips, C. I. 1970, "Applanation tension and axial length of eyeball", *Br.J.Ophthalmol.*, vol. 54, no. 8, pp. 548.
- Tomlinson, A. & Phillips, C. I. 1972, "Unequal axial length of eyeball and ocular tension", *Acta Ophthalmologica*, vol. 50, no. 6, pp. 872-876.
- Traquair, H. M. 1924, "Essential considerations in regard to the field of vision: contraction or depression?", *Br.J.Ophthalmol.*, vol. 8, no. 2, pp. 49-58.
- Tscherning M., 1924, *Physiologic Optics*. 4<sup>th</sup> Ed., Philadelphia: Keystone Publishing Co. pp. 150-154.
- Tsutsui, K., Uozato, H., Handa, T., Shoji, N., Mukuno, K., & Shimizu, K. 2003, "Diurnal variation of axial length and intraocular pressure in young adults", *Invest Ophthalmol.Vis.Sci*, vol. 44, p. 436.
- Twelker, J. D., Mitchell, G. L., Messer, D. H., Bhakta, R., Jones, L. A., Mutti, D. O., Cotter, S. A., Klenstein, R. N., Manny, R. E., & Zadnik, K. 2009, "Children's Ocular Components and Age, Gender, and Ethnicity", *Optom.Vis.Sci.*, vol. 86, no. 8, pp. 918-935.
- Twomey, J. M., Gilvarry, A., Restori, M., Kirkness, C. M., Moore, A. T., & Holden, A. L. 1990, "Ocular Enlargement Following Infantile Corneal Opacification", *Eye*, vol. 4, pp. 497-503.
- Van Aphen, G.W.H.M., 1961, "On emmetropia and ametropia", *Ophthalmologica.*, vol. 142 (Suppl.), pp.1-92.
- Vera-Diaz, F. A., McGraw, P. V., Strang, N. C., & Whitaker, D., 2005, "A psychophysical investigation of ocular expansion in human eyes", *Invest Ophthalmol.Vis.Sci.*, vol. 46, no. 2, pp. 758-763.
- Vitale, S., Ellwein, L., Cotch, M. F., Ferris, F. L., III, & Sperduto, R. 2008, "Prevalence of refractive error in the United States, 1999-2004", *Arch.Ophthalmol.*, vol. 126, no. 8, pp. 1111-1119.
- Vitale, S., Sperduto, R. D., & Ferris, F. L., III 2009, "Prevalence of refractive error in the United States, 1999-2004", *Arch.Ophthalmol.*, vol. 127, no. 12, pp. 1632-1639.
- Wallman, J. & Winawer, J. 2004, "Homeostasis of eye growth and the question of myopia", *Neuron*, vol. 43, no. 4, pp. 447-468.
- Wani J. S., M. S, Nasti A.R.. 2005, *Automated Perimetry-- Interpreting the Data. JK-Practitioner* 2005, vol. 12, no. 4 pp.219-223.
- Weinreb, R. N. & Perlman, J. P. 1986, "The effect of refractive correction on automated perimetric thresholds", *Am.J.Ophthalmol.*, vol. 101, no. 6, pp. 706-709.
- Westall, C. A., Dhaliwal, H. S., Panton, C. M., Sigesmun, D., Levin, A. V., Nischal, K. K., & Heon, E. 2001, "Values of electroretinogram responses according to axial length", *Doc.Ophthalmol.*, vol. 102, no. 2, pp. 115-130.

- Westbrook C, Kaut C. 2003, "MRI in practice". Blackwell Publishing 2<sup>nd</sup> ed
- Williams, D. R. 1985, "Aliasing in human foveal vision", *Vision Res.*, vol. 25, no. 2, pp. 195-205.
- Wilson, S. E., Netto, M., & Ambrosio, R., Jr. 2003, "Corneal cells: chatty in development, homeostasis, wound healing, and disease", *Am J Ophthalmol*, vol. 136, no. 3, pp. 530-536.
- Wojciechowski, R., Congdon, N., Bowie, H., Munoz, B., Gilbert, D., & West, S. K. 2005, "Heritability of refractive error and familial aggregation of myopia in an elderly American population", *Invest Ophthalmol.Vis.Sci*, vol. 46, no. 5, pp. 1588-1592.
- Wolsley, C. J., Saunders, K. J., Silvestri, G., & Anderson, R. S. 2008, "Investigation of changes in the myopic retina using multifocal electroretinograms, optical coherence tomography and peripheral resolution acuity", *Vision Res.*, vol. 48, no. 14, pp. 1554-1561.
- Yap, M., Wu, M., Liu, Z. M., Lee, F. L., & Wang, S. H. 1993, "Role of Heredity in the Genesis of Myopia", *Ophthalmic and Physiological Optics*, vol. 13, no. 3, pp. 316-319.
- Yeung L., Hung P.T., Lin L.L., Yang C.H., Chiou G.C., 2001, "Effects of dopamine antagonists in human eye accommodation", *J Ocul Pharmacol Ther.*, vol. 17, no. 1, pp. 11-7.
- Young, T. L., Metlapally, R., & Shay, A. E. 2007, "Complex trait genetics of refractive error", *Archives of Ophthalmology*, vol. 125, no. 1, pp. 38-48.
- Young, T. 1801, "The Bakerian Lecture: on the mechanism of the eye", *Philos Trans Roy Soc Lond (Biol)*, vol. 91 no. 23 pp. 88.
- Young, W. O., Stewart, W. C., Hunt, H., & Crosswell, H. 1990, "Static threshold variability in the peripheral visual field in normal subjects", *Graefe's Archive for Clinical and Experimental Ophthalmology*, vol. 228, no. 5, pp. 454-457.
- Zadnik, K., Mutti, D. O., Friedman, N. E., Qualley, P. A., Jones, L. A., Qiu, P. H., Kim, H. S., Hsu, J. C., & Moeschberger, M. L. 1999, "Ocular predictors of the onset of juvenile myopia", *Invest Ophthalmol.Vis.Sci.*, vol. 40, no. 9, pp. 1936-1943.
- Zadnik, K., Satariano, W. A., Mutti, D. O., Sholtz, R. I., & Adams, A. J. 1994, "The Effect of Parental History of Myopia on Childrens Eye Size", *Jama-Journal of the American Medical Association*, vol. 271, no. 17, pp. 1323-1327.
- Zaidi, F. H., Hull, J. T., Peirson, S. N., Wulff, K., Aeschbach, D., Gooley, J. J., Brainard, G. C., Gregory-Evans, K., Rizzo, J. F., III, Czeisler, C. A., Foster, R. G., Moseley, M. J., & Lockley, S. W. 2007, "Short-wavelength light sensitivity of circadian, pupillary, and visual awareness in humans lacking an outer retina", *Curr.Biol.*, vol. 17, no. 24, pp. 2122-2128.
- Zhu, X., Liu, Y., & Wallman, J. 2005, "Glucagon increases choroidal thickness of chick eyes by acting on the retinal pigment epithelium", *Invest Ophthalmol.Vis.Sci*, vol. 46.

# MYOPIA: STRUCTURAL AND FUNCTIONAL CORRELATES

## APPENDICES

## LIST OF APPENDICES

APPENDIX 1: LIST OF ABBREVIATIONS	240
APPENDIX 2: STUDY ETHICAL CONSENT FORMS AND INFORMATION	241
APPENDIX 3: OCULAR HEALTH AND HISTORY QUESTIONNAIRE	274
APPENDIX 4: MRI DERIVED AXIAL LENGTHS AND VOLUMES	277
APPENDIX 5: QUADRANT DATA FOR MRI WORK	282
APPENDIX 6: LEFT PERIPHERAL REFRACTION DATA	295
APPENDIX 7: RIGHT PERIPHERAL REFRACTION AND RETFIT DATA	300
APPENDIX 8: VISUAL FIELDS	317
APPENDIX 9: MFERG RING CONFIGURATION RESPONSES	330
APPENDIX 10: GANGLION CELL DENSITY: DETECTION TASK DATA	340
APPENDIX 11: GANGLION CELL DENSITY: DIRECTION DISCRIMINATION TASK DATA	341

## APPENDIX 1: LIST OF ABBREVIATIONS

ACD: Anterior chamber depth

AL:CR: Axial Length : Corneal radius ratio

D: Dioptres

IN: Inferior-nasal

IT: Inferior-temporal

IV: Interval Variance

MfERG: Multifocal electroretinogram

MRI: Magnetic Resonance Imaging

MS: Maximum Sensitivity

MSE: Mean Spherical Error in D

SN: Superior-nasal

ST: Superior-temporal

TD: Total Deviation

VERIS: Visual Evoked Response Imaging System

XQ: Describes the superior, inferior, nasal, and temporal quadrant configuration

+Q: Describes the superior-nasal, superior-temporal, inferior-nasal, and inferior-temporal quadrant configuration

## APPENDIX 2: STUDY ETHICAL CONSENT FORMS AND INFORMATION

Ethical consent forms were prepared by Professor Bernard Gilmartin with my contribution being largely in the form of proofreading. The ethical form template was used by myself to draft the questionnaire ethics which were a later addition to the project, again with the guidance of Professor Bernard Gilmartin.

MEMORANDUM

REGISTRY & PLANNING SERVICES

DATE: 30 March 2007

TO: Professor Bernard Gilmartin,  
Life & Health Sciences

FROM: John Walter,  
Academic Registrar

SUBJECT: "Structural and functional correlates of eye globe conformation in  
adult human myopia" (07/1)

I am writing to inform you that a Sub-Group of the University's Ethics Committee has approved the above project proposals as amended in the light of the Sub-Group's comments.

The details of the investigation will be placed on file. You should notify me of any difficulties experienced by the volunteer subjects, and any significant changes which may be planned for this project in the future.

Best wishes,



Secretary to the Ethics Committee

**Figure 126 Scanned copy of Aston University project consent by the Ethics Committee**

Project Title:

Structural and functional correlates of eye globe conformation in adult human myopia.

Project Convener: Professor Bernard Gilmartin

## SUMMARY INFORMATION SHEET FOR RESEARCH PARTICIPANTS

### Invitation

You are being invited to take part in a research study. Before you decide it is important for you to understand why the research is being done and what it will involve. Please take time to read the following information carefully.

What is the purpose of the study?

We are using a variety of measurements on the eyes to study a wide range of eye conditions including long-sighted and short-sighted eyes (i.e. myopic eyes). Myopic eyes are out of focus for distance and we are especially interested in these eyes as myopia is becoming much more common in Europe and other parts of the world and it may be possible to treat myopia in the future with special types of eye drops or contact lenses.

Why have I been chosen?

You have been chosen to take part in this study because you have eyes that are a representative example of the range of eyes that occur in the normal population. You may also have been chosen because you have a high level of myopia or a big difference in myopia between the two eyes.

What measurements would you like to take?

The measurements we would like to take are divided into four separate sections:

- 1) Magnetic Resonance Imaging (MRI). MRI scans of different types of eyes are taken so that we can look at their shape in 3-dimensions. We are doing this to help us understand how the different dimensions of the eye can affect how well they focus at distance;
- 2) Multifocal electrophysiology (mfERG). mfERG measures how different eye shapes can affect how they function in terms of the variation in sensitivity of the light receptors at the back of the eye;
- 3) Measurements of retinal response using computer patterns. These measures how densely packed the cells are in the retina (i.e. ganglion cell density);

4) Standard instruments that measure various dimensions of the eye (called ocular biometry). These measurements are taken so that comparisons can be made with the measurements in 1), 2) and 3) above.

Do I have to agree to have all these measurements taken?

You do not have to agree to have all of the above four sets of measurements taken. You will be asked to agree to take part in each of the above studies separately and will be given for each study a set of further information on what the study involves together with separate consent forms for each study.

How long do these measurements take?

Not all of these measurements can be taken on the same day and are taken in different locations within Aston University. The list below will show you how much time is normally involved with each of the four studies, that is how much time you would need to put to one side if you agree to participate.

- 1) Magnetic Resonance Imaging (MRI): 60 minutes
  
- 2) Multifocal electrophysiology (mfERG): 90 minutes
  
- 3) Measurements of retinal response using computer patterns: 120 minutes
  
- 4) Standard instruments that measure eye dimensions: 180 minutes (total)

Parts 1) 2) and 3) of the study would normally take place on different days. There does not have to be a set time between measurements – the different measurements would be taken at a time that is convenient to you. Although there is no fixed time period for taking the measurements we would aim to take all of the above four sets of measurements within three months from the time you agreed to take part in all measurements.

For part 4) of the study nine different instruments are used and it takes around 20 minutes for each of the measurements to be taken. These measurements would not necessarily be taken all at the same time. Sometimes they will be taken before or after the measurements in 1) 2) and 3) above. You will be fully informed when this occurs and be given full details of what you have agreed to do.

Agreeing to have just some of the measurements taken does not mean you have agreed to have all the measurements taken. You will be able to say that you wish to stop the testing and leave at any time, without giving a reason. This would not

affect your relationship with the Staff or University in any way. No sanctions will be taken against any student of the University who refuses to participate in or withdraws from the study.

Expenses and payments:

Subjects will not receive financial re-imburement for taking part in the study.

Who is organising and funding the research?

The investigators involved in the study are listed below. All investigators apart from Professor Krish Singh are located in Aston University (School of Life and health Sciences, Birmingham B4 7ET) The telephone numbers are internal – for outside calls prefix the number with 0121 204. The PhD student involved in the project, Ms Manbir Nagra, is funded by a Research Scholarship from the College of Optometrists, London.

Investigator(s): Department/address: Telephone:

Prof. B. Gilmartin (convener) Life and Health Sciences 3881

Dr N. Logan Life and Health Sciences 4128

Prof. Paul Furlong Life and Health Sciences 4058

Professor Stephen Anderson Life and Health Sciences 3880

Dr R. Cubbidge Life and Health Sciences 4107

Dr M Conway Life and Health Sciences 4149

Ms M Nagra (PG student) Life and Health Sciences 12166

Prof. K.D. Singh Cardiff University (CUBRIC & Sch. of Psychology)

External collaborator (0)2920 874690 / 874007

Ms A Scott Chief Clinical Life and Health Sciences 4149

Physiologist mfERG

Ms Elizabeth Wilkinson Life and Health Sciences 3865

MRI Superintendent Radiographer

Who has reviewed the study?

The study described here has been approved by Aston University's Ethics Committee. The Committee has to be informed of, and approve, any changes to the study.

Who do I contact if something goes wrong or I need further information?

You should contact Professor Bernard Gilmartin, the convener of the project, if something goes wrong with any aspect of the project – [b.gilmartin@aston.ac.uk](mailto:b.gilmartin@aston.ac.uk) or telephone 0121 204 3881 or any of the project members listed above although, for this part of the main study, contact in the first instance should be made with any of those members highlighted in bold above.

Who do I contact if I wish to make a complaint about the way in which the research is conducted?

If you have any concerns about the way in which the study has been conducted, you should contact the Secretary of the University Research Ethics Committee at [j.g.walter@aston.ac.uk](mailto:j.g.walter@aston.ac.uk) or telephone 0121 2044665.

Project Title:

Structural and functional correlates of eye globe conformation in adult human myopia.

Project Convener: Professor Bernard Gilmartin

#### SCHEDULE OF DATA COLLECTION FOR A TYPICAL VOLUNTEER RESEARCH

#### PARTICIPANT

Not all of the measurements can be taken on the same day and are taken in different locations within Aston University. The time normally allocated to each of the four studies is detailed below, that is how much time a participant would need to put to one side if he/she agrees to participate.

Please refer to the separate experimental protocols for each of the studies detailed in Appendices B1, C1, D1 and E1 and to Appendix A2 which explains the schedule of measurements to the participant.

1) Magnetic Resonance Imaging (MRI): 60 minutes

2) Multifocal electrophysiology (mfERG): 90 minutes

3) Measurements of retinal response using computer patterns: 120 minutes

4) Standard instruments that measure eye dimensions: 180 minutes (total)

Parts 1) 2) and 3) of the study would normally take place on different days. There does not have to be a set time between measurements – the different measurements would be taken at a time that is convenient to the subject. Although there is no fixed time period for taking the measurements we would aim to take all of the above four sets of measurements within three months from the time the subject agrees to take part in all measurements.

For part 4) of the study nine different instruments are used and it takes around 20 minutes for each of the measurements to be taken. These measurements would not necessarily be taken all at the same time. Sometimes they will be taken before or after the measurements in 1) 2) and 3) above. The subject will be fully informed when this occurs and will be given full details of what they have agreed to do.

Project Title:

Structural and functional correlates of eye globe conformation in adult human myopia.

Project Convener: Professor Bernard Gilmartin

## EXPERIMENTAL PROTOCOL

Magnetic Resonance Imaging (MRI)

(to be read in conjunction with the Rules and Procedures document – pdf attached)

Scientific purpose of the study and potential benefits

It is known from conventional ultrasound and light scanning techniques of the eye that ocular biometry differs between individuals. However, both these methods are limited in how deeply they penetrate into the eye and are affected by the structures (such as the cornea and lens) which they have to pass through. Magnetic Resonance Imaging offers a non-invasive way of evaluating the accuracy of these techniques and a novel method of assessing in more detail the biometry of the eye. Our particular interest is in how the 3D shape of the eye differs in myopic (i.e. short-sighted) eyes compared to hyperopic (i.e. longsighted) eyes and eyes that do not need a refractive correction (i.e. emmetropic eyes). Understanding these differences will help to clarify further the developmental features of these conditions.

The research programme is unique in myopia research as it couples a new MRI technique (using the standard head coil attached to the 3-Tesla Magnetic Resonance Imaging system housed within the Aston Academy of Life Sciences) for the complete *in vivo* 3-D structural representation of the myopic eye with established multifocal electroretinography (mfERG; the VERIS system housed in the Vision Sciences Building). MRI data will provide a topography of retinal stretch over the posterior segment and mfERG data will assess

concomitantly the effect of ocular stretch on retinal function. The data are further complemented by a series of psychometric and biometric data to establish the most comprehensive data base on human adult myopia available to date.

The project wills novel foundations for the investigation:

- 1) the stratification and analysis of eye shape, volume and sphericity and how they contribute to identifying specific biometric parameters that predispose individuals subsequently to develop myopia;
- 2) the nature of asymmetry of ocular stretch and the effect of peripheral and central stretch on ocular aberrations, receptor orientation, image quality and the risk of pathology in high myopia;
- 3) the role of sagittal and tangential peripheral image shells in refractive development which an essential pre-requisite for the optimum design of optic appliances (e.g. specialist contact lenses) to be used in myopia treatment.

#### Selection and screening process

Participants will be recruited from the staff and student population of Aston University.

Participants will undergo a two-stage questionnaire screening process before they are scanned using the Magnetic Resonance Imaging (MRI) system (3-Tesla, housed in the Aston Academy of Life Sciences). The first-stage is carried out off site and is designed to ensure that unsuitable volunteers do not make a wasted trip to the scan suite. The second screening process occurs before the scan and is the final safety check before participants are admitted to the scanner (see screening forms in Appendix A3).

#### Scan sequence

After verbal briefing and paradigm training, participants will be admitted to the scan room, and placed on the MR scan bed. They will be given an alarm buzzer that can be pressed at any time and will summon the operator to remove them from the MR system. Ear-plugs and defenders will be used to guard against the noise generated by the MR system while it is

scanning, When they are in the scanner they can communicate with the operator using the built in intercom system, which is still audible to the participant even with the earplugs *in situ*. Once in the scanner, subjects will simply be asked to view a distant fixation spot for the duration of the scan.

A typical scan sequence will be:

Scan 1: Localiser scan (30 seconds).

Scan 2: Eye scan lasting 5-10 minutes.

The participant is in the scanner for no more than 15 minutes

Project Title:

Structural and functional correlates of eye globe conformation in adult human myopia.

Project Convener: Professor Bernard Gilmartin

MAGNETIC RESONANCE IMAGING (MRI)

INFORMATION SHEET FOR RESEARCH PARTICIPANTS

**Project title:** Eye shape and function in short-sighted people

Invitation

You are being invited to take part in a research study. Before you decide it is important for you to understand why the research is being done and what it will involve. Please take time to read the following information carefully.

What is the purpose of the study?

This study is part of a large study that is taking measurements of the eye using:

- 1) Magnetic Resonance Imaging (MRI). MRI scans of different types of eyes are taken so that we can look at their shape in 3-dimensions. We are doing this to help us understand how the different dimensions of the eye can affect how well they focus at distance;
- 2) Multifocal electrophysiology (mfERG). mfERG measures how different eye shapes can affect how they function in terms of the variation in sensitivity of the light receptors at the back of the eye;
- 3) Measurements of retinal response using computer patterns. This measure how densely packed the cells are in the retina (i.e. ganglion cell density);
- 4) Standard instruments that measure various dimensions of the eye (called ocular biometry). These measurements are taken so that comparisons can be made with the measurements in 1), 2) and 3) above.

This is part 1) of the study that takes MRI measurements.

We are using all of the measurements above to study a wide range of eyes including long-sighted and short-sighted eyes (i.e. myopic eyes). Myopic eyes are out of focus for distance and we are especially interested in these eyes as myopia is becoming much more common in Europe and other parts of the world and it may be possible to treat myopia with special types of eye drops or contact lenses.

Why have I been chosen?

You have been chosen to take part in this study because you have eyes that are a representative example of the range of eyes that occur in the normal population. You may also have been chosen because you have a high level of myopia or a big difference in myopia between the two eyes.

What will happen to me if I take part?

In this study you will be asked to have an MRI scan. All the scanning procedures used are standard procedures.

Before the scan

You will be asked to complete a questionnaire (the Initial Screening Form) which asks about various matters to determine whether it is safe for you to be scanned.

If you agree to participate you will be asked to sign the initial screening form that accompanies this information sheet in the presence of an appropriate member of staff (or other witness, who should countersign the form giving their name and address, if this is not practical). It is perfectly in order for you to take time to consider whether to participate, or discuss the study with other people, before signing. After signing, you will still have the right to withdraw at any time before or during the experiment, without giving a reason.

The study will not benefit you directly and does not form part of any medical diagnosis or treatment but you will be asked to give the name and address of your Family Doctor. This is because there is a very small chance that the scan could reveal something which requires investigation by a doctor. If that happened, we would contact your doctor directly. By signing the consent form, you authorise us to do this. We are also required to state that the information we report to your doctor may potentially have an impact on your eligibility for life insurance or private medical insurance. You will also be asked to complete a second, shorter, screening form immediately before the scan.

You are perfectly free to ask any questions about any aspect of the study or the scanning procedure before completing the initial screening form.

The scanning procedure

MRI is a method for producing non-invasive images of the internal structures of the body. It involves placing the participant inside a large, powerful magnet, which forms part of the brain scanner. Radiofrequency signals are also used as part of the imaging process. No ionizing radiation, such as X-rays, is used in MRI.

To be scanned, you will lie on your back on a narrow bed on runners, on which you will be moved until your head is inside the magnet. The scanning process itself creates intermittent loud noises and you must therefore wear ear-plugs or sound-attenuating headphones. We are able to talk to you while you are in the scanner through an intercom. If you are likely to become very uneasy in this relatively confined space (suffer from claustrophobia), you should NOT take part in the study. If you do take part and this happens, you will be able to alert the staff by activating an alarm and will then be removed from the scanner quickly. It is important that you keep your head as still as possible during the scan, and to help you with this, your head will be partially restrained with padded headrests. We shall ask you to relax your head and keep it still for the period of the scan. If this becomes unacceptably difficult or uncomfortable, you may demand to be removed from the scanner.

During the scan we will ask you to look through a mirror at a distant “spot” and to move your eyes as little as possible. The whole procedure will typically take about 15 minutes, plus another 15 minutes to discuss with you the purposes of the study and answer any questions about it which you may raise.

Are there any potential risks in taking part in the study?

As far as we know, this procedure poses no direct health risks. However, the Department of Health advises that certain people should NOT be scanned. Because the scanner magnet is very powerful, it can interfere with heart pacemakers and clips or other metal items which have been implanted into the body by a surgeon, or with body-piercing items. If you have had surgery which may have involved the use of metal items you should NOT take part. Note that only ferro-magnetic materials (e.g. steel) are likely to cause significant problems. Thus normal dental amalgam fillings do not prohibit you from being scanned, though a dental plate which contained metal would do so, and you would be asked to remove it. You will be asked to remove metal from your pockets (coins, keys), remove articles of clothing which have metal fasteners (belts, bras, etc), as well as most jewellery. Ideally, you should come for the scan in warm comfortable clothes that do not contain any metal – sweatshirt and jogging trousers are ideal. You can bring these and change in the MR suite as we have our own private changing room. Watches and credit cards should not be taken into the scanner since it can interfere with their operation.

Do I have to take part?

You will be able to say that you wish to stop the testing and leave at any time, without giving a reason. This would not affect your relationship with the Staff or University in any way. No sanctions will be taken against any student of the University who refuses to participate in or withdraws from the study.

Expenses and payments:

Subjects will not receive financial re-imburement for taking part in the study.

Will my taking part in this study be kept confidential?

The images of your body will be held securely and you will not be identified by name in any publications that might arise from the study. The information in the two screening forms will also be treated as strictly confidential and the forms will be held securely until eventually destroyed.

What will happen to the results of the research study?

The findings of the research will be submitted for publication in well-known scientific journals that are highly regarded for publishing the results of studies that have produced valuable results. It is hoped that we will be able to publish at least some of the results by the end of 2007. Your own results will not be identified in the publications. If you would like to see any of the published data then contact the project convener, Professor Bernard Gilmartin towards the end of 2007.

Who is organising and funding the research?

The investigators involved in the study are listed below. All investigators apart from Professor Krish Singh are located in Aston University (School of Life and Health Sciences, Birmingham B4 7ET) The telephone numbers are internal – for outside calls prefix the number with 0121 204. The PhD student involved in the project, Ms Manbir Nagra, is funded by a Research Scholarship from the College of Optometrists, London.

Investigator(s): Department/address: Telephone:

Prof. B. Gilmartin (convener) Life and Health Sciences 3881

Dr N. Logan Life and Health Sciences 4128

Prof. Paul Furlong Life and Health Sciences 4058

Professor Stephen Anderson Life and Health Sciences 3880

Dr M Conway Life and Health Sciences

Ms M Nagra (PG student) Life and Health Sciences 12166

Prof. K.D. Singh Cardiff University (CUBRIC & Sch. of Psychology)

External collaborator (0)2920 874690 / 874007

Ms A Scott Chief Clinical Life and Health Sciences 4149

Physiologist mfERG

Ms Elizabeth Wilkinson Life and Health Sciences

MRI Radiographer

Who has reviewed the study?

The study described here has been approved by Aston University's Ethics Committee. The Committee has to be informed of, and approve, any changes to the study.

Who do I contact if something goes wrong or I need further information?

You should contact Professor Bernard Gilmartin, the convener of the project, if something goes wrong with any aspect of the project – [b.gilmartin@aston.ac.uk](mailto:b.gilmartin@aston.ac.uk) or telephone 0121 204 3881 or any of the project members listed above although, for this part of the main study, contact in the first instance should be made with any of those members highlighted in bold above.

Who do I contact if I wish to make a complaint about the way in which the research is conducted?

If you have any concerns about the way in which the study has been conducted, you should contact the Secretary of the University Research Ethics Committee at [j.g.walter@aston.ac.uk](mailto:j.g.walter@aston.ac.uk) or telephone 0121 2044665.

Pages 257, 258, 259 and 260 have been removed for copyright restrictions.

Project Title:

Structural and functional correlates of eye globe conformation in adult human myopia.

Project Convener: Professor Bernard Gilmartin

## EXPERIMENTAL PROTOCOL

Questionnaire

Scientific purpose of the study and potential benefits

It is known from conventional ultrasound and light scanning techniques of the eye that ocular biometry differs between individuals. However, both these methods are limited in how deeply they penetrate into the eye and are affected by the structures (such as the cornea and lens) which they have to pass through. Magnetic Resonance Imaging offers a non-invasive way of evaluating the accuracy of these techniques and a novel method of assessing in more detail the biometry of the eye. Our particular interest is in how the 3D shape of the eye differs in myopic (i.e. short-sighted) eyes compared to hyperopic (i.e. longsighted) eyes and eyes that do not need a refractive correction (i.e. emmetropic eyes). Understanding these differences will help to clarify further the developmental features of these conditions.

The research programme is unique in myopia research as it couples a new MRI technique (using the standard head coil attached to the 3-Tesla Magnetic Resonance Imaging system housed within the Aston Academy of Life Sciences) for the complete *in vivo* 3-D structural representation of the myopic eye with established multifocal electroretinography (mfERG; the VERIS system housed in the Vision Sciences Building). MRI data will provide a topography of retinal stretch over the posterior segment and mfERG data will assess concomitantly the effect of ocular stretch on retinal function. The data are further complemented by a series of psychometric and biometric data to establish the most comprehensive data base on human adult myopia available to date.

The project will provide novel foundations for the investigation:

- 1) the stratification and analysis of eye shape, volume and sphericity and how they contribute to identifying specific biometric parameters that predispose individuals subsequently to develop myopia;

2) the nature of asymmetry of ocular stretch and the effect of peripheral and central stretch on ocular aberrations, receptor orientation, image quality and the risk of pathology in high myopia;

3) the role of sagittal and tangential peripheral image shells in refractive development which an essential pre-requisite for the optimum design of optic appliances (e.g. specialist contact lenses) to be used in myopia treatment.

Selection and screening process

Participants will be recruited from the staff and student population of Aston University.

There are no known risks to this procedure. The procedure is widely used in research.

Questionnaire procedure

The questionnaire will be given to each subject to complete in their own time. It should take approx. 15-20 mins.

Project Title:

Structural and functional correlates of eye globe conformation in adult human myopia.

Project Convener: Professor Bernard Gilmartin

Questionnaire

## INFORMATION SHEET FOR RESEARCH PARTICIPANTS

**Project title:** Eye shape and function in short-sighted people

### Invitation

You are being invited to take part in a research study. Before you decide it is important for you to understand why the research is being done and what it will involve. Please take time to read the following information carefully.

What is the purpose of the study?

This study is part of a large study that is taking measurements of the eye using:

- 1) Magnetic Resonance Imaging (MRI). MRI scans of different types of eyes are taken so that we can look at their shape in 3-dimensions. We are doing this to help us understand how the different dimensions of the eye can affect how well they focus at distance;
- 2) Multifocal electrophysiology (mfERG). mfERG measures how different eye shapes can affect how they function in terms of the variation in sensitivity of the light receptors at the back of the eye;
- 3) Measurements of retinal response using computer patterns. This measures how densely packed the cells are in the retina (i.e. ganglion cell density);
- 4) Standard instruments that measure various dimensions of the eye (called ocular biometry). These measurements are taken so that comparisons can be made with the measurements in 1), 2) and 3) above.
- 5) Questionnaire, this is to obtain information about you're the type of eye correction you are currently using and how you use it. Questions will also be asked how much you read, your hobbies and whether members of your family have their vision corrected.

This is part 5) of the study which concerns the questionnaire.

We are using all of the measurements above to study a wide range of eyes including long-sighted and short-sighted eyes (i.e. myopic eyes). Myopic eyes are out of focus for distance and we are especially interested in these eyes as myopia is becoming much more common in Europe and other parts of the world and it may be possible to treat myopia with special types of eye drops or contact lenses.

Why have I been chosen?

You have been chosen to take part in this study because you have eyes that are a representative example of the range of eyes that occur in the normal population. You may also have been chosen because you have a high level of myopia or a big difference in myopia between the two eyes.

What will happen to me if I take part?

Before completing the questionnaire

If you agree to participate you will be asked to sign a consent form that accompanies this information sheet, in the presence of an appropriate member of staff. It is perfectly in order for you to take time to consider whether to participate, or discuss the study with other people, before signing. After signing, you will still have the right to withdraw at any time before or during the experiment, without giving a reason.

The study will not benefit you directly and does not form part of any medical diagnosis or treatment but you will be asked to give the name and address of your Family Doctor. This is because there is a very small chance that you may mention something in your answers that could reveal something requiring investigation by a doctor. If that happened, we would contact your doctor directly. By signing the consent form, you authorise us to do this. We are also required to state that the information we report to your doctor may potentially have an impact on your eligibility for life insurance or private medical insurance.

You are perfectly free to ask any questions about any aspect of the study or the scanning procedure before completing the initial screening form.

You will be asked to complete a short questionnaire

Are there any potential risks in taking part in the study?

There are no known risks to this procedure.

Do I have to take part?

You will be able to say that you wish to stop or refuse to answer some questions and leave at any time, without giving a reason. This would not affect your relationship with the Staff or University in any way. No sanctions will be taken against any student of the University who refuses to participate in or withdraws from the study.

Expenses and payments:

Subjects will not receive financial re-imburement for taking part in the study.

Will my taking part in this study be kept confidential?

The information we collect will be held securely until eventually destroyed and you will not be identified by name in any publications that might arise from the study.

What will happen to the results of the research study?

The findings of the research will be submitted for publication in well-known scientific journals that are highly regarded for publishing the results of studies that have produced valuable results. It is hoped that we will be able to publish at least some of the results by the end of 2007. Your own results will not be identified in the publications. If you would like to see any of the published data then contact the project convener, Professor Bernard Gilmartin towards the end of 2007.

Who is organising and funding the research?

The investigators involved in the study are listed below. All investigators apart from Professor Krish Singh are located in Aston University (School of Life and health Sciences, Birmingham B4 7ET) The telephone numbers are internal – for outside calls prefix the number with 0121 204. The PhD student involved in the project, Ms Manbir Nagra, is funded by a Research Scholarship from the College of Optometrists, London.

Investigator(s): Department/address: Telephone:

Prof. B. Gilmartin (convener) Life and Health Sciences 3881

Dr N. Logan Life and Health Sciences 4128

Prof. Paul Furlong Life and Health Sciences 4058

Professor Stephen Anderson Life and Health Sciences 3880

Dr M Conway Life and Health Sciences 3881

Ms M Nagra (PG student) Life and Health Sciences 12166

Prof. K.D. Singh Cardiff University (CUBRIC & Sch. of Psychology)

External collaborator (0)2920 874690 / 874007

Ms A Scott Chief Clinical Life and Health Sciences 4149

Physiologist mfERG

Ms Elizabeth Wilkinson Life and Health Sciences 3881

MRI Radiographer

Who has reviewed the study?

The study described here has been approved by Aston University's Ethics Committee. The Committee has to be informed of, and approve, any changes to the study.

Who do I contact if something goes wrong or I need further information?

You should contact Professor Bernard Gilmartin, the convener of the project, if something goes wrong with any aspect of the project – [b.gilmartin@aston.ac.uk](mailto:b.gilmartin@aston.ac.uk) or telephone 0121 204 3881 or any of the project members listed above although, for this part of the main study, contact in the first instance should be made with any of those members highlighted in bold above.

Who do I contact if I wish to make a complaint about the way in which the research is conducted?

If you have any concerns about the way in which the study has been conducted, you should contact the Secretary of the University Research Ethics Committee at [j.g.walter@aston.ac.uk](mailto:j.g.walter@aston.ac.uk) or telephone 0121 2044665.

Project Title:

Structural and functional correlates of eye globe conformation in adult human myopia.

Project Convener: Professor Bernard Gilmartin

### QUESTIONNAIRE

This questionnaire forms part of a study examining the shape of your eye, any glasses or contact lens prescription you may have and the functional ability of your eye.

All the data will be confidential. The information we collect will be held securely until eventually destroyed and you will not be identified by name in any publications that might arise from the study.

The first part of the questionnaire asks about any glasses or contact lenses you may wear now or you may have worn in the past

Do you wear glasses or contact lenses?

- Glasses only please go to question 2
- Contact lenses only please go to question 3
- Both please answer all questions ignoring any instructions to skip questions
- Neither please go to question 4

What do you wear your glasses for?

- Reading (close work)
- Distance (driving/TV)
- Reading and distance only
- All the time

Please go to question 5

What do you wear your contact lenses for?

- For seeing at distance
- For seeing at distance and near
- For cosmetic purposes only e.g. coloured contact lenses

Please answer question 4

In the past have you ever worn glasses?

- Yes please answer questions 6 and 7
- No please answer question 8
- Was advised to but didn't wear *please go to question 6*

How often do you wear your glasses

.....Hours/days per week

Please go to question 7

How often do you wear your contact lenses?

.....Hours per day/days per week

Please answer question 8

How old were you when you were advised to first wear glasses?

.....

If exact age unknown please give approx by ticking one of the following:

- Less than 5 years
- 5-10 yrs
- 10-15 yrs
- 15-20 yrs

20+

What were these glasses for?

Reading close work

Distance

All the time

Continue to question 8

What was your initial prescription? If unsure please give approximate

Right Eye.....

Left Eye.....

This should be in your original optician records [please give approx if unsure]

Continue to question 9 if glasses worn in past

Continue to question 10 if contact lenses worn not glasses

Please answer question 13 if neither worn

How old were you when you actually started wearing glasses?

.....

If exact age unknown please give approx by ticking one of the following:

Less than 5 years

5-10 yrs

10-15 yrs

15-20 yrs

20+

Please answer question 11

How old were you when you actually started wearing contact lenses?

10-15 yrs

15-20 yrs

20+

Proceed to question 12

At any point did you stop wearing glasses? Please state when and reasons why

.....  
.....

Proceed to question 13

At any point did you stop wearing contact lenses? Please state when and reasons why

.....  
.....

When was your last eye test?

Never had one

More than 2 years ago

1-2 years

6months- 1 year

Less than 6 months

Unknown

What is your current prescription?

(Even if you do not wear glasses you should have a prescription given to you following your eye test this should have the prescription written on)

Right Eye.....

Left Eye.....

How long is it since you have had your prescription changed?

Approx no. of years.....

This part asks about any problems you may have or had in the past with your eyes as this may explain any differences in the test results of your eyes

Do you have any special eye conditions not related to glasses or contact lenses?

Yes

No

If yes please state...

Have you had any previous surgery or medical treatment of the eyes? (e.g. laser, exercises, eye drops)

Yes

No

If yes please state reason and type of treatment

This next part asks about eye and general health of your family, this can be important especially where eye conditions are passed down in the family

Does anyone in the immediate family wear glasses?

Yes

No

If yes please state who wears glasses and what they wear them for e.g. 'father wears for driving only' (If possible please give approx. prescription for glasses)

.....  
.....

Do you suffer from any general health disorders?

Yes

No

If yes please state...

Are there any inherited disorders in the family?

Yes

No

If yes please state.....

This next part asks about lifestyle and ethnicity. Both of these factors can affect your eyes

Do you have any particular hobbies or interests that require a lot of close work? E.g. sewing, crosswords, studying

How much time on average do you spend each day doing close work such as reading?

How much time on average do you spend each day at a VDU?

How much time do you spend outdoors each day?

On average how many pieces of fruit and veg do you consume on a daily basis?

Do you take any special vitamins or supplements that are not prescribed by your GP?

Which best describes your ethnicity?

White

Indian

Pakistani

Bangladeshi

Black African

Black Caribbean

Chinese

Japanese

Other please give details.....

THANK YOU FOR TAKING TIME TO COMPLETE THIS QUESTIONNAIRE

IF YOU WISH TO COMMENT ON THE QUESTIONNAIRE PLEASE DO SO  
BELOW.....

## APPENDIX 3: OCULAR HEALTH AND HISTORY QUESTIONNAIRE

### **Methods**

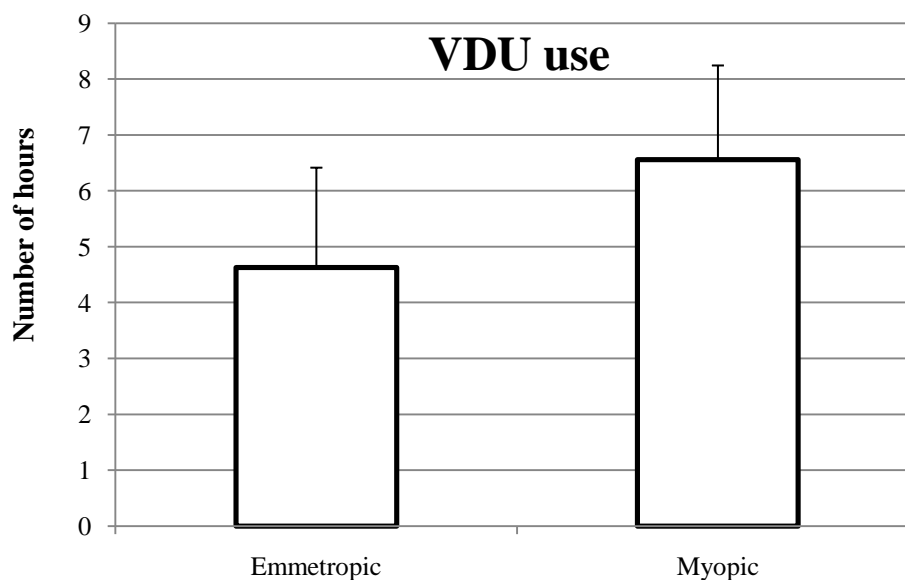
In order to gain further information about the daily visual activities of the subjects who'd undergone MR scanning, questionnaires were circulated to all subjects. The questionnaire sought information on the visual activities of subjects, in particular the levels of near and VDU work. Subjects were also asked questions regarding ocular history, refractive corrections and family ocular health and history.

Copies of questionnaires were circulated via email along with the consent and information forms. Following a poor response; questionnaires were recirculated to all subjects. The final response was 23 subjects, (this excludes myopes  $>-15D$ ).

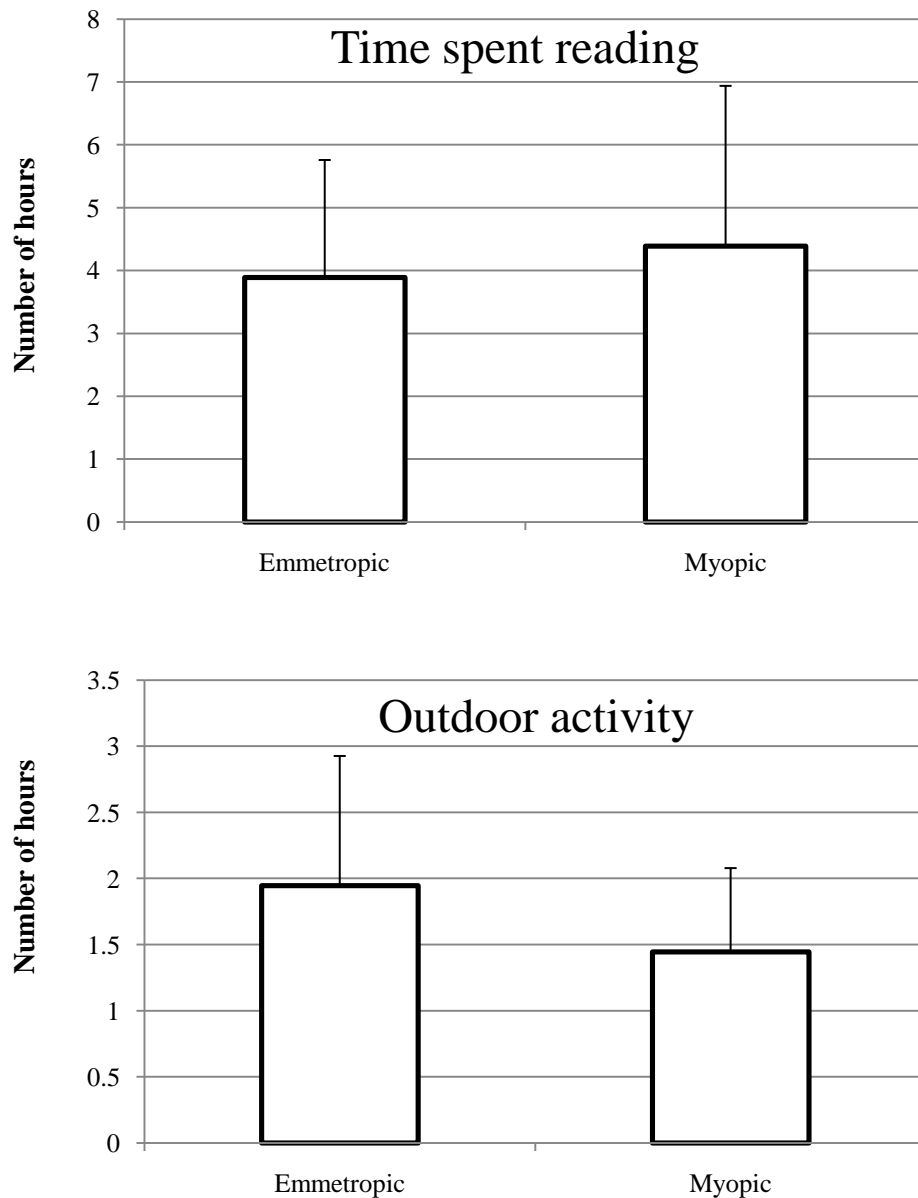
Due to the low numbers of subjects responding to the questionnaire full analysis was not carried out for factors such as family history *vs.* level of myopia. Responses for near, VDU and outdoor activity were correlated with refractive error.

### **Results**

Results showed that myopic subjects spent longer periods of time using a VDU on a daily basis compared to emmetropes. The results did not, however, show that VDU usage was related to the magnitude of refractive error.



In addition to spending longer periods of time using a VDU, myopic subjects were found to spend longer reading than emmetropic subjects. The time spent reading varied with refractive group, but not with the magnitude of refractive error. Furthermore, myopic subjects were found to spend less time outdoors than their emmetropic counterparts.



### **Discussion and Conclusions**

Near work and VDU usage have long been implicated in the development of myopia. The amount of time spent outdoors has also recently become a subject of much interest with the publication of reports suggesting that number of hours spent outdoors is directly related to

less myopia (Rose et al. 2008). The production of hormones, for which sunlight is essential, are believed to be involved in myopic inhibition.

The findings presented by the current study are limited largely by number of participants, however, the results do concur with previous literature suggesting that myopic individuals spend less time outdoors and more time carrying out near tasks compared to emmetropic individuals.

The principal factor in reducing myopia progression through outdoor activity has been identified as the production of hormones such as dopamine, serotonin and melatonin. The production of serotonin and melatonin is regulated by the pineal gland located in the central region of the brain. The pineal gland is often referred to as the 'third eye', as much of its input is derived from the ocular photoreceptors in the retina. The retina possesses two main types of photoreceptor: rod cells and cone cells. In an outdoors environment the cone cells are likely to be of more importance as the pupil is more miosed and cone cells, which are more centrally located on the retina, are required to see. Previous work investigating the pineal gland with reference to form deprivation myopia has noted diurnal variations to the response elicited by image degradation.

In summary, the very limited data collected as part of this study has shown a strong link between close work and myopia. It would be of great value to have questionnaire responses from all subjects who underwent the ocular MRI.

APPENDIX 4: MRI DERIVED AXIAL LENGTHS AND VOLUMES

(RIGHT EYES)

*IOLMaster* measurements of axial length (AL), keratometry (K) and anterior chamber depth (ACD).

Right eye data

R AL MRI	R MSE	R Total Vol	R Post Vol	R Ant Vol	R AL IOL	R ACD IOL	R AL MRI - IOL	RE K	AXIS	RE K	AXIS
28.73	-10.56	11777	10646	1131	28.12	3.71	0.61	8.2	38	7.99	128
26.62	-10.55	8908	7791	1117	26.29	3.63	0.33	7.46	20	7.28	110
25.67	-9.995	7934	7027	907	25.08		0.59	7	173	6.89	83
29.7	-9.245	10013	9033	980	27.51	3.32	2.19	8.06	3	7.71	93
26.64	-9.055	8484	7553	931	25.87	3.81	0.77	7.5	172	7.36	82
26.77	-9	9188	8028	1160	27.3	3.73	-0.53				
27.13	-8.87	9533	8345	1188	26.48	3.66	0.65	7.71	46	7.62	136
25.96	-8.62	9258	7882	1376	26.64	4.01	-0.68	7.62	4	7.5	94
27.69	-8.5	9554	8625	929	26.68	3.83	1.01	7.9	176	7.61	86
26.15	-8.347	8055	7074	981	25.88	3.94	0.27	7.4	104	7.25	14
25.67	-7.12	9815	8603	1212	26.22	3.59	-0.55	7.65	128	7.59	98
28.57	-7	10745	9739	1006	27.99	3.51	0.58	8.3	17	8.12	107
26.76	-6.805	9684	8606	1078	25.72	4.39	1.04	7.47	120	7.36	90
25.68	-6.68	7562	6563	999	25.16	3.31	0.52	7.5	138	7.44	48
26.61	-6.625	10291	9081	1210	26.84	3.69	-0.23	7.99	2	7.86	92
24.63	-6.625	7721	6588	1133	25.02	3.57	-0.39	7.68	177	7.47	87
25.65	-6.55	8480	7464	1016	26.14	3.60	-0.49	7.97	178	7.85	88
25.62	-6.435	8577	7600	977	25.23	4.03	0.39	7.35	6	7.15	96
26.27	-5.75	8818	7846	972	25.81	3.15	0.46	7.53	110	7.45	20
26.62	-5.55	8419	7320	1099	25.84	3.92	0.78	7.66	171	7.58	81
25.62	-5.5	9445	8313	1132	25.77	4.07	-0.15	7.76	9	7.59	99
25.33	-5.245	8029	7220	809	25.22	3.87	0.12	7.56	2	7.39	92
26.66	-4.75	8314	7047	1267	25.94	4.02	0.72				
25.74	-3.81	8014	6905	1109	24.49	3.34	1.25	7.65	10	7.13	100
26.64	-3.75	10932	9643	1289	26.35	3.9	0.29	8.32	7	8.03	97
24.74	-3.24	8528	7395	1133	25.38	3.95	-0.64	7.76	83	7.71	173
24.62	-3.183	7362	6212	1150	24.28	3.59	0.34	7.69	170	7.46	80
26.71	-3.125	8950	7986	964	25.72	3.95	0.99	7.92	151	7.84	61
24.45	-3	6724	5637	1087	23.33	3.87	1.12	7.27	1	7	91
25.67	-3	7958	6889	1069	25.3	3.7	0.37	7.89	178	7.84	88
26.65	-2.5	8918	7783	1135							
24.77	-2.31	8086	6672	1414	24.84	3.91	-0.07	7.62	27	7.49	117
23.81	-2.055	7213	6046	1167	24.41	3.27	-0.6	7.93	4	7.68	94
23.11	-1.68	7262	6329	933	23.58	3.83	-0.47	7.82	128	7.53	38
25.68	-1.555	7936	6891	1045	24.55	3.84	1.13	8.01		7.91	
24.49	-1.31	7857	6928	929	23.72	2.67	0.77	7.64	22	7.44	112
24.6	-0.87	7836	6926	910	23.19	3.61	1.41	7.69	178	7.52	88
24.72	-0.81	7521	6888	633	24.15	3.48	0.57	8.11	5	8.01	95
23.64	-0.75	7645	6580	1065	23.49	3.46	0.15	7.79	20	7.64	110
23.17	-0.75	7493	6526	967	23.17		0				

23.66	-0.68	7625	6364	1261	23.41	3.31	0.25	8.05	177	7.82	87
24.04	-0.5	7657	6413	1244	23.9	3.76	0.14	7.76	4	7.58	94
24.78	-0.435	7955	6603	1352	23.54	3.69	1.24	7.61	88	7.51	178
23.69	-0.31	7479	6376	1103	22.63	3.48	1.06	7.72	1	7.49	91
24.14	-0.3	7134	6032	1102	23.86	3.66	0.28	8.07		7.9	
25.64	-0.245	8361	7018	1343	24.39	3.7	1.25	8	4	7.92	94
22.96	-0.185	7670	6480	1190	22.96	3.32	0	7.93	116	7.86	26
24.04	-0.18	6845	5898	947	23.22	3.562	0.82	7.83	8	7.69	98
25.65	-0.12	7708	6393	1315	24.21	3.68	1.44	8.1	161	8.04	161
25.68	-0.06	8307	7241	1066	23.54	3.56	2.14	7.93	129	7.87	39
23.64	-0.06	7194	6079	1115	23.75	3.34	-0.11	7.77	2	7.57	92
25.65	-0.005	9285	8209	1076	24.64	3.68	1.01	8.14	177	7.9	87
23.61	0	8021	6989	1032							
23.25	0	8658	7236	1422	24.09	3.04	-0.84	8.01	16	7.82	106
25.67	0.12	9052	7972	1080	25.26	3.17	0.41	8.48	162	8.27	72
24.71	0.173	8337	7171	1167	24.43	3.57	0.28	8.2		8.05	
23.68	0.19	6909	5747	1162	23.22	3.09	0.46	8.06	28	7.98	118
25.67	0.19	8478	7432	1046	23.56	3.09	2.11	8.42	170	8.22	80
24.7	0.245	7995	6841	1154	23.53	3.53	1.17	7.72	1	7.49	91
24.62	0.25	8464	7313	1151	24.34	3.53	0.28	7.99	83	7.92	173
23.61	0.37	7738	6513	1225	23.27	3.13	0.34	7.88	135	7.8	45
22.65	0.435	6598	5547	1051	22.44	3.32	0.21	7.5	2	7.24	92
23.73	0.5	7268	6222	1046	23.4	3.48	0.33	7.97	10	7.85	100
23.78	0.5	8293	7202	1091	23.81	3.68	-0.03	8.06	172	7.87	82
23.62	0.56	7318	6126	1192	22.85	3.362	0.77	7.72	102	7.7	12
24.6	1.185	7780	6666	1114	22.83	3.16	1.77	7.94	171	7.87	81
21.6	1.495	6615	5525	1090	21.72	3.5	-0.12	7.88	2	7.54	92
24.63	1.56	7445	6232	1213	23.47	3.59	1.16	7.72	135	7.69	45
22.85	2.685	7661	6612	1049	22.89	3.26	-0.04	8.5	14	8.02	104
22.9	3.25	6584	5455	1129	22.59	3.54	0.31	7.86	5	7.77	95
21.6	3.815	6895	5830	1065	22.22	3.31	-0.62	8	12	7.44	102
21.65	4.375	5036	4017	1019	21.75	3.47	-0.1	7.65	136	7.57	46
20.91	9.5	5586	4510	1076	20.32	3.38	0.59				

Radius band averages for each refractive group

EMM: Emmetropes

LM: Low Myopes

HM: High Myopes

HYP: Hyperopes

SD: Standard Deviation

<b>Dist along geometric axis (%)</b>	<b>EMM</b>	<b>EMM SD</b>	<b>LM</b>	<b>LM SD</b>	<b>HM</b>	<b>HM SD</b>	<b>HYP</b>	<b>HYP SD</b>
<b>1</b>	8.123	0.688	7.958	0.710	7.545	0.596	8.341	1.637
<b>2</b>	16.041	1.397	16.024	1.485	15.202	1.340	16.025	2.253
<b>3</b>	15.748	1.929	16.093	1.510	15.127	1.716	15.890	1.801
<b>4</b>	15.990	2.577	16.337	1.886	14.722	2.232	15.828	2.051
<b>5</b>	16.057	3.435	16.509	2.846	14.422	4.048	15.350	3.880
<b>6</b>	15.569	5.128	15.302	3.880	12.609	4.633	14.791	6.069
<b>7</b>	12.531	5.641	15.316	4.233	12.414	5.471	14.939	6.198
<b>8</b>	12.521	5.689	14.994	4.848	12.691	6.137	15.339	6.635
<b>9</b>	11.870	4.717	14.978	5.898	12.364	5.935	14.792	6.067
<b>10</b>	12.031	4.613	14.711	4.511	11.413	3.885	14.520	5.796
<b>11</b>	11.753	3.049	13.366	3.290	11.141	2.494	13.502	5.929
<b>12</b>	11.907	1.692	12.326	1.718	11.623	2.109	10.829	2.215
<b>13</b>	12.257	1.237	12.431	1.187	12.039	1.592	11.055	1.666
<b>14</b>	12.662	1.099	12.811	1.214	12.731	1.339	11.393	1.542
<b>15</b>	13.092	0.918	12.965	1.170	13.042	0.916	12.015	1.062
<b>16</b>	13.363	0.948	13.072	0.757	13.439	0.846	12.380	1.386
<b>17</b>	13.297	0.703	12.995	0.701	13.557	0.908	12.193	1.216
<b>18</b>	13.333	0.860	13.158	0.702	13.673	0.759	12.378	1.349
<b>19</b>	13.384	0.721	13.204	0.669	13.648	0.871	12.550	1.208
<b>20</b>	13.509	0.721	13.300	0.594	13.511	0.771	12.789	1.176
<b>21</b>	13.450	0.614	13.273	0.595	13.532	0.889	12.692	1.116
<b>22</b>	13.245	0.693	13.334	0.516	13.483	0.829	12.973	1.309

23	13.344	0.661	13.258	0.527	13.453	0.787	13.027	0.951
24	13.302	0.616	13.115	0.603	13.490	0.962	12.699	1.131
25	13.287	0.626	13.218	0.554	13.286	0.852	12.619	0.961
26	13.148	0.554	13.271	0.481	13.149	0.689	12.707	0.773
27	13.216	0.522	13.264	0.551	13.337	0.850	12.946	0.774
28	13.182	0.637	12.956	0.712	13.298	0.895	12.352	0.773
29	13.140	0.561	13.160	0.551	13.276	0.942	12.539	0.803
30	13.045	0.557	13.225	0.516	13.263	0.822	12.359	1.036
31	13.093	0.453	12.984	0.606	13.184	0.681	12.556	0.753
32	13.138	0.600	13.146	0.533	13.309	0.893	12.155	0.734
33	13.080	0.719	13.191	0.487	13.282	0.948	12.369	0.830
34	12.916	0.584	13.035	0.505	13.526	0.801	12.206	0.815
35	13.113	0.551	13.192	0.424	13.229	0.751	12.415	0.713
36	13.039	0.617	13.020	0.559	13.192	0.732	12.057	0.884
37	13.033	0.754	13.152	0.531	13.438	0.796	12.170	0.800
38	12.926	0.663	13.057	0.557	13.530	0.752	12.592	1.092
39	13.154	0.576	13.055	0.581	13.500	0.870	12.001	0.586
40	13.104	0.629	13.149	0.630	13.373	0.734	12.201	1.066
41	12.900	0.601	13.201	0.662	13.384	0.818	12.564	1.016
42	13.062	0.715	12.904	0.562	13.460	0.728	11.803	0.612
43	13.155	0.487	13.116	0.439	13.431	0.989	12.506	0.892
44	12.985	0.564	13.032	0.813	13.429	0.767	12.347	0.741
45	12.972	0.692	13.143	0.723	13.605	0.746	11.873	0.824
46	13.130	0.520	13.105	0.526	13.259	0.855	12.399	0.869
47	13.008	0.504	13.080	0.604	13.366	0.956	12.104	0.805
48	12.944	0.540	12.980	0.456	13.438	0.834	12.033	0.739
49	13.024	0.417	13.113	0.632	13.650	0.739	12.364	0.883
50	13.046	0.534	13.065	0.560	13.283	0.729	12.186	0.944
51	12.937	0.703	13.100	0.428	13.237	1.127	12.165	0.642
52	12.974	0.430	13.094	0.511	13.608	0.779	12.201	0.874
53	13.104	0.458	12.929	0.801	13.526	0.641	12.002	0.656
54	12.995	0.641	13.178	0.410	13.324	0.704	12.313	0.718
55	12.903	0.493	13.064	0.367	13.394	1.120	12.234	0.783
56	12.982	0.461	12.972	0.764	13.375	0.791	12.049	0.997
57	13.197	0.593	13.183	0.751	13.605	0.734	12.159	0.631

<b>58</b>	12.902	0.611	13.039	0.373	13.315	0.737	12.488	0.926
<b>59</b>	12.908	0.564	13.002	0.651	13.429	1.016	12.050	0.693
<b>60</b>	13.160	0.604	13.108	0.667	13.401	0.688	11.833	0.679
<b>61</b>	12.941	0.601	13.198	0.488	13.400	0.702	12.666	0.970
<b>62</b>	12.895	0.660	13.005	0.623	13.506	0.910	12.197	0.953
<b>63</b>	13.097	0.496	13.154	0.637	13.166	0.918	12.244	0.859
<b>64</b>	13.109	0.620	13.110	0.461	13.701	0.667	12.163	0.961
<b>65</b>	12.919	0.516	13.058	0.489	13.189	0.579	12.160	0.818
<b>66</b>	12.943	0.532	13.167	0.691	13.497	0.882	12.597	1.079
<b>67</b>	13.149	0.553	13.160	0.465	13.439	0.937	12.093	1.034
<b>68</b>	12.990	0.470	13.055	0.635	13.377	0.748	12.110	0.793
<b>69</b>	13.028	0.534	13.203	0.658	13.394	0.752	12.356	0.800
<b>70</b>	13.174	0.568	13.133	0.477	13.214	0.681	12.378	0.773
<b>71</b>	13.096	0.601	13.150	0.663	13.482	0.769	12.441	0.833
<b>72</b>	13.158	0.516	13.274	0.751	13.437	0.906	12.160	0.695
<b>73</b>	13.147	0.777	13.228	0.407	13.302	0.818	12.415	0.619
<b>74</b>	13.167	0.457	13.258	0.533	13.398	0.707	12.715	1.146
<b>75</b>	13.171	0.585	13.213	0.513	13.482	0.750	12.360	0.836
<b>76</b>	13.160	0.575	13.401	0.615	13.374	0.754	12.475	0.769
<b>77</b>	13.339	0.564	13.172	0.571	13.257	1.005	12.754	0.880
<b>78</b>	13.179	0.551	13.397	0.373	13.451	0.859	12.691	0.743
<b>79</b>	13.360	0.614	13.325	0.634	13.334	0.860	12.448	0.637
<b>80</b>	13.432	0.580	13.398	0.638	13.243	0.827	12.513	0.820
<b>81</b>	13.379	0.514	13.512	0.519	13.222	0.929	12.668	0.618
<b>82</b>	13.489	0.624	13.520	0.659	13.401	0.962	12.783	0.759
<b>83</b>	13.476	0.683	13.586	0.590	13.329	0.804	12.859	0.817
<b>84</b>	13.662	0.634	13.506	0.668	13.428	1.041	12.826	0.664
<b>85</b>	13.644	0.590	13.619	0.703	13.427	1.027	12.814	0.648
<b>86</b>	13.658	0.675	13.676	0.724	13.318	1.127	13.190	0.856
<b>87</b>	13.820	0.689	13.769	0.936	13.403	1.087	13.042	0.981
<b>88</b>	13.924	0.675	13.693	0.951	13.367	1.201	13.044	0.939
<b>89</b>	13.967	0.732	13.639	1.014	13.291	1.213	13.409	0.989
<b>90</b>	13.998	0.679	13.683	1.145	13.197	1.185	13.355	0.651
<b>91</b>	14.057	0.879	13.697	1.336	13.217	1.330	13.663	1.289

APPENDIX 5: QUADRANT DATA FOR MRI WORK

The pages that follow provide various parameters for both XQ and +Q. The table below outlines the data provided for each set of quadrants

MSE	X <sup>2</sup> Post 25%	X <sup>2</sup> 25-75	X <sup>2</sup> 25-75	IV Post 25%	IV NASAL 25-75	IV TEMP 25-75	Ratio MAX NT Dist:AL	Mean Post Volume	Mean Axial Length
Mean Sph Error	X <sup>2</sup> coefficient of the second order polynomial curve fitted to data comprising the posterior 25% of the eye	X <sup>2</sup> coefficient of the second order polynomial curve fitted to data comprising the region 25-75% for a particular quadrant	X <sup>2</sup> coefficient of the second order polynomial curve fitted to data comprising the region 25-75% for a particular quadrant	Interval Variance for the data comprising the posterior 25%	Interval Variance for the data comprising the posterior 25% for a particular quadrant	Interval Variance for the data comprising the posterior 25% for a particular quadrant	The ratio between the maximum distances of two parallel quadrants	The mean volume of the posterior 25% of the eye in mm <sup>3</sup>	The mean axial length of the two corresponding quadrants

NASAL-TEMPORAL QUADRANT DATA

MSE	X^2 Post 25%	X^2 NASAL 25-75	X^2 TEMP 25-75	IV Post 25%	IV NASAL 25-75	IV TEMP 25-75	Ratio MAX NT Dist:AL	Mean Post Volume	Mean Axial Length
-10.56	-0.0382	-0.0355	0.0311	6.550214061	1.017000102	1.035565102	1.063288133	1954.473606	27.57697588
-10.555	-0.055	-0.0399	0.0382	5.221370344	0.997084097	1.045796015	0.960608753	1245.113054	26.4110575
-9.995	-0.0582	-0.0356	0.0407	5.370571971	0.92934619	1.282087798	0.960734886	1087.61731	25.39215735
-9.245	-0.0538	-0.0332	0.0386	5.313963754	1.019177441	1.186803833	0.931321622	1532.75652	28.9819616
-9.055	-0.0561	-0.0391	0.0404	5.066020037	1.001759781	1.206774848	0.937107014	1213.635977	26.33453805
-9	-0.0509	-0.04	0.0458	5.386507893	1.045711087	1.348732936	0.997856332	1382.473106	26.77239905
-8.87	-0.0484	-0.036	0.0384	5.56326608	0.986234326	1.196912891	0.997109511	1491.692501	27.11829538
-8.62	-0.0455	-0.0363	0.0378	5.727914909	0.872267812	1.097907912	1.009724523	1444.193808	25.8713142
-8.5	-0.0515	-0.0344	0.0441	5.558711213	0.929034146	1.542703863	0.938289495	143.6286976	27.44885788
-8.347	-0.0521	-0.0421	0.047	5.209295959	0.961180097	1.232310873	0.982202369	1221.778608	25.4633285
-7.12	-0.0458	-0.0417	0.0373	5.573012947	0.957788128	0.96034608	1.039179761	1431.062105	25.83818674
-7	-0.0453	-0.0402	0.0503	5.804556666	1.152583872	1.579369372	1.01011167	1704.243664	28.04238825
-6.805	-0.0419	-0.0511	0.0448	6.027823824	1.401075669	1.392970028	1.0511904	1610.813872	26.21982235
-6.68	-0.0571	-0.0382	0.0477	4.923698161	0.876902552	1.051663982	0.946995844	1113.119265	25.44420914
-6.625	-0.0507	-0.0388	0.0349	5.530258188	1.078573039	0.963188896	1.023307259	1341.340185	26.31924945
-6.625	-0.0575	9.4569	0.0444	4.804890961	0.998866665	0.974696491	1.01008123	1007.308287	24.28931005
-6.55	-0.0499	-0.0373	0.0375	5.400457345	0.955841974	1.003815235	0.993595646	1368.965429	26.3782856
-6.435	-0.0463	-0.0402	0.0432	16.33378095	0.98842505	1.066672065	1.006243989	1410.731587	25.7936465
-5.75	-0.0453	-0.0378	0.0422	5.655597367	0.911647275	1.020281935	1.045085826	1387.338773	25.301159
-5.55	-0.0484	-0.0376	0.0428	5.308229868	0.946007633	1.200225338	0.982458043	1383.001058	26.1116304
-5.5	-0.0464	-0.0423	0.0427	5.55157812	1.090905432	1.001961915	1.051818185	1356.413646	25.3194996
-5.245	-0.0508	-0.0406	0.0331	5.299620199	0.953803244	1.097891169	0.988693241	1236.339795	25.29302849
-4.75	-0.0563	-0.0435	0.043	5.153052477	1.106074031	1.296196489	0.962426893	1220.716888	26.45828722

-3.81	-0.0456	-0.0433	0.0504	5.594099547	0.926366945	1.441840564	1.055083607	1279.246612	24.3758412
-3.75	-0.0396	-0.0391	0.0414	6.136918551	0.980081377	1.389299226	1.080072116	1708.19224	26.24919675
-3.24	-0.0458	-0.0418	0.0481	5.488888001	0.903932504	1.45919926	1.035520371	1278.318415	24.4203742
-3.183	-0.0493	-0.0437	0.0366	5.133601854	0.947890763	1.188606881	1.003124811	1179.727997	24.3396571
-3.125	-0.0478	-0.041	0.0479	5.537569899	1.016857119	1.185377409	1.052994151	1319.912242	25.3505
-3	-0.0542	-0.0558	0.0522	4.852704587	1.110952452	1.209062418	1.015538573	1006.933611	23.5776282
-3	-0.0544	-0.0409	0.0393	5.227989991	1.092280004	0.99045647	0.995449986	1155.448446	25.3031616
-2.5	-0.0495	-0.0375	0.0443	5.501279088	0.979268736	1.183481887	0.98178588	1380.031879	26.37832482
-2.31	-0.0496	-0.0479	0.0477	5.337513011	1.03830064	1.241324753	1.020195983	1212.3146	24.7484816
-2.055	-0.0552	-0.0424	0.0454	4.877452912	1.008157619	0.919602233	1.03292767	972.9840347	23.38958137
-1.68	-0.0466	-0.0429	0.0471	5.136978483	0.805753085	1.116397061	1.063015638	1124.918621	23.10753205
-1.555	-0.0428	-0.0436	0.0392	5.891771468	0.94775476	1.359021027	1.080125525	1356.879441	24.3216239
-1.31	-0.0408	-0.0515	0.048	6.043241148	1.499773317	1.562808895	1.076445516	1591.210923	25.71544299
-0.87	-0.0461	-0.0522	0.0479	5.323877608	1.205124193	1.020265343	1.052985692	1234.592257	24.07754981
-0.81	-0.051	-0.0364	0.0505	5.101653316	1.049461073	1.100042062	1.049976763	1132.56144	24.25582365
-0.75	-0.0421	-0.0525	0.0477	5.837992506	1.049079845	1.476957764	1.108500197	1280.093606	23.42944305
-0.75	-0.0478	-0.0488	0.0443	5.326304336	1.003723393	1.011111617	1.065548483	1132.113098	23.47788163
-0.68	-0.0501	-0.0461	0.0533	5.119672984	0.927784393	1.053093567	1.051551165	1070.117757	23.36870795
-0.5	-0.0488	-0.0377	0.0395	5.308970933	0.824669201	0.795274685	1.03504409	1115.212018	23.54445729
-0.435	-0.0458	-0.0418	0.0481	5.510223155	0.903932504	0.912820735	1.034097293	1278.318415	24.4203742
-0.31	-0.0462	-0.0469	0.0503	5.36042028	0.931269526	1.148641098	1.075536258	1161.895049	23.38322945
-0.3	-0.0456	-0.0636	0.0449	5.37577299	1.366800999	1.003552383	1.087831983	1268.216017	24.27052055
-0.245	-0.045	-0.0378	0.0429	5.748370356	0.924901	1.384572398	1.011369348	1404.691979	25.37446305
-0.185	-0.0467	-0.0476	0.0463	5.539188634	0.935543526	1.305173633	1.083033475	1142.239572	23.309722
-0.18	-0.0434	-0.0339	0.0422	5.439852059	0.65927463	0.996322894	1.070667299	1170.353051	22.74591246
-0.12	-0.0477	-0.0388	0.052	5.170920823	0.896911692	1.151195577	1.048651587	1181.751002	23.9619541
-0.06	-0.0452	-0.0512	0.0443	5.614016136	1.133176415	1.249814614	1.057427539	1320.513147	24.6570227

-0.06	-0.0478	-0.0442	0.0499	5.229505922	0.866322812	1.179901301	1.042800986	1117.974097	23.33081295
-0.005	-0.0439	-0.0436	0.0459	5.756091331	1.012946477	1.283128489	1.066475197	1433.795999	25.32071675
0	-0.0459	-0.0468	0.0434	5.613321524	0.924239309	1.309847725	1.074867226	1165.217596	23.34048697
0	-0.0449	-0.0428	0.0542	5.515077068	1.064109881	1.106054522	1.124413678	1194.894092	23.37695443
0.12	-0.0471	-0.0427	0.0509	5.541756461	0.987529514	1.180273223	1.076882999	1231.235077	24.3041813
0.173	-0.0442	-0.0389	0.0483	5.488228847	0.871199015	1.223420621	1.099078661	1213.284285	23.37181681
0.19	-0.0478	-0.0381	0.0517	5.121678515	0.809891045	0.978840403	1.08587397	1023.887113	22.32749699
0.19	-0.0483	-0.0503	0.0473	5.46783049	1.127860217	1.233602139	1.030664229	1280.929975	25.1036177
0.245	-0.0497	-0.0417	0.044	5.300097245	0.90799174	1.094561554	1.016864333	1186.317976	24.50635965
0.25	-0.048	-0.0498	0.0449	5.554786418	1.067728463	1.206482349	1.055759978	1216.636972	24.38940338
0.37	-0.0451	-0.0404	0.0492	5.718817255	0.807918278	1.218784223	1.090163353	1185.518883	23.33686757
0.435	-0.0513	-0.0517	0.0504	5.136670643	0.933229281	1.237473655	1.062512261	958.487195	22.379578
0.5	-0.0463	-0.0468	0.0457	5.455364194	0.954176215	1.220497577	1.048648905	1191.484975	23.7047202
0.5	-0.0486	-0.0407	0.0511	5.047003132	0.880511877	1.09635495	1.048626157	1154.73626	23.90889965
0.56	-0.0467	-0.0404	0.0366	5.51184983	0.895780162	1.075634717	1.090148269	1097.120923	22.84471487
1.185	-0.0549	-0.0381	0.0484	4.981538357	0.912036915	1.269666264	1.025759568	1055.512364	24.29505505
1.495	-0.048	-0.0491	0.0526	5.158669421	0.945784849	1.061936408	1.115436897	919.8334292	21.20680612
1.56	-0.0497	-0.0476	0.0471	5.265260714	1.093691446	1.463149196	0.996144419	1217.442991	24.82576065
2.685	-0.0401	-0.0554	-0.0484	16.12934613	1.086827985	1.226800968	1.162538818	1237.867232	22.4858481
3.25	-0.0472	-0.0512	-0.0558	5.315615113	0.994136868	1.343890365	1.051166847	1093.892643	22.93286967
3.815	-0.0452	-0.0547	0.0564	5.422559999	1.043876474	1.167450364	1.156578443	987.7923435	21.3256412
4.375	-0.0563	-0.0505	0.0456	4.697622601	0.840206901	1.044453561	0.995873851	813.1174053	21.59388971
9.5	-0.0548	-0.0623	0.0566	4.716019543	1.357063036	4.987715491	1.098837639	766.0415561	20.67837929

SUPERIOR-INFERIOR QUADRANT DATA

MSE	X^2 Post 25%	X^2 SUP 25-75	X^2 INF 25-75	IV Post 25%	IV SUP 25-75	IV INF 25-75	Ratio MAX SI Dist:AL	Posterior 25% Vol	Mean Axial Length
-10.56	-0.0438	-0.0348	0.0289	6.18937828	1.132587517	0.948517767	1.064964546	1695.158975	27.50060985
-10.555	-0.047	-0.0444	0.0364	5.5882157	1.149548037	1.131253109	0.995449461	1453.926191	26.38275605
-9.995	-0.0481	-0.0428	0.0368	5.734519913	1.32476912	0.958445821	1.022683074	1273.939098	24.9831344
-9.245	-0.059	-0.0383	0.0376	5.062183006	1.209516796	1.137648898	0.887933922	1413.762295	29.14836881
-9.055	-0.0505	-0.0459	0.0444	5.596163954	1.280129565	1.247238466	0.987690822	1350.573123	26.35753509
-9	-0.0563	-0.0424	0.0455	5.179297109	1.128491394	1.154003933	0.972598427	1251.274622	26.78740035
-8.87	-0.0494	-0.0393	0.0373	5.48132114	1.224121803	0.989006991	0.998451339	1449.891679	27.01041805
-8.62	-0.0496	-0.0411	0.089	5.493286845	1.059186127	0.955575902	0.846681164	1323.798981	25.8613929
-8.5	-0.0468	-0.0453	0.0397	5.425288668	1.491973759	1.032590876	0.995030743	1572.651742	27.38036665
-8.347	-0.0557	-0.0488	0.0502	5.047543227	1.176014525	1.168868061	0.974139778	1144.991163	25.4875868
-7.12	-0.0451	-0.0413	0.0383	5.60762112	0.976614701	0.971843004	1.050210207	1432.518486	25.65301655
-7	-0.0491	-0.0454	0.0459	5.657332197	1.382141324	1.344094584	0.983679164	1579.516445	28.10624805
-6.805	-0.0434	-0.0479	0.046	5.774766223	1.294041215	1.29896106	1.032713215	1558.00086	26.24392356
-6.68	-0.0589	-0.0448	0.0464	4.835816793	1.036115405	1.0844057	0.950173402	1073.101927	25.37337205
-6.625	-0.048	-0.0423	0.0398	5.504981274	1.157520283	1.035839259	1.046496878	1416.645564	26.31790255
-6.625	-0.0554	-0.0488	0.0408	4.855555057	1.089442457	0.988575482	1.019586387	1046.221121	24.29778455
-6.55	-0.05	-0.0386	0.0415	5.388832141	1.047283234	1.084939526	1.004333471	1365.244715	26.3687964
-6.435	-0.049	-0.042	0.0453	5.439220811	1.115533394	1.220755269	0.998124733	1317.179623	25.64015195
-5.75	-0.0439	-0.0462	0.0448	5.63337695	1.085338594	1.170373871	1.0751082	1430.500088	25.29159725
-5.55	-0.05	-0.0441	0.0401	5.327827457	1.168702411	1.067764693	0.970427422	1350.167915	26.222793
-5.5	-0.0441	-0.0439	0.042	5.753655304	1.155903482	0.980094184	1.063305507	1423.05031	25.28305065
-5.245	-0.0476	-0.0426	0.0438	5.508128673	1.185540707	1.027667346	1.017229609	1320.173276	25.29991125
-4.75	-0.0555	-0.0479	0.0401	5.095530283	1.267044408	1.129525766	0.955448335	1234.593697	26.41852535
-3.81	-0.0483	-0.0469	0.0456	5.455554596	1.201917661	1.016438673	1.048606654	1207.916293	24.37766125

-3.75	-0.0442	-0.0418	0.0409	5.830012869	1.077071845	0.996893995	1.060429186	1509.567889	26.06978875
-3.24	-0.0439	-0.0456	0.051	5.712040891	1.252376592	1.180189279	1.053093236	1345.722067	24.53070331
-3.183	-0.0496	-0.0464	0.0507	5.085460775	1.036925399	1.112862923	1.030880527	1163.699507	24.24718445
-3.125	-0.0502	-0.0408	0.0444	5.262459648	0.970839105	1.09832483	1.024541227	1255.366063	25.33594475
-3	-0.051	-0.0548	0.0523	5.133114605	1.227326315	1.148288798	1.027596475	1077.865313	23.66286843
-3	-0.0471	-0.0393	0.0402	5.447599487	1.028551511	0.939495741	1.023456235	1334.714037	25.3048997
-2.5	-0.0508	-0.042	0.0383	5.226452281	1.062164987	0.905112438	0.989126724	1337.394703	26.3064175
-2.31	-0.0476	-0.0443	0.056	5.521178257	1.12363291	1.228707412	1.055636218	1274.520354	24.85861435
-2.055	-0.0539	-0.0386	0.0419	4.812756275	0.76372326	0.835858814	1.040550596	977.4436343	23.1654263
-1.68	-0.0433	-0.0548	0.0507	5.475057979	1.124051085	1.046188086	1.091668377	1231.836226	23.30883067
-1.555	-0.0438	-0.0444	0.049	5.855974056	1.256584197	1.110742284	1.082188736	1326.281991	24.32512297
-1.31	-0.0448	-0.0461	0.0519	5.741427166	1.497408781	1.442604519	1.028333032	1446.739703	25.69415028
-0.87	-0.0418	-0.057	0.0575	5.588070092	1.605627142	1.209450681	1.111610395	1335.819268	23.84855365
-0.81	-0.0499	-0.0506	0.0434	5.235681641	1.120894755	1.170699043	1.064124177	1154.212007	24.22105855
-0.75	-0.0455	-0.0427	0.0522	5.516193071	1.016468484	1.218743245	1.059812758	1185.280584	23.4377726
-0.75	-0.0464	-0.0491	0.0437	5.108491568	1.097198016	0.929516836	1.0768077	1158.526298	23.3997917
-0.68	-0.0447	-0.0484	0.0528	5.574884461	1.052407279	1.295215432	1.092161517	1203.939021	23.4129458
-0.5	-0.0475	-0.0463	0.0453	5.310106929	0.997464963	0.907774964	1.067773196	1143.128371	23.51767365
-0.435	-0.0444	-0.0456	0.051	5.741385717	1.252376592	1.180189279	1.053763952	1330.567539	24.53070331
-0.31	-0.0458	-0.0522	0.0408	5.517168605	1.190760927	0.864124422	1.062619208	1178.860255	23.45113975
-0.3	-0.0455	-0.0455	0.0507	5.396924859	1.040153853	1.103498686	1.051570117	1283.856481	24.39293115
-0.245	-0.0478	-0.0402	0.0372	5.534520765	1.064067931	0.976583171	0.986187814	1320.412378	25.3553024
-0.185	-0.0458	-0.0518	0.0421	5.665784396	1.37965268	0.875793541	1.090144274	1165.112138	23.31399265
-0.18	-0.0406	-0.0489	0.0428	5.662937883	0.951697365	0.780961599	1.156149948	1222.482251	22.4845578
-0.12	-0.0473	-0.053	0.0494	5.239980072	1.156150303	1.085294428	1.064276596	1201.882005	24.06365207
-0.06	-0.0432	-0.0479	0.054	5.710688223	1.192949427	1.251964188	1.061710112	1385.823114	24.6942492
-0.06	-0.0451	-0.0508	0.0608	5.369125605	1.046399236	1.227455515	1.085026516	1177.338528	23.2562133

-0.005	-0.0421	-0.049	0.048	5.991530138	1.309383968	1.205404546	1.075655815	1500.229253	25.36412679
0	-0.0445	-0.0502	0.0557	5.624675982	1.375098891	1.163218879	1.106271076	1202.336457	23.34495635
0	-0.0472	-0.0474	0.0453	4.936053384	1.099670112	0.890398781	1.133488647	1127.421195	23.2816711
0.12	-0.0425	-0.0471	0.054	5.793954995	1.199539021	1.176003709	1.132839829	1364.491279	24.30411995
0.173	-0.0431	-0.0461	0.0511	5.329584232	1.015369739	1.47943599	1.123072204	1244.492395	23.37409535
0.19	-0.0501	-0.0533	0.0488	4.721666002	1.009701024	0.859819311	1.120212588	959.9643482	22.13331515
0.19	-0.0431	-0.0486	0.051	5.636023124	1.180984892	1.231586649	1.059633367	1438.650951	25.13138402
0.245	-0.0462	-0.0455	0.0473	5.450170644	1.029926999	1.032209286	1.061219514	1268.628275	24.43364355
0.25	-0.0431	-0.0442	0.0485	5.807480037	1.118969829	1.134225411	1.078680546	1351.368628	24.3571014
0.37	-0.0491	-0.0474	0.0474	5.307622629	1.025250105	0.979109345	1.064138469	1090.190451	23.35027425
0.435	-0.0452	-0.0531	0.0512	5.491804635	1.180789158	0.995616329	1.104484784	1093.143983	22.434064
0.5	-0.0478	-0.0444	0.0401	5.395095005	1.088157413	0.912844892	1.016282462	1154.195566	23.7057501
0.5	-0.042	-0.0495	0.0465	5.297522277	1.035796084	1.381606462	1.139385582	1314.183943	23.71115865
0.56	-0.0395	-0.0506	0.0453	5.548834222	1.163812546	1.076438709	1.152591511	1271.433921	22.6175468
1.185	-0.0591	-0.0471	0.0412	4.760533953	1.248714094	0.990031784	1.015258726	980.829785	24.29912393
1.495	-0.0442	-0.0558	0.0438	5.142831495	2.198017263	2.233250869	1.163502053	1007.194079	21.2945158
1.56	-0.0482	-0.0506	0.0479	5.318154944	1.386478243	1.146378899	1.001738142	1253.76122	24.8102413
2.685	-0.0448	-0.0557	-0.0549	5.448122262	1.155848993	1.01786485	1.116060521	1120.697693	22.61430779
3.25	-0.0492	-0.0555	0.0522	4.845816916	1.250154335	1.078092971	1.044531019	1041.470342	22.84578355
3.815	-0.0448	-0.0564	0.0363	5.396280591	1.030435941	0.689610167	1.157561519	996.0648241	21.319787
4.375	-0.0515	-0.0527	0.0491	4.715486958	1.057115909	0.9579836	1.030304885	882.1330372	21.5115008
9.5	-0.049	-0.0524	0.0563	4.601325628	1.896587161	2.515601567	1.130528969	838.5197058	20.4576022

SUPERIOR-TEMPORAL AND INFERIOR-NASAL QUADRANT DATA

MSE	X^2 Post 25%	X^2 SUP TEMP 25-75	X^2 INF NASAL 25- 75	IV Post 25%	IV IN 25-75	IV ST 25-75	Ratio MAX ST-IN Dist:AL	Mean Post Volume	Mean Axial Length
-10.56	-0.0402	-0.0357	0.0358	6.183303688	1.076447456	1.015446558	1.053169612	1867.862122	27.65575295
-10.555	-0.051	-0.0405	0.038	5.371023074	1.075421583	0.969601631	0.975149187	1341.140579	26.39503805
-9.995	-0.0483	-0.00456	0.0371	5.640603802	5.732493216	0.977001272	0.993380693	1312.190959	25.408097
-9.245	-0.0527	-0.0407	0.0353	5.315069165	1.235320746	1.109562574	0.927202928	1565.983417	28.99338615
-9.055	-0.0525	-0.0434	0.0386	5.40046625	1.243806444	1.055228705	0.96697587	1297.091947	26.33692615
-9	-0.0517	-0.0437	0.0392	5.444247413	1.212339924	1.087257959	0.990431892	1361.548928	26.77700197
-8.87	-0.0478	-0.0433	0.039	5.834329743	1.289651006	1.064331725	1.030003155	1490.205698	26.93624856
-8.62	-0.0448	-0.0398	0.0365	5.775079867	1.040205063	0.890011891	1.022248109	1467.822447	25.8806883
-8.5	-0.048	-0.0462	0.032	5.687786845	1.645180249	0.939951737	0.960841175	1535.783406	27.4022142
-8.347	-0.0536	-0.0525	0.0477	5.10166257	1.254765004	1.055586844	0.980610642	1187.77231	25.4653146
-7.12	-0.0461	-0.0365	0.039	5.590480139	0.868538173	0.952922331	1.045538814	1411.090977	25.7411546
-7	-0.0478	-0.0488	0.0389	5.705821227	1.534153759	1.27534768	1.001309863	1612.239093	28.0174577
-6.805	-0.0426	-0.047	0.0517	5.877585306	1.372659159	1.394790689	1.05573966	1581.847323	26.19914595
-6.68	-0.0571	-0.0438	0.0423	5.062882288	1.115123987	0.982399667	0.950327235	1110.292353	25.41187915
-6.625	-0.0494	-0.0378	0.0353	5.539520247	0.985323274	0.970371345	1.037483658	1376.929344	26.3220285
-6.625	-0.0557	-0.0456	0.0387	4.962004395	0.98988519	0.979829828	1.011911518	1041.401896	24.30730624
-6.55	-0.0496	-0.0525	0.0477	5.515930427	1.003263547	0.936099874	1.001518862	1377.544802	26.38115207
-6.435	-0.0472	-0.0448	0.0411	5.614064271	1.343853722	1.016534938	1.002549927	1377.695233	25.73639005
-5.75	-0.0443	-0.0441	0.0377	5.715986011	1.044228066	0.889064745	1.060565321	1419.652929	25.31005025
-5.55	-0.0484	-0.0483	0.0373	5.209179938	1.17411994	0.876696656	1.015207866	1322.793445	25.5369338
-5.5	-0.0466	-0.0458	0.043	5.476695962	1.084508395	1.029168754	1.04866393	1348.8415	25.3030848
-5.245	-0.0467	-0.0342	0.0396	5.520673408	1.234472614	0.955896719	0.995158618	1404.777192	25.85009936
-4.75	-0.0552	-0.0477	0.0419	5.186749345	1.279647255	1.077457133	0.969566209	1244.389393	26.4513439

-3.81	-0.0445	-0.0535	0.0426	5.371237251	1.107518675	0.94829885	1.098896503	1240.060199	23.70835615
-3.75	-0.0448	-0.0406	0.0384	6.028859791	1.106999489	0.959801253	1.077949309	1498.756425	26.1519808
-3.24	-0.0468	-0.0473	0.0423	5.310551367	1.064901152	0.936987137	1.065643043	1273.133143	24.6354155
-3.183	-0.0493	-0.0451	0.043	5.168199655	1.082359879	0.949332193	1.008337615	1182.756311	24.37087654
-3.125	-0.0494	-0.0427	0.0522	5.399666806	0.957005852	1.238730616	1.039125452	1298.158043	25.35023395
-3	-0.0518	-0.0508	0.0529	5.052371064	1.350594504	1.079008925	1.005136976	1074.327029	23.808563
-3	-0.0486	-0.0361	0.0361	5.263919544	0.850638814	0.930804798	1.022288539	1252.454316	24.8999878
-2.5	-0.049	-0.0525	0.0477	5.230621593	0.978873047	0.755079164	1.054189011	1216.926275	24.6450797
-2.31	-0.0478	-0.0454	0.0515	5.516158884	1.193310202	1.135664968	1.047658381	1266.616768	24.8334248
-2.055	-0.055	-0.0427	0.0358	4.874748375	0.888521929	1.020988094	1.034000058	962.6902126	23.22333975
-1.68	-0.0439	-0.0268	-0.026	5.564239386	0.961494538	0.857281011	1.102076246	1202.126612	23.185017
-1.555	-0.0405	-0.0479	0.0418	5.617074659	1.18362505	0.911676552	1.11062513	1421.013851	24.21178005
-1.31	-0.0426	-0.0532	0.0541	5.551301315	1.27785663	1.239892401	1.090518847	1378.380764	24.45622685
-0.87	-0.0432	-0.0509	0.05	5.548236063	1.146720177	1.113300971	1.137446294	1166.099446	22.65216523
-0.81	-0.0502	-0.0482	0.0402	5.273621372	1.133884882	1.135023304	1.045105394	1173.610391	24.4970554
-0.75	-0.0419	-0.0435	0.0486	5.788175309	1.010730294	0.988622833	1.138953656	1165.648381	22.3044155
-0.75	-0.0462	-0.044	0.0461	5.39447911	0.941118903	0.93437042	1.076328605	1169.40154	23.4586422
-0.68	-0.05	-0.048	0.0466	5.153515055	1.09431824	0.959913624	1.048075571	1072.824247	23.37487759
-0.5	-0.0467	-0.0381	0.0365	5.108386373	0.777537397	0.777209956	1.054038145	1154.187471	23.43131545
-0.435	-0.044	-0.044	-0.046	5.624274334	1.354984346	1.332089887	1.048901045	1337.662787	24.48497776
-0.31	-0.0441	-0.0534	0.0411	5.669389487	1.234235639	0.837761859	1.082765111	1223.731197	23.44565464
-0.3	-0.0421	-0.0444	0.0563	5.465821043	1.051729675	1.226717652	1.090915968	1311.266002	23.713
-0.245	-0.0453	-0.0406	0.0361	5.669660285	1.203617425	0.883644828	1.003855986	1392.755953	25.35050793
-0.185	-0.0452	-0.0498	0.0443	5.705089725	1.378841913	0.888533741	1.097592945	1181.150332	23.3196409
-0.18	-0.0407	-0.0491	0.0378	16.29596869	1.020942068	0.737512991	1.130073124	1221.915039	22.50700785
-0.12	-0.0477	-0.0526	0.0438	5.251491177	1.122035491	1.044977203	1.061824132	1189.091079	24.036255
-0.06	-0.0443	-0.044	0.0523	5.722887155	1.21619745	1.151692133	1.055653144	1352.434099	24.70358438

-0.06	-0.0469	-0.0497	0.048	5.39156866	1.105305381	0.947127891	1.062384312	1137.404717	23.31009195
-0.005	-0.0437	-0.046	0.0451	5.850877591	1.32233049	5.334730107	1.069210311	1441.062943	25.3269123
0	-0.051	-0.0525	0.0477	5.755495645	1.339516588	1.059670706	1.113039675	1049.86345	23.35347695
0	-0.0465	-0.0503	0.0427	5.304835032	1.043351728	0.944575134	1.124746051	1148.844536	23.32690715
0.12	-0.0442	-0.0477	0.0454	5.793036588	1.302939979	1.127549527	1.088870427	1373.658586	24.86855723
0.173	-0.045	-0.0488	0.037	5.495821579	1.186924165	0.869613107	1.074304162	1263.766959	24.0679892
0.19	-0.0483	-0.0526	0.0438	5.148193722	0.960215869	0.853110582	1.114679973	1002.961231	22.21343345
0.19	-0.0456	-0.0458	0.0487	5.614717256	1.170908501	1.100285186	1.043859223	1353.561775	25.07387836
0.245	-0.0464	-0.0492	0.0427	6.274518331	1.136597022	0.946825032	1.054346042	1267.224049	24.4729175
0.25	-0.0443	-0.0451	0.0519	5.823372512	1.123785233	1.136192785	1.082258313	1317.795222	24.3851752
0.37	-0.0462	-0.0494	0.0394	5.562288661	1.16664094	0.802518695	1.078706287	1156.99779	23.33389855
0.435	-0.0484	-0.048	0.051	5.374383709	1.222402892	0.933459119	1.08304423	1017.186478	22.39355392
0.5	-0.047	-0.0445	0.0429	5.518351828	1.171044225	0.901445209	1.033876451	1176.451986	23.7320954
0.5	-0.045	-0.0482	0.0397	5.534240177	1.088220971	0.850497863	1.092370026	1240.287746	23.8433644
0.56	-0.0412	-0.0508	0.0533	5.715358355	1.161409991	1.008299776	1.144871571	1231.733486	22.7356322
1.185	-0.0546	-0.0514	0.0378	4.999930269	1.150892413	0.945882668	1.048719919	1061.561933	24.2979169
1.495	-0.0468	-0.0574	0.0455	14.6674168	1.046581413	0.900767738	1.141281771	948.1175747	21.2595505
1.56	-0.0485	-0.0505	0.0466	5.389060769	1.461579971	1.09389114	1.012213967	1253.442721	24.8841705
2.685	-0.0434	-0.0508	0.0541	5.550782124	1.102016139	1.022353289	1.121215303	1157.418643	22.61987258
3.25	-0.0471	-0.0549	0.0501	5.301912236	1.353962391	0.986328704	1.052436508	1095.675258	22.92722188
3.815	-0.0442	-0.0579	0.0441	5.497102819	1.095494956	0.801112319	1.166227547	1010.241031	21.32670144
4.375	-0.0536	-0.0497	0.0503	4.85257909	1.105060665	0.855874715	1.018046112	853.0720115	21.58118533
9.5	-0.0498	-0.0549	0.057	5.233622274	1.221448512	1.380260454	1.139416744	840.6459261	20.65005823

SUPERIOR-NASAL AND INFERIOR TEMPORAL QUADRANT DATA

MSE	X <sup>2</sup> Post 25%	X <sup>2</sup> SUPNASAL 25-75	X <sup>2</sup> INF TEMP 25-75	IV Post SN- IT 25%	IV SN 25-75	IV IT 25-75	Ratio MAX SN-IT Dist:AL	Posterior 25% Vol	Mean Axial Length
-10.56	-0.0404	-0.0367	0.0366	6.21275594	1.036404164	1.05064957	1.05915771	1877.253397	27.79407243
-10.555	-0.0503	-0.0436	0.0375	5.43220893	1.156149111	1.13865022	0.980318855	1359.314887	26.3902851
-9.995	-0.0511	-0.0426	0.0411	17.0456762	1.154312064	1.20144439	0.971431184	1239.516521	25.4001723
-9.245	-0.0602	-0.0349	0.0365	5.01976375	1.080663706	1.17251315	0.890075436	1390.767186	29.20286871
-9.055	-0.0539	-0.0432	0.0432	5.29709909	1.1806719	1.2592272	0.957529288	1265.403754	26.35779007
-9	-0.055	-0.0439	0.0476	5.13573932	1.136657586	1.26807349	0.980651679	1278.509597	26.7629137
-8.87	-0.05	-0.0427	0.0522	5.38153285	0.924323729	0.98246528	0.985493886	1415.818562	26.8527554
-8.62	-0.0484	-0.04	0.0383	5.50091888	0.977320755	1.01308012	0.99528432	1342.11191	25.72273235
-8.5	-0.049	-0.0397	0.0448	5.60781346	1.159599119	1.36443844	0.971287495	1505.865908	27.41518895
-8.347	-0.0543	-0.0427	0.0522	5.14823287	1.052661988	1.20447046	0.9751675	1175.714684	25.5006317
-7.12	-0.0447	-0.0428	0.0399	5.63267759	1.038033627	1.06592777	1.044664609	1451.963894	25.7117551
-7	-0.0464	-0.041	0.0483	5.83912105	1.228372779	1.47129668	0.996546761	1663.268815	28.0375632
-6.805	-0.0423	-0.0491	0.0426	5.90424582	1.380029137	1.30867792	1.0250406	1611.873152	26.35334013
-6.68	-0.0582	-0.0419	0.0471	4.89998102	0.994051576	1.18187015	0.964109794	1088.184109	25.3987729
-6.625	-0.0496	-0.0423	0.0408	5.42645928	1.198199728	1.03847099	1.032447965	1370.754722	26.31605385
-6.625	-0.0573	-0.0488	0.044	4.69576552	1.129738521	0.97931761	1.017147256	1007.530157	24.24970115
-6.55	-0.0506	-0.0397	0.0416	5.26648896	1.038338978	1.06093642	0.995554676	1348.216568	26.3605909
-6.435	-0.0483	-0.0416	0.0431	5.47711477	1.060143743	1.29645611	1.001265727	1345.018594	25.72395625
-5.75	-0.045	-0.0438	0.0455	5.63229041	1.07517965	1.0757013	1.0597235	1396.504317	25.3004037
-5.55	-0.0485	-0.0394	0.0417	5.13072366	0.975155598	1.01289602	0.984220199	1326.893667	25.60288955
-5.5	-0.0441	-0.0428	0.0443	5.87327876	1.098334196	1.38016631	1.034317107	1533.851042	26.24888985
-5.245	-0.051	-0.0388	0.0389	5.2418869	0.946609078	1.11603007	0.965474622	1284.634932	25.83300955
-4.75	-0.0569	-0.0453	0.042	5.02254692	1.163272099	1.25681464	0.948908153	1204.111777	26.41737055

-3.81	-0.0482	-0.0437	0.0472	5.22411179	0.929925207	1.00475649	1.05871174	1157.223953	23.83593976
-3.75	-0.0429	-0.0415	0.0433	5.94164469	1.044667503	1.169669	1.060350083	1570.408517	26.1960023
-3.24	-0.0481	-0.035	0.0415	5.37479702	0.872756555	1.03066952	1.024845194	1247.196475	24.71951971
-3.183	-0.0496	-0.0498	0.0511	5.03389687	1.122921227	1.20227787	1.027222649	1155.85703	24.16534225
-3.125	-0.0486	-0.0427	0.0522	5.39966681	0.957005852	1.23873062	1.039125452	1298.158043	25.35023395
-3	-0.052	-0.0596	0.0542	4.96710436	1.302306615	1.23045006	1.02923731	1059.262063	23.6866386
-3	-0.05	-0.0445	0.0429	5.14034202	1.031318571	0.96860175	1.023738298	1216.340874	24.88930132
-2.5	-0.049	-0.0424	0.0141	5.24094353	0.967622565	0.93384218	1.051561251	1218.035179	24.65630585
-2.31	-0.0494	-0.047	0.0519	5.29942107	1.093356251	1.21717152	1.026806802	1224.123354	24.81853368
-2.055	-0.054	-0.0441	0.0466	4.89111292	1.01017449	0.9413667	1.036855174	995.4120178	23.39905793
-1.68	-0.0431	-0.0427	0.047	5.47016335	0.988710062	1.03149437	1.09050194	1233.037053	23.26626935
-1.555	-0.0413	-0.0427	0.0522	14.2797806	0.937546666	1.0063503	1.065291392	1399.396714	24.26305617
-1.31	-0.0458	-0.0466	0.0524	5.22053261	1.021462898	1.32703745	1.054216664	1283.962746	24.4742281
-0.87	-0.0446	-0.0475	-0.0559	5.27697963	0.938931531	1.03745869	1.130511963	1126.415695	22.62126195
-0.81	-0.0521	-0.042	0.0482	4.99338192	0.996958325	1.10516848	1.034064644	1130.170219	24.4901161
-0.75	-0.0439	-0.0519	0.0589	5.49251153	0.936887989	1.24196197	1.142335139	1113.272702	22.31172215
-0.75	-0.0476	-0.0502	0.046	5.15577722	1.016521953	1.09416455	1.064168867	1131.986665	23.42740495
-0.68	-0.0463	-0.05	0.0532	5.37270939	1.087764291	1.1096601	1.088779599	1158.710954	23.37642555
-0.5	-0.0494	-0.0377	0.0444	5.05592441	0.829490254	0.90585254	1.031882331	1112.277731	23.65757079
-0.435	-0.046	-0.044	0.0516	5.47531066	1.077206764	1.39952846	1.041129016	1278.065313	24.47121275
-0.31	-0.0486	-0.0513	0.0454	5.17620869	1.063154222	0.99370764	1.054359547	1105.209383	23.3905519
-0.3	-0.0459	-0.0573	0.0476	5.40947529	1.24835355	1.03877855	1.073324494	1270.878374	24.37577264
-0.245	-0.048	-0.043	0.0394	5.56471382	1.079957495	1.27497357	0.9941028	1315.641769	25.36235038
-0.185	-0.0464	-0.0502	0.0439	5.47004468	1.115407067	1.08012035	1.074920471	1149.593764	23.30940795
-0.18	-0.0434	-0.0375	0.0421	5.47948581	0.843529603	0.86468076	1.093751799	1159.676237	22.64192235
-0.12	-0.0471	-0.0446	0.0518	5.15470512	1.012515639	1.08674778	1.047575269	1204.151939	24.03538877
-0.06	-0.0447	-0.0515	0.0502	5.5636582	1.182367441	1.30957621	1.062756086	1330.153521	24.60960815

-0.06	-0.046	-0.0482	0.0598	5.2445295	1.023535033	1.25568999	1.065905224	1156.638316	23.2797202
-0.005	-0.0412	-0.049	0.0467	6.10793537	1.310563825	1.26404077	1.093736684	1530.703886	25.34511425
0	-0.0455	-0.0478	0.0471	5.50597051	1.042149485	1.20763794	1.065543842	1176.100707	23.3468346
0	-0.0449	-0.045	0.0503	5.4529455	1.189438817	1.11581298	1.131098446	1193.487529	23.36319135
0.12	-0.047	-0.0417	0.0522	5.31511265	0.979877688	1.11626975	1.064144639	1283.479172	24.78810885
0.173	-0.0461	-0.0443	0.0466	5.29837196	0.963357862	0.98282938	1.062945341	1240.533087	24.1354106
0.19	-0.0499	-0.0451	0.0487	4.87899252	0.932178822	0.9101128	1.09442434	966.5020201	22.16418205
0.19	-0.0455	-0.0519	0.0504	5.50396346	1.22283934	1.28578146	1.045468547	1366.758773	25.16817275
0.245	-0.0494	-0.0427	0.0442	5.25204199	0.9655268	1.04528461	1.022307869	1188.181165	24.45146355
0.25	-0.0471	-0.0447	0.0461	5.54933391	1.020225875	1.22046515	1.052093336	1237.133086	24.36232415
0.37	-0.0483	-0.045	0.0517	5.40473704	0.904295486	1.12387466	1.077142774	1107.849542	23.34608215
0.435	-0.048	-0.0558	0.05	5.24042761	1.15882397	1.12518796	1.085908658	1025.679285	22.39373135
0.5	-0.0473	-0.047	0.0422	5.37323364	1.073361534	1.10777787	1.031168536	1163.206635	23.673314
0.5	-0.0452	-0.045	0.0526	5.30917139	1.106485902	1.095527	1.096272002	1220.359554	23.70353795
0.56	-0.0439	-0.0469	0.0501	5.45200452	1.006250486	1.08657265	1.106616375	1145.340574	22.6307859
1.185	-0.0598	-0.0425	0.0438	4.76374495	1.004203719	0.99580024	0.992113334	969.2596012	24.29800968
1.495	-0.0455	-0.0532	0.0461	5.00780608	1.093610024	0.83017839	1.13333312	978.4695863	21.2950869
1.56	-0.0496	-0.0474	0.0494	5.22898951	1.140776683	1.3009019	0.987025768	1209.300776	24.7177
2.685	-0.0416	-0.0616	0.0509	5.52727408	1.168633619	1.19068698	1.146625162	1197.340569	22.52452115
3.25	-0.0494	-0.0534	0.0565	5.03976122	1.101614713	1.24309265	1.045705066	1035.324006	22.82452085
3.815	-0.046	-0.0578	0.0453	5.27852176	1.055330353	0.93054266	1.173954461	970.1950775	21.32104575
4.375	-0.0543	-0.0523	0.0455	4.60154662	0.971574715	0.98767844	1.006660868	838.3781728	21.533764
9.5	-0.0533	-0.0572	0.0594	4.31831615	0.941873364	0.92525626	1.089000562	771.2391105	20.46247585

APPENDIX 6: LEFT PERIPHERAL REFRACTION DATA

Eccentricity	High myopes	Low myopes	Emmetropes
30n	-6.85±3.44	-0.09±1.38	-0.51±1.07
25n	-6.44±2.44	-0.83±1.62	0.12±0.95
20n	-7.12±1.75	-1.23±1.60	0.36±0.55
15n	-7.51±2.07	-1.40±1.6	0.34±0.45
10n	-7.84±1.72	-1.52±1.47	0.12±0.63
5n	-7.50±1.27	-1.69±1.34	0.16±0.59
0	-7.45±1.13	-1.82±1.23	0.20±0.51
5t	-7.22±1.16	-1.92±1.19	0.32±0.65
10t	-7.38±0.90	-1.97±1.27	0.20±0.57
20t	-6.75±2.49	-1.72±1.49	0.15±0.82
25t	--5.81±3.12	-1.49±1.71	0.37±1.10
30t	-5.12±0.00	-1.16 ±2.25	0.21±0.92

Table 30 Mean MSE at each eccentricity for left eyes

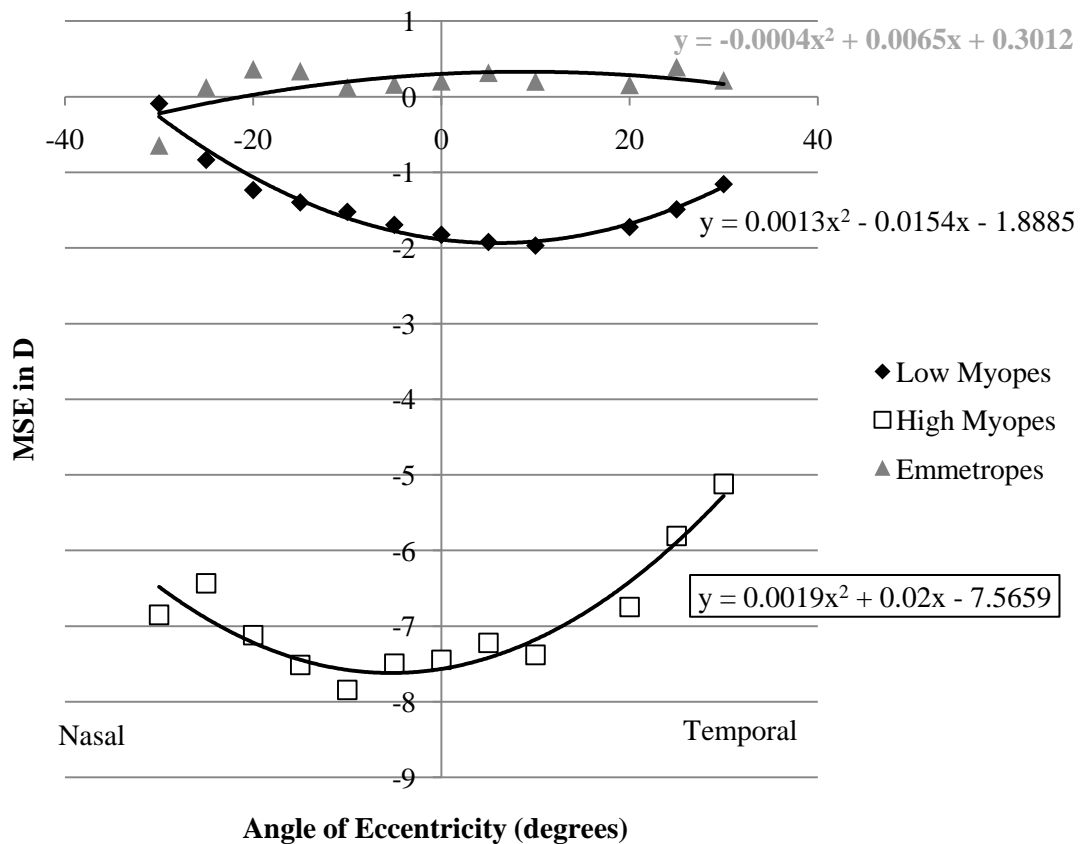
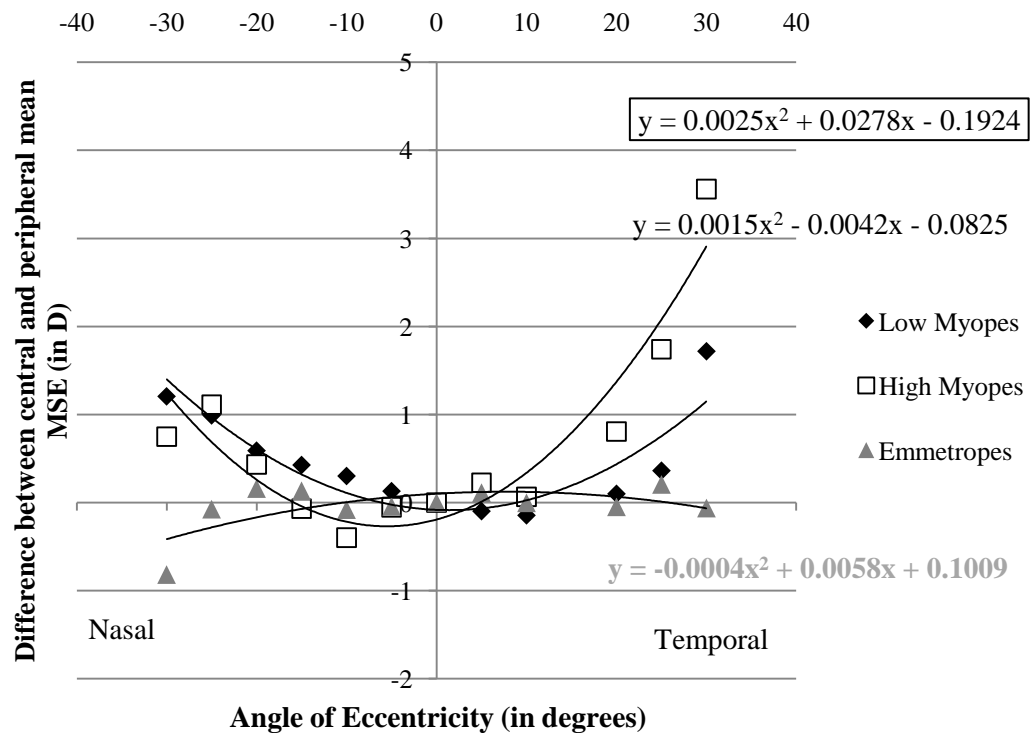


Figure 127 Graph of the mean peripheral refractive error for left eyes fitted with 2<sup>nd</sup> order polynomial curves

Eccentricity	High myopes	Low myopes	Emmetropes
30n	0.75±2.30	1.21±1.18	-0.82±1.25
25n	1.11±1.58	0.99±1.30	-0.07±1.20
20n	0.43±1.02	0.59±1.05	0.16±0.62
15n	-0.07±1.27	0.43±0.92	0.13±0.46
10n	-0.40±0.89	0.30±0.64	-0.08±0.57
5n	-0.05±0.35	0.13±0.47	-0.04±0.34
5t	0.23±0.19	-0.10±0.34	0.01±0.33
10t	0.07±0.33	-0.14±0.59	0.00±0.23
20t	0.81±1.86	0.10±1.21	-0.05±0.78
25t	1.74±2.46	0.36±1.98	0.21±1.15
30t	3.56±0.00	1.72±0.30	-0.06±0.57

**Table 31 Mean difference in MSE values between central and peripheral locations, data is shown for left eyes**



**Figure 128 Graphical representation of the mean difference in MSE between the central and peripheral locations, left eyes**

Eccentricity	High myopes	Emmetropes	Low myopes
30n	0.38±0.19	-1.07±0.74	0.01±0.94
25n	0.32±0.48	-0.43±0.69	0.12±0.81
20n	0.28±0.34	-0.24±0.42	0.22±0.70
15n	0.35±0.60	-0.08±0.38	0.38±0.47
10n	0.53±0.39	-0.06±0.30	0.30±0.44
5n	0.13±0.31	0.02±0.28	0.30±0.43
0	-0.07±0.30	0.01±0.24	0.22±0.43
5t	0.02±0.59	-0.06±0.26	0.16±0.55
10t	-0.19±0.94	-0.07±0.34	-0.04±0.59
20t	-0.11±0.76	-0.56±0.57	-0.28±0.84
25t	0.12±1.05	-0.63±0.85	-0.51±1.08
30t	-0.23±0.00	-0.81±0.54	-0.14±0.84

Table 32 Mean  $J_{180}$  values left eye based on eccentricity

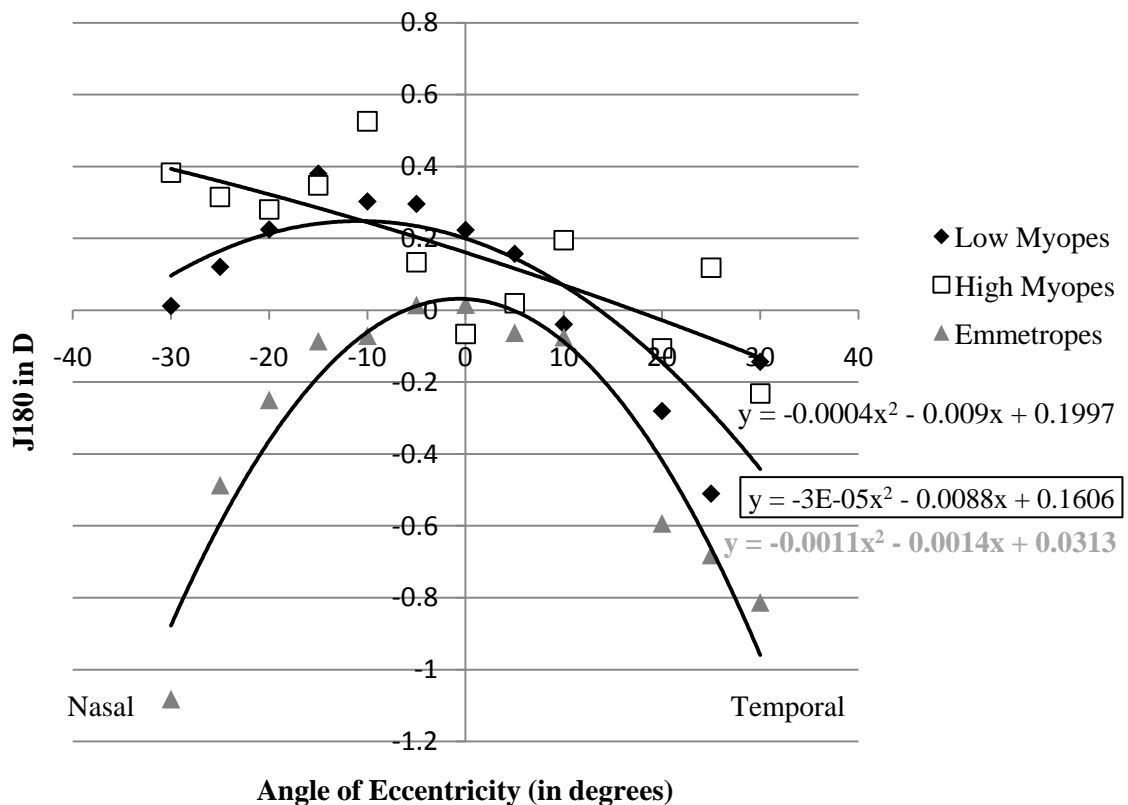


Figure 129 Mean  $J_{180}$  values for left eyes, fitted with 2<sup>nd</sup> order polynomial curves

Eccentricity	High myopes	Low myopes	Emmetropes
30n	-0.10±0.46	0.14±0.19	0.22±0.46
25n	0.04±0.30	0.13±0.31	0.16±0.31
20n	-0.06±0.35	0.10±0.29	0.23±0.29
15n	-0.33±0.54	0.00±0.25	0.07±0.27
10n	-0.06±0.40	0.03±0.26	0.17±0.28
5n	-0.32±0.34	-0.02±0.27	0.12±0.15
0	-0.24±0.36	0.14±0.38	0.05±0.14
5t	-0.26±0.23	0.07±0.38	0.06±0.17
10t	-0.15±0.31	0.05±0.42	-0.04±0.26
20t	-0.20±0.33	-0.03±0.48	0.03±0.47
25t	-0.04±0.73	-0.14±0.62	0.05±0.48
30t	-0.09±0.00	-0.07±0.71	0.63±0.34

Table 33 J<sub>45</sub> left eye, based on eccentricity

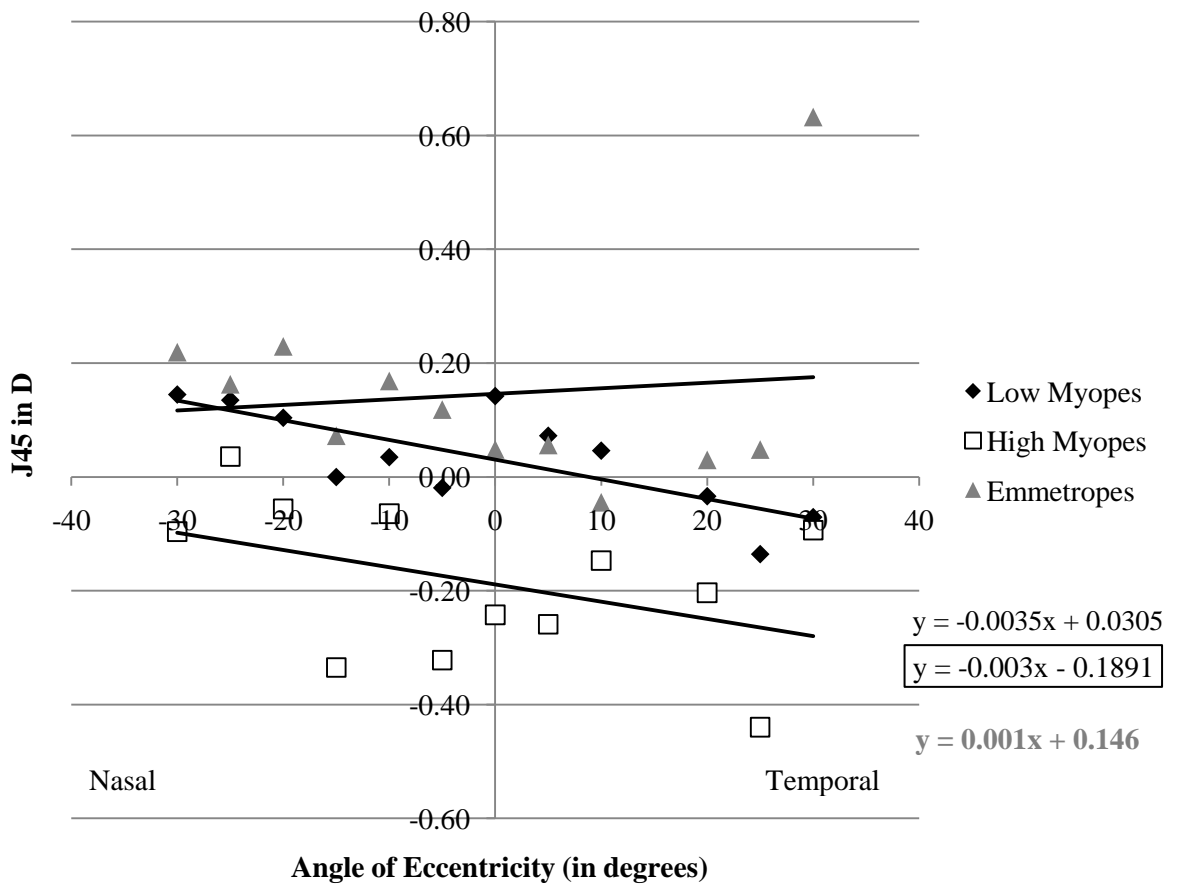
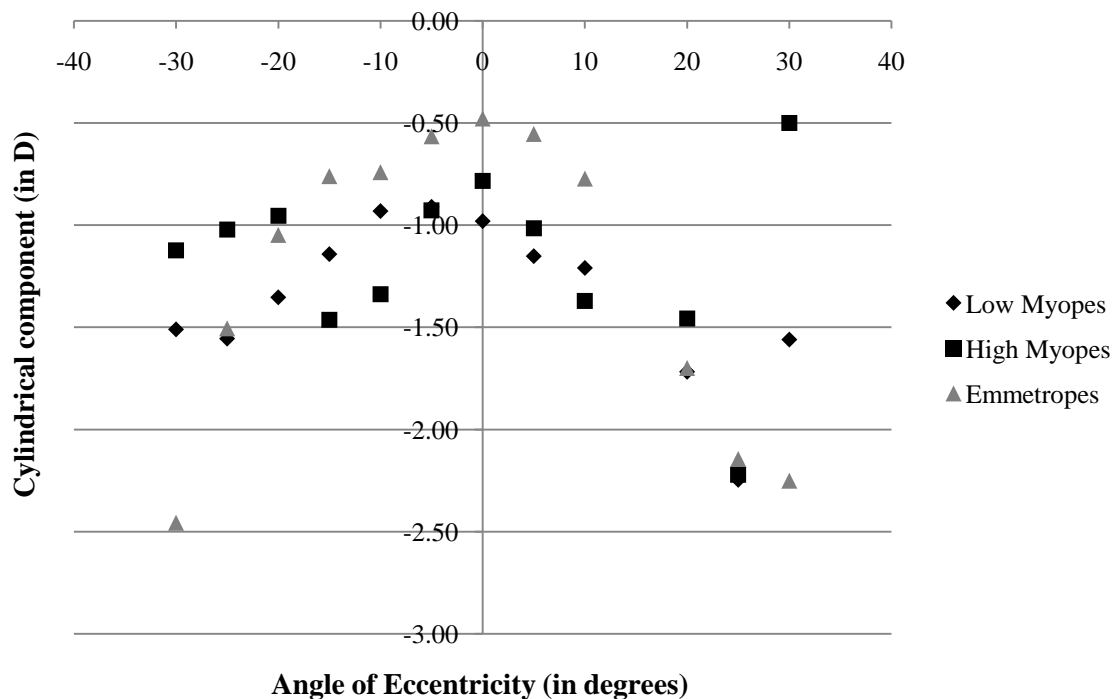


Figure 130 Mean J<sub>45</sub> values for left eyes, fitted with linear trend lines

Eccentricity	High myopes	Low myopes	Emmetropes
30n	-1.12±0.22	-1.51±0.91	-2.46±1.29
25n	-1.02±0.69	-1.56±0.74	-1.50±0.91
20n	-0.96±0.51	-1.35±0.77	-1.05±0.58
15n	-1.46±1.09	-1.14±0.58	-0.76±0.57
10n	-1.34±0.69	-0.93±0.72	-0.74±0.49
5n	-0.93±0.65	-0.91±0.70	-0.57±0.37
0	-0.78±0.67	-0.98±0.76	-0.48±0.30
5t	-1.02±0.83	-1.15±0.68	-0.55±0.31
10t	-1.37±1.41	-1.21±0.73	-0.77±0.40
20t	-1.46±0.69	-1.72±0.94	-1.70±0.68
25t	-2.22±1.16	-2.25±1.40	-2.14±0.98
30t	-0.50±0.00	-1.56±0.44	-2.25±0.74

**Table 34 Cylindrical component calculated from vector components  $J_{180}$  and  $J_{45}$ . Left eye data is shown**



**Table 35 Graphical representation of the cylindrical component, left eyes only**

APPENDIX 7: RIGHT PERIPHERAL REFRACTION AND RETFIT DATA

Raw RE refraction data and values for sagittal refraction and interval of sturm as described in section 11.6

	N	N	N	N	N	N	N	T	T	T	T	T	tang K
Eccentricity	-30	-25	-20	-15	-10	-5	0	5	10	20	25	30	8.04
Sph	0.37	0.12	-0.5	-0.5	-0.8	-0.1	-0.4	-0.8	-0.9	-0.6	-0.1	-0.9	
Cyl	-3	-2.4	-1.5	-1.1	-0.9	-0.4	-0.6	-0.9	-0.5	-0.5	-1.6	-0.4	
Axis	108	106	112	110	137	134	111	51	117	120	69	132	
Int sturm	3	2.37	1.5	1.12	-0.9	0.37	0.62	0.87	0.5	0.5	1.62	0.37	
sag	0.37	0.12	-0.5	-0.5	-1.6	-0.1	-0.4	-0.8	-0.9	-0.6	-0.1	-0.9	
Eccentricity	-30	-25	-20	-15	-10	-5	0	5	10	20	25	30	7.76
Sph		1.62	0.62	0.25	0.12	-0.3	-0.3	-0.3	0.37	1.75	2.12		
Cyl		-1.6	-1.3	-0.9	-1	-0.5	-0.5	-0.3	-0.9	-1.3	-1.5		
Axis		136	120	116	140	120	114	56	68	48	48		
Int sturm	-1.6	1.25	0.87	-1	0.5	0.5	0.25	0.87	1.25	1.5			
sag		0	0.62	0.25	-0.9	-0.3	-0.3	-0.3	0.37	1.75	2.12		
Eccentricity	-30	-25	-20	-15	-10	-5	0	5	10	20	25	30	7.65
Sph	5.87	5.87	6.12	5	5.12	4.87	4.75	4.37	4.25	4.62	5.37		
Cyl	-1.4	-1.6	-1.8	-1.3	-1.1	-1.3	-0.8	-0.4	-0.6	-1.1	-1		
Axis	109	109	111	102	109	109	113	123	116	82	81		
Int sturm	1.37	1.62	1.75	1.25	1.12	1.25	0.75	0.37	0.62	1.12	1		
Sag	5.87	5.87	6.12	5	5.12	4.87	4.75	4.37	4.25	4.62	5.37		
Eccentricity	-30	-25	-20	-15	-10	-5	0	5	10	20	25	30	7.67
Sph	-0.6	0.12	0.25	0.62	0.5	0.5	1.12	0.87	0.25	1.5	1.62		
Cyl	-2	-1.6	-1.6	-2.3	-0.6	-0.8	-1.1	-1.3	-0.6	-3.3	-3.3		
Axis	104	89	100	119	87	99	101	100	94	87	82		
Int sturm	2	1.62	1.62	2.25	0.62	0.75	1.12	1.25	0.62	3.25	3.25		
sag	-0.6	0.12	0.25	0.62	0.5	0.5	1.12	0.87	0.25	1.5	1.62		
Eccentricity	-30	-25	-20	-15	-10	-5	0	5	10	20	25	30	7.79
Sph	2.75	3.37	2.25	1.12	1.25	0.87	-0.3	-1.1	-1.9	2.37			
Cyl	-1.8	-2.1	-1.5	-1.4	-1.8	-1.1	-1	-0.5	-1.4	-4.9			
Axis	4	175	13	15	12	7	34	49	83	81			
Int sturm	-1.8	-2.1	-1.5	-1.4	-1.8	-1.1	-1	0.5	1.37	4.87			
sag	1	1.25	0.75	-0.3	-0.5	-0.3	-1.3	-1.1	-1.9	2.37			
Eccentricity	-30	-25	-20	-15	-10	-5	0	5	10	20	25	30	7.71
Sph		-3.6	-7.8	-8.1	-8.8	-8.1	-7.9	-8.6	-7.9	-7.6	-6.6		
Cyl		-4.1	-1.3	-1.8	-0.6	-1.1	-1	-1.1	-0.9	-1.5	-1.8		
Axis		163	176	162	180	172	150	139	130	117	125		
Int sturm	-4.1	-1.3	-1.8	-0.6	-1.1	-1	-1.1	0.87	1.5	1.75			

sag		-7.7	-9	-9.9	-9.4	-9.2	-8.9	-9.7	-7.9	-7.6	-6.6		
Eccentricity	-30	-25	-20	-15	-10	-5	0	5	10	20	25	30	7.57
sph	-2	-3.1	-3.8	-5	-4.9	-5.5	-4.4	-5.3	-5.6	-4.6	-4	0.5	
Cyl	-3.1	-2.6	-2.6	-1.5	-1.4	-0.9	-0.8	-0.8	-0.5	-2	-0.9		
Axis	172	180	3	6	154	168	170	171	131	93	155		
Int sturm	-3.1	-2.6	-2.6	-1.5	-1.4	-0.9	-0.8	-0.8	0.5	2	-0.9		
sag	-5.1	-5.7	-6.4	-6.5	-6.2	-6.4	-5.1	-6	-5.6	-4.6	-4.9		
Eccentricity	-30	-25	-20	-15	-10	-5	0	5	10	20	25	30	8.11
		1.12	0.75	-0.3	-0.1	0	0.25	0.87	0.38	-0.3	0.62	0.5	
Cyl		-1.9	-1.4	-0.5	-0.5	-0.5	-1.1	-1.3	-1.3	-1.3	-1.8		
Axis		103	89	57	115	92	81	74	89	93	94		
Int sturm	1.87	1.37	0.5	0.5	0.5	1.12	1.25	1.25	1.25	1.75			
sag		1.12	0.75	-0.3	-0.1	0	0.25	0.87	0.38	-0.3	0.62		
Eccentricity	-30	-25	-20	-15	-10	-5	0	5	10	20	25	30	8.26
Sph			-6.8	-6.6	-6.8	-6.9	-6.6	-6.1	-5.1				
Cyl			-0.5	-0.8	-0.8	-0.9	-0.9	-0.8	-1.9				
Axis			25	65	95	5	11	13	89				
Int sturm		-0.5	0.75	0.75	-0.9	-0.9	-0.8	1.87					
sag			-7.3	-6.6	-6.8	-7.7	-7.5	-6.9	-5.1				
Eccentricity	-30	-25	-20	-15	-10	-5	0	5	10	20	25	30	7.62
Sph	-7.3	-7.9	-8	-8.5	-8	-8.3	-8.9	-8	-7.8	-6.4	-5.9		
Cyl	-0.5	-0.5	-0.9	-0.5	-0.8	-0.4	-0.5	-1	-2	-2.4	-0.9		
Axis	142	144	143	159	14	163	111	82	75	60	74		
Int sturm	-0.5	-0.5	-0.9	-0.5	-0.8	-0.4	0.5	1	2	2.37	0.87		
sag	-7.8	-8.4	-8.9	-9	-8.8	-8.6	-8.9	-8	-7.8	-6.4	-5.9		
Eccentricity	-30	-25	-20	-15	-10	-5	0	5	10	20	25	30	7.69
Sph	1.12	0.75	0.12	-0.5	0	-0.1	-0.3	-0.1	-0.6	-1.4	0.5		
Cyl	-1.3	-0.9	-0.8	-0.4	-0.5	-0.5	-0.1	-1.1	-0.5	-0.6	-0.8		
Axis	117	113	120	27	167	21	13	17	59	59	28		
Int sturm	1.25	0.87	0.75	-0.4	-0.5	-0.5	-0.1	-1.1	0.5	0.62	-0.8		
sag	1.12	0.75	0.12	-0.9	-0.5	-0.6	-0.4	-1.2	-0.6	-1.4	-0.3		
Eccentricity	-30	-25	-20	-15	-10	-5	0	5	10	20	25	30	7.8
Sph	2.87	1.37	1.25	1	0.62	0.5	0.5	0.75	1	2.5			
Cyl	-2.3	-1.3	-1.5	-1.4	-0.5	-0.4	-0.3	-0.4	-0.8	-0.8			
Axis	171	167	150	164	164	135	51	82	66	2			
Int sturm	-2.3	-1.3	-1.5	-1.4	-0.5	0.37	0.25	0.37	0.75	-0.8			
Sag	0.62	0.12	-0.3	-0.4	0.12	0.5	0.5	0.75	1	1.75			
Eccentricity	-30	-25	-20	-15	-10	-5	0	5	10	20	25	30	7.78
Sph	1.75	1.25	0.75	0.12	0	0	0	0.12	0.25	0	0.75		
Cyl	-0.9	-0.4	-1.6	-0.5		-0.1	-0.1		-0.3		-0.6		
Axis	85	75	114	65		128	55		71		100		

Int sturm	0.87	0.37	1.62	0.5	0	0.12	0.12	0	0.25	0	0.62		
Sag	1.75	1.25	0.75	0.12	0	0	0	0.12	0.25	0	0.75		
Eccentricity	-30	-25	-20	-15	-10	-5	0	5	10	20	25	30	7.66
Sph	`	-5.4	-6	-5.8	-5.5	-5.1	-5.4	-5.1	-4.9	-4.5			
Cyl		-0.4	-0.6	-2.3	-1.1	-1.3	-0.4	-0.6	-0.5	-1			
Axis		174	166	175	174	154	97	110	95	100			
Int sturm	-0.4	-0.6	-2.3	0	-1.3	0.37	0.62	0.5	1				
Sag		-5.7	-6.6	-8	-6.6	-6.4	-5.4	-5.1	-4.9	-4.5			
Eccentricity	-30	-25	-20	-15	-10	-5	0	5	10	20	25	30	7.8
Sph	`	2.25	1.25	0.75	0.25	0	0.12	0.12	0.5	0.87	1.62		
Cyl		-1.4	-0.6	-0.4	-1.3	-0.1	-0.3	-0.3	-0.6	-1.3	-2		
Axis		90	108	107	36	151	143	46	95	85	73		
Int sturm	1.37	0.62	0.37	-1.3	-0.1	-0.3	0.25	0.62	1.25	2			
Sag		2.25	1.25	0.75	-1	-0.1	-0.1	0.12	0.5	0.87	1.62		
Eccentricity	-30	-25	-20	-15	-10	-5	0	5	10	20	25	30	8.14
Sph	1.62	1.5	1.62	0.37	0.75	0.25	0.12	0.5	0.87	1.62	2.25		
Cyl		-0.4	-0.5	-1	-1	-0.4	-0.3	-0.1	-0.5	-1.1	-1.1		
Axis		5	172	22	21	33	171	30	10	175	33		
Int sturm	0	-0.4	-0.5	-1	-1	-0.4	-0.3	-0.1	-0.5	-1.1	-1.1		
Sag	1.62	1.13	1.12	-0.6	-0.3	-0.1	-0.1	0.38	0.37	0.5	1.13		
Eccentricity	-30	-25	-20	-15	-10	-5	0	5	10	20	25	30	7.88
Sph	-0.6	0.25	0.12	0.12	0.37	0	0.25	0.25	0.12	-0.5	-0.3		
Cyl	-2.1	-1.1	-0.9	-1.1	-0.8	-0.6	-0.9	-0.8	-1.3	-2.8	-1.8		
Axis	104	83	117	123	118	119	98	95	70	82	83		
Int sturm	2.12	1.12	0.87	1.12	0.75	0.62	0.87	0.75	1.25	2.75	1.75		
Sag	-0.6	0.25	0.12	0.12	0.37	0	0.25	0.25	0.12	-0.5	-0.3		
Eccentricity	-30	-25	-20	-15	-10	-5	0	5	10	20	25	30	7.9
Sph	2.75	1.12	-0.1	-0.6	-1.1	-2.3	-2.8	-2.4	-2.6	-2.6	-2	-1.1	
Cyl	-2.8	-1.6	-0.9	-1.9	-1.8	-0.8	-0.3	-0.6	-0.6	-0.5	-0.4	-0.8	
Axis	17	24	31	43	161	30	103	96	141	77	140	159	
Int sturm	-2.8	-1.6	-0.9	-1.9	-1.8	-0.8	0.25	0.62	-0.6	0.5	-0.4	-0.8	
Sag	0	-0.5	-1	-2.5	-2.9	-3	-2.8	-2.4	-3.2	-2.6	-2.4	-1.9	
Eccentricity	-30	-25	-20	-15	-10	-5	0	5	10	20	25	30	7.98
Sph	1.25	1.37	1.12	1	0.75	0.5	0.75	0.12	0.12	0.12	0		
Cyl	-2.5	-1.1	-0.4	-0.8	-0.1	-0.1	-0.5	-0.1	-0.5	-2.4	-2.8		
Axis	74	77	51	37	13	159	17	20	70	88	90		
Int sturm	2.5	1.12	0.37	-0.8	-0.1	-0.1	-0.5	-0.1	0.5	2.37	2.75		
Sag	1.25	1.37	1.12	0.25	0.63	0.38	0.25	0	0.12	0.12	0		
Eccentricity	-30	-25	-20	-15	-10	-5	0	5	10	20	25	30	8.42
Sph		-0.8	0.75	0.12	0.12	0.12	-0.3	0	0.25	0.87			
Cyl		-3.1	-1.1	-0.4	-0.1	-0.3	-0.1	-0.6	-1.5	-3.6			

Axis		93	98	91	151	52	106	90	82	73			
Int sturm	3.12	1.12	0.37	-0.1	0.25	0.12	0.62	1.5	3.62				
Sag		-0.8	0.75	0.12		0.12	-0.3	0	0.25	0.87			
Eccentricity	-30	-25	-20	-15	-10	-5	0	5	10	20	25	30	7.51
Sph	0.25	0.37	0	-0.5	0	0	-0.3	0	0.25	0.25	0.37		
Cyl	-1.1	-1.3	-0.6	-0.4	-0.6	-0.6	-0.4	-0.8	-1.9	-2.9	-2.5		
Axis	89	98	77	165	99	88	90	70	80	90	86		
Int sturm	1.12	1.25	0.62	-0.4	0.62	0.62	0.37	0.75	1.87	2.87	2.5		
Sag	0.25	0.37	0	-0.9		0	-0.3	0	0.25	0.25	0.37		
Eccentricity	-30	-25	-20	-15	-10	-5	0	5	10	20	25	30	7.23
sph	-1.3	-3.6	-6.4	-6.6	-7.5	-7.5	-7.9	-7.6	-7.4	-5.5	-1	-1.5	
Cyl	-2.6	-1.6	-0.6	-1.1	-1	-0.6	-1	-1.4	-1.3	-0.5	-2	-2	
Axis	177	178	132	137	134	114	97	92	93	23	176	1	
Int sturm	-2.6	-1.6	0.62	-1.1	1	0.62	1	1.37	1.25	-0.5	-2	-2	
Sag	-3.9	-5.2	-6.4	-7.7	-7.5	-7.5	-7.9	-7.6	-7.4	-6	-3	-3.5	
Eccentricity	-30	-25	-20	-15	-10	-5	0	5	10	20	25	30	7.87
Sph		0.12	0.12	0.37	0.62	0.12	0	0.12	-0.1	0.12	0.5	0.37	
Cyl		-2.8	-3	-1.9	-1	-0.4	-0.1	-0.5	-0.8	-1.8	-1.6	-2.3	
Axis		75	76	77	75	72	76	116	122	96	111	112	
Int sturm	2.75	3	1.87	1	0.37	0.12	0.5	0.75	1.75	1.62	2.25		
Sag		0.12	0.12	0.37	0.62	0.12		0.12	-0.1	0.12	0.5	0.37	
Eccentricity	-30	-25	-20	-15	-10	-5	0	5	10	20	25	30	8.19
Sph	-10	-11	-11	-11	-10	-11	-9.8	-9.9	-9.6	-9.5	-6.6		
Cyl	-1.8	-1.3	-2.4	-2.9	-1.8	-1.3	-1.6	-1.4	-3.4	-1.8	-4		
Axis	13	46	49	47	48	35	51	46	48	54	24		
Int sturm	-1.8	1.25	2.37	2.87	1.75	-1.3	1.62	1.37	3.37	1.75	-4		
Sag	-12	-11	-11	-11	-10	-12	-9.8	-9.9	-9.6	-9.5	-11		
Eccentricity	-30	-25	-20	-15	-10	-5	0	5	10	20	25	30	7.65
sph		-1.6	-1.8	-1.8	-2	-2.5	-2.4	-1.8					
Cyl		-3.9	-2.9	-3	-2.3	-2.3	-1.9	-3.5					
Axis		180	5	5	5	28	8	19					
Int sturm	-3.9	-2.9	-3	-2.3	-2.3	-1.9	-3.5						
Sag		-5.5	-4.6	-4.8	-4.3	-4.8	-4.2	-5.3					
Eccentricity	-30	-25	-20	-15	-10	-5	0	5	10	20	25	30	7.69
Sph	-1.9	-1.9	-2.1	-2.6	-2.6	-2.9	-2.5	-2.4	-2.3	-1.6	-1		
Cyl	-3.3	-3.3	-3.1	-0.8	-1	-0.4	-0.4	-0.5	-0.6	-1.8	-3.1		
Axis	97	100	90	80	86	112	157	123	122	90	90		
Int sturm	3.25	3.25	3.12	0.75	1	0.37	-0.4	0.5	0.62	1.75	3.12		
Sag	-1.9	-1.9	-2.1	-2.6	-2.6	-2.9	-2.9	-2.4	-2.3	-1.6	-1		
Eccentricity	-30	-25	-20	-15	-10	-5	0	5	10	20	25	30	7.63
Sph	1.62	1	0.25	-0.9	-1.6	-1.9	-2.3	-1.9	-1.8	-0.6	0.12	1	

Cyl	-5.6	-4	-1.9	-1.4	-0.8	-0.8	-0.1	-0.8	-1	-1.1	-1.4	-1.5	
Axis	90	83	72	71	65	36	12	179	7	172	168	171	
Int sturm	5.62	4	1.87	1.37	0.75	-0.8	-0.1	-0.8	-1	-1.1	-1.4	-1.5	
Sag	1.62	1	0.25	-0.9	-1.6	-2.6	-2.4	-2.6	-2.8	-1.7	-1.3	-0.5	
Eccentricity	-30	-25	-20	-15	-10	-5	0	5	10	20	25	30	7.64
Sph	2.37	1.25	0.87	0	0.25	0.13	-0.1	-0.8	-1	-1.9	-1.9	-1.8	
Cyl	-4.3	-3.1	-2.6	-1.6	-2	-1.8	-1.4	-1	-1.1	-2	-2.1	-2	
Axis	2	178	177	175	4	5	14	23	36	71	64	71	
Int sturm	-4.3	-3.1	-2.6	-1.6	-2	-1.8	-1.4	-1	-1.1	2	2.12	2	
Sag	-1.9	-1.9	-1.8	-1.6	-1.8	-1.6	-1.5	-1.8	-2.1	-1.9	-1.9	-1.8	
Eccentricity	-30	-25	-20	-15	-10	-5	0	5	10	20	25	30	7.64
Sph	-0.1	-1.3	-1.8	-2.1	-2.4	-2	-1.6	-1.4	-1.3	-0.6	0.25	1.25	
Cyl	-1.4	-1.4	-1	-1.1	-2	-1.1	-0.6	-0.8	-0.6	-0.9	-1.9	-1.8	
Axis	131	149	148	163	167	11	155	148	113	105	98	102	
Int sturm	1.37	-1.4	-1	-1.1	-2	-1.1	-0.6	-0.8	0.62	0.87	1.87	1.75	
Sag	-0.1	-2.6	-2.8	-3.2	-4.4	-3.1	-2.2	-2.1	-1.3	-0.6	0.25	1.25	
Eccentricity	-30	-25	-20	-15	-10	-5	0	5	10	20	25	30	7.91
Sph	`		1.37	0.87	0.12	0.25	0.62	0.62	0.87	0.87			
Cyl			-0.8	-0.8	-0.4	-0.6	-0.8	-0.9	-1	-1.8			
Axis			50	88	59	83	87	96	99	105			
Int sturm		0.75	0.75	0.37	0.62	0.75	0.87	1	1.75				
Sag			1.37	0.87	0.12	0.25	0.62	0.62	0.87	0.87			
Eccentricity	-30	-25	-20	-15	-10	-5	0	5	10	20	25	30	8.06
Sph	1.87	2.37	1.62	1.12	0.87	0.75	0.75	0.37	0.62	1.25	1.37		
Cyl	-1.3	-0.6	-0.5	-0.9	-0.4	-0.4	-0.5	-0.4	-0.5	-2.4	-3.6		
Axis	62	59	165	174	47	69	180	53	95	88	91		
Int sturm	1.25	0.62	-0.5	-0.9	0.37	0.37	-0.5	0.37	0.5	2.37	3.62		
Sag	1.87	2.37	1.12	0.25	0.87	0.75	0.25	0.37	0.62	1.25	1.37		
Eccentricity	-30	-25	-20	-15	-10	-5	0	5	10	20	25	30	7.88
Sph	`	0.37	1.37	1.62	2	2.37	1.62	1.37	1.12	1.12	1.5		
Cyl		-1.8	-0.3	-0.3	-0.8	-0.4	-0.3	-0.4	-0.3	-2.1	-0.9		
Axis		77	47	14	169	179	7	19	72	89	90		
Int sturm	1.75	0.25	-0.3	-0.8	-0.4	-0.3	-0.4	0.25	2.12	0.87			
Sag		0.37	1.37	1.37	1.25	2	1.37	1	1.12	1.12	1.5		
Eccentricity	-30	-25	-20	-15	-10	-5	0	5	10	20	25	30	7.7
Sph			-0.5	-0.6	-1.3	-0.6	-0.6	-0.1	-0.3	-0.1	0.13		
Cyl			-1.8	-1.3	-1	-0.3	-0.5	-0.4	-0.4	-0.6	-1.1		
Axis			97	112	125	147	132	155	120	89	87		
Int sturm		1.75	1.25	1	-0.3	0.5	-0.4	0.37	0.62	1.12			
Sag			-0.5	-0.6	-1.3	-0.9	-0.6	-0.5	-0.3	-0.1	0.13		
Eccentricity	-30	-25	-20	-15	-10	-5	0	5	10	20	25	30	7.93

Sph	-1.3	-1.9	-2.6	-2.9	-2.5	-2.9	-2.5	-2.6	-2.4	-3	-2.9		
Cyl	-2.5	-1.1	-0.5		-0.6	-1.3	-0.8	-0.5	-1.5	-4.6	-4.6		
Axis	70	67	59		176	176	175	98	96	97	99		
Int sturm	2.5	1.12	0.5	0	-0.6	-1.3	-0.8	0.5	1.5	4.62	4.62		
Sag	-1.3	-1.9	-2.6	-2.9	-3.1	-4.1	-3.3	-2.6	-2.4	-3	-2.9		
Eccentricity	-30	-25	-20	-15	-10	-5	0	5	10	20	25	30	7.94
Sph	0.5	0.87	1	1	1.12	0.87	1.37	1.37	1.5	1.75	1.5		
Cyl	-4.5	-1.8	-1.4	-0.9	-0.5	-0.4	-0.4	-0.5	-0.8	-2.4	-2.9		
Axis	98	113	102	99	104	119	83	99	83	77	81		
Int sturm	4.5	1.75	1.37	0.87	0.5	0.37	0.37	0.5	0.75	2.37	2.87		
Sag	0.5	0.87	1	1	1.12	0.87	1.37	1.37	1.5	1.75	1.5		
Eccentricity	-30	-25	-20	-15	-10	-5	0	5	10	20	25	30	8.09
Sph	0.37	0.12	0.62	1	0.75	0.62	0.12	0.37	0.37	0.87	1.12		
Cyl	-3.1	-1.9	-1	-1.1	-0.3	-0.5	-0.4	-0.5	-0.5	-1.4	-2.1		
Axis	97	104	133	136	92	131	103	58	63	73	83		
Int sturm	3.12	1.87	1	-1.1	0.27	0.5	0.37	0.5	0.5	1.37	2.12		
Sag	0.37	0.12	0.62	-0.1	0.75	0.62	0.12	0.37	0.37	0.87	1.12		
Eccentricity	-30	-25	-20	-15	-10	-5	0	5	10	20	25	30	7.7
Sph	1.62	2	2.12	2.87	2.25	2.12	1.87	2	1.75	1.87	2.25		
Cyl	-1.5	-1	-0.8	-0.4	-0.5	-0.3	-0.6	-0.8	-1.3	-2.5	-1.3		
Axis	108	120	125	37	28	1	86	90	86	79	89		
Int sturm	1.5	1	0.75	-0.4	-0.5	-0.3	0.62	0.75	1.25	2.5	1.25		
Sag	1.62	2	2.12	2.5	1.75	1.87	1.87	2	1.75	1.87	2.25		
Eccentricity	-30	-25	-20	-15	-10	-5	0	5	10	20	25	30	8.06
Sph	0.87	0.87	0.75	-0.1	0.38	0.5	0.62	0.87	0.87	0.5	0.38		
Cyl	-3.8	-1.3	-1.1	-1.1	-0.9	-0.8	-0.4	-1	-1.1	-4.1	-5.4		
Axis	100	117	118	136	116	112	83	78	77	87	82		
Int sturm	3.75	1.25	1.12	-1.1	0.87	0.75	0.37	1	1.12	4.12	5.37		
Sag	0.87	0.87	0.75	-1.2	0.38	0.5	0.62	0.87	0.87	0.5	0.38		
Eccentricity	-30	-25	-20	-15	-10	-5	0	5	10	20	25	30	7.53
Sph	-0.6	-0.6	-0.8	-0.8	-0.4	-0.6	-0.8	-1.3	-0.8	-0.5	-0.1		
Cyl	-0.8	-0.8	-0.6	-1.3	-1.4	-1.6	-1.9	-1.9	-2.6	-3.4	-6.6		
Axis	107	128	150	129	127	125	123	109	108	99	82		
Int sturm	0.75	0.75	-0.6	1.25	1.37	1.62	1.87	1.87	2.62	3.37	6.62		
Sag	-0.6	-0.6	-1.4	-0.8	-0.4	-0.6	-0.8	-1.3	-0.8	-0.5	-0.1		
Eccentricity	-30	-25	-20	-15	-10	-5	0	5	10	20	25	30	8
Sph	0.75	0	0	-0.3	-0.3	-0.4	-0.1	-0.3	-0.1	0.12	0.25		
Cyl	-1.3	-0.8	-0.9	-0.9	-0.6	-0.3	-0.3	-0.3	-0.5	-1	-1		
Axis	165	151	140	75	156	178	22	77	57	73	64		
Int sturm	-1.3	-0.8	-0.9	0.87	-0.6	-0.3	-0.3	0.25	0.5	1	1		
Sag	-0.5	-0.8	-0.9	-0.3	-0.9	-0.6	-0.4	-0.3	-0.1	0.12	0.25		

Eccentricity	-30	-25	-20	-15	-10	-5	0	5	10	20	25	30	7.51
Sph		0.87	0.12	0	0	0	0.12	0	0.25				
Cyl		-0.8	-0.8	-0.9	-0.3	-0.1	-0.8	-0.4	-0.5				
Axis		100	31	20	28	19	6	150	167				
Int sturm	0.75	-0.8	-0.9	-0.3	-0.1	-0.8	-0.4	-0.5					
Sag		0.87	-0.6	-0.9	-0.3	-0.1	-0.6	-0.4	-0.3				
Eccentricity	-30	-25	-20	-15	-10	-5	0	5	10	20	25	30	7.5
Sph	-2.5	-4.1	-4.8	-5.1	-6.3	-6.8	-6.9	-6.1	-6	-4.4	-2.9	-2.4	
Cyl	-2.5	-2.3	-2.4	-1.8	-2.1		-0.4	-0.6	-1	-1	-2.5	-1.9	
Axis	168	168	168	153	173		156	106	88	74	33	13	
Int sturm	-2.5	-2.3	-2.4	-1.8	-2.1	0	-0.4	0.62	1	1	-2.5	-1.9	
Sag	-5	-6.4	-7.1	-6.9	-8.4	-6.8	-7.2	-6.1	-6	-4.4	-5.4	-4.2	

Apical radius (r) and conic constant values (p) derived through use of RetFit x and y<sup>2</sup> coordinates and SPSS statistical package v.16

SUBJECT	b1	b2	Radius	Conic
1	-24.461	-2.686	-12.2305	2.686
2	-27.879	-5.564	-13.9395	5.564
3	-21.984	-6.509	-10.992	6.509
4	-11.961	0.903	-5.9805	-0.903
5	-9.504	1.387	-4.752	-1.387
6	-10.677	5.592	-5.3385	-5.592
7	-19.175	-1.958	-9.5875	1.958
8	-14.166	-1.637	-7.083	1.637
9	-20.231	-2.067	-10.1155	2.067
10	-13.529	1.505	-6.7645	-1.505
11	-10.604	0.548	-5.302	-0.548
12	-25.786	-6.106	-12.893	6.106
13	-19.642	-2.717	-9.821	2.717
14	-33.08	-10.283	-16.54	10.283
15	0.476	2.196	0.238	-2.196
16	15.13	15.628	7.565	-15.628
17	-8.211	0.767	-4.1055	-0.767
18	5.479	5.55	2.7395	-5.55
19	-13.121	-0.31	-6.5605	0.31
20	-31.199	-7.731	-15.5995	7.731
21	-17.085	-0.228	-8.5425	0.228
22	-33.523	-11.291	-16.7615	11.291
23	-12.211	8.026	-6.1055	-8.026
24	-25.327	-3.81	-12.6635	3.81
25	-10.298	0.549	-5.149	-0.549
26	-13.855	1.439	-6.9275	-1.439
27	-36.535	-11.005	-18.2675	11.005
28	-22.672	-4.114	-11.336	4.114
29	-24.151	-3.47	-12.0755	3.47
30	-2.236	4.131	-1.118	-4.131
31	-8.017	3.761	-4.0085	-3.761
32	-22.38	-2.934	-11.19	2.934
33	-20.866	-2.496	-10.433	2.496
34	-24.557	-2.582	-12.2785	2.582
35	1.512	5.884	0.756	-5.884
36	-23.081	-0.83	-11.5405	0.83
37	-39.467	-8.658	-19.7335	8.658
38	-17.851	-0.919	-8.9255	0.919
39	-17.182	-1.188	-8.591	1.188
40	-21.84	-3.911	-10.92	3.911
41	-13.306	0.346	-6.653	-0.346

Calculated values of Y from fixed X values from peripheral refraction

As described in section 11.6

30°	20°	10°
7.008942959	5.351725105	2.869201108
5.797886994	5.279861589	3.012649996
2.746097067	4.235821101	2.626223048
6.620898753	4.269174768	2.072912806
6.388808864	3.969499062	1.869841571
9.050815941	5.0382204	2.102848069
6.3109852	4.767880535	2.543893669
5.265111233	4.053588188	2.181184884
6.481628137	4.897181353	2.612975794
7.342108723	4.640704903	2.217997408
6.050217748	3.959435717	1.94384413
4.744669578	4.894528946	2.876997567
5.868503071	4.683129851	2.55770747
2.641619144	5.105629716	3.212216135
4.267226219	1.87754691	0.320015625
9.719937387	2.980362931	
5.60427932	3.576570257	1.722732568
8.124023941	4.257985439	1.611683902
6.038241383	4.185285653	2.13409817
4.916207573	5.322753385	3.157942764
7.003271179	4.810727263	2.439635219
	4.975857675	3.217126435
10.40500517	5.668853006	2.292822496
6.454916653	5.262651043	2.897882848
5.974875304	3.905989708	1.916129562
7.368259896	4.675503353	2.241768833
3.294518098	5.427741519	3.382179401
5.568636153	4.842794483	2.726029163
6.417892411	5.169150027	2.833332843
6.604331389	3.309494886	1.135186108
7.589107069	4.269181233	1.807393842
6.378553645	5.029601416	2.733785837
6.330469998	4.903233382	2.645248571
7.095216121	5.382517924	2.877265195
7.558070415	3.645826326	1.118029517
7.848051159	5.501920392	2.824300798
6.372043958	6.16248041	3.571112572
6.720010275	4.783747109	2.476948223
6.383834365	4.631277664	2.422430598
5.507891511	4.763516726	2.67673355
6.54814589	4.361330347	2.16782956

Apical radius (r) and conic constant (p) values as derived from statistical program SPSS (v16) using MR data (RE data)

	b1	b2	Radius	Conic
1	28.651	-1.62	14.3255	1.62
2	25.138	-0.625	12.569	0.625
3	27.67	-1.377	13.835	1.377
4	22.615	-0.027	11.3075	0.027
5	22.111	-0.567	11.0555	0.567
6	27.245	-0.936	13.6225	0.936
7	21.287	0.778	10.6435	-0.778
8	38.818	-5.424	19.409	5.424
9	31.275	-1.324	15.6375	1.324
10	24.369	-0.135	12.1845	0.135
11	21.734	-0.659	10.867	0.659
12	19.675	1.623	9.8375	-1.623
13	22.785	-0.203	11.3925	0.203
14	30.109	-1.593	15.0545	1.593
15	44.443	-4.973	22.2215	4.973
16	22.822	-0.031	11.411	0.031
17	47.897	-4.283	23.9485	4.283
18	31.361	-1.649	15.6805	1.649
19	29.252	-2.189	14.626	2.189
20	37.797	-3.893	18.8985	3.893
21	20.747	-0.581	10.3735	0.581
22	30.547	-1.751	15.2735	1.751
23	47.737	-6.202	23.8685	6.202
24	22.688	0.454	11.344	-0.454

25	25.673	-1.202	12.8365	1.202
26	23.786	0.263	11.893	-0.263
27	32.184	-2.37	16.092	2.37
28	28.36	-1.385	14.18	1.385
29	-0.0999	7.411	-0.04995	-7.411
30	37.389	-3.893	18.6945	3.893
31	26.746	-1.213	13.373	1.213
32	24.723	-0.124	12.3615	0.124
33	14.983	2.172	7.4915	-2.172
34	22.932	-0.054	11.466	0.054
35	19.471	0.675	9.7355	-0.675
36	32.34	-2.046	16.17	2.046
37	34.961	-4.396	17.4805	4.396
38	15.567	1.75	7.7835	-1.75
39	26.997	-1.997	13.4985	1.997
40	8.231	4.137	4.1155	-4.137
41	21.412	-0.873	10.706	0.873

Calculated values of Y from fixed X values from MRI data

30 degrees eccentricity from the	20 degrees eccentricity from the	10 degrees eccentricity from the
8.437033128	6.037652855	3.135187395
8.341166435	5.787934865	2.953258793
8.391828305	5.963408522	3.084771872
8.208377873	5.581870762	2.812817538
7.812992596	5.42525439	2.769366805
8.549538958	5.984612068	3.069379416
8.402590541	5.554969235	2.746953767
8.220384273	6.57566532	3.594698875
9.037453048	6.37479995	3.283909256
8.46501013	5.776861259	2.917638172
7.687205871	5.360776101	2.743387049
8.563762742	5.499303701	2.66177901
8.143237053	5.572854457	2.819553599
8.705419617	6.206183272	3.216054648
9.403480882	7.201441439	3.865987261
8.243824167	5.606721288	2.825580029
10.24312363	7.611919259	4.029799313
8.889722442	6.335441926	3.282430121
8.239757345	6.016562839	3.157538202
8.843597724	6.689247402	3.57100231
7.539186422	5.246370517	2.68146928
8.699506589	6.230590309	3.236812089

9.342758147	7.35295663	3.993520377
8.479146502	5.672216286	2.827793309
8.12503968	5.756704891	2.972928691
8.571545152	5.772827487	2.890902541
8.662685669	6.316683624	3.312714144
8.509662831	6.041457275	3.123513647
8.158050141	3.775098727	0.970985324
8.774354717	6.64702872	3.550951633
8.314216662	5.882129104	3.035211278
8.533064959	5.820789843	2.939023647
8.013555216	4.981254541	2.34736448
8.251297752	5.61634422	2.83188718
8.015788015	5.306170936	2.626316337
8.854668565	6.382225129	3.326915238
8.07667694	6.314620939	3.42021052
7.886095675	4.981481707	2.379669095
7.928912302	5.783837238	3.033861813
7.848304511	4.386032695	1.840552227
7.497811194	5.280721428	2.717950975

Differences between MRI and RetinaFit results

Differences between the calculated y value at each fixed x value for each subject is listed below.

Subject	30 degrees eccentricity from fovea	20 degrees eccentricity from fovea	10 degrees eccentricity from fovea
1	1.4281	0.6859	0.2660
2	2.5433	0.5081	-0.0594
3	5.6457	1.7276	0.4585
4	1.5875	1.3127	0.7399
5	1.4242	1.4558	0.8995
6	-0.5013	0.9464	0.9665
7	2.0916	0.7871	0.2031
8	2.9553	2.5221	1.4135
9	2.5558	1.4776	0.6709
10	1.1229	1.1362	0.6996
11	1.6370	1.4013	0.7995
12	3.8191	0.6048	-0.2152
13	2.2747	0.8897	0.2618
14	6.0638	1.1006	0.0038
15	5.1363	5.3239	3.5460
16	-1.4761	2.6264	
17	4.6388	4.0353	2.3071
18	0.7657	2.0775	1.6707
19	2.2015	1.8313	1.0234
20	3.9274	1.3665	0.4131
21	0.5359	0.4356	0.2418

22		1.2547	0.0197
23	-1.0622	1.6841	1.7007
24	2.0242	0.4096	-0.0701
25	2.1502	1.8507	1.0568
26	1.2033	1.0973	0.6491
27	5.3682	0.8889	-0.0695
28	2.9410	1.1987	0.3975
29	1.7402	-1.3941	-1.8623
30	2.1700	3.3375	2.4158
31	0.7251	1.6129	1.2278
32	2.1545	0.7912	0.2052
33	1.6831	0.0780	-0.2979
34	1.1561	0.2338	-0.0454
35	0.4577	1.6603	1.5083
36	1.0066	0.8803	0.5026
37	1.7046	0.1521	-0.1509
38	1.1661	0.1977	-0.0973
39	1.5451	1.1526	0.6114
40	2.3404	-0.3775	-0.8362
41	0.9497	0.9194	0.5501
42	2.0450	1.2654	0.5931
43	1.6743	1.1463	0.9293

### Case Study RC

Case study RC was a 45 year old highly anisomyopic male subject. MSEs were R: -19.76D L:-2.75D, and thus helped demonstrate an extreme case of myopia in the right eye while allowing the left eye to act as a control. Ocular biometric data for subject RC are listed in the table below.

Eye	Axial length	Corneal curvature	A/C depth
Right	27.87	7.32@101/7.29@11	3.50
Left	21.93	7.38@7/ 7.12@97	3.28

**Table 36 Biometry data for subject RC measured using the Zeiss IOL Master (in mm)**

### Results

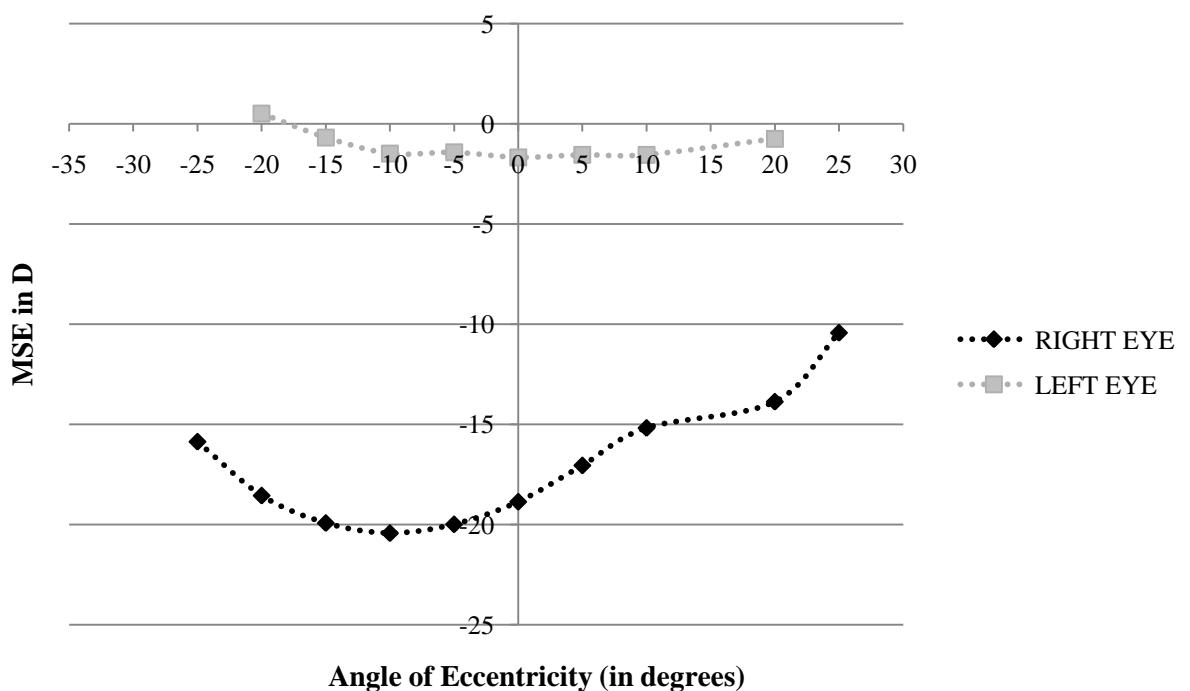


**Figure 131 Peripheral refraction MSE results for subject RC**

Consistent with the main study the nasal aspect was shown to be more myopic than the temporal.

### Case Study JP

Case Study JP was a 49 year old highly myopic subject. MSEs were R:-15.50d L:-14.37D. Ocular biometric data for subject JP is listed in the table below

Eye	Axial length	Corneal curvature	A/C depth
Right	28.13	7.48@175/7.35@85	3.86
Left	28.78	7.61@163/ 7.28@86	3.72

**Table 37 Ocular biometry data for subject JP (in mm)**

In addition to taking peripheral refraction measurements as taken in all subjects, peripheral refractive measures were also taken with soft contact lenses in situ.

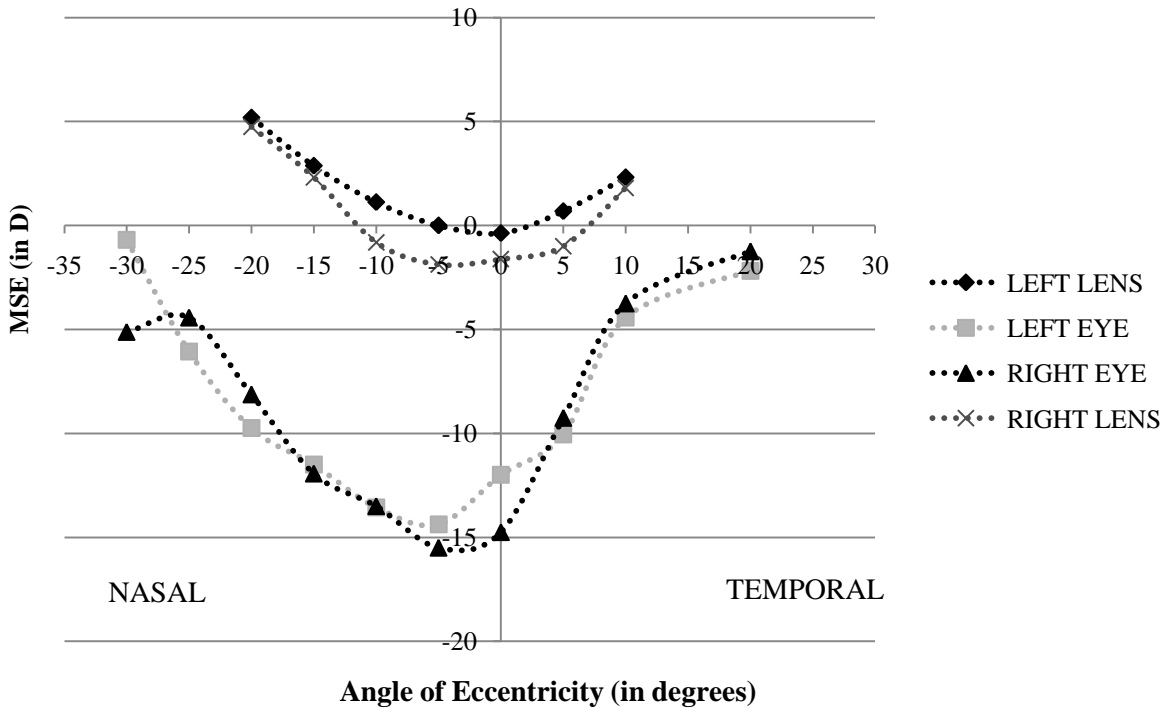


**Figure 132 MSE results for subject JP, with and without contact lenses in situ**

Both eyes showed similar nasal-temporal asymmetries. The nasal region appeared to be more myopic, which is consistent with results from the main peripheral refraction study. A similar asymmetry between the nasal and temporal regions was retained with the contact lenses in situ. As shown on the graph measurements, particularly with the contact lenses in situ, were difficult to obtain thus they do not extend to 30°. Of particular note is the relative peripheral hyperopic defocus with the contact lens in situ. This subject suffered from pathological myopia in the form of a longstanding posterior staphyloma.

APPENDIX 8: VISUAL FIELDS

Mean maximum sensitivity plot responses per quadrant (Right eyes  $n=40$ )

Subj	Inf	Sup	Temp	Nasal	Inf Temp	Inf Nasal	Sup Temp	Sup Nasal
1	31.21	32.37	33.16	32.29	32.36	31.33	32.68	32.61
2	32.58	32.53	32.05	33.24	32.05	32.83	32.37	33.11
3	30.53	31.58	31.89	31.71	31.26	30.56	31.84	32.00
4	31.11	31.26	32.32	32.82	31.58	31.94	31.68	32.22
5	30.05	31.16	30.63	30.88	30.37	30.33	30.79	31.22
6	30.05	32.89	31.68	32.82	30.74	31.11	32.53	33.00
7	29.47	30.95	31.11	31.82	30.68	29.89	30.47	32.22
8	29.42	30.63	31.16	31.06	30.26	29.83	30.95	31.17
9	28.68	29.68	31.53	30.82	30.00	29.61	30.53	30.50
10	29.21	30.32	30.53	30.35	29.84	30.11	30.11	30.33
11	31.95	32.89	32.68	32.82	32.32	32.17	32.79	33.06
12	28.89	30.21	30.21	31.24	29.11	29.78	30.37	31.22
13	30.63	31.89	32.21	32.35	31.53	30.78	31.74	33.00
14	28.89	31.32	30.58	31.12	29.68	29.67	31.32	31.17
15	30.79	30.05	30.95	30.59	31.00	30.72	30.32	30.33
16	30.74	31.42	31.84	31.65	31.42	30.67	31.84	31.67
17	28.53	30.32	30.16	30.47	29.42	28.72	30.42	30.83
18	28.84	31.84	30.79	30.94	29.84	29.22	31.68	31.61
19	30.00	31.00	31.05	31.76	30.21	30.67	31.32	31.56
20	28.68	29.68	30.63	28.94	29.32	29.11	30.53	29.00
21	29.11	31.74	30.95	31.53	30.32	29.78	30.95	32.22
22	30.79	29.74	31.26	31.76	31.32	30.94	30.21	31.00
23	27.63	30.26	29.05	29.41	28.05	27.89	30.00	30.39

24	30.53	31.26	30.79	31.12	30.63	30.61	31.26	31.17
25	28.53	31.05	30.32	31.35	29.21	29.28	31.05	31.61
26	29.95	31.26	31.42	31.29	30.95	30.00	31.37	31.56
27	29.00	31.16	30.84	31.65	29.89	30.06	30.95	31.67
28	28.37	31.21	30.47	31.82	28.89	30.00	30.95	31.94
29	29.47	31.32	31.21	31.41	31.11	29.61	31.00	31.61
30	31.00	32.42	31.84	32.12	31.32	31.28	32.16	32.61
31	28.95	30.95	32.00	31.65	31.00	29.61	31.32	31.50
32	28.37	31.42	29.53	30.71	28.58	29.00	30.89	31.50
33	30.05	31.53	31.16	32.71	30.05	31.33	31.79	32.17
34	29.42	32.00	31.26	32.18	30.84	29.72	31.84	32.33
35	30.63	32.68	32.68	31.29	31.26	30.89	33.05	32.11
36	29.32	30.89	31.05	31.71	30.47	29.94	30.68	31.78
37	29.89	31.58	30.16	30.82	30.37	29.61	30.68	31.78
38	31.21	32.16	32.16	32.29	31.95	31.17	32.11	32.56
39	30.58	31.47	31.42	30.82	31.11	30.67	31.58	30.94
40	29.74	30.63	30.42	30.88	29.42	30.83	31.00	30.39

Mean total deviation plot results per quadrant (Right eyes  $n=40$ )

Subj	Inf Nasal	Inf Temp	Sup Temp	Sup Nasal	Inf	Sup	Temp	Nasal
1	0.89	1.68	1.26	0.78	1.33	0.78	1.84	0.59
2	1.67	1.00	0.42	0.89	2.11	0.61	0.21	1.00
3	0.50	0.89	0.79	0.56	0.94	0.39	0.89	0.47
4	0.67	0.32	-0.11	-0.06	0.61	-0.61	0.42	0.41
5	-0.61	-0.79	-0.68	-0.78	-0.33	-0.50	-0.95	-1.06
6	-1.44	-1.95	-0.11	-0.33	-1.94	0.17	-1.26	-0.71
7	-0.67	-0.11	-0.89	0.56	-0.67	-0.39	-0.32	0.12
8	-1.44	-0.95	-0.84	-1.11	-1.00	-1.28	-0.63	-1.29
9	-0.61	-0.37	-0.42	-1.06	-0.72	-1.67	0.58	-0.59
0	-2.11	-1.42	-1.63	-2.00	-1.39	-1.44	-1.37	-3.06
11	1.83	1.84	1.53	1.44	2.22	1.50	1.47	1.35
12	-0.78	-1.68	-1.05	-0.72	-1.11	-1.39	-1.21	-0.59
13	-0.50	0.16	-0.11	0.56	-0.11	-0.06	0.26	0.00
14	-1.28	-1.37	-0.32	-1.06	-1.50	-0.50	-1.00	-1.00
15	0.06	0.26	-1.16	-1.67	0.61	-1.61	-0.37	-1.29
16	-0.61	0.21	0.00	-0.67	-0.06	-0.61	0.05	-0.65
17	-1.00	-0.47	-0.42	-0.44	-0.67	-0.78	-0.32	-0.65
18	-0.89	-0.68	0.37	-0.11	-0.83	0.39	-0.37	-0.47
19	-0.11	-0.74	-0.11	-0.33	-0.33	-0.44	-0.42	-0.18
20	0.67	0.58	-0.63	-1.56	0.94	-1.22	-0.11	-0.71
21	-0.33	0.21	0.05	0.39	-0.39	0.56	0.26	-0.18
22	0.39	0.37	-1.11	-0.83	0.39	-1.72	-0.05	0.00
23	-1.39	-1.53	-0.42	-0.61	-1.17	-0.28	-1.21	-1.35
24	-0.11	-0.26	-0.32	-0.67	0.56	-0.22	-0.74	-0.82
25	-1.94	-1.68	-0.47	-0.44	-2.06	-0.67	-1.11	-0.82

26	-0.89	-0.32	-0.42	-0.67	-0.33	-0.72	-0.37	-0.82
27	-1.22	-0.74	0.05	-1.06	-1.22	-0.94	-0.11	-0.76
28	-0.06	-1.63	-0.11	0.33	-1.28	0.00	-0.74	0.47
29	-1.39	-0.16	-0.47	-0.50	-1.17	-0.33	-0.37	-0.71
30	0.78	0.58	1.00	1.00	1.11	1.11	0.58	0.65
31	-0.83	0.26	0.05	-0.33	-0.89	-0.56	0.74	-0.12
32	-1.78	-2.37	-0.74	-0.44	-1.72	-0.44	-2.00	-1.00
33	1.00	-0.26	0.47	0.61	0.56	0.22	0.16	1.18
34	-0.94	-0.11	0.37	0.33	-0.78	0.44	-0.21	0.29
35	1.22	1.47	2.47	0.89	1.50	1.89	2.16	0.29
36	0.67	0.26	0.63	0.44	0.11	1.00	0.26	0.53
37	-0.61	0.16	-0.21	0.44	0.22	0.61	-0.53	-0.59
38	-0.83	-1.37	-0.63	-0.06	-0.72	-0.39	-1.26	-0.47
39	0.78	0.84	0.79	-0.39	1.28	0.39	0.68	-0.35
40	-0.39	-1.21	-0.37	-1.11	-0.72	-0.83	-1.05	-0.65

Surface area (in mm<sup>2</sup>)

For Visual fields data (Right eyes)

Subj	Nasal	Temp	Sup	Inf	Sup Temp	Inf Nas	Sup Nas	Inf Temp
1	189.3	229.4	203.5	227.4	205.0	233.9	226.4	220.5
2	201.5	220.4	249.2	268.3	236.6	225.4	234.9	222.2
3	323.6	320.7	280.1	320.2	275.9	346.5	274.0	337.9
4	225.8	245.9	242.9	225.2	251.3	237.1	224.5	223.6
5	225.2	204.6	229.8	252.7	221.0	254.7	223.9	217.9
6	219.9	235.4	236.0	237.2	241.3	229.1	221.7	226.6
7	245.9	261.7	275.6	257.3	273.1	257.4	252.8	251.0
8	219.7	213.8	231.8	212.6	242.3	270.2	248.6	174.0
9	205.5	208.7	200.0	190.6	200.2	198.4	206.7	197.9
10	216.7	216.1	217.0	205.2	222.1	220.0	221.0	206.0
11	200.6	227.0	208.2	218.2	226.5	213.3	194.4	220.2
12	226.4	251.1	266.0	259.9	260.6	236.5	273.1	261.6
13	211.2	198.6	228.2	202.2	216.3	207.8	222.2	199.3
14	243.2	185.1	199.8	188.6	227.8	236.4	247.8	231.9
15	258.0	268.2	245.9	249.9	275.4	302.9	251.5	284.3
16	213.2	235.4	232.1	217.1	240.6	228.5	201.3	219.0
17	263.8	235.2	229.3	252.5	226.5	274.7	248.1	238.2
18	205.0	203.3	225.0	240.9	216.0	222.6	227.8	222.7
19	218.5	218.7	233.2	229.3	212.3	192.2	222.8	189.1
20	166.1	168.8	163.7	199.3	165.1	199.2	164.8	188.6
21	195.3	192.6	183.6	173.0	193.8	194.0	185.1	172.2
22	225.8	245.9	241.0	228.3	219.5	286.6	220.5	251.6
23	298.7	238.4	262.9	242.4	243.4	284.4	281.7	241.6
24	200.7	221.9	245.8	225.9	245.2	215.0	213.0	221.7

25	183.2	194.0	207.1	214.7	198.3	183.1	197.7	187.5
26	188.3	249.9	208.7	238.9	230.3	233.1	221.5	248.8
27	238.7	244.4	228.0	284.3	236.4	281.4	223.3	261.0
28	205.9	194.4	198.6	211.0	196.5	215.6	203.0	196.8
29	202.0	184.4	241.2	194.8	215.2	206.2	208.6	192.9
30	174.5	184.8	160.1	194.9	163.2	190.1	152.8	194.5
31	226.8	257.5	240.8	227.1	233.9	226.8	215.0	215.3
32	243.4	279.2	270.5	272.2	293.7	267.5	250.7	286.4
33	169.2	178.8	179.0	203.8	177.1	186.1	173.3	186.1
34	206.1	223.2	229.1	220.5	240.7	211.7	228.0	188.0
35	149.0	177.8	206.8	164.8	194.6	161.5	175.0	175.9
36	213.2	210.8	256.8	266.3	228.0	251.6	225.4	236.6
37	172.4	214.2	256.6	208.3	234.2	180.1	219.0	219.4
38	183.8	200.0	224.8	210.9	211.6	203.2	208.6	197.0
39	177.8	181.8	229.1	209.4	211.7	181.8	209.5	209.2
40	192.0	228.2	248.3	236.1	267.5	217.0	201.0	219.5

Interval Variance for visual fields subjects (Right eyes) derived by multiplying the standard deviation of the data in the posterior 25% of each quadrant by 1.96

Subj	Nasal	Temp	Sup	Inf	Sup Temp	Inf Nasal	Sup Nasal	Inf Temp
1	5.18	4.91	5.18	4.91	5.25	4.88	5.17	5.13
2	5.08	5.94	5.94	5.45	6.08	5.15	5.40	5.70
3	6.20	6.85	6.48	5.90	6.49	5.80	6.25	6.18
4	5.11	5.77	6.00	5.40	5.09	5.23	5.38	5.57
5	5.04	5.74	5.83	5.42	5.85	5.21	5.34	5.65
6	5.07	5.65	5.60	5.11	5.74	5.07	5.32	5.42
7	5.36	6.06	5.69	5.38	5.97	5.30	5.49	5.65
8	5.09	5.61	5.79	5.34	5.97	5.22	5.25	5.42
9	5.20	5.82	5.55	4.99	5.77	4.93	5.37	5.44
10	5.02	5.92	5.86	5.43	6.13	5.10	5.31	5.62
11	4.90	5.40	5.37	5.10	5.48	4.97	5.04	5.27
12	5.33	6.04	6.26	5.65	6.13	5.39	6.24	5.97
13	4.88	5.64	5.65	5.23	5.93	5.10	5.22	5.30
14	4.83	5.30	5.62	5.29	5.64	5.34	5.29	5.64
15	5.55	5.82	5.54	5.42	5.92	5.49	5.44	5.57
16	5.06	5.63	5.74	5.26	5.96	5.28	5.13	5.23
17	5.22	6.12	5.55	5.04	5.97	5.02	5.33	5.49
18	4.97	5.44	5.49	5.21	5.66	5.00	5.09	5.40
19	5.19	5.43	5.29	5.36	5.46	4.97	5.04	5.18
20	4.49	5.08	5.30	4.96	5.43	4.58	4.94	4.95
21	4.83	5.13	4.85	4.67	5.19	4.79	4.79	4.75
22	5.05	5.77	5.91	5.40	5.75	4.87	2.77	5.33
23	5.76	5.87	5.74	5.55	5.86	5.54	5.95	5.68
24	5.20	5.79	6.03	5.50	6.22	5.07	5.35	5.30
25	4.69	5.40	5.51	4.80	5.74	4.60	5.06	4.94

26	5.13	6.00	5.77	5.06	5.88	5.10	5.46	5.58
27	5.09	5.74	5.98	5.32	6.13	5.26	5.46	5.51
28	5.12	5.48	5.18	4.85	5.63	4.93	5.06	5.03
29	4.76	5.68	5.83	4.75	6.13	4.71	5.41	5.10
30	4.73	5.41	4.69	4.70	5.29	4.87	4.64	5.13
31	5.43	6.12	5.75	5.23	6.14	5.24	5.45	5.54
32	5.40	5.68	5.57	5.29	6.04	5.30	5.34	5.43
33	4.62	5.05	4.95	4.57	5.10	4.41	4.64	5.13
34	5.63	4.93	5.51	5.08	5.51	4.62	5.12	5.01
35	4.44	4.82	4.76	4.77	5.07	4.51	4.50	4.68
36	5.09	5.83	5.36	5.47	6.04	5.22	5.32	5.56
37	4.70	5.71	5.48	5.15	5.86	4.79	4.99	5.42
38	4.65	5.46	5.76	5.16	5.79	4.71	5.10	5.37
39	5.00	5.24	5.84	5.24	5.25	5.01	5.38	5.38
40	4.87	5.19	5.79	4.66	5.69	5.13	5.19	5.41

Visual fields sensitivity per quadrant for left eyes  $n=42$  (Sita Standard 30-2)

1	Inf	Sup	Temp	Nasal	Inf Temp	Inf Nas	Sup Temp	Sup Nas
2	30.79	30.58	31.79	31.53	31.37	31.06	31.21	31.00
3	30.53	31.63	31.84	32.59	31.53	30.94	31.47	32.56
4	31.05	31.42	30.95	32.00	31.05	31.22	31.05	32.06
5	31.16	31.32	31.58	32.65	31.37	31.39	31.42	32.44
6	28.95	31.32	29.89	31.29	29.26	29.78	30.74	31.61
7	29.42	31.79	31.84	31.94	30.58	30.50	32.26	31.56
8	28.42	29.84	29.84	31.06	29.42	29.00	29.63	31.00
9	27.89	30.68	29.68	30.71	28.47	28.61	30.53	31.28
10	27.84	29.79	29.68	30.06	28.37	28.78	30.26	29.89
11	29.37	30.42	30.63	31.53	29.68	30.50	31.05	30.61
12	30.84	32.37	31.26	33.47	31.11	31.44	32.47	32.78
13	27.95	31.11	30.63	30.94	29.95	28.44	30.47	31.67
14	30.63	31.89	31.53	32.00	30.95	31.33	31.47	32.28
15	30.05	32.74	31.26	32.53	30.74	31.50	31.47	32.83
16	28.58	30.68	30.05	31.00	29.16	29.89	29.95	31.28
17	28.74	31.37	30.47	31.71	29.84	29.56	30.68	32.11
18	29.42	31.16	30.74	31.24	29.63	30.78	31.16	30.94
19	27.84	29.89	29.21	29.94	28.84	28.17	29.37	30.44
20	30.05	30.53	30.21	32.12	29.95	30.78	30.37	31.72
21	28.89	29.32	30.00	29.35	29.58	29.11	29.47	29.39
22	30.26	30.63	31.37	31.82	30.89	30.67	30.95	31.50
23	30.00	30.79	29.47	32.06	29.68	30.72	29.89	31.94
24	27.84	31.32	29.00	32.12	28.53	29.11	30.53	31.94
25	29.58	30.74	30.21	30.76	29.95	30.00	30.37	30.94

26	27.42	31.74	30.21	30.59	29.26	27.94	31.00	31.67
27	29.53	30.84	29.84	31.65	29.89	30.00	30.05	31.83
28	29.00	30.42	30.79	31.29	29.68	29.78	30.37	31.61
29	28.47	31.37	31.63	30.88	29.68	29.44	31.47	31.72
30	27.53	30.68	31.26	31.29	29.68	29.00	30.74	31.22
31	30.47	32.05	31.26	31.65	31.16	30.33	31.42	32.50
32	29.16	31.11	30.74	31.82	30.53	29.22	30.89	32.06
33	28.79	30.95	29.53	31.94	29.26	29.89	30.47	31.44

Visual fields sensitivity Sita Standard 10-2 (in dB)

<b>Subj</b>	<b>1</b>	<b>1</b>	<b>2</b>	<b>2</b>	<b>3</b>	<b>3</b>	<b>4</b>	<b>4</b>	<b>5</b>	<b>5</b>	<b>6</b>	<b>6</b>	<b>7</b>	<b>7</b>	<b>8</b>	<b>8</b>	<b>9</b>	<b>9</b>
<b>Location</b>	R	L	R	L	R	L	R	L	R	L	R	L	R	L	R	L	R	L
<b>1</b>	34	36	32	32	33	32	31	31	33	31	31	33	33	33	32	31	29	30
<b>2</b>	33	33	31	33	32	34	32	32	31	31	34	31	32	32	32	31	31	27
<b>3</b>	33	38	34	33	34	31	31	31	30	31	34	33	31	32	32	32	32	32
<b>4</b>	33	32	33	33	33	34	33	31	33	33	31	31	32	33	31	33	30	31
<b>5</b>	33	32	32	33	32	32	31	33	33	34	32	32	34	34	33	31	33	31
<b>6</b>	33	34	32	32	32	34	31	32	30	33	32	34	32	33	32	31	32	31
<b>7</b>	34	33	33	32	34	31	31	34	31	33	33	33	33	33	31	33	32	33
<b>8</b>	33	33	32	32	33	33	28	32	32	32	33	32	31	31	31	32	33	31
<b>9</b>	32	34	34	33	34	33	32	31	34	34	32	32	32	32	33	34	34	32
<b>10</b>	34	35	33	33	33	34	32	32	31	34	33	32	33	31	33	33	33	34
<b>11</b>	35	33	34	35	34	34	31	33	32	34	34	34	33	32	34	32	34	33
<b>12</b>	34	34	35	35	33	34	33	32	32	33	35	35	34	33	33	32	35	34
<b>13</b>	33	33	33	33	33	34	34	31	32	32	33	34	33	31	33	32	35	33
<b>14</b>	34	33	33	34	33	33	33	33	31	32	34	33	33	31	33	33	33	33
<b>15</b>	34	32	33	33	34	34	30	32	31	33	34	34	34	31	32	32	32	32
<b>16</b>	34	36	33	33	34	33	33	33	33	32	32	35	34	33	33	32	29	31
<b>17</b>	34	34	35	35	33	34	33	32	33	32	34	32	35	37	34	32	33	34
<b>18</b>	35	34	34	33	34	36	33	33	32	33	34	34	33	33	35	33	34	35
<b>19</b>	35	34	35	33	36	35	33	34	34	33	34	35	33	33	35	34	35	35
<b>20</b>	35	33	34	34	34	36	33	33	34	33	34	34	34	32	34	34	34	35

<b>21</b>	34	33	34	33	35	35	33	32	34	34	34	36	32	32	35	34	34	34
<b>22</b>	33	34	34	34	34	33	33	33	33	33	35	35	33	35	35	34	35	35
<b>23</b>	35	34	35	35	32	34	34	33	33	33	33	34	34	34	33	34	34	34
<b>24</b>	34	34	34	33	33	33	31	32	34	34	31	32	36	31	32	34	33	32
<b>25</b>	33	35	33	33	33	31	34	33	33	32	34	33	32	33	34	31	32	35
<b>26</b>	35	33	33	33	34	32	33	32	34	33	33	33	34	33	35	33	33	33
<b>27</b>	34	35	35	35	33	34	34	33	33	33	34	35	35	34	32	33	35	35
<b>28</b>	35	34	34	35	33	35	35	35	34	34	36	33	35	34	36	34	34	34
<b>29</b>	34	35	35	35	35	35	34	33	34	33	36	33	36	35	36	34	35	34
<b>30</b>	35	35	35	34	33	35	33	34	36	36	35	35	34	35	36	36	36	35
<b>31</b>	34	34	34	31	36	35	35	34	35	35	35	36	37	34	34	36	36	34
<b>32</b>	34	33	34	33	34	35	34	34	37	34	34	36	34	35	33	35	36	33
<b>33</b>	35	34	33	32	34	35	32	34	33	34	34	32	33	33	32	33	33	34
<b>34</b>	34	32	35	32	33	34	33	34	31	32	34	33	33	33	33	32	32	31
<b>35</b>	33	34	35	35	32	33	31	32	32	33	34	32	32	32	34	33	33	32
<b>36</b>	34	33	33	34	33	33	32	34	33	34	35	34	35	33	35	33	33	33
<b>37</b>	34	35	34	35	33	34	34	33	35	33	34	34	35	33	34	35	35	34
<b>38</b>	33	34	36	34	32	35	35	34	34	34	36	32	35	35	36	34	38	36
<b>39</b>	34	35	36	36	34	36	34	33	35	35	34	32	35	37	36	33	353	36
<b>40</b>	34	36	36	35	33	35	35	33	34	36	34	36	36	36	36	36	6	36
<b>41</b>	36	35	35	34	36	36	36	33	35	34	36	35	34	35	33	36	36	35
<b>42</b>	36	34	34	35	34	36	36	33	35	33	34	35	33	34	33	34	34	34
<b>43</b>	34	34	34	33	34	33	33	34	34	32	34	34	33	34	32	32	34	32
<b>44</b>	34	32	33	33	33	33	34	34	32	32	34	35	32	32	34	34	31	32
<b>45</b>	35	33	34	35	34	34	32	32	33	33	33	34	33	32	34	32	34	33

<b>46</b>	34	34	35	34	33	36	32	34	34	32	34	33	33	32	34	33	35	35
<b>47</b>	35	35	35	35	34	35	32	35	35	33	35	33	33	33	35	33	34	34
<b>48</b>	35	34	35	35	34	34	34	35	34	34	34	34	34	33	34	34	34	34
<b>49</b>	34	34	34	34	35	36	36	33	34	35	34	36	35	34	36	34	34	35
<b>50</b>	36	35	35	35	35	35	35	34	34	35	35	34	35	34	35	35	35	34
<b>51</b>	34	34	34	34	34	34	34	34	33	34	34	33	34	34	34	34	33	33
<b>52</b>	36	37	32	34	33	34	32	34	34	34	34	33	33	37	34	34	32	30
<b>53</b>	37	34	34	33	32	36	34	32	32	31	32	34	34	32	34	31	34	33
<b>54</b>	34	33	34	33	33	34	33	34	33	32	33	33	34	31	33	32	34	33
<b>55</b>	36	34	33	34	33	34	33	34	34	34	34	33	35	33	34	35	33	35
<b>56</b>	36	35	34	33	32	33	34	33	33	33	33	34	35	36	33	35	32	33
<b>57</b>	35	33	33	33	33	33	34	32	34	34	33	34	32	35	33	35	33	34
<b>58</b>	34	34	34	34	34	34	34	33	33	32	34	35	32	34	34	34	34	33
<b>59</b>	33	33	35	33	35	33	33	32	33	34	32	34	34	33	33	33	32	33
<b>60</b>	35	34	35	34	33	34	32	34	34	34	32	33	33	33	34	32	31	33
<b>61</b>	34	32	33	33	34	33	33	33	32	31	32	33	30	33	32	33	34	33
<b>62</b>	33	33	35	34	33	34	30	33	33	33	32	31	31	32	33	33	33	32
<b>63</b>	34	35	33	32	33	34	32	32	34	32	32	33	32	33	32	33	33	32
<b>64</b>	33	34	33	32	32	33	32	31	32	32	34	33	33	32	32	31	34	34
<b>65</b>	33	33	35	33	33	34	32	31	32	34	32	32	33	31	34	33	33	32
<b>66</b>	33	33	34	32	33	32	34	31	32	34	32	32	34	35	36	34	32	32
<b>67</b>	33	32	33	31	33	34	29	31	32	33	31	33	34	33	33	32	33	31
<b>68</b>	34	30	33	31	32	32	31	30	33	32	33	33	33	33	34	34	33	32

APPENDIX 9: MFERG RING CONFIGURATION RESPONSES

Ring 1						Ring 2					
n1		p1		n2		n1		p1		n2	
ms	nv/deg <sup>2</sup>	ms	nv/deg <sup>2</sup>	ms	nv/deg <sup>2</sup>	ms	nv/deg <sup>2</sup>	Ms	nv/deg <sup>2</sup>	ms	nv/deg <sup>2</sup>
16.3	-48.1	29.6	88.1	48.8	-50.6	12.5	-18.8	28.3	38.1	43.3	-23.1
13.3	-45.6	27.5	88.8	50.4	-44.4	14.2	-19.4	27.1	39.4	43.3	-26.3
14.6	-53.1	28.3	83.8	44.2	-1.3	14.2	-24.4	28.3	44.4	42.9	-36.3
14.2	-38.1	26.7	65.0	45.8	-41.9	15.8	-20.6	27.5	35.0	41.3	-19.4
15.8	-66.3	29.2	153.1	43.8	-83.1	15.0	-32.5	29.2	66.9	45.4	-55.6
15.8	-59.4	27.5	87.5	50.0	-51.9	11.3	-16.9	27.5	32.5	42.1	-24.4
14.2	-41.9	32.1	75.0	49.2	-53.1	15.4	-18.8	29.2	33.8	43.8	-20.0
14.2	-86.3	29.2	137.5	44.2	-103.8	15.8	-38.8	27.5	63.8	42.5	-47.5
15.8	-41.3	27.9	68.8	45.8	-39.4	14.6	-22.0	27.1	31.9	42.9	-25.0
13.8	-41.3	27.1	74.4	41.3	-66.9	11.3	-20.0	26.3	44.4	41.3	-31.3
15.8	-40.0	27.1	67.5	48.3	4.4	15.0	-19.4	28.8	30.6	42.1	-21.3
13.3	-30.0	28.3	43.8	55.0	-21.3	14.2	-13.8	25.8	23.8	45.0	-21.3
15.4	-55.0	26.7	91.9	45.4	-58.1	14.2	-20.0	27.1	38.8	41.3	-28.8
15.4	-41.3	31.7	86.3	44.6	-51.3	13.3	-19.4	29.2	36.3	43.3	-26.3
18.3	-39.4	30.0	93.8	43.3	7.5	16.7	-18.8	30.4	32.5	44.2	-21.9
15.0	-52.5	29.2	128.8	44.6	-98.1	13.8	-28.1	27.1	50.6	42.9	-33.8
14.6	-47.5	30.8	165.0	47.9	-111.3	16.3	-25.0	30.4	61.3	45.0	-43.8
11.7	-45.0	26.7	72.5	43.3	56.3	15.8	-17.5	24.2	31.3	45.0	-28.8
15.4	-46.9	27.5	106.3	46.7	-54.4	14.2	-31.3	26.3	48.1	42.9	-32.5
17.1	-68.1	30.0	105.0	51.3	3.8	16.3	-31.3	29.2	41.9	43.8	-33.1
15.8	-36.9	27.9	80.6	43.3	-48.1	16.3	-18.8	27.1	36.3	43.8	-30.0
16.7	-46.5	30.4	81.9	46.3	-1.3	14.6	-18.1	29.2	35.0	44.2	-21.9
13.3	-68.1	30.4	129.4	49.6	-84.4	15.0	-28.8	29.6	49.4	46.7	-37.5

Ring 3						Ring 4					
n1		p1		n2		n1		p1		n2	
ms	nv/deg <sup>2</sup>	ms	nv/deg <sup>2</sup>	ms	nv/deg <sup>2</sup>	ms	nv/deg <sup>2</sup>	Ms	nv/deg <sup>2</sup>	ms	nv/deg <sup>2</sup>
13.8	-11.3	28.8	18.1	42.9	-15.0	15.4	-10.6	28.0	14.4	41.3	-10.0
15.0	-11.9	28.3	21.3	42.5	-16.3	14.6	-8.8	29.6	14.4	42.5	-12.5
13.8	-12.5	28.3	25.6	42.1	-23.1	14.6	-9.4	28.8	15.0	42.1	-15.0
13.8	-13.1	26.3	23.8	40.4	-15.0	13.8	-9.4	29.2	13.1	41.6	-10.0
15.8	-20.6	28.3	33.8	42.9	-36.9	15.0	-16.9	28.8	23.1	43.8	-19.4
14.2	-11.3	27.1	18.8	41.3	-15.6	12.9	-8.1	28.3	10.6	40.8	-10.6
13.3	-9.4	27.9	16.9	40.4	-13.1	13.8	-6.3	27.1	9.4	40.4	-10.0
15.0	-18.8	29.2	32.5	41.7	-28.8	15.0	-12.5	28.3	26.3	42.5	-17.5
14.6	-13.8	29.6	20.0	42.5	-15.6	14.2	-9.4	29.6	15.0	42.1	-11.3
11.7	-8.8	25.8	21.3	39.6	-18.8	12.5	-6.3	26.3	11.3	40.8	-10.0
14.6	-12.5	29.6	20.6	41.7	-13.8	15.4	-11.3	28.8	14.4	42.5	-11.9
14.2	-10.0	27.5	16.3	41.7	-11.3	14.2	-6.3	28.3	10.0	40.8	-10.0
14.2	-14.4	27.1	25.0	40.4	-19.4	14.6	-12.5	28.3	16.9	41.3	-14.4
13.8	-11.3	29.6	17.5	42.5	-15.6	15.8	-9.4	29.6	13.8	41.7	-11.3
15.8	-12.5	29.6	18.8	43.3	-17.5	13.3	-8.8	30.8	12.5	44.2	-10.6
14.2	-15.0	27.9	26.5	42.1	-20.6	14.2	-10.0	27.9	16.9	41.7	-15.0
16.7	-16.3	29.2	28.8	43.3	-23.8	16.3	-11.3	31.3	16.3	43.3	-11.3
15.8	-11.3	25.8	18.8	40.0	-18.8	13.3	-11.3	27.5	15.0	39.2	-8.8
15.0	-16.9	27.5	26.9	40.4	-19.4	13.8	-11.9	25.8	15.0	40.0	-11.3
15.0	-18.1	29.6	25.0	41.3	-18.8	14.2	-12.5	29.2	20.0	41.3	-13.1
12.9	-11.3	27.9	18.8	40.4	-14.4	14.6	-8.8	28.3	14.4	42.1	-11.9
15.4	-10.6	29.6	16.3	42.9	-14.4	14.2	-8.1	27.9	12.5	41.7	-9.4
16.3	-18.1	29.2	26.9	43.8	-22.5	15.8	-12.5	28.3	18.1	42.9	-14.4

Ring 5					Ring 6						
n1		p1		n2		n1		p1		n2	
ms	nv/deg <sup>2</sup>	ms	nv/deg <sup>2</sup>	ms	nv/deg <sup>2</sup>	ms	nv/deg <sup>2</sup>	ms	nv/deg <sup>2</sup>	ms	nv/deg <sup>2</sup>
14.2	-8.8	28.8	12.5	42.1	-10.0	14.2	-7.5	28.3	8.8	41.7	-7.5
15.4	-7.5	30.8	10.0	43.3	-10.6	15.4	-6.3	30.8	7.5	42.5	-6.9
15.0	-7.5	29.6	11.3	42.5	-10.0	15.4	-6.9	30.8	8.1	42.5	-7.5
15.4	-8.8	28.3	9.4	42.5	-8.1	14.6	-6.3	29.2	8.1	42.5	-6.9
15.0	-12.5	27.9	17.5	44.2	-15.0	15.0	-6.9	29.6	10.6	45.0	-9.4
13.3	-6.3	27.9	8.1	42.5	-6.9	14.2	-5.0	29.2	5.6	40.8	-5.6
11.7	-5.0	27.9	8.8	41.7	-6.3	13.8	-4.4	29.2	5.6	42.5	-6.3
15.0	-11.3	29.2	17.5	43.3	-15.0	14.2	-7.5	29.2	11.3	42.5	-8.8
14.6	-7.5	30.0	10.6	42.9	-8.8	15.0	-6.3	30.8	7.5	43.3	-7.5
14.2	-6.3	25.4	10.0	40.0	-6.9	11.7	-3.8	29.2	5.0	42.1	-5.6
15.0	-7.5	30.0	11.3	43.3	-9.4	15.8	-7.5	30.0	11.3	43.3	-10.0
14.2	-6.3	29.2	7.5	43.3	-8.8	14.2	-5.0	29.2	6.3	41.7	-6.3
14.6	-9.4	28.3	13.1	42.1	-11.3	14.6	-7.5	29.2	8.8	42.5	-8.8
15.4	-7.5	30.0	10.0	42.9	-8.1	15.0	-6.3	30.8	6.3	43.3	-6.3
16.3	-8.1	30.8	10.0	43.8	-8.1	16.3	-5.0	32.1	4.4	43.3	-5.0
15.0	-10.0	28.3	12.5	41.7	-10.6	15.0	-8.1	28.8	9.4	41.7	-8.1
17.5	-8.8	32.5	11.9	47.5	-11.3	17.5	-5.6	34.2	8.1	47.9	-8.1
15.0	-8.8	29.2	10.0	40.0	-7.5	12.5	-6.3	29.2	8.8	40.8	6.3
15.4	-10.0	29.2	11.9	42.9	-10.0	15.0	-8.1	25.8	11.3	42.1	-7.5
15.4	-10.0	30.0	13.8	41.7	-10.0	15.0	-5.6	30.0	7.5	41.3	-5.6
15.4	-8.1	28.8	10.6	42.1	-8.8	14.6	-6.3	28.8	8.8	42.5	-7.5
14.6	-6.9	30.4	8.1	42.5	-6.9	14.2	-5.6	30.4	8.1	42.1	-6.3
16.3	-11.3	30.0	12.5	43.8	-10.0	14.2	-7.5	30.0	10.0	42.9	-7.5

+Q Configuration responses

INFERIOR NASAL					INFERIOR TEMP						
n1		p1		n2		n1		p1		n2	
ms	nv/deg^2	ms	nv/deg^2	ms	nv/deg^2	ms	nv/deg^2	Ms	nv/deg^2	ms	nv/deg^2
14.6	-8.1	28.8	10.0	42.1	-8.1	16.1	-7.5	28.3	11.3	42.1	-8.8
15.8	-6.9	30.4	8.8	42.9	-8.1	15.8	-8.8	30.4	12.5	42.9	-10.6
14.2	-6.9	29.6	10.6	42.1	-10.0	15.4	-6.9	29.2	12.5	41.7	-10.6
14.2	-6.9	28.3	9.4	42.1	-6.9	15.0	-8.1	28.3	10.6	41.3	-8.1
15.4	-8.8	28.8	13.8	44.2	-11.3	15.8	-10.6	29.2	15.6	44.2	-13.8
13.8	-5.6	28.3	6.3	40.8	-6.9	12.5	-6.3	29.2	8.8	39.6	-6.9
14.2	-5.0	27.9	6.9	41.7	-6.3	13.3	-5.6	28.3	8.1	41.7	-7.5
15.0	-10.0	30.0	15.0	42.5	-11.3	15.8	-11.3	29.2	17.5	42.5	-12.5
15.0	-7.5	30.0	8.8	42.9	-7.5	14.2	-6.9	29.6	11.9	42.5	-8.8
12.9	-3.8	27.9	6.3	39.2	-5.0	15.0	-6.3	26.7	9.4	38.3	-7.5
15.4	-8.1	30.8	10.6	43.8	-9.4	15.8	-8.8	29.2	13.1	42.5	-11.3
13.3	-6.3	29.2	6.3	39.2	-3.8	15.8	-6.3	27.5	8.8	40.8	-7.5
13.3	-7.5	28.8	10.0	42.5	-8.8	15.0	-9.4	28.8	13.1	42.5	-12.5
15.0	-6.9	30.0	7.5	42.1	-6.3	15.8	-7.5	30.0	9.4	42.5	-9.4
13.8	-4.4	31.3	6.3	41.7	-5.0	15.4	-5.0	30.4	7.5	42.5	-5.6
14.6	-8.8	27.9	11.9	42.1	-8.8	15.0	-10.0	27.1	14.4	41.3	-11.3
17.5	-8.1	33.3	11.3	47.9	-8.8	15.8	-6.9	32.1	11.3	45.8	-0.6
13.3	-6.3	27.5	8.8	40.8	-7.5	15.8	-8.8	29.2	11.3	40.8	-8.8
13.8	-8.8	27.1	10.6	41.3	-8.1	15.4	-9.4	27.5	13.8	42.5	-9.4
12.5	-7.5	30.0	10.6	40.8	-6.9	15.4	-8.8	29.6	11.3	41.7	-9.4
14.2	-6.9	29.2	8.8	42.5	-8.1	12.9	-6.9	28.8	11.9	42.1	-9.4
15.0	-5.6	29.2	7.5	42.9	-5.6	14.6	-8.1	29.6	11.9	42.1	-8.8
15.4	-8.8	30.0	10.6	45.0	-8.1	15.4	-9.4	30.0	13.1	42.9	-11.3

SUPERIOR NASAL				SUPERIOR TEMP							
n1		p1		n2		n1		p1		n2	
ms	nv/deg^2	ms	nv/deg^2	ms	nv/deg^2	ms	nv/deg^2	ms	nv/deg^2	ms	nv/deg^2
13.8	-8.8	30.4	10.6	41.3	-8.1	14.6	-10.6	27.9	13.8	41.7	-10.6
14.2	-6.3	30.0	10.0	43.3	-9.4	15.8	-8.8	28.3	12.5	42.9	-11.3
14.2	-7.5	29.6	10.6	42.1	-9.4	15.0	-9.4	30.0	13.1	41.7	-11.3
13.8	-7.5	30.0	10.0	41.7	-7.5	15.0	-8.1	28.3	12.5	42.9	-9.4
15.0	-11.3	28.8	16.3	43.8	-14.4	15.0	-12.5	28.7	19.4	43.3	-15.6
12.1	-5.6	27.1	7.5	40.8	-6.9	15.0	-8.1	28.8	10.0	41.3	-8.8
13.8	-5.6	29.2	6.9	41.7	-6.9	12.5	-5.6	27.1	10.0	40.4	-8.1
12.5	-8.8	29.2	15.0	44.2	-13.8	15.8	-12.5	28.3	20.0	43.3	-15.0
15.0	-7.5	30.4	9.4	42.9	-8.1	14.6	-9.4	30.0	12.5	42.9	-10.6
12.5	-5.0	26.3	7.5	40.4	-6.3	12.1	-6.9	26.7	12.5	40.0	-8.8
15.8	-8.1	30.8	11.9	43.3	-8.8	15.4	-10.0	29.6	13.8	28.3	-12.5
14.2	-6.3	28.3	8.8	41.7	-8.8	15.0	-7.5	29.2	10.0	42.5	-10.0
14.6	-9.4	28.8	11.3	42.5	-11.3	14.2	-10.6	27.9	16.3	41.7	-12.5
15.0	-7.5	30.4	9.4	43.7	-7.5	16.3	-9.4	30.4	11.3	42.5	-9.4
12.5	-6.9	30.4	10.0	42.9	-9.4	15.4	-8.8	30.8	11.3	44.2	-9.4
12.9	-7.5	29.2	11.3	42.5	-11.3	13.8	-10.6	27.5	16.3	41.7	-11.9
17.5	-7.5	33.8	11.3	47.5	-9.4	17.5	-10.0	31.3	15.0	46.3	-13.1
15.8	-7.5	29.2	8.8	40.0	-6.3	15.8	-11.3	28.3	13.8	40.0	-10.0
15.0	-9.4	29.6	10.6	41.3	-8.8	14.2	-10.6	26.3	16.9	40.4	-10.6
15.0	-9.4	29.6	13.8	41.7	-7.5	14.6	-9.4	30.4	13.1	41.3	-10.0
15.4	-7.5	28.8	10.0	42.5	-10.0	14.6	-8.1	28.8	12.5	41.3	-9.4
13.8	-6.3	29.2	8.1	42.1	-6.3	15.0	-8.1	30.4	11.3	43.8	-9.4
15.4	-10.0	30.8	12.5	44.2	-10.0	15.4	-12.5	28.8	16.9	42.9	-11.9

XQ Configuration responses

INFERIOR						SUPERIOR					
n1		p1		n2		n1		p1		n2	
ms	nv/deg <sup>2</sup>	ms	nv/deg <sup>2</sup>	ms	nv/deg <sup>2</sup>	ms	nv/deg <sup>2</sup>	Ms	nv/deg <sup>2</sup>	ms	nv/deg <sup>2</sup>
15.8	-8.1	28.3	11.9	43.3	-9.4	13.8	-9.4	30.0	12.5	41.7	-9.4
16.7	-8.8	31.3	11.3	42.1	-8.8	15.4	-8.8	29.2	13.1	43.3	-10.6
15.0	-7.5	29.2	13.1	42.5	-10.6	15.4	-9.4	30.0	12.6	26.7	-10.6
15.8	-8.8	28.3	11.3	42.1	-6.9	15.8	-9.4	28.8	11.9	42.5	-8.1
15.8	-9.4	30.0	14.4	44.6	-11.9	14.6	-13.1	27.9	19.4	43.3	-16.9
13.8	-6.9	27.9	8.8	40.4	-6.9	12.9	-7.5	27.9	9.4	41.7	-8.8
12.9	-5.6	28.3	8.8	40.4	-6.3	12.9	-6.3	26.3	9.4	42.1	-7.5
15.8	-11.3	29.2	18.8	42.5	-12.5	15.8	-12.5	27.5	20.0	43.3	-16.3
13.8	-7.5	30.0	10.6	43.3	-8.8	15.0	-9.4	30.4	11.3	42.9	-10.0
13.8	-5.0	25.8	9.4	40.4	-6.3	12.9	-7.5	26.3	11.9	40.0	-8.1
15.8	-9.4	28.3	13.8	42.1	-9.4	15.8	-9.4	29.6	12.5	43.3	-10.0
14.2	-7.5	27.5	8.8	40.8	-7.5	15.0	-7.5	29.2	12.5	42.5	-10.0
15.0	-8.8	28.3	12.5	43.3	-10.6	13.3	-9.4	27.9	15.0	42.1	-13.1
15.0	-6.9	29.2	10.0	42.5	-8.8	15.0	-8.8	30.0	11.9	43.3	-9.4
16.7	-5.6	30.8	6.9	43.8	-5.0	15.0	-9.4	30.4	13.1	43.8	-10.6
14.2	-10.0	27.5	15.0	41.7	-11.3	15.0	-11.3	28.8	13.8	42.1	-12.5
16.3	-7.5	31.7	11.9	45.8	-10.0	17.5	-10.6	32.5	15.0	46.7	-11.9
14.2	-7.5	29.2	10.0	40.0	-8.8	14.2	-10.0	27.5	12.5	42.5	-8.8
15.4	-8.8	27.9	11.3	42.1	-9.4	14.2	-11.3	26.3	15.6	41.7	-11.3
15.4	-8.8	29.6	12.5	40.8	-8.8	15.4	-10.0	30.0	14.4	43.8	-10.0
13.8	-6.9	28.8	10.6	42.1	-9.4	14.6	-8.1	27.3	11.3	42.9	-11.3
15.0	-7.5	28.3	10.0	43.3	-7.5	14.6	-8.1	29.6	11.3	42.9	-8.1
16.7	-10.0	30.0	11.9	43.8	-10.0	15.4	-11.9	30.0	17.5	45.0	-13.1

NASAL						TEMPORAL					
n1		p1		n2		n1		p1		n2	
ms	nv/deg^2	ms	nv/deg^2	ms	nv/deg^2	ms	nv/deg^2	ms	nv/deg^2	ms	nv/deg^2
13.3	-7.5	28.8	10.0	41.7	-7.5	14.6	-9.4	28.3	11.3	41.7	-10.0
14.6	-5.6	30.4	7.5	43.3	-7.5	15.8	-8.1	30.8	11.3	42.9	-11.3
14.6	-6.9	29.6	8.8	42.5	-8.8	15.4	-8.8	29.6	12.5	42.5	-11.9
15.4	-7.5	30.4	8.1	41.7	-7.5	15.4	-8.1	28.3	11.3	42.5	-8.8
14.6	-9.4	28.3	13.8	43.8	-12.5	14.2	-10.6	27.9	17.5	44.2	-14.4
12.1	-4.4	29.6	5.0	40.8	-6.3	15.4	-7.5	29.2	9.4	41.3	-8.1
15.0	-5.0	28.3	5.6	41.7	-6.9	13.8	-5.6	27.1	9.4	42.5	-8.8
15.0	-8.8	30.0	13.8	42.5	-11.3	15.8	-11.3	28.3	16.3	43.3	-13.8
15.0	-6.3	30.0	7.5	43.3	-7.5	16.3	-8.8	30.0	11.9	42.9	-10.6
12.9	-3.8	29.2	5.0	40.4	-5.0	15.0	-6.9	25.8	10.6	39.2	-8.8
16.3	-6.9	30.8	10.6	43.3	-8.8	15.4	-8.8	30.0	13.8	42.5	-12.5
14.2	-6.3	31.7	3.8	40.0	-5.0	15.0	-6.3	29.2	8.8	42.5	-10.0
15.0	-8.8	29.6	8.1	42.1	-8.1	14.6	-10.0	28.8	14.4	42.1	-12.5
14.6	-6.3	30.0	6.9	42.9	-5.6	15.0	-7.5	30.0	10.6	42.5	-9.4
12.9	0.0	30.0	7.5	42.9	-6.9	14.6	-6.3	30.8	7.5	42.5	-6.9
15.0	-6.9	28.8	9.4	42.1	-9.4	14.2	-9.4	27.5	15.0	41.7	-11.9
18.3	-6.9	34.2	9.4	47.1	-6.9	17.5	-8.1	32.9	11.3	46.3	-11.3
13.3	-6.3	29.2	7.5	42.5	-6.3	15.0	-10.0	27.5	13.8	40.0	-8.8
14.2	-7.5	30.4	9.4	41.7	-8.1	13.8	-10.0	26.7	16.9	42.1	-10.6
15.8	-7.5	29.6	13.1	41.3	-8.8	15.8	-9.4	30.0	11.3	41.3	-9.4
14.2	-6.9	28.3	9.4	42.9	-7.5	15.4	-8.1	28.8	11.9	41.7	-9.4
15.0	-5.6	29.6	6.9	42.9	-5.6	14.6	-8.1	29.6	11.9	42.5	-9.4
15.4	-8.1	30.4	10.6	42.5	-7.5	15.4	-11.3	27.5	15.6	42.9	-11.9

Multifocal ERG subject details

MSE: Mean Spherical Error

AL: Axial Length

IV: Interval Variance

		IV	IV	IV	IV	IV	IV	IV	IV
Left MSE	Left AL IOL	SUP	INF	NASAL	TEMP	SUP TEMP	INF NASAL	INF TEMP	SUP NASAL
0.50	23.12	5.34	5.00	5.82	5.05	5.16	5.55	5.65	4.95
-7.25	26.22	5.25	4.77	5.85	4.87	5.19	5.17	5.61	4.52
-4.25	25.15	NO MR DATA							
-0.19	22.95	5.94	5.19	5.85	5.29	5.56	5.69	6.03	5.10
-2.00	24.13	NO MR DATA							
0.00	24.17	4.60	4.70	5.55	4.98	4.67	5.11	5.47	5.37
-4.75	25.29	5.60	5.23	5.85	5.11	5.37	5.63	6.19	5.34
-0.63	23.28	5.82	5.33	5.58	5.08	5.25	5.37	6.01	5.19
0.25	23.27	5.37	4.98	5.50	5.08	5.18	5.15	5.18	4.97
-8.68	26.84	5.65	5.39	5.97	5.10	5.33	5.88	5.94	5.11
-8.00	27.24	6.44	5.75	6.47	5.80	5.79	5.81	6.44	5.74
0.13	23.39	6.03	5.57	5.72	5.58	5.56	5.59	6.04	5.32
-1.13	24.03	5.52	4.81	4.69	5.41	5.03	5.07	5.63	4.62
-6.63	25.52	5.48	4.98	5.69	4.97	5.36	5.42	5.69	5.02
-1.12	23.48	5.47	5.49	5.41	4.97	5.14	5.46	5.62	5.29
-3.00	25.19	5.77	5.13	5.51	5.23	5.41	5.28	5.73	5.13
0.25	23.50	5.70	5.09	5.64	5.03	5.35	5.41	5.71	5.06
-9.31	26.41	5.90	5.33	6.15	5.42	5.47	5.73	5.85	5.66
-0.07	24.31	5.85	5.33	5.63	4.98	5.44	5.58	5.73	5.07
-0.07	23.68	5.63	4.91	5.64	4.86	5.56	5.85	6.26	5.45
-0.18	23.70	5.51	5.64	5.64	4.93	5.20	5.41	5.68	5.00
-0.31	22.93	5.69	5.16	5.60	5.23	5.46	5.45	5.66	5.10
-0.75	24.33	5.61	5.05	5.50	4.74	5.13	5.30	5.72	4.85

SURFACE AREAS FOR MFERG SUBJECTSXQ DATASURFACE AREAS IN mm<sup>2</sup>

<b>MSE (D)</b>	<b>SUP</b>	<b>INF</b>	<b>NASAL</b>	<b>TEMP</b>
0.495	220.5121	231.6063	212.0273	247.1733
-7.25	240.2087	218.6113	203.9558	245.1092
-4.25	NO MR DATA			
-0.185	228.5753	220.6947	228.6536	234.2750
-1.995	NO MR DATA			
0	215.7808	227.5891	264.7641	243.9464
-4.75	257.6212	270.3276	273.6055	232.1776
-0.625	224.7261	235.0683	213.6098	227.5266
0.245	211.4910	220.7778	227.8496	204.4018
-8.68	271.8368	292.8415	283.6517	261.6697
-8	308.1347	285.7326	332.4242	309.9796
0.125	262.6133	240.4372	240.4700	231.6088
-1.125	206.7012	214.7728	182.7880	193.3873
-6.625	205.9602	242.8201	239.5309	220.4595
-1.12	230.0244	212.9193	214.0497	200.1824
-3	247.8121	229.8404	222.9243	249.7332
0.245	212.6054	214.0648	192.8345	232.4840
-9.31	237.9476	260.4218	253.1010	277.5386
-0.065	239.3049	261.9538	218.0068	237.9423
-0.065	231.7679	253.4496	213.3948	232.7510
-0.18	224.2802	245.0085	196.0024	213.2033
-0.31	210.4789	229.4705	210.4921	229.4853
-0.75	207.6813	226.3243	200.2533	217.9766

## SURFACE AREAS FOR MFERG SUBJECTS

### +Q DATA

#### SURFACE AREAS IN mm<sup>2</sup>

<b>MSE (D)</b>	<b>SUP TEMP</b>	<b>INF NASAL</b>	<b>INF TEMP</b>	<b>SUP NASAL</b>
0.495	228.995	220.893	201.993	219.931
-7.25	230.640	205.276	204.889	228.456
-4.25	NO MR DATA			
-0.185	241.470	223.376	229.823	227.686
-1.995	NO MR DATA			
0	199.886	240.797	222.870	229.002
-4.75	239.939	274.079	282.777	249.885
-0.625	227.165	223.032	381.416	444.166
0.245	201.977	224.117	190.752	196.597
-8.68	274.048	290.478	262.627	283.142
-8	249.129	325.232	257.585	296.791
0.125	236.829	223.005	221.415	217.222
-1.125	238.315	270.037	195.226	203.463
-6.625	220.628	259.240	235.684	231.237
-1.12	208.042	205.342	207.681	242.480
-3	246.462	230.063	232.114	239.774
0.245	228.247	198.569	202.867	219.340
-9.31	292.378	299.246	278.918	309.175
-0.065	260.664	263.864	239.597	222.162
-0.065	265.579	229.875	240.530	263.464
-0.18	235.572	206.517	246.863	207.394
-0.31	214.238	204.062	220.660	231.870
-0.75	214.077	204.062	205.702	208.842

APPENDIX 10: GANGLION CELL DENSITY: DETECTION TASK DATA

	<b>AVERAGE OF % CORRECT</b>	
<b>Spatial Frequency c/deg</b>	<b>Subject a</b>	<b>Subject b</b>
1	98	100
2	100	96
3	86.67	88
4	76	81.33
5	69.33	84
6	45.33	52
7		48
	<b>AVERAGE OF % CORRECT</b>	
<b>Spatial Frequency c/deg</b>	<b>Subject c</b>	<b>Subject d</b>
1	88	98
2	82	92
3	82	72
3.5		68
4	60	50
5	54	42
6	54	
7	46	

APPENDIX 11: GANGLION CELL DENSITY: DIRECTION DISCRIMINATION TASK  
DATA

	<b>AVERAGE OF % CORRECT</b>	
<b>Spatial Frequency c/deg</b>	<b>Subject a</b>	<b>Subject b</b>
1	100	100
2	98	96
3	70	64
3.5	68	52
4	56	57.33
5	48	56
6		48
<b>AVERAGE OF % CORRECT</b>		
<b>Spatial Frequency c/deg</b>	<b>Subject c</b>	<b>Subject d</b>
1	98.67	64.33
2	72	58
2.5		50.17
3	50	41
3.5	46	
4	54.67	26.67
5		39

Ganglion cell Density: Case Study R.C raw data

Detection

<b>Spatial frequency c/deg</b>	<b>Right eye % correct</b>	<b>Left eye % correct</b>
1	96	100
2	88	84
3	76	100
4	56	80
4.5		84
5	52	56
5.5	56	
6	58	56
6.5		56

Direction discrimination

<b>Spatial frequency c/deg</b>	<b>Right eye % correct</b>	<b>Left eye % correct</b>
1	92	96
1.5	64	88
2	48	38
2.5	40	68